SPREAD-SPECTRUM MULTIPLE ACCESS FOR INTERACTIVE DATA COMMUNICATIONS

by

VICTOR CHUNG MING LEUNG

B.A.Sc., University of British Columbia, 1977

A THESIS SUBMITTED IN PARTIAL FULFILLMENT OF

THE REQUIREMENTS FOR THE DEGREE OF

DOCTOR OF PHILOSOPHY

in

THE FACULTY OF GRADUATE STUDIES

Department of Electrical Engineering

We accept this thesis as conforming

to the required standard

THE UNIVERSITY OF BRITISH COLUMBIA

December 1981

In presenting this thesis in partial fulfilment of the requirements for an advanced degree at the University of British Columbia, I agree that the Library shall make it freely available for reference and study. I further agree that permission for extensive copying of this thesis for scholarly purposes may be granted by the head of my department or by his or her representatives. It is understood that copying or publication of this thesis for financial gain shall not be allowed without my written permission.

Department of Electrical Engineering

The University of British Columbia
2075 Wesbrook Place
Vancouver, Canada
V6T 1W5

Date Jan 30, 1982

ABSTRACT

Spread-spectrum multiple access (SSMA) is conceptually attractive for interactive data communications over broadcast channel shared by a large number of potential users. The present thesis involves a study of asynchronous direct sequence SSMA interactive data communication systems. The study includes a unified analysis and assessment of system delay-throughput performance.

Two important message delay components which are affected by the design of the transmitter/receiver pair result from code acquisition and bit-errors. A new code synchronizer design featuring a number of parallel correlators is developed, and an analysis of synchronizer performance as it relates to SSMA applications is provided. It is shown that average acquisition delay decreases in proportion to increase in the number of correlators when this number is small. Receiver bit-error probability for any given channel occupancy is derived. Three protocols suitable for SSMA transmissions under different operating conditions are proposed. Using one of these protocols, the expected number of transmissions before a message is received error-free is estimated by averaging bit-error probabilities over a postulated channel occupancy probability distribution. This distribution is verified using data obtained from channel simulations.

Delay-throughput characteristics of the SSMA system are thus obtained by evaluating the above delays and other exogenous delays at various traffic levels. Results relevant to the given system and traffic models, transmission protocol, and transmitter/receiver structure are obtained assuming that users'

codes are uncorrelated. Subsequently, it is shown that the results are easily modified to account for code cross-correlations.

Assessment of SSMA delay-throughput performance is accomplished by comparisons with pure ALOHA, slotted ALOHA and queueing channels. These comparisons necessitate extension of existing analysis of slotted ALOHA channels to include the effects of Gaussian channel noise, as well as development of an analysis procedure for noisy pure ALOHA channels. It is shown that in power-limited situations, the capacities of ALOHA and queueing channels can be maximized with respect to the transmission bit rate. Delay-throughput comparisons show that at throughput levels much lower than the capacities of these channels, average delays for SSMA are higher than those of the other channels. However, capacities of SSMA channels are generally higher than those of the other channels, which occupy only a fraction of the available bandwidth at power levels favourable to SSMA. In such cases, the throughput which results for a given delay clearly favours SSMA.

Comparisons are also performed with respect to m-parallel ALOHA or queueing channels, where m is the number of channels accommodated by the available bandwidth. In this case the capacities of SSMA channels are generally less than those of m-parallel slotted ALOHA or queueing channels, but approximately equal to those of m-parallel pure ALOHA channels. Therefore, SSMA presents a viable alternative to m-parallel pure ALOHA multiple access for interactive data communications. SSMA is especially favourable for transmissions of long messages in a wide-band broadcast channel with limited power.

TABLE OF CONTENTS

LIST OF TABLES

LIST OF ILLUSTRATIONS

ACKNOWLEDGEMENT

I am deeply grateful to my research supervisor, Dr. R.W. Donaldson, for his encouragement and many helpful suggestions during the course of this thesis.

Grateful acknowledgement is extended to the Natural Sciences and Engineering Research Council for financial support received under the Postgraduate Scholarships Program, and to the National Research Council for support under Grant NRC A-3308.

Special thanks are also extended to Mr. A. Mackenzie for his technical assistance and to Mrs. Kathy Brindamour for typing the manuscript.

Finally, I am thankful to my parents and sisters for their patience and encouragement.

1. INTRODUCTION

1.1 Motivation and Objectives

Advances in digital technology have led to growing interest in interactive data communications for a variety of applications including data base updating and retrieval, electronic funds transfer, electronic mail, interactive distance education, placing of reservations for travel, accommodation and entertainment, point of sale information processing, and remote monitoring of property and equipment. Communication nodes include homes, business establishments, data storage locations, educational institutions and mobile transceivers. These applications motivate the use of readily available broadcast communication facilities such as satellite links, cable networks and radio networks for wide-band point-to-point and multipoint interactive data communications.

Pseudonoise (PN)-coded spread-spectrum multiple access (SSMA) communication systems enable a large number of users to share a common broadcast channel. Although SSMA receiver performance in terms of bit-error probability has been determined by others, system development has been impeded by the lack of comprehensive evaluations of overall system performance. The primary objective of this thesis is performance evaluation for PN-coded direct sequence SSMA interactive data communication systems.

An important measure of interactive data communication system performance is the delay-throughput characteristic. System throughput is the amount of information transferred from all sources to destinations per unit time. It is a function of the total traffic generated, an entity not within control of the system. However, the feasible level of system throughput is constrained by the

acceptability of the corresponding message delay. Therefore throughput is treated as an independent variable for the evaluation of message delay, where delay is the elapsed time between the input of a message from its source to the system and the correct reception of the entire message at its destination. For interactive data communications, short message delays are desirable, especially when human interaction is involved. Message delays averaging two to three seconds with standard deviations of one to two seconds are considered acceptable [M1, R1].

In SSMA communications, PN-code synchronization is a primary cause of delay. In this thesis a code synchronizer suitable for direct sequence SSMA applications is introduced and its acquisition time and hold-in time statistics are obtained. System and data traffic models as well as appropriate signal transmission protocols are established to facilitate delay-throughput analysis in relation to synchronization delay, bit-error probability and message length. Delay-throughput characteristics for other multiple accessing schemes including pure ALOHA, slotted ALOHA and queueing are obtained, and are used for comparison purposes. The effects of transmission errors caused by random noise as well as "collisions" are included in the analysis.

1.2 Spread-Spectrum Multiple Access

Spread-spectrum techniques [D1,D2] are employed in communications, ranging, direction finding and position location. Spreading of the signal spectrum may be achieved by direct multiplication of the signal with a code sequence at a high clock rate (direct sequence technique) or by varying the carrier frequency in a time-coded fashion (frequency hopping technique).

Combinations of the two techniques and other techniques may also be used. The received signal is de-spread by application of the spreading technique in reverse so that the desired information is restored to its original bandwidth while uncorrelated noise and interference remain spread to the transmission bandwidth. Thus, a spread-spectrum gain results when filtering extracts the information and rejects most of the noise and interference.

Advantages of spread spectrum communications are as follows:

1. Spectrum spreading enhances the signal to noise ratio of the de-spread signal in the presence of noise and co-channel jamming and thereby reduces the transmitter power required.
2. Because spread-spectrum signals have wideband spectra with low spectral densities which are noise-like when PN codes are used, they are less susceptible to eavesdropping. Furthermore, an intercepted signal cannot be decoded without knowledge of the spread-spectrum code, although codes that are not cryptographically safe may be reconstructed using suitable processing techniques.
3. The inherent frequency diversity of spectrum spreading effectively combats passive interference such as fading, multipath and intersymbol interference.

The inherent attractiveness of SSMA as a means of point-to-point communication on broadcast channels is a direct consequence of the above features. Thus the channel is shared by a number of users, each of which is assigned a unique code sequence chosen from a set of codes with low mutual cross-correlations. As a result, the signal transmitted by each user appears

as noise to all other users, and each user sees himself as the only occupant of a noisy channel. Further to advantages cited above, SSMA possesses the following advantages:

4. Compared with other multiple accessing schemes, SSMA does not require universal timing as in time division multiple access and all slotted contention multiple accessing schemes, or frequency guard-bands as in frequency division multiple access. Users may transmit at any time using the entire bandwidth available to the system, and collision with other users does not necessitate retransmission as in ALOHA and carrier-sense multiple access.

5. Because of low spectral densities and noise-like spectra of SSMA signals, co-existence of SSMA with other services in the same channel is possible, with only a slight degradation to all received signals. It is therefore feasible to phase in SSMA over a period of time to replace existing services.

6. Hardware for all users is standardized and could benefit from large scale integration with sufficient demand. The PN-code generator is easily realized by a shift register with feedback connections determined by the user's code.

7. Priority messages can be accommodated by simply increasing the transmitter power, or by other means.

Potential disadvantages of SSMA communications are as follows:

1. Large channel bandwidth, which is often scarce and costly, is needed. However sharing of the channel among a number of users considerably reduces this potential disadvantage, particularly when the user traffic is bursty. In this case the law of large number applies to average and smooth the demand placed on the channel, with a small subset of the totality of potential users actually occupying the channel at any instant.
2. Spread-spectrum receivers are somewhat more complex than those used in other multiplexing schemes. However, continued decreases in costs of digital electronics largely obviate this problem.
3. Some form of power control may be required in some applications where received power from different users varies in accordance with transmitter-receiver distance separation; for example on a cable network. In such cases an indirect form of power control would involve limiting the network to a star configuration.

The ultimate question is this: "How does the efficiency of SSMA compare with that of other multiplexing schemes for point-to-point communication on broadcast channels?" This thesis deals with this question.

1.3 Review of Previous Work

Although the basic principles of spread-spectrum systems have been known for many years, most of the early development was done in the military domain because implementation was costly. In the late 1960's advances in satellite technology attracted much interest in multiple accessing the satellite channel. Schwartz et al. [S1] analysed several modulation techniques, including spread-

spectrum, for multiple access to satellite repeaters. Aein [A1] derived the optimum bandwidth and the resulting maximum number of simultaneous users for SSMA to a hard-limiting satellite repeater. Anderson and Wintz [A2] analysed a SSMA system with a hard limiter by computing the signal to noise ratio at the output of a correlation detector. The analysis included the effects of cross-correlations of the PN codes.

Advances in digital computer technologies since the 1970's has led to growing demand for interactive data communications. Advantages in sharing computer and communication resources [K1, K2] have spawned schemes for packet transmission over broadcast channels, including ALOHA [K3, L1, C1], carrier sense and busy tone [K4, T1] multiple access, and polling [T2]. Analysis has centered on the delay-throughput characteristics of these schemes. However, delay-throughput analysis for SSMA is lacking.

Spread-spectrum transceiver hardware such as megabits-per-second code generators [D5], surface acoustic wave devices [G1] and digital correlators [E1] are becoming available as digital technologies advance. As a result, there is growing interest in spread-spectrum for data communications. Signal to noise ratio and bit-error probability of SSMA receivers were analysed by Pursley [P1] and Yao [Y1]. The effects of code sequence parameters were further considered by Pursley and Sarwate [P2]. While these authors assumed equal power for all co-channel users at the receiving site, the effects of geographical distribution of users were considered by Musa and Wasylkiwskyj [M2].

The proper operation of a SSMA communication system depends on the assignment of codes with low mutual cross-correlations to the system users. For

direct sequence applications, Gold [G1] presented a method of generating a large number of non-pseudonoise codes with bounded cross-correlations from a pair of PN codes, and Anderson [A3] described a strategy of selecting a subset of PN codes with bounded cross-correlations from the set of all PN codes which have identical lengths. For frequency hopping applications, the formulation of optimal frequency hopping sequences for SSMA was investigated by Solomon [S2], and the design of a time-frequency coded signal set with low cross-correlations was presented by Yates and Cooper [Y2].

The delay characteristics of a SSMA communication system are related closely to the spread-spectrum code acquisition time if code synchronizers are used. When the received signal frequency and the receiver's environmental temperature are stable, information can be extracted using a matched filter for the intended code sequence and code acquisition is not necessary. Matched filter receivers are usually implemented using surface acoustic wave (SAW) or charge coupled (CCD) devices [B1,B2,V2,M3]. SAW devices are only applicable for short code lengths (less than 200 chips) because of physical limitations on length of delay line, resolution of taps, and signal attenuation. Performance of SAW filters deteriorates when signal frequency or environmental temperature fluctuates. CCD filters are only useful for code rates of 5 MHz or less, and are also subjected to attenuation problems for long code lengths. SAW and CCD filters are expensive because they are not currently mass-produced. For SSMA applications, other methods of demodulation, usually involving the use of a code synchronizer, are normally more appropriate and less expensive.

A code synchronizer generally performs two tasks, acquisition and tracking. The acquisition process brings the receiver generated code in phase with

the received code. The tracking process then keeps the codes in phase. Delay-lock loops [S3] or dithering loops [H1] are usually used for tracking. Various methods of code acquisition have been proposed. Sequential estimation [W1,K5,W2] achieves rapid acquisition by initializing the receiver's code generator with an estimate of the received code. Because this estimate is made without the benefit of spread-spectrum gain, it is unreliable when a number of coded signals are present. Therefore sequential estimation is unsuitable for SSMA applications. Another method of acquisition uses the sliding correlator [D1] whereby the phases of the local code and received code slide past each other until a match occurs. Analysis of various forms of sliding correlators was offered by Sage [S4], Holmes and Chen [H2] and Hopkins [H3]. These correlators are well suited for SSMA applications, although acquisition time is quite long. Hopkins' synchronizer is particularly interesting because both acquisition and tracking are treated in a unified manner and the eventuality of losing lock is also taken into consideration. It appears that acquisition time and hold-in time performance of code synchronizers in SSMA data communication systems has not been investigated in the literature.

The application of SSMA in a cellular mobile radio system has recently been investigated by Cooper, Nettleton and Grybos [C2,C3,N1,N2,N3,G3]. Their suggestion that SSMA is spectrally more efficient than conventional narrow band FM techniques for cellular mobile radio service has been a subject of dispute [H4].

Applications of spread-spectrum techniques to enhance the performance of ALOHA-type contention multiplexing schemes in packet radio networks were described by Kahn et al. [K6]. The throughput-delay characteristics of a system

which employs SSMA to reduce the message-obliterating effect of collisions in slotted ALOHA multiple access were recently analysed by Raychaudhiru [R2]. In this analysis, perfect code-synchronization between transmitter/receiver pairs and perfect block-synchronization among system users were assumed.

Use of SSMA for interactive data communications involving a large user population is new, and comprehensive results on performance analysis and optimization of such systems are unavailable. In particular, analysis in synchronizer performance and delay-throughput characteristics for asynchronous SSMA communication systems is lacking.

1.4 Outline of the Thesis

In Chapter 2 models for a spread-spectrum transmitter/receiver pair and the multiple access channel are specified. The bit-error probability at the receiver output is derived for the case where co-channel interferers are modelled as Gaussian white noise. An upper bound for the bit-error probability is also obtained by taking into consideration the maximum cross-correlation between the code sequences. A numerical example using a specific set of system parameters is presented.

A code synchronizer employing a number of sliding correlators working in parallel is presented in Chapter 3. In addition to having the advantages of Hopkins' synchronizer [H3] cited earlier, the design of this synchronizer reduces the mean and standard deviation of acquisition time in proportion to the number of parallel correlators used. In the special case where the number of parallel correlators equals one, this synchronizer reduces to the one proposed by Hopkins. The means and variances of acquisition time and hold-in time

are derived. An acquisition time confidence estimate is obtained using Chebyshev's inequality. It is also demonstrated that the hold-in time probability distribution is approximately exponential. Finally, to show the effect of some synchronizer and system parameters on acquisition time and hold-in time, a number of graphs are presented using a set of fixed synchronizer parameters and the system parameters specified in Chapter 2.

The overall SSMA data communication system performance is considered in Chapter 4. Protocols suitable for SSMA signal transmission under different conditions of propagation delay and acknowledgement delay in relation to acquisition time and message duration are described. Average message delays are derived for these protocols. A probability distribution for the number of active users is approximated using simulation techniques. Delay-versus-throughput curves are obtained for different message lengths using results from Chapters 2 and 3. It is shown that the SSMA channel is subjected to instability when it is operating near capacity. This property is common to other forms of contention multiple access.

In Chapter 5, delay-throughput characteristics are derived for pure ALOHA and slotted ALOHA channels where retransmissions are caused not only by collisions but also by random errors resulting from channel noise. Consideration of the effects of random errors is essential for proper system performance comparisons. It is shown that the capacities of these channels can be maximized at some optimum data rates under conditions of fixed power and unlimited bandwidth. The same analysis is repeated for a M/D/1 queueing channel. Comparison between delay-throughput characteristics of SSMA, pure ALOHA,

slotted ALOHA and queueing channels shows that SSMA is quite favorable, especially in limited power, wide-bandwidth-available situations.

Chapter 6 concludes the thesis with a summary of the results and some suggestions for further research.

2. SYSTEM MODEL

2.1 Structure of the Transmitter and Receiver

Simplified block diagrams of a direct sequence spread-spectrum transmitter/receiver pair are shown in Fig. 2.1.1. The signals indicated are those used for and resulting from the modulation and demodulation of a message sequence generated by a typical (i-th) user of the channel.

The transmitted signal $s_i(t)$ is formed by biphase-modulating a sinusoidal carrier of angular frequency ω_c and average power P by a binary sequence which is a product of the message (information) sequence $m_i(t)$ and the code sequence $c_i(t)$ assigned to the i-th user. That is,

$$s_i(t) = \sqrt{2P}\, m_i(t)\, c_i(t) \cos(\omega_c t + \theta_i) \qquad (2.1.1)$$

where θ_i is a random time invariant phase angle, uniformly distributed between 0 and 2π. Both binary sequences $m_i(t)$ and $c_i(t)$ consist of unit amplitude, positive and negative rectangular pulses. The pulse duration T_b of $m_i(t)$ is assumed to be related to the pulse duration T_c and period (length) L of $c_i(t)$ by

$$T_b = L \cdot T_c \qquad (2.1.2)$$

The modulation process thus spreads the information bandwidth B_m in the baseband to a much wider transmission bandwidth B_t in the passband. These bandwidths are related to the pulse durations by

$$B_m = 1/T_b \qquad (2.1.3)$$

$$B_t = 2/T_c \qquad (2.1.4)$$

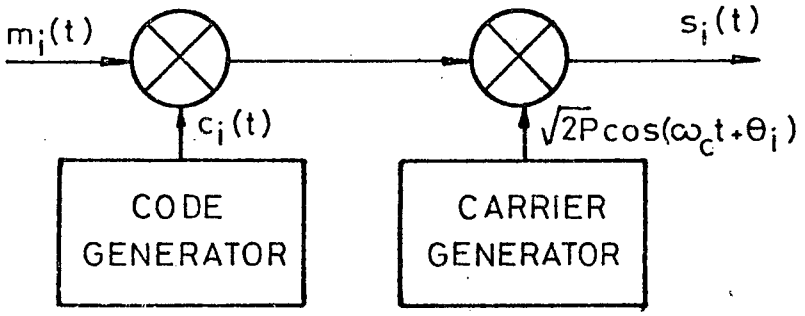

(a) TRANSMITTER

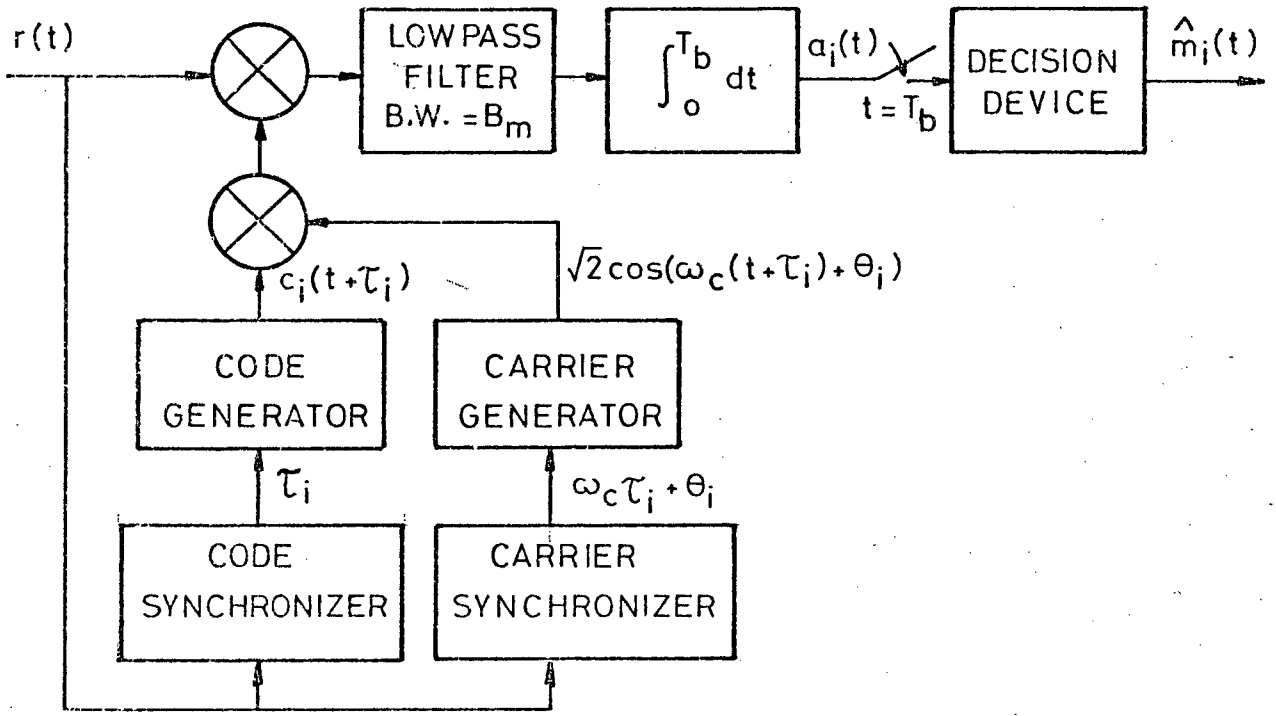

(b) RECEIVER

Fig. 2.1.1 Direct sequence spread-spectrum transmitter/receiver pair.

The receiver correlates the received signal r(t) with a locally generated signal which is a product of a replica of $c_i(t)$ and a sinusoid phase-coherent with the carrier of $s_i(t)$. This process restores the desired information to its baseband bandwidth B_m and rejects most of the interference and noise power which has a baseband bandwidth greater than $B_t/2$. The resulting signal $a_i(t)$ is sampled at the information bit rate. A decision device then reconstructs an estimate $\hat{m}_i(t)$ of the message sequence from the samples. Successful demodulation of the desired information requires that synchronization with $s_i(t)$ be established at the code word, code bit (chip) and carrier levels.

2.2 Multiple Access Channel Model

Consider M active users simultaneously accessing a SSMA channel. The SSMA channel and its signal sources and sinks are shown in Fig. 2.2.1.

The sources and sinks consist of M matching transmitter/receiver pairs as described in Section 2.1. The output of each transmitter is subjected to an independent random delay τ uniformly distributed between 0 and T_b which accounts for the asynchronous nature of the M signals. Assuming that the SSMA channel is a linear Gaussian noise channel with zero attenuation, all receivers therefore receive a composite signal

$$r(t) = s(t) + n(t) \tag{2.2.1}$$

where

$$s(t) = \sum_{i=1}^{M} s_i(t-\tau_i) \tag{2.2.2}$$

and n(t) is the channel noise generated by a white Gaussian process with two-

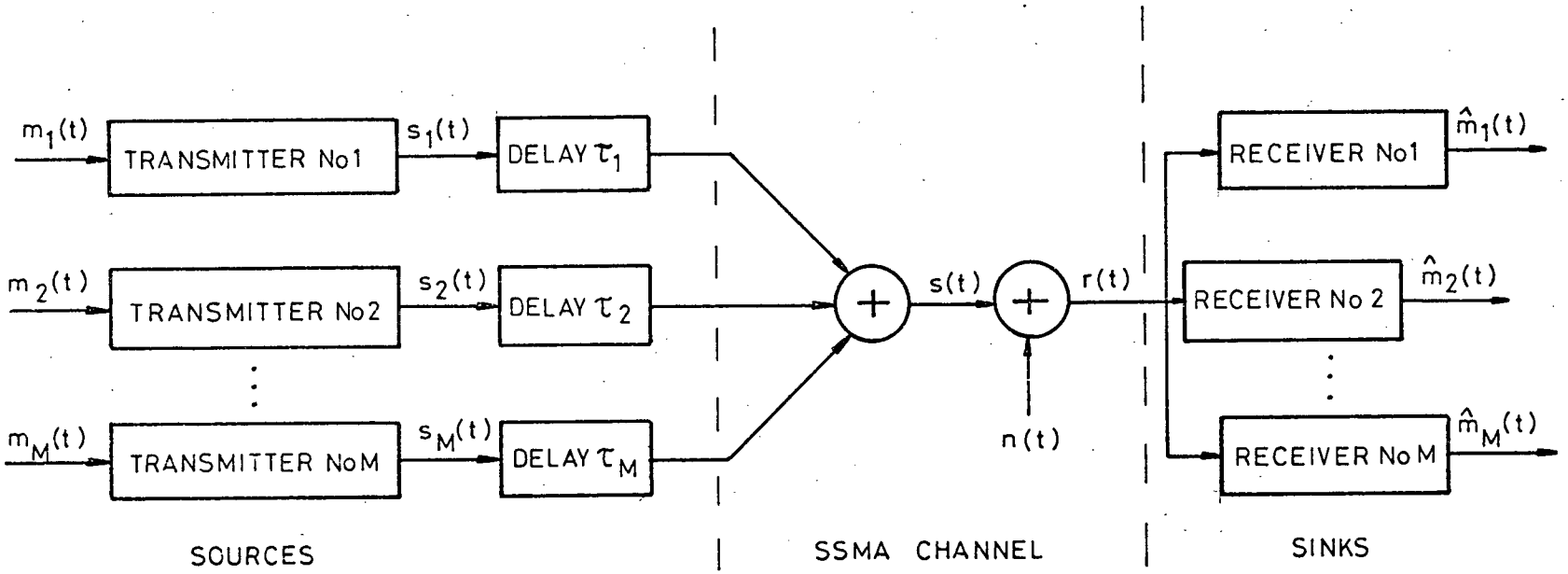

Fig. 2.2.1 Model of SSMA channel and its sources and sinks.

side spectral density $N_0/2$. In eqn. (2.2.2), $s_i(t)$ is given by eqn. (2.1.1). Each of the M signals presents an equal average power P to all receivers. A single user power to (single-sided) noise-density ratio (PNR) at the input to the receivers can be defined as

$$PNR = P/N_0 \tag{2.2.3}$$

The above channel model is applicable to a centralized network where the user population communicates only with a fixed central node over a common Gaussian noise channel. Located at the central node is one receiver for each potential user. With suitable controls, signal power contributed by each active user can be maintained constant at all receivers. Such a network may be realized through the use of:

(i) a satellite transponder not driven to saturation, with a single earth station as the central node;

(ii) a satellite which acts as the central node itself, that is, all receivers are on board the satellite;

(iii) a coaxial cable linking all users to the central node;

(iv) a radio network, with all users as well as central node stationary.

With some modifications, the channel model is also applicable to other SSMA channels such as VHF and UHF mobile radio channels.

In many multiple access applications, direct user-to-user communication is desirable, and the resulting network configuration is fully connected. Application of SSMA to this network configuration is hindered by two major problems: power control and contention.

Geographical dispersion of receiving sites in a connected network results in difficulties in controlling transmitter power to enable all users to present equal signal power to all other users. If it is only required that received power from all other users be constant at a user's receiving site, but that this power may vary from one receiving site to another, then a central transponder may be used to equalize the path attenuation between any one user and all other remaining users. In this case the power control requirement is the same as that of a centralized network, with the transponder replacing the central node. The network remains fully connected because the transponder retransmits all received signals without demodulating them. However, transponding doubles the transmission bandwidth requirement.

The contention problem is caused by the desirability of minimizing the number of receivers at user's site. Contention is not a problem if each user has as many receivers as there are other users, in which case the total number of receivers required for an n-user population is $n(n-1)$, a very large number if n is large. If each user has only one receiver, then the total number of receivers is reduced to n, a much smaller number. However, in this case contention arises when two or more users try to communicate with another user at the same time. Contention generally lowers the performance of the SSMA channel, but analysis is probably very difficult because the time that each user spends in the channel is not constant. An additional problem that accompanies contention is addressing. When there is one receiver per user, the best addressing scheme is to assign to each receiver a unique code which every transmitter incorporates into its transmission to that receiver. Alternatively, if each user is assigned a unique code for transmission rather than recep-

tion, then the originating user must, probably through a separate channel, identify himself and request that the destination receiver tune to the correct code sequence. In this case contention in the request channel is possible, as well as contention in the SSMA channel.

In this thesis detailed analysis of SSMA performance will be restricted to centralized networks. This problem is itself very important, and our methods and results would be useful in analyzing SSMA performance in networks where contention is involved.

2.3 Bit-Error Probability at the Receiver Output

2.3.1 Derivations

Referring to the receiver block diagram shown in Fig. 2.1.1(b), the signal to noise (power) ratio (SNR) of the sampled integrator output $a_i(T_b)$ for the i-th receiver is

$$SNR = \frac{(E[a_i(T_b)])^2}{Var[a_i(T_b)]} \tag{2.3.1}$$

where E[x] and Var[x] denote expected value (mean) and variance of random variable x, respectively. The decision device is a two level quantizer which makes a transition when $a_i(T_b)$ changes sign. If the noise components of $a_i(T_b)$ are Gaussian, the bit-error probability p_B at the output of the decision device is

$$p_B = 0.5 \text{ erfc } (\sqrt{SNR}) \tag{2.3.2}$$

where

$$\text{erfc}(x) = \frac{2}{\sqrt{\pi}} \int_x^\infty e^{-t^2} dt \qquad (2.3.3)$$

In SSMA communications, the noise components of $a_i(T_b)$ contributed by co-channel interferers are not truly Gaussian. Therefore p_B as given by eqn. (2.3.2) represents an approximation to the exact p_B which is too complicated to obtain. Fortunately, this approximation is usually quite good because the sum of the noise components aproaches a Gaussian distribution as the channel occupancy increases in accordance with the central limit theorem [P3].

It is convenient to distinguish between the noise and signal components of $a_i(T_b)$. Thus

$$a_i(T_b) = a_i^S(T_b) + a_i^N(T_b) \qquad (2.3.4)$$

where $a_i^S(T_b)$ is the signal component and $a_i^N(T_b)$ is the noise component. It can be shown that $a_i^N(T_b)$ has zero expected value and $a_i^S(T_b)$ has zero variance. The squared expected value of $a_i(T_b)$ or $a_i^S(T_b)$ is

$$(E[a_i(T_b)])^2 = (E[a_i^S(T_b)])^2 = \frac{1}{2} PT_b^2 \qquad (2.3.5)$$

To calculate the variance of $a_i(T_b)$ or $a_i^N(T_b)$, consider two different cases.

Case 1: Interference from other users of the channel behaves as independent sources of Gaussian noise, each of which has a uniform spectral density $P/2B_t$ over the transmission bandwidth. In this case [1]

---

[1] See Appendix 1 for derivation.

$$\mathrm{Var}\left[a_i(T_b)\right] = \mathrm{Var}\left[a_i^{N}(T_b)\right] = 0.9\ N_D/B_m \tag{2.3.6}$$

where N_D is the spectral density of noise plus interference from (M-1) other channel users given by

$$N_D = \frac{N_o}{2} + (M-1)\frac{P}{2B_t} \tag{2.3.7}$$

The SNR is therefore

$$\mathrm{SNR} = \frac{1.11\ P}{N_o B_m + (M-1)P(B_m/B_t)} \tag{2.3.8}$$

Define the spread-spectrum processing gain G_{ss} by

$$G_{ss} = B_t/(2B_m) = L \tag{2.3.9}$$

Thus

$$\mathrm{SNR} = \frac{2.22 \cdot \mathrm{PNR} \cdot G_{ss}}{(M-1) \cdot \mathrm{PNR} + B_t} \tag{2.3.10}$$

and p_B may be calculated using eqn. (2.3.2).

Case 2: The cross-correlations between the code sequences assigned to all potential users are upper-bounded by the maximum cross correlation ψ_{max}. In this case [2]

$$\mathrm{Var}\left[a_i^{N}(T_b)\right] \leq (M-1)\psi_{max}^{2}\ P/2 + 0.45\ N_o/B_m \tag{2.3.11}$$

and the SNR is given by

---

[2] See Appendix 2 for derivation.

$$SNR > \frac{2.22 \cdot PNR \cdot G_{ss}}{1.11 \cdot (M-1) \cdot \psi_{max}^2 \cdot B_t \cdot B_m \cdot PNR + B_t} \qquad (2.3.12)$$

Substituting the right hand side of eqn. (2.3.12) into eqn. (2.3.2), the p_B thus calculated gives an upper bound to the actual P_B.

Case 1 is applicable when the user propulation (UP) is sufficiently small that codes with low cross-correlations may be assigned. Mazo [M4] has shown that for UP << $d^2/2$, where $d = 2B_tT_b$, codes may be assigned so that each receiver's bit-error probability is at least as good as that calculated under case 1. If the set of codes is restricted to PN codes with length L for ease of generation and good auto-correlation, then case 1 is applicable only if UP << L. Selection of a set of codes with low cross-correlations usually involves extensive searching using a digital computer.

If a large UP is desired, procedures exist for construction of a large set of codes with higher but bounded cross-correlations, and results obtained under case 2 may be used to bound p_B. One such procedure was proposed by Gold [G2]. It provides for construction of 2^n+1 code sequences of length 2^n-1 from a pair of PN codes of the same length. The cross-correlations of these sequences are bounded by

$$\psi_{max} = \begin{cases} (2^{(n+1)/2} + 1)T_c, & n \text{ odd} \\ (2^{(n+2)/2} + 1)T_c, & n \text{ even} \end{cases} \qquad (2.3.13)$$

2.3.2 Numerical Examples

A set of signal parameters typical for moderate-speed spread-spectrum data communications is shown in Table 2.3.1.

TABLE 2.3.1 SSMA Signal Parameters

Information bit rate	$1/T_b$ = 50 KBits/sec.
Information (baseband) bandwidth	B_m = 50 KHz
Spread-spectrum code length	L = 511 chips
Spread-spectrum code rate	$1/T_c$ = 25.55 MBits/sec.
Transmission bandwidth	B_t = 51.1 MHz

Assuming case 1 is valid, a family of bit-error probability (p_B) vs. number of active user (M) curves at different PNR's is shown in Fig. 2.3.1. These curves show that at low PNR's p_B is insensitive to changes in M because channel noise predominates over co-channel interference. At moderate to high PNR's, p_B increases with M. If M stays constant, p_B decreases with increasing PNR but at a decreasing rate so that beyond a certain PNR (about 80 dB-Hz in this case) increase in PNR does not bring about any improvement in p_B. This is because at high PNR's co-channel interference predominates (i.e. (M-1) PNR >> B_t). Thus eqn. (2.3.10) becomes SNR $\approx$ 2.22 $G_{ss}/(M-1)$ and p_B is independent of PNR.

Using a set of Gold codes [G2] with signal parameters listed in Table 2.3.1 and applying results derived under case 2, bit-error probability upper bounds are plotted against number of active users at different PNR's as shown

in Fig. 2.3.2. Except for a compressed horizontal axis, these curves are similar to the ones in Fig. 2.3.1 and the previous observations regarding Fig. 2.3.1 are all applicable to Fig. 2.3.2. For Gold codes of length L = 511, $\psi_{max} = 33T_c$. Since $G_{ss} = L$, eqn. (2.3.12) becomes

$$SNR \geq \frac{2.22 \cdot PNR \cdot G_{ss}}{4.73 \cdot (M-1) \cdot PNR + B_t} \qquad (2.3.14)$$

This lower bound on SNR equals the SNR value in eqn. (2.3.10) if the number of co-channel interferers in eqn. (2.3.10) is multiplied by 4.73. Thus, with uncorrelated user codes (case 1), the SSMA system can accommodate more than four times the number of active users than when Gold codes are used while achieving the same bit-error probability p_B. However, Gold codes can support a much higher user population (UP $\leq$ 513 in this case) than PN codes which satisfy the uncorrelated codes assumption of case 1.

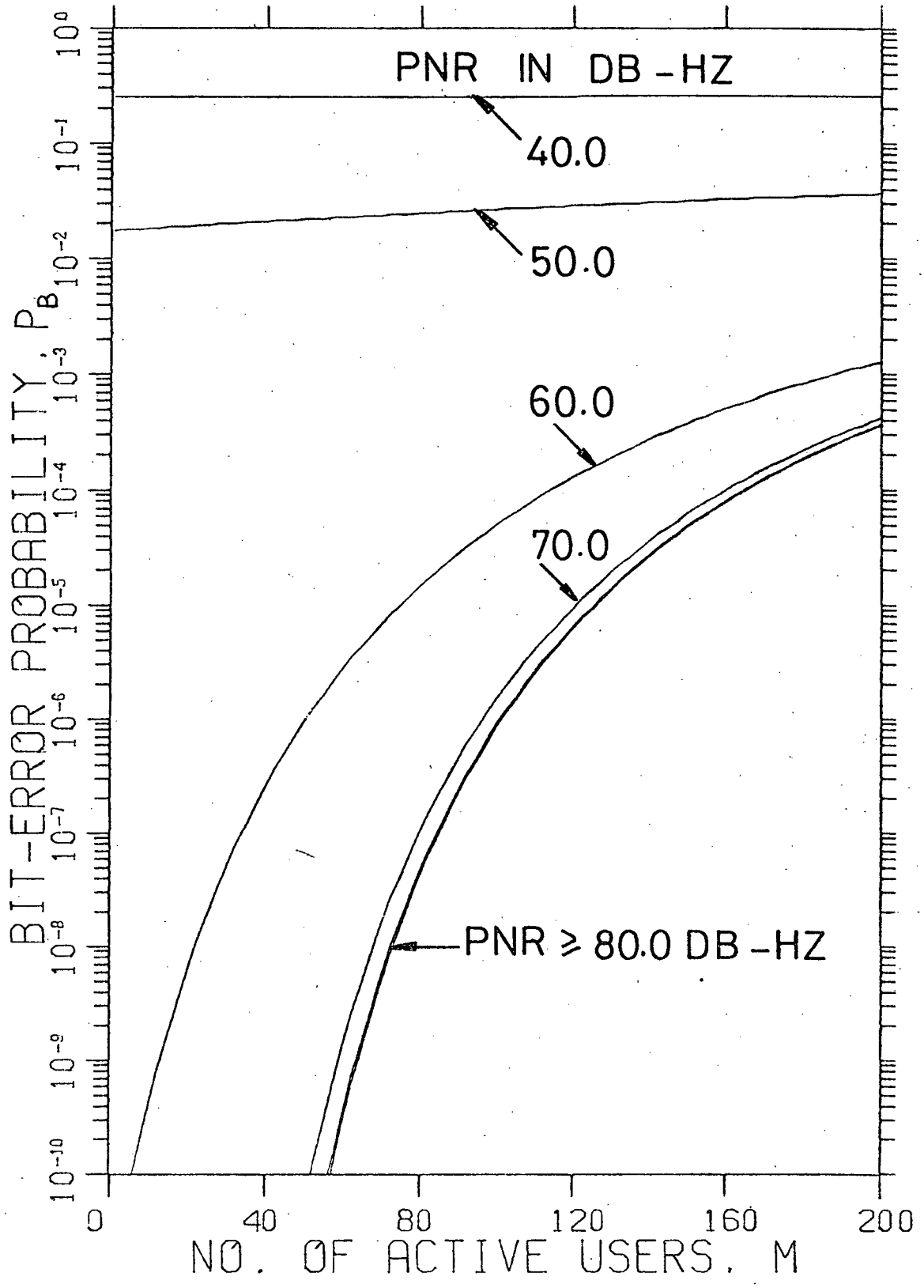

Fig. 2.3.1 Bit-error probability p_B vs. number of active users M for various PNR values, co-channel interferers modelled as Gaussian noise sources.

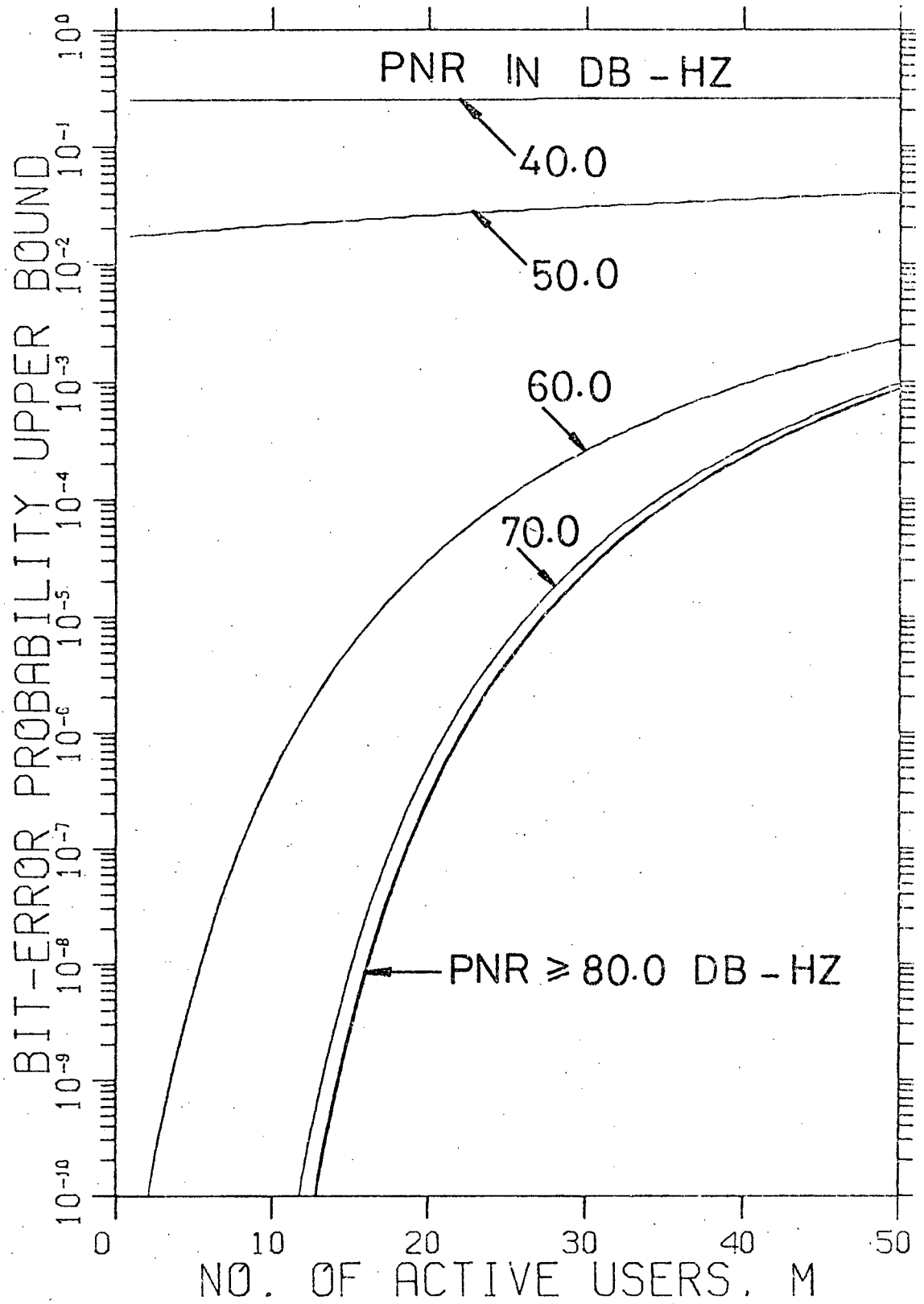

Fig. 2.3.2 Bit-error probability upper bound vs. number of active users M for various PNR values, showing the effects of cross-correlations between 511-bit Gold's codes.

3. SPREAD-SPECTRUM CODE SYNCHRONIZATION

3.1 Introduction

Acquisition and tracking of the spread-spectrum code sequence is essential for successful demodulation of the desired signal using the correlation receiver described in Section 2.1. A code synchronizer is employed for these purposes.

Code synchronizers incorporating a sliding correlator for acquisition and a delay lock loop for tracking are well suited for SSMA applications. A typical example is Hopkins' synchronizer [H3] which also includes a search/lock strategy (SLS) to arbitrate the transitions between acquisition and tracking. The SLS can be modelled as a finite Markov chain with absorbing boundaries which facilitates analysis of the acquisition time and hold-in time performance of the code synchronizer. Such analysis is important because acquisition time is a major cause of message delay and a long hold-in time is needed to avoid loss of synchronization before transmission of a message is complete.

Sliding correlators acquire a code sequence by searching serially through all code cells[1] to detect the (correct) cell that synchronizes with the desired signal. Acquisition delay results because on the average the correct cell is located after testing N/2 cells, where N is the total number of code cells. Acquisition delay may be reduced by parallel/serial searches whereby K cells, each displaced from the next by approximately N/K consecutive cells, are simul-

[1] Code cells are the phases of the code sequence in discreet and equally spaced steps.

taneously tested. In this case the correct cell is located after an average of N/(2K) cell-tests.

A code synchronizer incorporating a sliding correlator with parallel/-serial searching, a delay lock loop and a SLS is described and analyzed in this chapter. In the special case of K = 1, this synchronizer reduces to the one proposed by Hopkins. This synchronizer is chosen for ease of implementation and analysis, and because its performance seems acceptable for some applications. The synchronizer may not be optimum, however.

3.2 Structure of the Code Synchronizer

A block diagram of the code synchronizer is shown in Fig. 3.2.1. The dashed lines divides the blocks into three functional groups: the synchronization detector, the SLS and the delay lock loop.

The heart of the code synchronizer is the local code generator which supplies K code cells to the synchronization detector for testing. It also supplies the appropriate code phases to the delay lock phase detector via a phase selector controlled by the SLS. The phase and frequency of the code generator is coarse-controlled by the synchronization detector via the SLS during acquisition and fine-controlled by the delay lock loop during tracking.

The synchronization detector employs K sliding envelope correlators to perform a parallel/serial search during acquisition. The K cells, each displaced from the next by approximately N/K consecutive cells, slide past the received code sequence to search for the cell which is the best match to the phase of the received code sequence. The detector detects the maximum output of the K correlators which also exceeds a given threshold and declares the

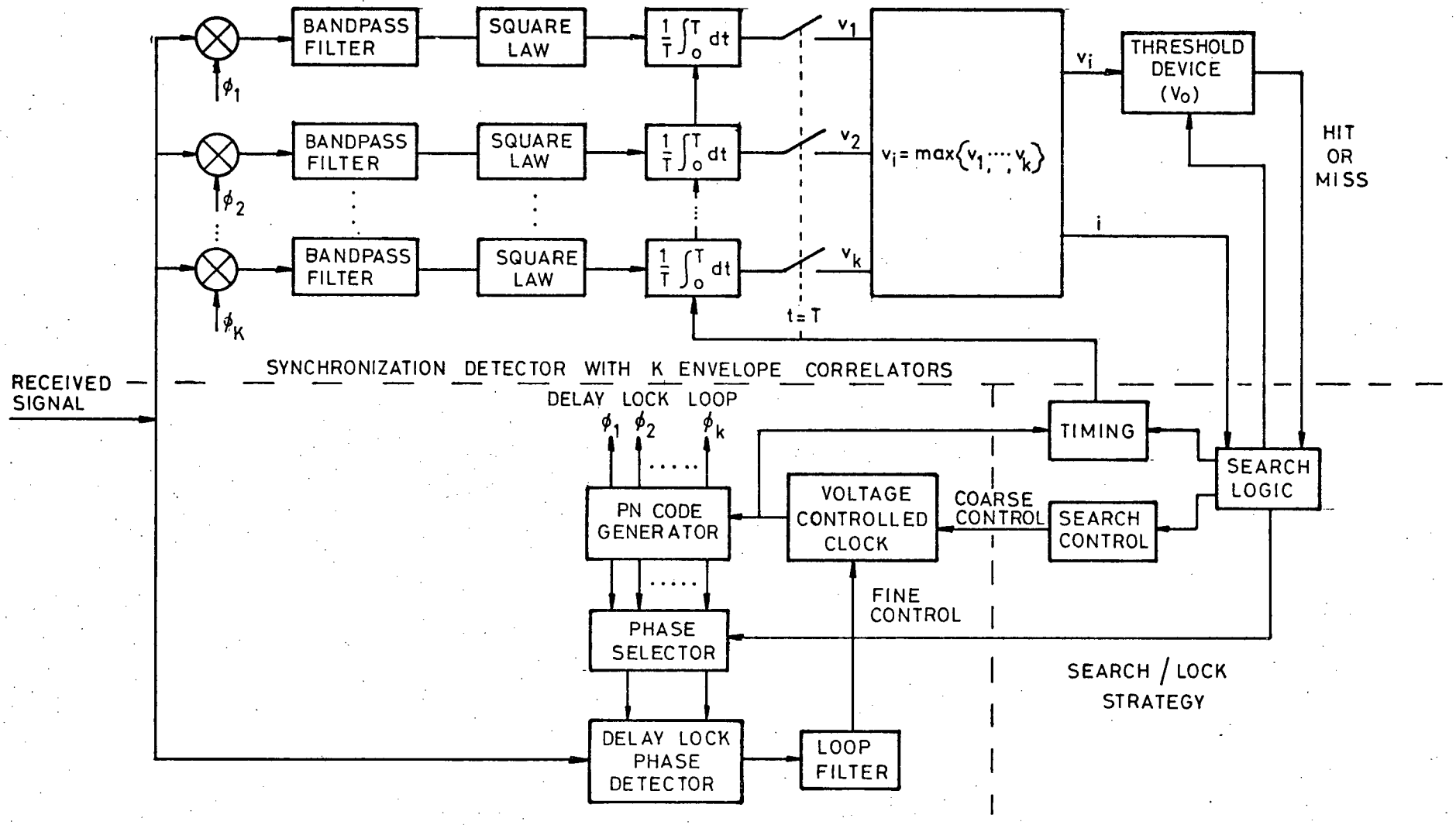

Fig. 3.2.1 Direct sequence spread-spectrum code synchronizer

corresponding cell as correct (a hit). The SLS uses the information supplied by the synchronization detector to control the transitions between acquisition (search) and tracking (lock) modes by means of a logical procedure. It also alters the correlator integration time and decision threshold when a change of mode occurs.

When the phase of local code closely matches that of the received code, the phase difference is detected by the delay lock loop which generates an error signal to fine-control the phase of the code generator. As a result, the local code tracks the received code. Detailed discussions of delay lock loop design and operation [S5] will not be repeated here. It is assumed that with proper choice of loop filter parameters the delay lock loop will operate as desired. In this case the local code will lock onto the received code within a sufficiently short time after the acquisition procedure brings the phase difference to less than half a chip.

3.3 The Synchronization Detector

3.3.1 Description

The synchronization detector consists of K envelope correlators and a decision device. Each envelope correlator multiplies the local code corresponding to a given code cell to the received signal. The product is then bandpassed to remove most noise and interference, squared and lowpassed to extract the envelope, then integrated for T seconds and sampled at the end of the integration period. The K correlator outputs are fed to the decision device consisting of a maximum signal extractor and a threshold device. The maximum signal extractor extracts the maximum from the K correlator outputs and

identifies the correlator (i-th correlator) corresponding to it. If the maximum exceeds a given threshold, the decision that the i-th correlator produces a hit is made. If the maximum is less than the threshold, the decision is that all correlators have missed. The probability density of each correlator output and some probabilities attributed to the synchronization decisions are derived in the following sections.

3.3.2 Probability Density of Correlator Outputs

A block diagram of the envelope correlator is shown in Fig. 3.3.1. Each of the K correlators are identical except for the local code sequence fed to the multiplier. The code sequences for the K correlators satisfy the relation that the code cell ϕ_i $(i = 1,2,\cdots,K)$ to be tested by the i-th correlator differs in phase from the cells tested by the adjacent correlators, $\phi_{(i-1)\text{mod}K}$ and $\phi_{(i+1)\text{mod}K}$, by $\lceil N/K \rceil$ consecutive cells, where $\lceil x \rceil$ denotes the smallest integer greater than or equal to x.

Let x(t) be the signal at the square-law envelope detector input. Expressed in terms of its envelope a(t), its phase angle α and the carrier frequency ω_c,

$$x(t) = a(t) \cos \left(\omega_c t + \alpha\right) \tag{3.3.1}$$

The output of the square law device is

$$kx^2(t) = {}^1/_2\, ka^2(t) \left[1 + \cos \left(2\omega_c t + 2\alpha\right)\right] \tag{3.3.2}$$

The low-pass filter rejects the double frequency term to give

$$u(t) = {}^1/_2\, ka^2(t) \tag{3.3.3}$$

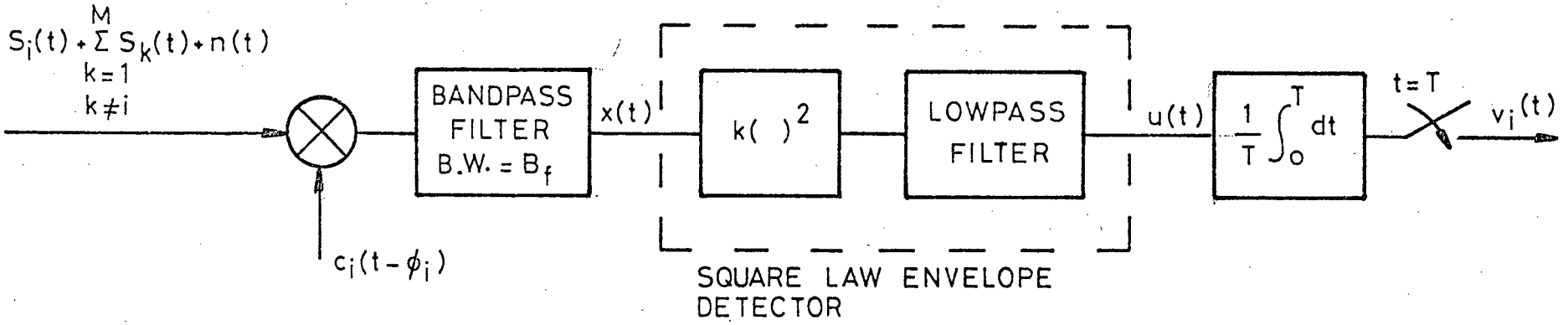

Fig. 3.3.1 One of K envelope correlators in code synchronizer

at the envelope detector output.

The bandpass filter output envelope a(t) has a correlation time of $1/B_f$ where B_f is the bandpass filter bandwidth. If a(t) has a random component it is reasonable to assume that values of a(t) and thus of u(t) when separated by $1/B_f$ seconds are independent. Let U_k be random variables representing values of u(t) $1/B_f$ seconds apart. The integration can therefore be approximated by the summation of $n = B_f T$ independent identically distributed random variables U_k/B_f, $k = 1,2,\cdots,n$. Let V_i be a random variable representing the i-th sampled integrator output $v_i(T)$. If n is large, the central limit theorem [P3] is applicable and the probability density function (pdf) of V_i, $f_{V_i}(v_i)$, is approximately Gaussian. Thus

$$f_{V_i}(v_i) = \frac{1}{\sqrt{2\pi}\,\sigma} \exp\left[-\frac{1}{2}\left(\frac{v_i-\mu}{\sigma}\right)^2\right] \tag{3.3.4}$$

where mean μ and variance σ^2 are given by

$$\mu = (n/T)E[U/B_f] = E[U] \tag{3.3.5}$$

$$\sigma^2 = (n/T^2)\mathrm{Var}[U/B_f] = \mathrm{Var}[U]/(B_f T) \tag{3.3.6}$$

Given that ϕ_i is in synchronization (event S) or not in synchronization (event $\bar{S}$) with the received signal, two conditional pdf's, $f_{V|S}(v|S)$ and $f_{V|\bar{S}}(v|\bar{S})$ can be obtained from the conditional means and variances of U. The subscript i is dropped because the conditional pdf's are identical for all correlator outputs.

To derive the conditional means and variances of U, consider two different cases.

Case 1: Assume co-channel interferers behave as independent sources of Gaussian noise with uniform two-sided spectral density of $P/(2B_t)$ over the transmission bandwidth.

From the channel model in Section 2.2, the total noise power contributed by (M-1) co-channel interferers and the channel noise in the bandpass filter bandwidth is

$$N_T = N_0 B_f + (M-1)PB_f/B_t \tag{3.3.7}$$

When ϕ_i is not synchronized with the received code, a(t) is the noise envelope [Z1] which has a Rayleigh pdf given by

$$f_{A|\bar{S}}(a|\bar{S}) = \begin{cases} \frac{a}{N_T} e^{-\frac{a^2}{2N_T}}, & a \geq 0 \\ 0, & a < 0 \end{cases} \tag{3.3.8}$$

Applying the transformation

$$U = {}^1/_2 \, kA^2 \tag{3.3.9}$$

to eqn. (3.3.8) yields

$$f_{U|\bar{S}}(u|\bar{S}) = \begin{cases} \frac{1}{kN_T} e^{-\frac{u}{kN_T}}, & u \geq 0 \\ 0, & u < 0 \end{cases} \tag{3.3.10}$$

which is an exponential pdf with mean

$$E[U|\bar{S}] = kN_T \tag{3.3.11}$$

and variance

$$Var[U|\bar{S}] = (kN_T)^2 \tag{3.3.12}$$

When ϕ_i synchronizes with the received code, the bandpass filter output has an additional signal component $\pm\sqrt{2P}\cos(\omega_c t)$. The envelope a(t) has a Rician pdf given by [Z1]

$$f_{A|S}(a|S) = \begin{cases} \frac{a}{N_T} e^{-\frac{(2P+a^2)}{2N_T}} I_0\left(\frac{\sqrt{2P}\,a}{N_T}\right), & a \geq 0 \\ 0, & a < 0 \end{cases} \tag{3.3.13}$$

where $I_0(\cdot)$ is the modified Bessel function of the first kind and zero order. Define the signal-to-noise power ratio in the filter bandwidth as

$$\rho = P/N_T \tag{3.3.14}$$

Define a random variable Z by the transformation

$$Z = A^2/(2N_T) \tag{3.3.15}$$

Eqn. (3.3.15) transforms eqn. (3.3.13) to give the pdf of Z,

$$f_{Z|S}(z|S) = \begin{cases} e^{-(z+\rho)} I_0(2\sqrt{z\rho}), & z \geq 0 \\ 0, & z < 0 \end{cases} \tag{3.3.16}$$

The moment generating function for Z is

$$C_{Z|S}(\omega) = \int_{-\infty}^{\infty} f_{Z|S}(z|S)\, e^{-j\omega z}\, dz$$

$$= \frac{1}{1-j\omega}\, e^{\frac{j\omega\rho}{1-j\omega}} \tag{3.3.17}$$

Its first and second derivatives are

$$\frac{dC_{Z|S}(\omega)}{d\omega} = \frac{je^{\frac{j\omega\rho}{1-j\omega}}}{(1-j\omega)^3}(1 + \rho - j\omega) \tag{3.3.18}$$

$$\frac{d^2C_{Z|S}(\omega)}{d\omega^2} = -e^{\frac{j\omega\rho}{1-j\omega}}\left[\frac{\rho(\rho + 1 - j\omega)}{(1-j\omega)^5} + \frac{3(\rho + 1 - j\omega)}{(1-j\omega)^4} - \frac{1}{(1-j\omega)^3}\right] \tag{3.3.19}$$

The mean and variance of Z are therefore given by

$$E[Z|S] = -j\frac{dC_{Z|S}(0)}{d\omega} = 1 + \rho \tag{3.3.20}$$

$$E[Z^2|S] = (-j)^2\frac{d^2C_{Z|S}(0)}{d\omega^2} = \rho^2 + 4\rho + 2 \tag{3.3.21}$$

and

$$Var[Z|S] = E[Z^2|S] - \{E[Z|S]\}^2 = 1 + 2\rho \tag{3.3.22}$$

Since the random variable U is related to Z by

$$U = kN_T Z \tag{3.3.23}$$

the mean and variance of U conditioned on S are

$$E[U|S] = kN_T(1+\rho) \tag{3.3.24}$$

$$Var[U|S] = (kN_T)^2(1+2\rho) \tag{3.3.25}$$

To summarize, the conditional pdf's of the sampled integrator outputs are Gaussian with means

$$\mu|S = kN_T(1+\rho) \tag{3.3.26}$$

$$\mu|\bar{S} = kN_T \tag{3.3.27}$$

and variances

$$\sigma^2|S = (kN_T)^2(1+2\rho)/(B_fT) \tag{3.3.28}$$

$$\sigma^2|\bar{S} = (kN_T)^2/(B_fT) \tag{3.3.29}$$

These results are consistent with those derived by Marcum [M5] using a slightly different approach.

Case 2: Assume that cross-correlations between code sequences assigned to all potential users are bounded by ψ_{max}. Further assume that each co-channel interferer contributes a signal $\pm(\psi_{max}/T_b)\sqrt{2P}\cos(\omega_c t+\theta_i)$ to the bandpass filter output; θ_i is a random phase angle, uniformly distributed between $-\pi$ and π, which is unchanged in each correlation interval of duration $1/B_f$.

The sum of noise components at the bandpass filter output is

$$x_n(t) = \left[\sum_{i=1}^{M-1} (\psi_{max}/T_b)\sqrt{2P}\cos(\theta_i) + n_c(t)\right]\cos(\omega_0 t)$$

$$- \left[\sum_{i=1}^{M-1} (\psi_{max}/T_b) \sqrt{2P} \sin(\theta_i) + n_s(t) \right] \sin(\omega_0 t)$$

$$= x_c(t) \cos(\omega_0 t) + x_s(t) \sin(\omega_0 t) \qquad (3.3.30)$$

The terms $n_c(t)$ and $n_s(t)$ are Gaussian with zero means and variances of $N_0 B_f$. The pdf's for $C_i = \cos\theta_i$ and $S_i = \sin\theta_i$ are, respectively,

$$f_{C_i}(c_i) = \frac{1}{\pi\sqrt{1-c_i^2}} \quad , \quad |c_i| \leq 1 \qquad (3.3.31)$$

and

$$f_{S_i}(s_i) = \frac{1}{\pi\sqrt{1-s_i^2}} \quad , \quad |s_i| \leq 1 \qquad (3.3.32)$$

with means

$$E[C_i] = E[S_i] = 0 \qquad (3.3.33)$$

and variances

$$Var[C_i] = Var[S_i] = 1/2 \qquad (3.3.34)$$

If the number of simultaneous users M is large, the sine and cosine noise components contributed by (M-1) co-channel interferers are Gaussian with zero means and variances of $(M-1)(\psi_{max}/T_b)^2 P$, by virtue of the central limit theorem [P3]. Therefore, the total cosine and sine noise components, $x_c(t)$ and $x_s(t)$, are Gaussian with zero means and variance or total noise power of

$$N_T = N_0 B_f + (M-1)(\psi_{max}/T_b)^2 P \qquad (3.3.35)$$

With the total Gaussian noise power thus defined, equations (3.3.8) to (3.3.29) from Case 1 become valid and applicable to Case 2.

The total noise power for Case 1 and Case 2 may be compared using signal parameters listed in Table 2.3.1 with B_f = 100 KHz. The total noise power for Case 1 is

$$N_T = N_0 B_f + 0.00196\ (M-1)P \qquad (3.3.36)$$

Using a set of Gold's code with $\psi_{max} = 33\ T_c$, the total noise power for Case 2 is

$$N_T = N_0 B_f + 0.00417\ (M-1)P \qquad (3.3.37)$$

Therefore, to maintain the same total noise power and hence synchronizer performance, when Gold's codes of length L = 511 are used the channel can accommodate half the number of simultaneous users compared to the case where uncorrelated codes of the same length are used.

3.3.3 Probabilities Attributed to Synchronization Detector Decisions

Assuming that the K sampled integrator outputs $v_1(T)$, $v_2(T), \cdots, v_K(T)$ are independent, their joint pdf is simply the product of the individual pdf's derived in the last section.

Let (i) p_{FA}, (ii) p_D and (iii) p_{FD} be the probabilities of making the decision that ϕ_i is synchronous with the received code (i-th correlator produces a hit) when in fact the following conditions are true, respectively:

(i) None of $\phi_1, \phi_2, \cdots, \phi_K$ is synchronous with the received code.

(ii) ϕ_i is synchronous with the received code.

(iii) ϕ_j, $j \neq i$, is synchronous with the received code.

This decision is made if $v_i(T) = \max \{v_1(T), v_2(T), \cdots, v_K(T)\}$ and $v_i(T) \geq v_0$ where v_0 is a decision threshold. Therefore,

$$P_{FA} = \int_{v_0}^{\infty} f_{V|\bar{S}}(v|\bar{S}) \left[\int_{-\infty}^{v} f_{V|\bar{S}}(u|\bar{S})du \right]^{K-1} dv \tag{3.3.38}$$

$$P_D = \int_{v_0}^{\infty} f_{V|S}(v|S) \left[\int_{-\infty}^{v} f_{V|\bar{S}}(u|\bar{S})du \right]^{K-1} dv \tag{3.3.39}$$

$$P_{FD} = \int_{v_0}^{\infty} f_{V|\bar{S}}(v|\bar{S}) \left[\int_{-\infty}^{v} f_{V|\bar{S}}(u|\bar{S})du \right]^{K-2} \int_{-\infty}^{v} f_{V|S}(w|S)dwdv \tag{3.3.40}$$

Using the conditional pdf's derived before, the probabilities P_{FA}, P_D and P_{FD} may be evaluated using numerical integration techniques.

3.4 The Search/Lock Strategy

3.4.1 The SLS Logic

The SLS is a logical procedure which controls the operation of the code synchronizer. It supervises the transitions between search mode (acquisition) and lock mode (tracking), and adjusts the synchronization detector integration time T and decision threshold v_0 when mode transitions occur to achieve a reasonable trade-off between acquisition time and hold-in time. At the end of each integration period, the decision device of the synchronization detector provides the SLS with the information of whether one of the K correlators produces a hit or all correlators produce a miss. A correlator identifier (CI)

with possible values of 1,2,•••,K identifies the correlator that produces a hit.

A flow chart of the SLS logic is shown in Fig. 3.4.1. It is a modified version of the up-down counter strategy described by Hopkins [H3]. Briefly, Hopkins' SLS is analogous to an up-down counter with possible counts of 0, 1, 2 and 3. A new cell is tested at count 1 in the search mode. A hit increases the count by 1 to a maximum of 3 when the lock mode is entered, whereas a hit reduces the count by 1 to a minimum of 0 when the present cell is rejected in favour of a new cell and a transition to search mode is made if lock mode was previously entered. To control a parallel/serial search, Hopkins' SLS is modified so that K cells are simultaneously being tested. At count 2 in the search mode the CI is registered in a correlator identifier register (CIR) for reference. A hit with the same CI advances the count to 3 whereas a hit with a different CI causes the CIR to be updated. In the lock mode, only a hit which CI is the same as the current content of the CIR causes the count to be advanced, whereas a miss or a hit with a different CI causes the count to be retarded. At count 0 the phase of the code generator is changed by one step and a new set of K cells is presented for testing.

In the search mode the probability that one of the cells currently being tested is correct is small if $K \ll N$. In this case a short integration time T_S and a high threshold V_S serves to decrease p_{FA} and quicken acquisition. The converse is true in the lock mode. Therefore the integration time is increased to T_L and the threshold is reduced to V_L. An increased p_D results so that it would be harder for random disturbances to knock the synchronizer out of lock.

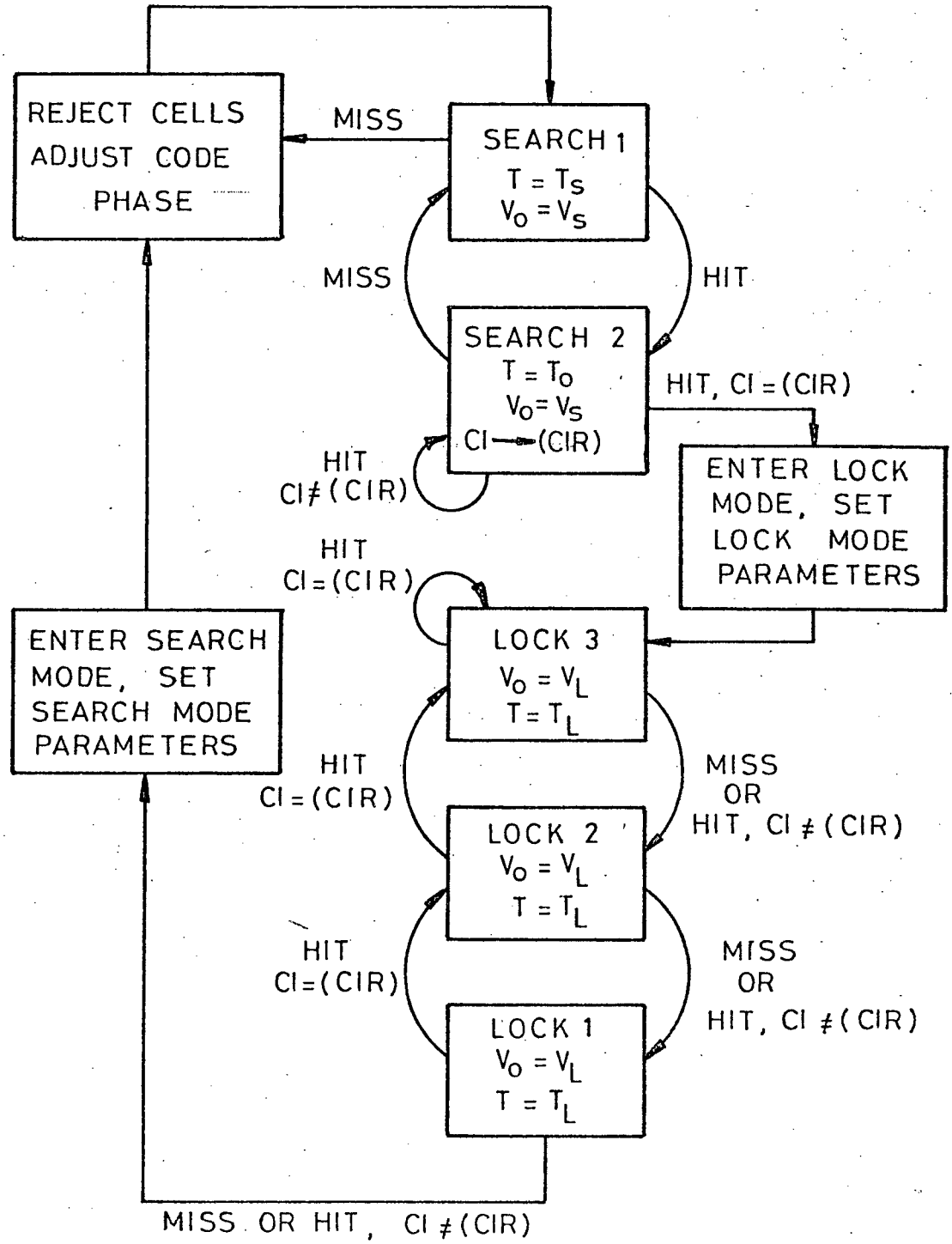

Legend: v_0 - decision threshold
T - synchronization detector integration time
CI - correlator identifier
→ - " is assigned to "
(CIR) - correlator identifier register

Fig. 3.4.1 The search/lock strategy logic.

Analysis of the SLS is simplified by representing the SLS by finite Markov chains with absorbing boundaries and applying the theory of finite Markov chains [K7]. A finite Markov chain is characterized by its transition matrix $[p_{ij}]$. Element p_{ij} is the probability of transition from state i to state j. $[p_{ij}]$ can be rearranged and partitioned to reflect the type of state transitions as follows.

$$[p_{ij}] = \begin{array}{c} \\ \text{absorbing} \\ \\ \text{transient} \end{array} \begin{array}{c} \begin{array}{cc} \text{absorbing} & \text{transient} \end{array} \\ \left[\begin{array}{cc} I & \Phi \\ \hline R & Q \end{array}\right] \end{array} \qquad (3.4.1)$$

where I is an identity matrix for probabilities of transitions among absorbing states, Φ is a zero matrix for the zero probabilities of transitions from absorbing states to transient states, R is a matrix of probabilities of transitions from transient states to absorbing states and Q is a matrix of probabilities of transitions among transient states.

Let Y be the event that one of the K cells being currently tested is synchronous with the received code and $\bar{Y}$ be the complement of Y. The finite Markov chain representations of the SLS under events Y and $\bar{Y}$ are shown in Figs. 3.4.2 and 3.4.3, respectively.

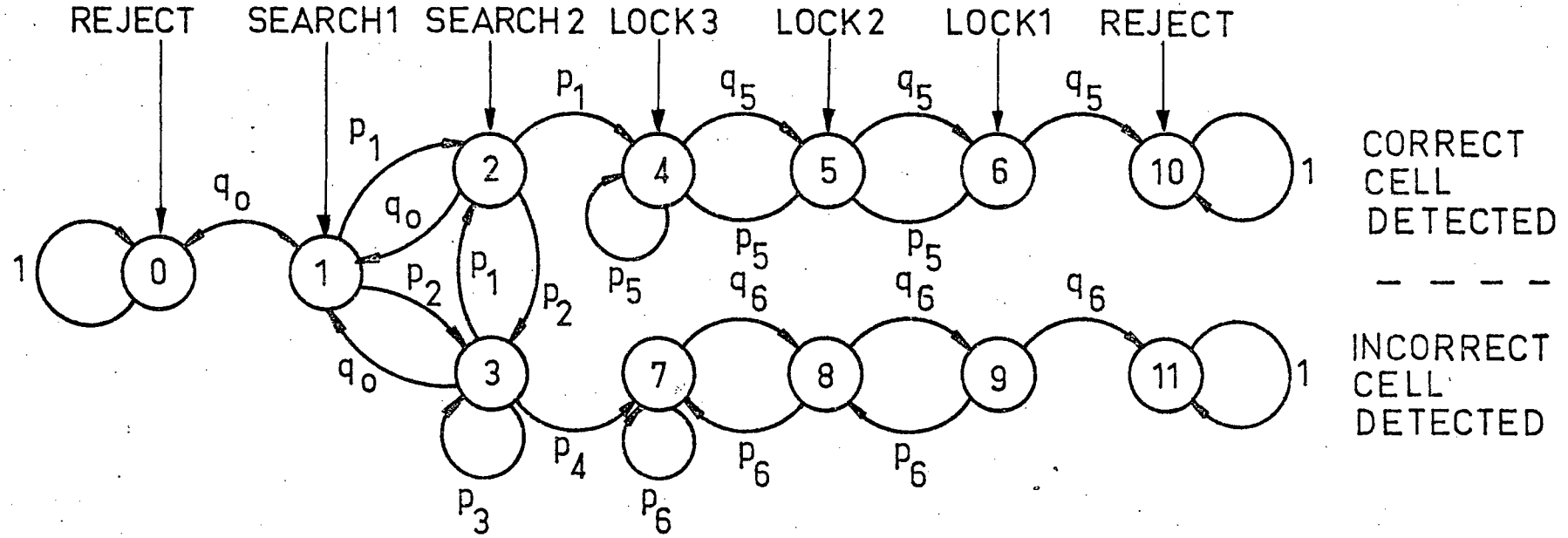

p_1 = SEARCH MODE p_D

p_2 = (K − 1) × (SEARCH MODE p_{FD})

p_3 = (K − 2) × (SEARCH MODE p_{FD})

p_4 = SEARCH MODE p_{FD}

p_5 = LOCK MODE p_D

p_6 = LOCK MODE p_{FD}

$q_0 = 1 - p_1 - p_2$

$q_5 = 1 - p_5$ $q_6 = 1 - p_6$

Fig. 3.4.2 Markov chain model of SLS given that one of the K cells being tested is in synchronization (event Y)

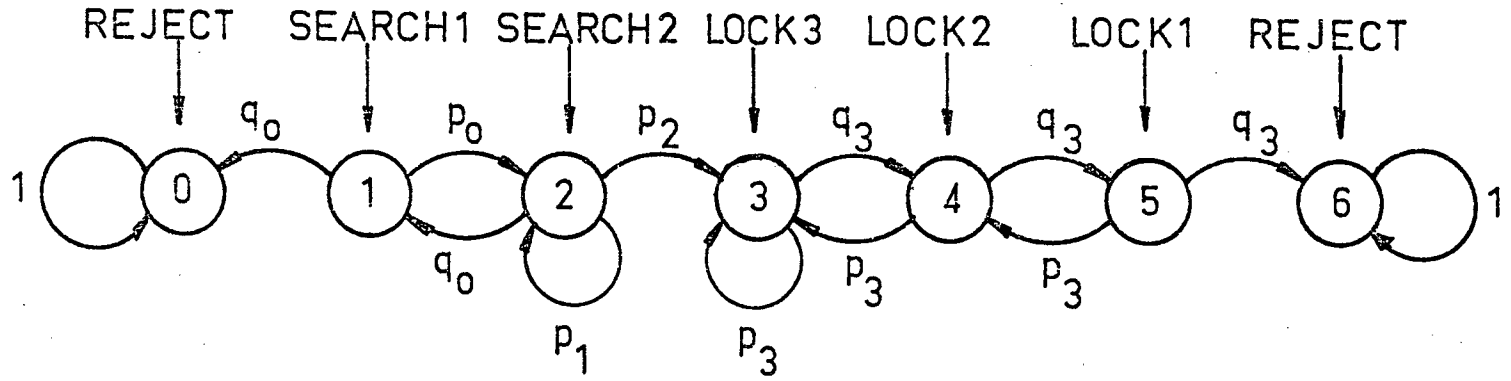

$P_0 = K \times (\text{SEARCH MODE } P_{FA})$ $\qquad q_0 = 1 - p_0$

$P_1 = (K-1) \times (\text{SEARCH MODE } P_{FA})$ $\qquad q_3 = 1 - p_3$

$P_2 = \text{SEARCH MODE } P_{FA}$

$P_3 = \text{LOCK MODE } P_{FA}$

Fig. 3.4.3 Markov chain model of SLS given that none of the K cells being tested are in sychronization (event $\overline{Y}$).

3.4.2 Mean and Mean-Squared Dwell Time

Dwell time is the time taken to reject a set of K cells without achieving synchronization with the received code.

Let T_{D1} and S_{D1} be the mean and mean-squared dwell time respectively when event $\bar{Y}$ is true. Referring to the Markov chain shown in Fig. 3.4.3, the dwell time for event $\bar{Y}$ is the absorption time from state 1 to any absorbing state.

Let Ω be the set of transient states and Ω^c be the complement of Ω, the set of absorbing states. Let s_k denotes state k. Let $t_{1,i}$ be the absorption time from transient state i to any absorbing state, and T_i be the transition time from state i. The mean absorption time from transient state i is

$$E[t_{1,i}] = \sum_{s_k \epsilon \Omega^c} p_{ik} T_i + \sum_{s_k \epsilon \Omega} p_{ik} E[T_i + t_{1,k}] \qquad (3.4.2)$$

Therefore the mean absorption times for all transient states satisfy the matrix equation

$$E[\bar{t}_1] = (I - Q_1)^{-1} \bar{T}_1 \qquad (3.4.3)$$

where $E[\bar{t}_1]$ is a vector of mean absorption times with elements $E[t_{1,i}]$ such that $s_i \epsilon \Omega$. For event $\bar{Y}$, matrix I in eqn. (3.4.3) is a 5×5 identity matrix, Q_1 is the matrix of probabilities of transitions among transient states given by

$$Q_1 = \begin{array}{c} \text{State} \\ 1 \\ 2 \\ 3 \\ 4 \\ 5 \end{array} \begin{array}{c} \begin{array}{ccccc} 1 & 2 & 3 & 4 & 5 \end{array} \\ \begin{bmatrix} 0 & p_0 & 0 & 0 & 0 \\ q_0 & p_1 & p_2 & 0 & 0 \\ 0 & 0 & p_3 & q_3 & 0 \\ 0 & 0 & p_3 & 0 & q_3 \\ 0 & 0 & 0 & p_3 & 0 \end{bmatrix} \end{array} \tag{3.4.4}$$

where the non-zero elements are defined in Fig. 3.4.3, and $\bar{T}_1$ is the vector of transition times given by

$$\bar{T}_1 = [T_S, T_S, T_L, T_L, T_L]^t \tag{3.4.5}$$

where T_S and T_L are the search mode and lock mode integration times respectively.

Thus the mean dwell time for event $\bar{Y}$ is

$$T_{D1} = \left(E[\bar{t}_1]\right)_1 \tag{3.4.6}$$

which is the element of vector $E[\bar{t}_1]$ corresponding to state 1.

Similarly the mean-squared absorption time from transient state i is

$$E[t_{1,i}^2] = \sum_{s_k \epsilon \Omega^c} p_{ik} T_i^2 + \sum_{s_k \epsilon \Omega} p_{ik} E[(T_i + t_{1,k})^2] \tag{3.4.7}$$

which results in the matrix equation

$$E[\bar{t}_1^2] = (I - Q_1)^{-1} \{\bar{T}_1^2 + 2D_{T1} Q_1 E[\bar{t}_1]\} \tag{3.4.8}$$

where the mean-square absorption time vector $E[\bar{t}_1^2]$ has elements $E[t_{1,i}^2]$, vector $\bar{T}_1^2$ is formed by element-by-element squaring of $\bar{T}_1$, and D_{T1} is a diagonal matrix given by

$$D_{T1} = \begin{bmatrix} T_S & 0 & 0 & 0 & 0 \\ 0 & T_S & 0 & 0 & 0 \\ 0 & 0 & T_L & 0 & 0 \\ 0 & 0 & 0 & T_L & 0 \\ 0 & 0 & 0 & 0 & T_L \end{bmatrix} \tag{3.4.9}$$

The mean-squared dwell time for event $\bar{Y}$ is therefore

$$S_{D1} = \left(E\left[\bar{t}_1^2\right]\right)_1 \tag{3.4.10}$$

When event Y is true, the dwell time is the absorption time from state 1 to absorbing states 0 or 11 of the Markov chain shown in Fig. 3.4.2. Let the mean and mean-squared dwell time for event Y be T_{D2} and S_{D2} respectively.

Let $t_{2,i}$ be the absorption time from transient state i to absorbing states 0 or 11. Since transitions from transient states 4, 5 and 6 to absorbing states 0 or 11 are impossible, these three transient states may be merged into absorbing state 10 with no adverse effects to the following derivations. The mean and mean-squared absorption times from transient state i to absorbing states 0 or 11 are

$$E\left[t_{2,i}\right] = \sum_{s_k \epsilon \Omega^c - \{s_{10}\}} p_{ik}\, T_i + \sum_{s_k \epsilon \Omega} p_{ik}\, E\left[T_i + t_{2,k}\right] \tag{3.4.11}$$

and

$$E\left[t_{2,i}^2\right] = \sum_{s_k \epsilon \Omega^c - \{s_{10}\}} p_{ik}\, T_i^2 + \sum_{s_k \epsilon \Omega} p_{ik}\, E\left[(T_i + t_{2,k})^2\right] \tag{3.4.12}$$

which result in the matrix equations

$$E[\bar{t}_2] = (I - Q_2)^{-1} D_{P2} \bar{T}_2 \tag{3.4.13}$$

and

$$E[\bar{t}_2^2] = (I - Q_2)^{-1} \{D_{P2} \bar{T}_2^2 + 2 D_{T2} Q_2 E[\bar{t}_2]\} \tag{3.4.14}$$

In eqns. (3.4.13) and (3.4.14), mean and mean-squared absorption time vectors $E[\bar{t}_2]$ and $E[\bar{t}_2^2]$ respectively have elements $E[t_{2,i}]$ and $E[t_{2,i}^2]$ with $s_i \epsilon \Omega$, $\bar{T}_2$ is the transition time vector given by

$$\bar{T}_2 = [T_S, T_S, T_S, T_L, T_L, T_L]^t \tag{3.4.15}$$

and $\bar{T}_2^2$ is $\bar{T}_2$ squared element-by-element, Q_2 is the transition probability matrix given by

$$Q_2 = \begin{array}{c} \text{State} \\ 1 \\ 2 \\ 3 \\ 7 \\ 8 \\ 9 \end{array} \begin{array}{c} \begin{array}{cccccc} 1 & 2 & 3 & 7 & 8 & 9 \end{array} \\ \begin{bmatrix} 0 & p_1 & p_2 & 0 & 0 & 0 \\ q_0 & 0 & p_2 & 0 & 0 & 0 \\ q_0 & p_1 & p_3 & p_4 & 0 & 0 \\ 0 & 0 & 0 & p_6 & q_6 & 0 \\ 0 & 0 & 0 & p_6 & 0 & q_6 \\ 0 & 0 & 0 & 0 & p_6 & 0 \end{bmatrix} \end{array} \tag{3.4.16}$$

where the non-zero elements are defined in Fig. 3.4.2, I is a 6×6 identity matrix, D_{P2} is a diagonal matrix given by

$$D_{P2} = \begin{bmatrix} 1 & 0 & 0 & 0 & 0 & 0 \\ 0 & (1-p_1) & 0 & 0 & 0 & 0 \\ 0 & 0 & 1 & 0 & 0 & 0 \\ 0 & 0 & 0 & 1 & 0 & 0 \\ 0 & 0 & 0 & 0 & 1 & 0 \\ 0 & 0 & 0 & 0 & 0 & 1 \end{bmatrix} \tag{3.4.17}$$

where p_1 is defined in Fig. 3.4.2, and D_{T2} is a diagonal matrix given by

$$D_{T2} = \begin{bmatrix} T_S & 0 & 0 & 0 & 0 & 0 \\ 0 & T_S & 0 & 0 & 0 & 0 \\ 0 & 0 & T_S & 0 & 0 & 0 \\ 0 & 0 & 0 & T_L & 0 & 0 \\ 0 & 0 & 0 & 0 & T_L & 0 \\ 0 & 0 & 0 & 0 & 0 & T_L \end{bmatrix} \tag{3.4.18}$$

Solving eqn. (3.4.13) and eqn. (3.4.14), the mean and mean-squared dwell times are respectively

$$T_{D2} = \left(E[\bar{t}_2]\right)_1 \tag{3.4.19}$$

and

$$S_{D2} = \left(E[\bar{t}_2^2]\right)_1 \tag{3.4.20}$$

3.4.3 Mean and Mean-Squared Time to Lock

When event Y is true, it is possible for the synchronizer to lock onto the received signal with the correct cell. If the SLS goes into lock mode with the correct cell, the elapsed time since the present group of K cells was first tested is the time to lock, which is the absorption time from state 1 to state 10'. Absorbing states 10' and 11' are formed by merging, respectively, states 4, 5, 6, 10 and states 7, 8, 9, 11 in Fig. 3.4.2. Let the mean and mean-squared times to lock be T_{LK} and S_{LK} respectively.

Let $t_{3,i}$ be the absorption time from transient state i to absorbing state 10'. As before, the vectors of mean and mean-squared absorption times satisfy the matrix equations

$$E[\bar{t}_3] = (I - Q_3)^{-1} D_{P3} \bar{T}_3 \tag{3.4.21}$$

and

$$E[\bar{t}_3^2] = (I - Q_3)^{-1} \{D_{P3} \bar{T}_3^2 + 2 T_S Q_3 E[\bar{t}_3]\} \tag{3.4.22}$$

where vectors $E[\bar{t}_3]$ and $E[\bar{t}_3^2]$ have elements $E[t_{3,i}]$ and $E[t_{3,i}^2]$ respectively, vectors

$$\bar{T}_3 = [T_S, T_S, T_S]^t \tag{3.4.23}$$

and $\bar{T}_3^2$ is $\bar{T}_3$ squared element-by-element, I is a 3×3 identity matrix, matrices

$$Q_3 = \begin{array}{c} \text{State} \\ 1 \\ 2 \\ 3 \end{array} \begin{array}{c} \begin{array}{ccc} 1 & 2 & 3 \end{array} \\ \begin{bmatrix} 0 & p_1 & p_2 \\ q_0 & 0 & p_2 \\ q_0 & p_1 & p_3 \end{bmatrix} \end{array} \tag{3.4.24}$$

and

$$D_{P3} = \begin{bmatrix} (1-q_0) & 0 & 0 \\ 0 & 1 & 0 \\ 0 & 0 & (1-p_4) \end{bmatrix} \tag{3.4.25}$$

where p_1, p_2, p_3, p_4 and q_0 are defined in Fig. 3.4.2. Solving the matrix equations results in

$$T_{LK} = \left(E[\bar{t}_3]\right)_1 \tag{3.4.26}$$

and

$$S_{LK} = \left(E[\bar{t}_3^2]\right)_1 \tag{3.4.27}$$

3.4.4 Probability of Entering Lock Mode with the Correct Cell

Let p_L be the probability that the SLS enters lock mode with the correct cell locking onto the received code when event Y is true.

Let B be the matrix which element B_{ij} is the probability of being absorbed in absorbing state j from an initial transient state i, given by

$$B_{ij} = p_{ij} + \sum_{s_k \epsilon \Omega} p_{ik} B_{kj} \quad , \quad s_i \epsilon \Omega \quad , \quad s_j \epsilon \Omega^c \tag{3.4.28}$$

Eqn. (3.4.28) satisfies the matrix equation

$$B = (I - Q)^{-1}R \tag{3.4.29}$$

where Q and R are submatrices of the transition matrix in eqn. (3.4.1).

Referring to the Markov chain in Fig. 3.4.2, it is obvious that transitions to states 4 or 7 guarantee absorption at states 10 or 11. By merging states 4, 5, 6, 10 into state 10' and states 7, 8, 9, 11 into state 11', the matrices Q and R in eqn. (3.4.29) can be simplified as follows.

$$Q = \begin{array}{c} \text{State} \\ 1 \\ 2 \\ 3 \end{array} \begin{array}{c} \begin{array}{ccc} 1 & 2 & 3 \end{array} \\ \begin{bmatrix} 0 & p_1 & p_2 \\ q_0 & 0 & p_2 \\ q_0 & p_1 & p_3 \end{bmatrix} \end{array} \tag{3.4.30}$$

$$R = \begin{array}{c} \text{State} \\ 1 \\ 2 \\ 3 \end{array} \begin{array}{c} \begin{array}{ccc} 0 & 10' & 11' \end{array} \\ \begin{bmatrix} q_0 & 0 & 0 \\ 0 & p_1 & 0 \\ 0 & 0 & p_4 \end{bmatrix} \end{array} \tag{3.4.31}$$

In eqns. (3.4.30) and (3.4.31), the non-zero elements are defined in Fig. 3.4.2. Solving eqn. (3.4.29) yields

$$p_L = B_{1,10'} \tag{3.4.32}$$

3.5 Acquisition Time

3.5.1 Mean Acquisition Time

An important performance measure of the code synchronizer is the probability distribution of the acquisition time random variable T_A. Acquisition time is the time taken by the synchronizer to lock onto the received code after the desired signal is present.

Let J be a random variable such that after the desired signal begins, event $\bar{Y}$ occurs J times before event Y occurs. The occurrence of event Y then repeats after every (N/K)-1 occurrences of event $\bar{Y}$, assuming henceforth that K is a factor of N. Since the desired signal may start at any time,

$$\Pr(J=j) = K/N \quad , \quad j=0,1,2,\cdots,(N/K)-1 \tag{3.5.1}$$

Define a set of random variables Z_m, $m=1,2,\cdots,N/K$, by

$$Z_m = \begin{cases} 1 \quad , \quad 1 \leq m \leq J \\ \\ 0 \quad , \quad J < m \leq N/K \end{cases} \tag{3.5.2}$$

Therefore the probability distribution of Z_m is given by

$$\Pr(Z_m=1) = \sum_{j=0}^{(N/K)-1} \Pr(Z_m=1 \,|\, J=j)\Pr(J=j)$$

$$= \sum_{j=m}^{(N/K)-1} K/N$$

$$= 1-(m\ K/N) \tag{3.5.3}$$

$$\Pr(Z_m=0) = 1-\Pr(Z_m=1) = m\ K/N \tag{3.5.4}$$

If the synchronizer locks onto the received code at the n-th occurrence of Y, the acquisition time is

$$(T_A \mid \text{lock at n-th Y})$$

$$= \sum_{i=1}^{n-1} \sum_{j=1}^{N/K} \tau_{(i-1)(N/K)+j} + \sum_{m=1}^{N/K} Z_m \, \tau_{(n-1)(N/K)+m} + \tau_{(n-1)(N/K)+J+1} \tag{3.5.5}$$

where, with reference to the set of K cells being tested when the desired signal begins (i=1),

$$\tau_i = \begin{cases} \text{dwell time of i-th set of cells,} & i \neq (n-1)(N/K)+J+1 \\ \text{time to lock,} & i=(n-1)(N/K)+J+1 \end{cases} \tag{3.5.6}$$

From Sections 3.4.2 and 3.4.3,

$$E[\tau_i] = \begin{cases} T_{D1}, & i \neq (\ell-1)(N/K)+J+1, \quad \ell=1,2,\cdots,n \\ T_{D2}, & i=(\ell-1)(N/K)+J+1, \quad \ell=1,2,\cdots,n-1 \\ T_{LK}, & i=(n-1)(N/K)+J+1 \end{cases} \tag{3.5.7}$$

From the probability distribution of Z_m,

$$E[Z_m] = Pr(Z_m=1) = 1-(mK/N) \tag{3.5.8}$$

and

$$\sum_{m=1}^{N/K} E[Z_m] = (N/K) - (K/N) \sum_{m=1}^{N/K} m = [(N/K)-1]/2 \tag{3.5.9}$$

Therefore

$$E[T_A \mid \text{lock at n-th Y}]$$

$$= (n-1)\left[\left(\frac{N}{K} - 1\right)T_{D1} + T_{D2}\right] + \frac{1}{2}\left(\frac{N}{K} - 1\right)T_{D1} + T_{LK} \tag{3.5.10}$$

The probability of locking onto the received code at the n-th occurrence of

Y is

$$\Pr(\text{lock at n-th Y}) = p_L(1-p_L)^{n-1} \tag{3.5.11}$$

The mean acquisition time is therefore

$$E[T_A] = \frac{1}{2}\left(\frac{N}{K} - 1\right)T_{D1} + T_{LK} + \left[\left(\frac{N}{K} - 1\right)T_{D1} + T_{D2}\right] p_L \sum_{n=1}^{\infty} (n-1)(1-p_L)^{n-1}$$

$$= \left(\frac{N}{K} - 1\right)\left(\frac{2-p_L}{2p_L}\right)T_{D1} + \left(\frac{1-p_L}{p_L}\right)T_{D2} + T_{LK} \tag{3.5.12}$$

3.5.2 Acquisition Time Variance

Squaring both sides of eqn. (3.5.5) and taking the mean, the mean-squared acquisition time given that acquisition is successful at the n-th occurrence of event Y is

$$E[T_A^2 \mid \text{lock at n-th Y}] = E\Big[\Big(\sum_{i=1}^{n-1}\sum_{j=1}^{N/K} \tau_{(i-1)(N/K)+j}\Big)^2$$

$$+ \Big(\sum_{m=1}^{N/K} Z_m\, \tau_{(n-1)(N/K)+m}\Big)^2 + \tau^2_{(n-1)(N/K)+J+1} +$$

$$2\sum_{i=1}^{n-1}\sum_{j=1}^{N/K} \tau_{(i-1)(N/K)+j} \sum_{m=1}^{N/K} Z_m \tau_{(n-1)(N/K)+m} +$$

$$2\tau_{(n-1)(N/K)+J+1}\Big(\sum_{i=1}^{n-1}\sum_{j=1}^{N/K} \tau_{(i-1)(N/K)+j} + \sum_{m=1}^{N/K} Z_m \tau_{(n-1)(N/K)+m}\Big)\Big] \tag{3.5.13}$$

From Sections 3.4.2 and 3.4.3,

$$E[\tau_i^2] = \begin{cases} S_{D1}, & i \neq (\ell-1)(N/K)+J+1, \quad \ell=1,2,\cdots,n \\ S_{D2}, & i=(\ell-1)(N/K)+J+1, \quad \ell=1,2,\cdots,n-1 \\ S_{LK}, & i=(n-1)(N/K)+J+1 \end{cases} \tag{3.5.14}$$

From the probability distribution of Z_m,

$$E[Z_m^2] = Pr(Z_m=1) = 1 - (mK/N) \tag{3.5.15}$$

Furthermore, definition of Z_m in eqn. (3.5.2) implies

$$Pr(Z_\ell = 1, Z_m = 1 \mid \ell < m) = \sum_{j=m}^{(N/K)-1} Pr(J=j) = 1 - (mK/N) \tag{3.5.16}$$

so that

$$E[Z_\ell Z_m] = 1 - (mK/N), \quad 1 \leq \ell < m \leq N/K \tag{3.5.17}$$

Substitutions into each term in the right hand side of eqn. (3.5.13) yield

$$E[(\sum_{i=1}^{n-1} \sum_{j=1}^{N/K} \tau_{(i-1)(N/K)+j})^2]$$

$$= (n-1)[(\tfrac{N}{K} - 1)S_{D1} + S_{D2} + (\tfrac{N}{K} - 1)(\tfrac{N}{K} - 2)T_{D1}^2 + 2(\tfrac{N}{K} - 1)T_{D1}\ T_{D2}]$$

$$+ (n-1)(n-2)[(\tfrac{N}{K} - 1)^2\ T_{D1}^2 + 2(\tfrac{N}{k} - 1)T_{D1}\ T_{D2} + T_{D2}^2] \tag{3.5.18}$$

$$E[(\sum_{m=1}^{N/K} Z_m\ \tau_{(n-1)(N/K)+m})^2] = E[\sum_{m=1}^{N/K} Z_m^2\ \tau_{(n-1)(N/K)+m}^2$$

$$+2 \sum_{\ell=1}^{(N/K)-1} \sum_{m=\ell+1}^{N/K} Z_\ell Z_m \tau_{(n-1)(N/K)+\ell}\ \tau_{(n-1)(N/K)+m}]$$

$$= \frac{1}{2}(\tfrac{N}{K} - 1)S_{D1} + \frac{1}{3}(\tfrac{N}{K} - 1)(\tfrac{N}{K} - 3)T_{D1}^2 \tag{3.5.19}$$

$$E\left[\tau^2_{(n-1)(N/K)+J+1}\right] = S_{LK} \tag{3.5.20}$$

$$E\left[2 \sum_{i=1}^{n-1} \sum_{j=1}^{N/K} \tau_{(i-1)(N/K)+j} \sum_{m=1}^{N/K} Z_m \, \tau_{(n-1)(N/K)+m}\right]$$

$$= (n-1)\left(\frac{N}{K} - 1\right)^2 T^2_{D1} + (n-1)\left(\frac{N}{K} - 1\right) T_{D1} \, T_{D2} \tag{3.5.21}$$

$$E\left[2\tau_{(n-1)(N/K)+J+1}\left(\sum_{i=1}^{n-1} \sum_{j=1}^{N/K} \tau_{(i-1)(N/K)+j} + \sum_{m=1}^{N/K} Z_m \, \tau_{(n-1)(N/K)+m}\right)\right]$$

$$= 2(n-1)T_{LK}\left[\left(\frac{N}{K} - 1\right)T_{D1} + T_{D2}\right] + \left(\frac{N}{K} - 1\right)T_{D1} \, T_{LK} \tag{3.5.22}$$

Multiplying the sum of equations (3.5.18) to (3.5.22) by Pr (lock at n-th Y) in eqn. (3.5.11) and summing the result over n from one to infinity, the mean-squared acquisition time thus obtained is

$$E\left[T_A^2\right] = \left(\frac{N}{K} - 1\right)\left(\frac{2-p_L}{2p_L}\right)S_{D1} + \left(\frac{1-p_L}{p_L}\right)S_{D2} + S_{LK}$$

$$+ \left[\frac{1}{3}\left(\frac{N}{K} - 3\right) + \left(\frac{2N}{K} - 3\right)\left(\frac{1-p_L}{p_L}\right) + 2\left(\frac{N}{K} - 1\right)\left(\frac{1-p_L}{p_L}\right)^2\right]\left(\frac{N}{K} - 1\right)T^2_{D1}$$

$$+ 2\left(\frac{1-p_L}{p_L}\right)^2 T^2_{D2} + \left[3+4\left(\frac{1-p_L}{p_L}\right)\right]\left(\frac{N}{K} - 1\right)\left(\frac{1-p_L}{p_L}\right)T_{D1} \, T_{D2}$$

$$+ \left(\frac{N}{K} - 1\right)\left(\frac{2-p_L}{p_L}\right)T_{D1} \, T_{LK} + 2\left(\frac{1-p_L}{p_L}\right)T_{D2} \, T_{LK} \tag{3.5.23}$$

The acquisition time variance is therefore

$$Var[T_A] = E[T_A^2] - \left(E[T_A]\right)^2 \tag{3.5.24}$$

where $E[T_A^2]$ amd $E[T_A]$ are given by eqn. (3.5.23) and eqn. (3.5.12) respectively.

3.5.3 Acquisition Time Confidence Estimates

The probability that the acquisition time is within a given time limit can be accurately calculated if the acquisition time pdf is available. Derivation of the acquisition time pdf requires the derivation of all the moments. The first and second moments have been formulated in the two previous sections. Derivation of higher moments seems practically impossible. However, a confidence estimate of the acquisition time can be obtained using Chebyshev inequality [D5] which states that

$$Pr\left(|T_A - E[T_A]| \geq \varepsilon\right) \leq Var[T_A]/\varepsilon^2 \qquad (3.5.25)$$

A confidence lower bound of x% is obtained by setting the right hand side of inequality (3.5.25) to 1-0.01x so that inequality (3.5.25) can be rewritten as

$$Pr(T_A \leq \beta) \geq 0.01x \qquad (3.5.26)$$

where, if x is given, the acquisition time upper bound is

$$\beta = E[T_A] + \sqrt{Var[T_A]/(1-0.01x)} \qquad (3.5.27)$$

or, if β is given,

$$x = 100\left[1-Var[T_A]/\left(\beta-E[T_A]\right)^2\right] \qquad (3.5.28)$$

Inequality (3.5.26) states that with confidence of at least x%, the acquisition time is upper-bounded by β.

3.6 Hold-In Time

3.6.1 Mean and Variance of Hold-In Time

In the lock mode, the synchronization detector continues to make a decision every T_L seconds causing an appropriate state transition in the SLS. In the presence of noise and co-channel interference, the lock mode detection probability p_D is close to but less than one. Therefore, after the SLS enters lock mode with acquisition of the correct cell, if the desired signal continues to be present, it is inevitable that the SLS eventually retards its count to zero, the search mode is re-entered and synchronization is lost. The time that the SLS spends in the lock mode when synchronization is maintained is the hold-in time T_H.

Referring to the Markov chain shown in Fig. 3.4.2, the hold-in time is the absorption time from state 4 to the only possible absorbing state 10. As before, the mean and mean-squared hold-in times are, respectively, elements corresponding to state 4 of the mean and mean-squared absorption time vectors $E[\bar{t}_4]$ and $E[\bar{t}_4^2]$ which satisfy the matrix equations

$$E[\bar{t}_4] = (I - Q_4)^{-1} \bar{T}_4 \tag{3.6.1}$$

$$E[\bar{t}_4^2] = (I - Q_4)^{-1} \{\bar{T}_4^2 + 2T_L Q_4 E[\bar{t}_4]\} \tag{3.6.2}$$

where Q_4 is the matrix

$$Q_4 = \begin{array}{c} \text{State} \\ 4 \\ 5 \\ 6 \end{array} \begin{array}{c} \begin{array}{ccc} 4 & 5 & 6 \end{array} \\ \begin{bmatrix} p_5 & q_5 & 0 \\ p_5 & 0 & q_5 \\ 0 & p_5 & 0 \end{bmatrix} \end{array} \tag{3.6.3}$$

with p_5 and q_5 defined in Fig. 3.4.2, $\bar{T}_4$ is the vector

$$\bar{T}_4 = [T_L, T_L, T_L]^t \tag{3.6.4}$$

and $\bar{T}_4^2$ is $\bar{T}_4$ squared element by element.

Solving eqn. (3.6.1), the mean hold-in time is

$$E[T_H] = \left(\frac{1}{q_5^3} + \frac{2}{q_5}\right)T_L \tag{3.6.5}$$

Substituting $E[\bar{t}_4]$ into eqn. (3.6.2) and solving the equation, the mean-squared hold-in time is

$$E[T_H^2] = \left(\frac{2}{q_5^6} + \frac{8}{q_5^4} - \frac{7}{q_5^3} + \frac{8}{q_5^2} - \frac{2}{q_5}\right)T_L^2 \tag{3.6.6}$$

Therefore the hold-in time variance is

$$\begin{aligned} Var[T_H] &= E[T_H^2] - \left(E[T_H]\right)^2 \\ &= \left(\frac{1}{q_5^6} + \frac{4}{q_5^4} - \frac{7}{q_5^3} + \frac{4}{q_5^2} - \frac{2}{q_5}\right)T_L^2 \end{aligned} \tag{3.6.7}$$

3.6.2 Approximation of Hold-In Time Probability Distribution

An important performance criterion for the code synchronizer is that the probability that the hold-in time is greater than the message transmission time should be close to one. This ensures that premature loss of synchronization does not occur most of the time. It is therefore of interest to calculate the synchronization loss probability.

Define $p_n(i)$ as the probability that nT_L seconds after the SLS enters lock mode with acquisition of the correct cell the SLS is in state i. Define vector

$$\bar{p}_n = [p_n(4), p_n(5), p_n(6), p_n(10)]^t \tag{3.6.8}$$

From the Markov chain shown in Fig. 3.4.2,

$$\bar{p}_n = G^t \bar{p}_{n-1} = (G^t)^n \bar{p}_0 \tag{3.6.9}$$

where

$$\bar{p}_0 = [1,0,0,0]^t \tag{3.6.10}$$

and state transition matrix

$$G = \begin{array}{c} \text{State} \\ 4 \\ 5 \\ 6 \\ 10 \end{array} \begin{array}{c} \begin{array}{cccc} 4 & 5 & 6 & 10 \end{array} \\ \begin{bmatrix} p_5 & q_5 & 0 & 0 \\ p_5 & 0 & q_5 & 0 \\ 0 & p_5 & 0 & q_5 \\ 0 & 0 & 0 & 1 \end{bmatrix} \end{array} \tag{3.6.11}$$

Iterative calculation of $\bar{p}_n$ yields the cumulative distribution for T_H, as follows.

$$Pr(T_H \leq nT_L) = p_n(10) \tag{3.6.12}$$

The probability of synchronization loss after at least nT_L seconds is

$$\Pr(T_H > nT_L) = 1 - p_n(10) \tag{3.6.13}$$

Let p_{DL} be the probability of detection in the lock mode. In eqn. (3.6.11), $p_5 = p_{DL}$ and $q_5 = 1 - p_{DL}$. Computations of the cumulative distribution for T_H reveal that for p_5 fixed and $p_n(10)<<1$, $p_n(10)$ increases approximately linearly with n, and to maintain a constant $p_n(10)$, n must increase by three order of magnitude for each order of magnitude decrease in q_5. Hence, for p_{DL} close to one, the number of iterations n and the computation time are large even for $p_n(10)$ close to zero. A better method to evaluate eqns. (3.6.12) and (3.6.13) is therefore needed. Unfortunately, the Chebyshev inequality cannot be applied to lower-bound the probability in eqn. (3.6.13).

When $p_{DL} \approx 1$ so that $q_5<<1$, the mean and variance of T_H derived in the last section may be reduced to

$$E[T_H] \approx (1/q_5^3)T_L \quad , \quad q_5<<1 \tag{3.6.14}$$

$$\mathrm{Var}[T_H] \approx (1/q_5^6)T_L^2 \quad , \quad q_5<<1 \tag{3.6.15}$$

The fact that the mean and standard deviation of T_H are nearly equal for $q_5<<1$ suggests that eqns. (3.6.12) and (3.6.13) may be approximated by an exponential distribution. To test this hypothesis, $1-p_n(10)$ from eqn. (3.6.13) is compared with

$$F(n) = \begin{cases} e^{-n/\bar{n}} & , \quad n \geq 0 \\ 0 & , \quad n < 0 \end{cases} \tag{3.6.16}$$

where

$$\bar{n} = (1 + 2q_5^2)/q_5^3 \tag{3.6.17}$$

and the percentage deviation

$$\delta = \frac{[1 - p_n(10)] - F(n)}{1 - p_n(10)} \times 100\% \tag{3.6.18}$$

is obtained. Values of δ are tabulated against different values of $1 - p_n(10)$, p_{DL} and n in Table 3.6.1.

Table 3.6.1 shows that the exponential distribution is an excellent approximation to the probability distribution of T_H for all values of $1 - p_n(10)$ and p_{DL} considered. The accuracy of the approximation improves with n, the number of iterations, and a large n is the condition under which the approximation becomes necessary.

3.7 Numerical Examples

Given the single user power to noise-density ratio PNR, the transmission bandwidth B_t, the filter bandwidth B_f, the number of simultaneous channel users M, the number of possible code cells N, the number of parallel envelope correlators K, the search mode integration time T_S and decision threshold V_S, and the lock mode integration time T_L and decision threshold V_L, the performance measures for the code synchronizer as derived in the previous sections may

$1-p_n(10)$	p_{DL}	n	Precision of n	Deviation δ (%)
0.9	0.9	110	± 0.5	-2.031×10^{-2}
	0.99	105,000	± 500	-2.538×10^{-5}
	0.9925	250,000	± 500	-1.085×10^{-5}
	0.995	845,000	±2500	-3.246×10^{-6}
0.99	0.9	13	± 0.5	3.639×10^{-3}
	0.99	10,100	± 50	-1.574×10^{-6}
	0.9925	23,800	± 50	-7.549×10^{-7}
	0.995	80,500	± 250	-2.538×10^{-7}
0.999	0.9	3	± 0.5	-2.011×10^{-3}
	0.99	1,000	± 5	7.091×10^{-7}
	0.9925	2,370	± 5	2.012×10^{-7}
	0.995	8,000	± 25	2.994×10^{-8}
	0.999	1,000,000	±5000	-1.294×10^{-9}

TABLE 3.6.1

Percent Deviation δ of Actual and Exponentially Approximated Hold-in Time Cumulative Distribution

be calculated using assumptions given under either case 1 or case 2 in Section 3.3.2. The means and standard deviations (square roots of the variances) of acquisition time and hold-in time are plotted against M using the signal parameters in Table 2.3.1 and a set of fixed synchronizer parameters tabulated in Table 3.7.1.

Table 3.7.1 Spread-Spectrum Code Synchronizer Parameters

Bandpass filter bandwidth	B_f =	100 KHz
Search mode integration time	T_S =	0.2 msec.
Lock mode integration time	T_L =	1.0 msec.
Search step size	Δ =	0.5 chips
Number of code cells[1]	N =	1024
Search mode decision threshold	V_S	see Figs. 3.7.3 to 3.7.21
Lock mode decision threshold	V_L	
Number of parallel correlators	K	

A series of graphs showing the dependence of these curves on each of the parameters V_S, V_L, PNR and K are obtained. Case 1 assumptions are used, but results for Case 2 are obtainable simply by halving the scale of the horizontal axis and will not be duplicated. The following discussions are generally valid for both Case 1 and Case 2.

Before the results are presented and discussed, some remarks regarding V_S

[1] To facilitate computations, two redundant cells have been appended to the 1022 possible code cells.

and V_L are in order. In eqns. (3.3.26) to (3.3.29), letting kN = 1, the conditional means and variances for the Gaussian pdf of the detector output become

$$\mu|S = 1 + \rho \tag{3.7.1}$$

$$\mu|\bar{S} = 1 \tag{3.7.2}$$

$$\sigma^2|S = (1+2\rho)/(B_f T) \tag{3.7.3}$$

$$\sigma^2|\bar{S} = 1/(B_f T) \tag{3.7.4}$$

The decision thresholds V_S and V_L specified with the results correspond to the Gaussian pdf's with means and variances given by eqns. (3.7.1) to (3.7.4). Figure 3.7.1 and Fig. 3.7.2 show the false alarm probability versus the decision threshold for different values of K, in the search mode and in the lock mode respectively.

Calculations reveal that when PNR = 50 dB-Hz or higher, the mean and standard deviation of acquisition time are insensitive to changes in V_L. The opposite is true for V_S, as illustrated by Figs. 3.7.3 to 3.7.5. Given PNR, K and the expected range of M, the mean acquisition time can be optimized with respect to V_S. For example, Fig. 3.7.3 shows that with PNR = 50 dB-Hz and K=4, optimum values for V_S are approximately 1.5 for $1 \leq M \leq 200$, 1.4 for $200 \leq M \leq 870$ and 1.3 for $M > 870$. Figures 3.7.4 and 3.7.5 show that V_S has the same effect on the mean and standard deviation of acquisition time.

The relationships between PNR and the mean and standard deviation of acquisition time are shown in Figs. 3.7.6 and 3.7.7. Both graphs display a minimum irreducible mean or standard deviation which occurs at large values of PNR and small values of M as a result of an "overhead" of searching through an

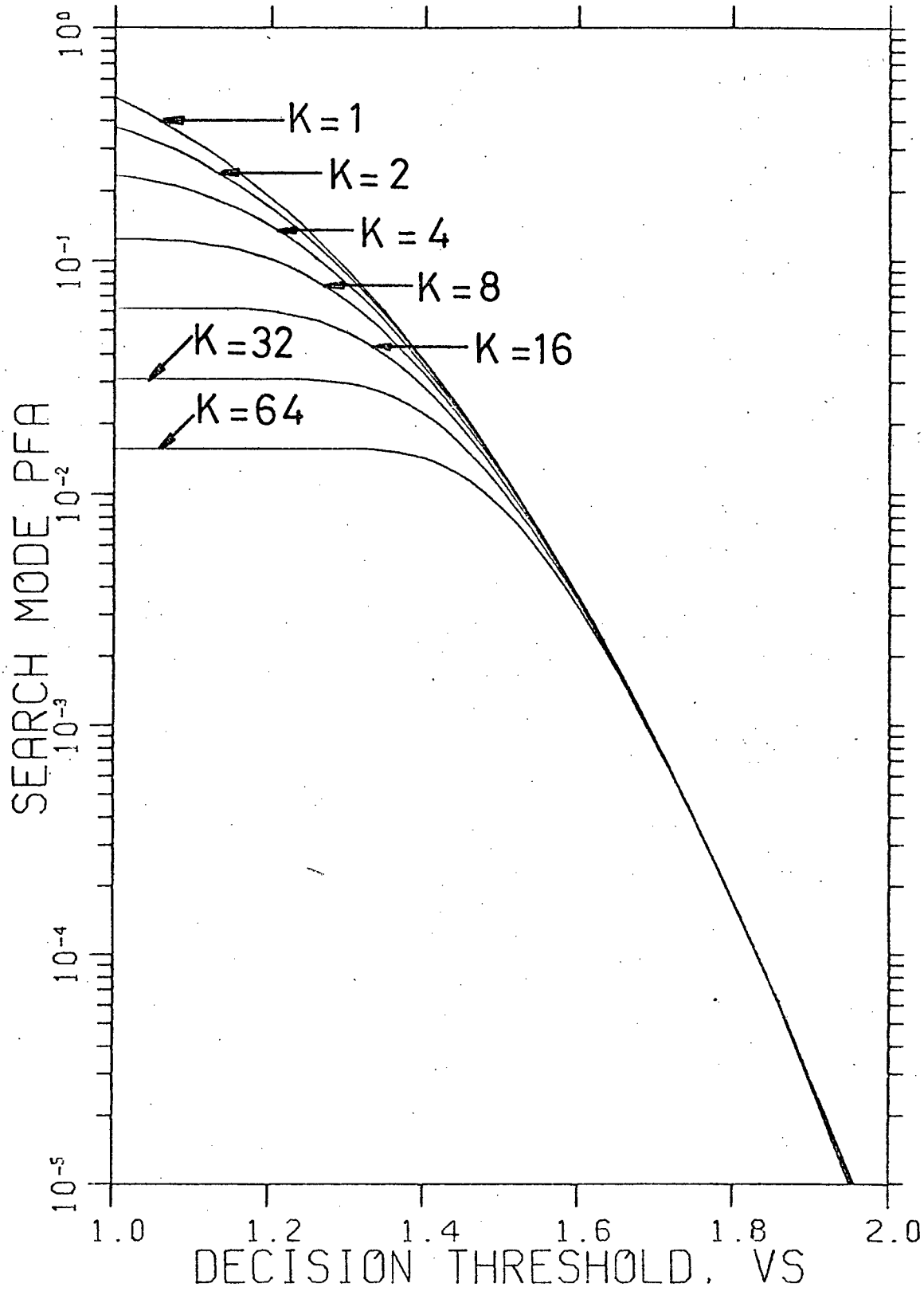

Fig. 3.7.1 False alarm probability p_{FA} vs. decision threshold V_S in the search mode.

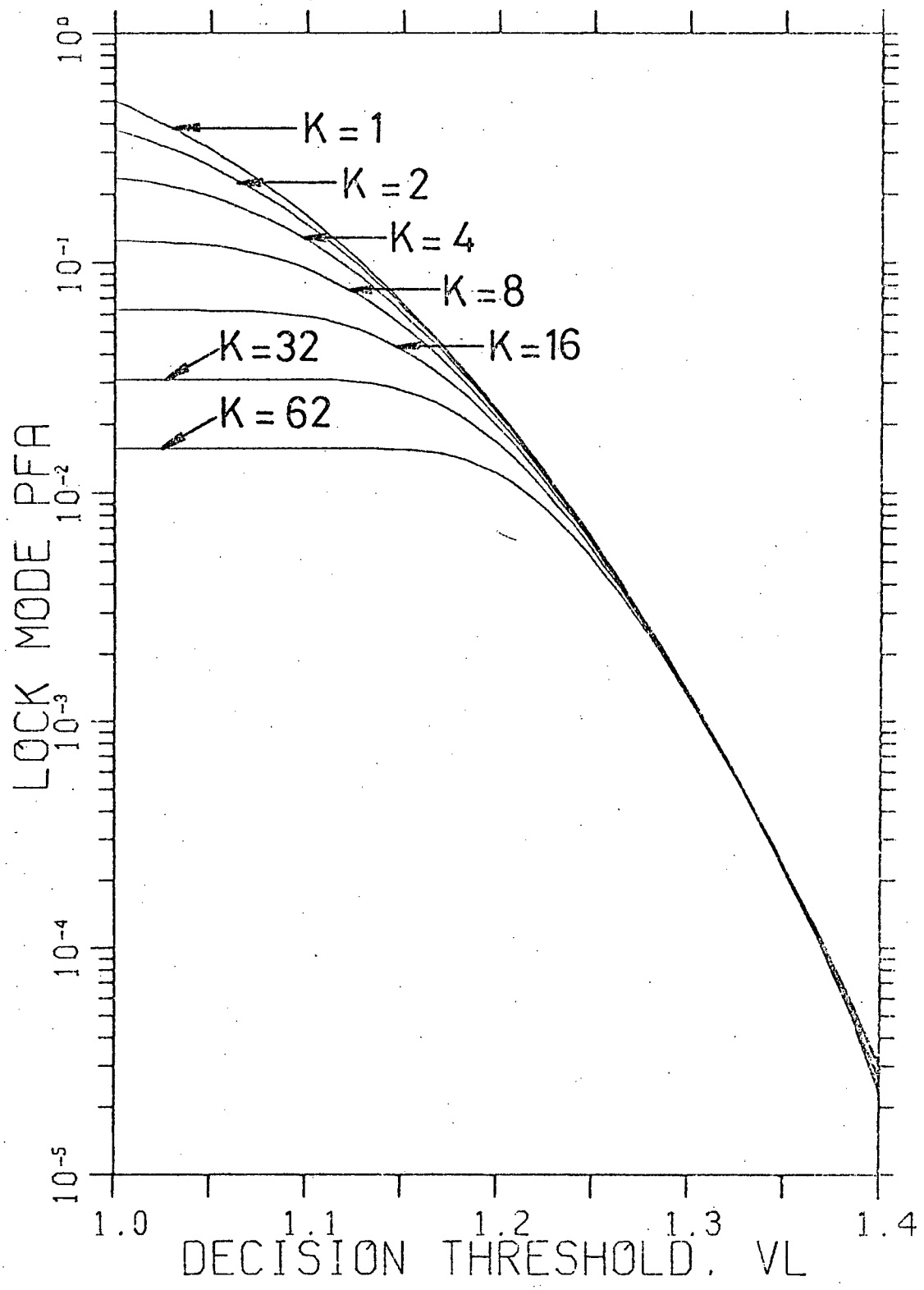

Fig. 3.7.2 False alarm probability p_{FA} vs. decision threshold V_L in the lock mode.

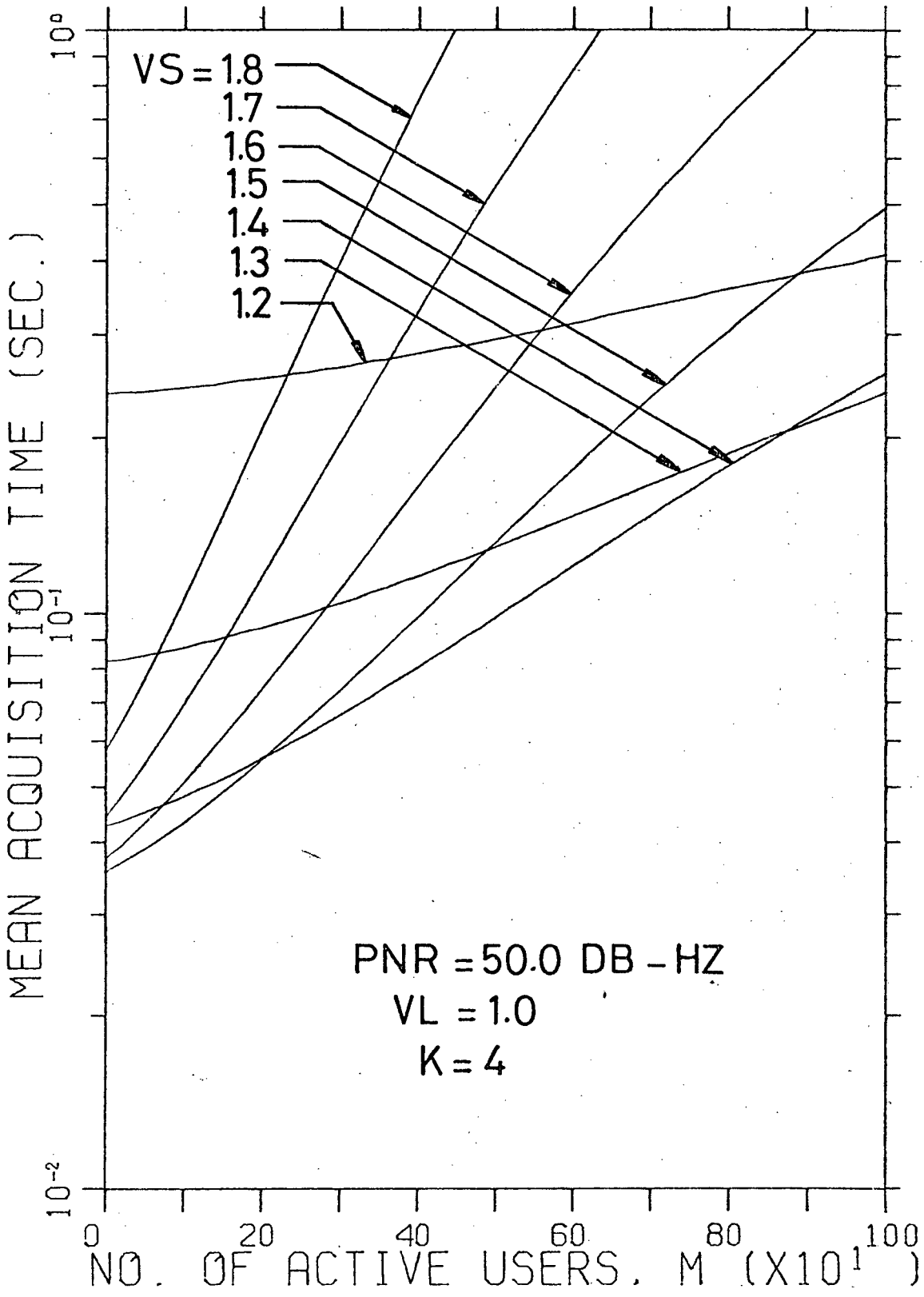

Fig. 3.7.3 Mean acquisition time vs. number of active users M for various V_S values with PNR = 50.0 dB-Hz.

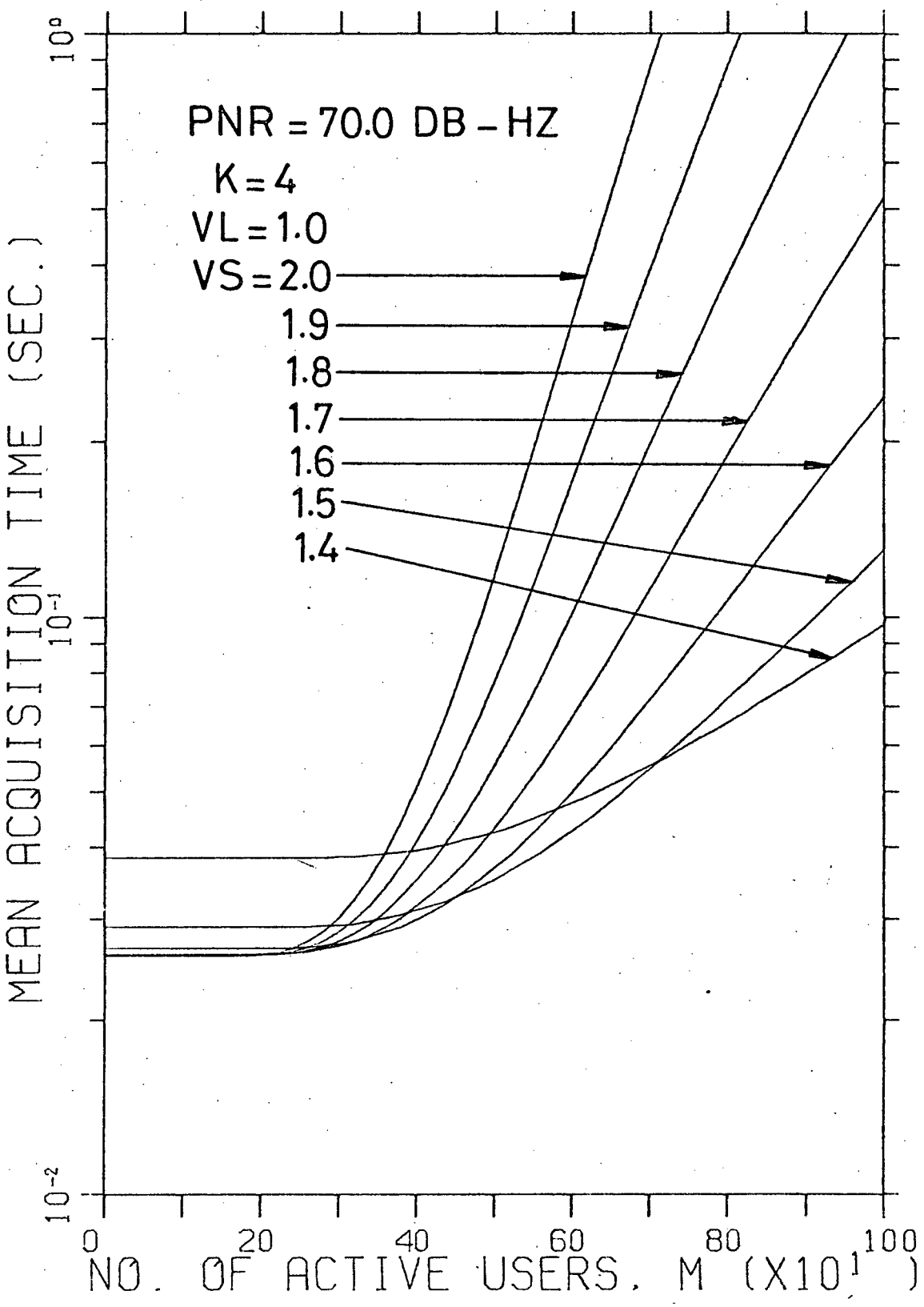

Fig. 3.7.4 Mean acquisition time vs. number of active users M for various V_S values with PNR = 70.0 dB-Hz.

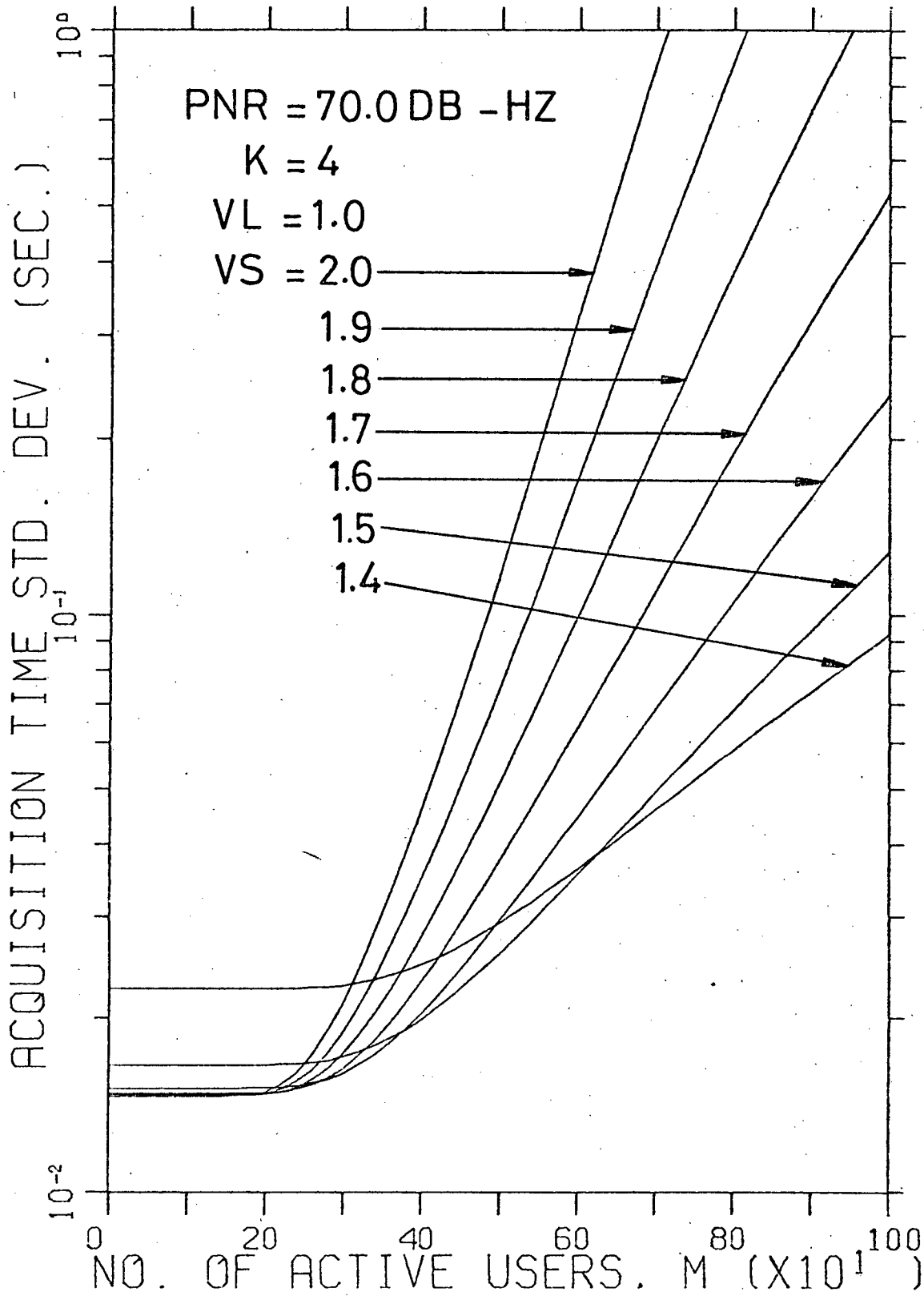

Fig. 3.7.5 Acquisition time standard deviation vs. number of active users M for various V_S values with PNR = 70.0 dB-Hz.

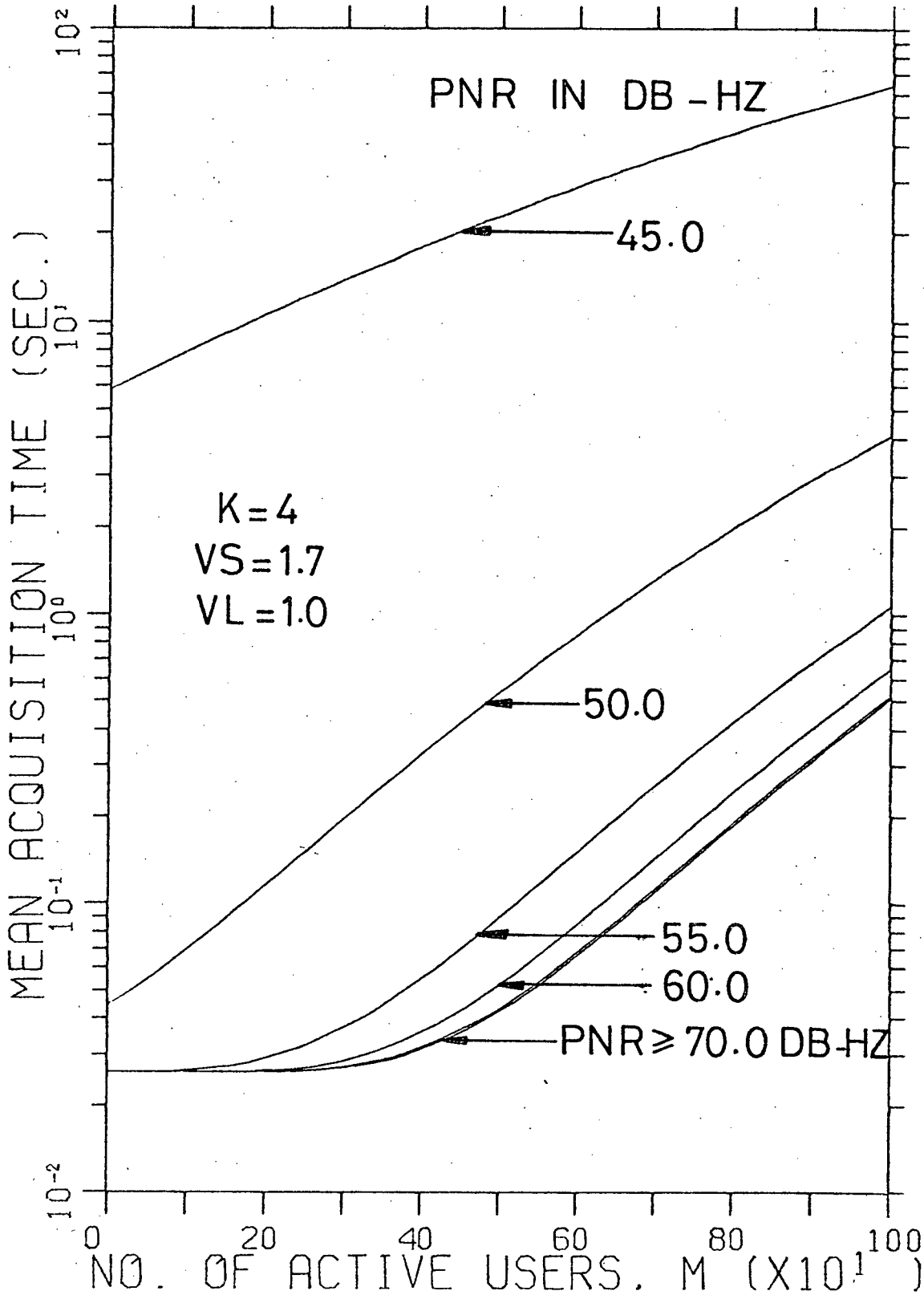

Fig. 3.7.6 Mean acquisition time vs. number of active users M for various PNR values

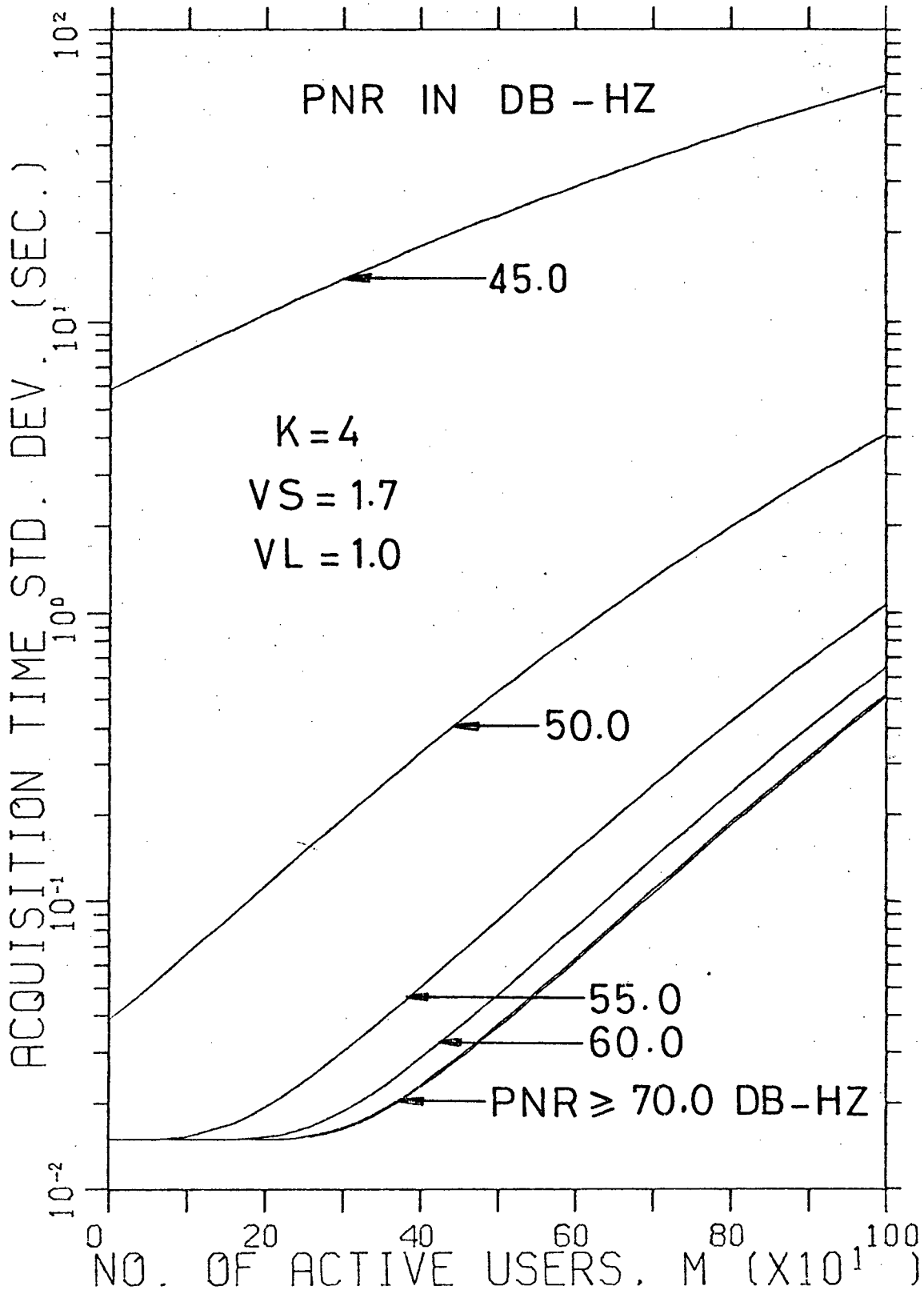

Fig. 3.7.7 Acquisition time standard deviation vs. number of active users M for various PNR values.

average of N/(2K) code cells to locate the correct cell for the first time. The relationships between PNR and receiver bit-error probability was discussed in Section 2.3. Therefore the choice of PNR affects the SSMA system performance as a whole. Although a high PNR level is generally desired, it is constrained by such considerations as government regulations, limitation of power supply, and cost, weight and physical size of the transmitter. Furthermore, increase in PNR beyond 80 dB-Hz does not bring about any improvement in acquisition time or bit-error probability as co-channel interference predominates over channel noise.

Figures 3.7.8, 3.7.9 and 3.7.10 show that the effect of increasing K is to reduce the mean and standard deviation of acquisition time. The rate of reduction decreases as K is increased. The ratio of reduction $RT = T_A(K)/T_A(1)$, where $T_A(K)$ is the minimum irreducible mean acquisition time for a synchronizer with K parallel correlators, is plotted against $\log_2(K)$ in Fig. 3.7.11. This graph shows that when K is small, reduction in mean acquisition time is almost proportional to increase in K. Another consequence of increasing K is that the complexity and therefore cost of the synchronizer also increase. Hence there is a trade-off between cost increase and acquisition time reduction.

Upper bounds for 90%, 99.9% and 99.999% confident acquisition time as derived in Section 3.5.3 are plotted against M for different values of PNR with $V_S = 1.7$, $V_L = 1.0$ and K = 1 in Figs. 3.7.12, 3.7.13 and 3.7.14 respectively. From these graphs, $T_A \leq 0.29$ sec. with probability of at least 0.9; $T_A \leq 1.97$ sec. with probability of at least 0.999 and $T_A \leq 18.8$ sec. with probability of at least 0.99999 for large PNR, small M and given values of V_S, V_L and K.

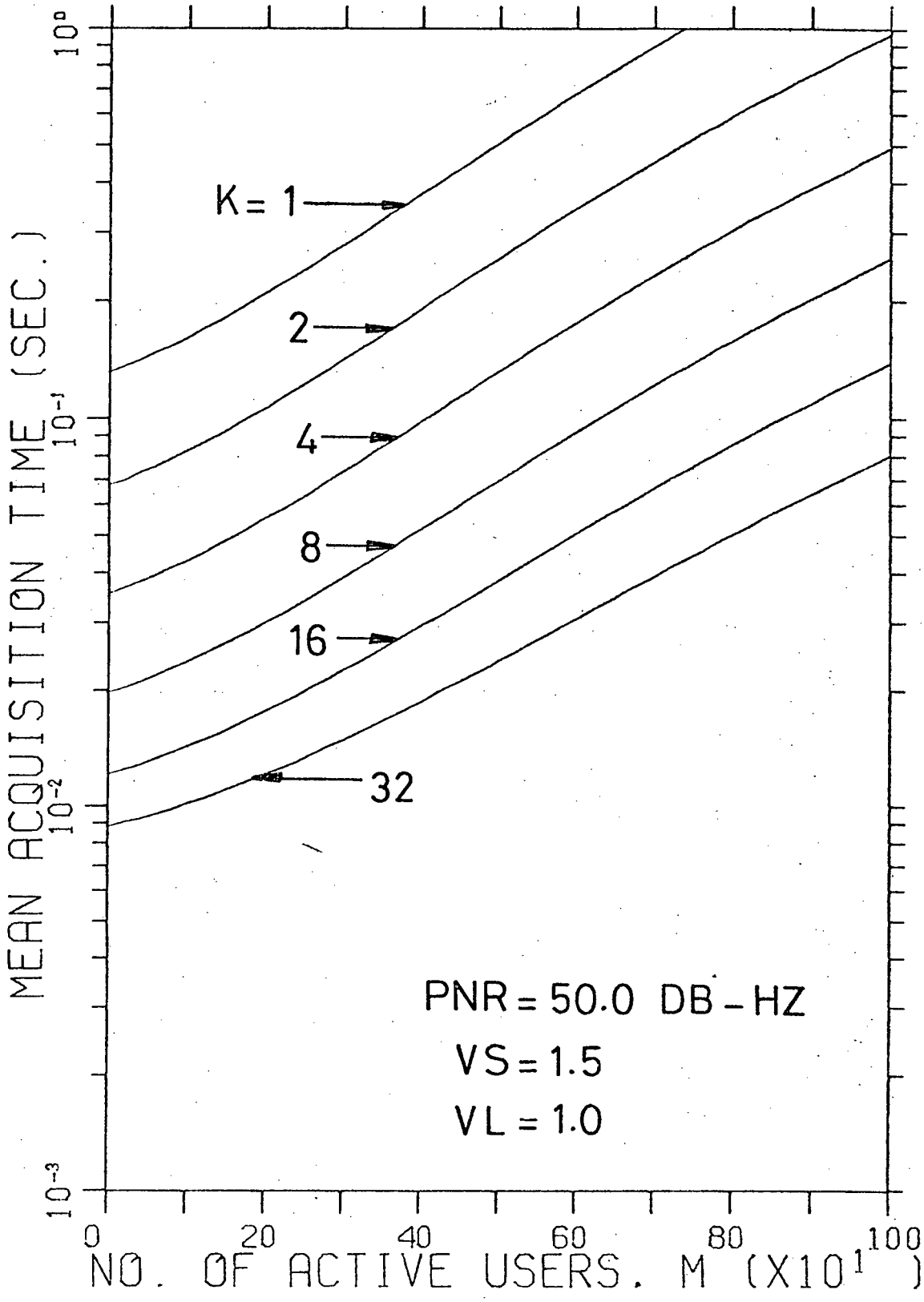

Fig. 3.7.8 Mean acquisition time vs. number of active users M for various K values with PNR = 50.0 dB-Hz.

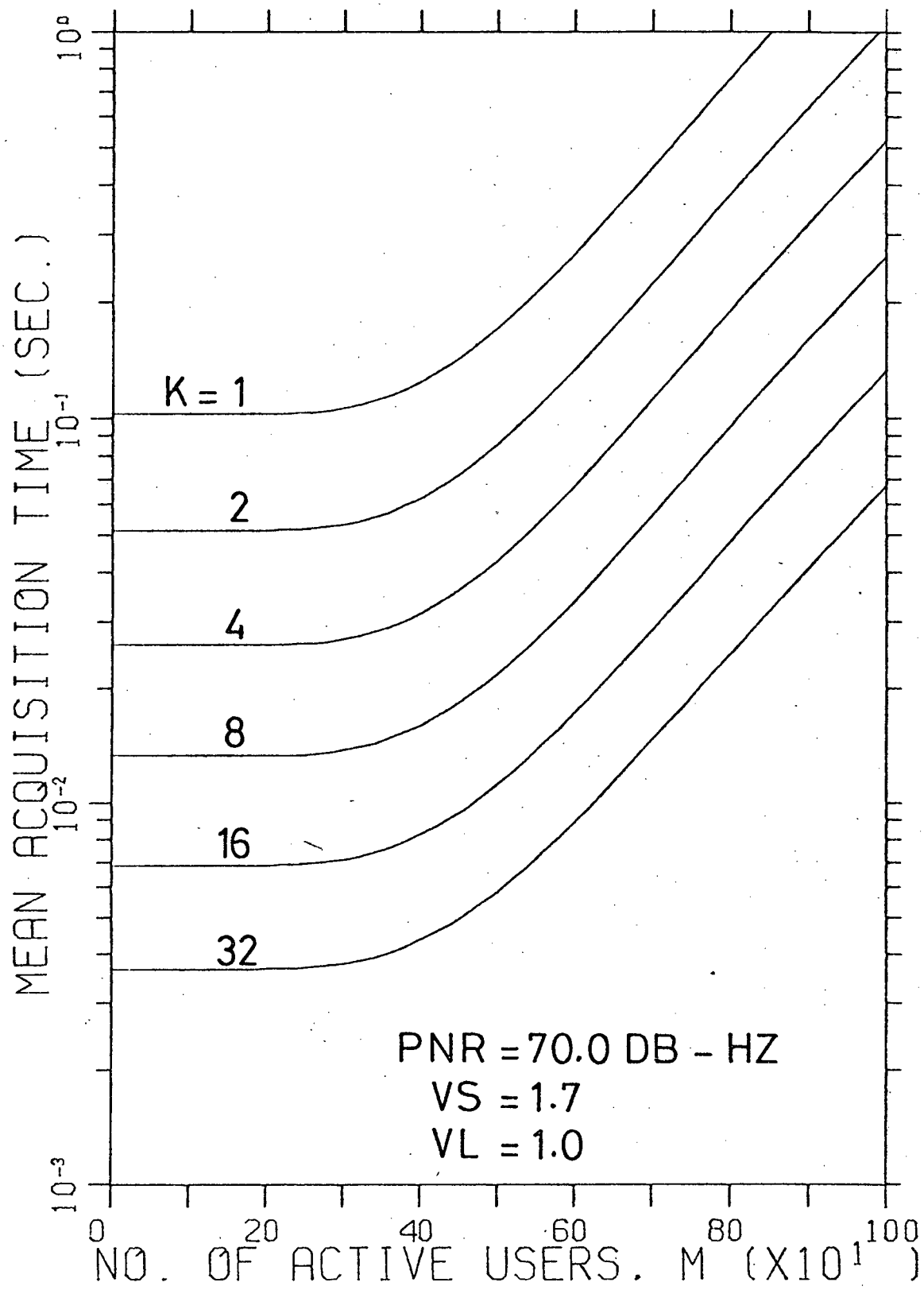

Fig. 3.7.9 Mean acquisition time vs. number of active users M for various K values with PNR = 70.0 dB-Hz.

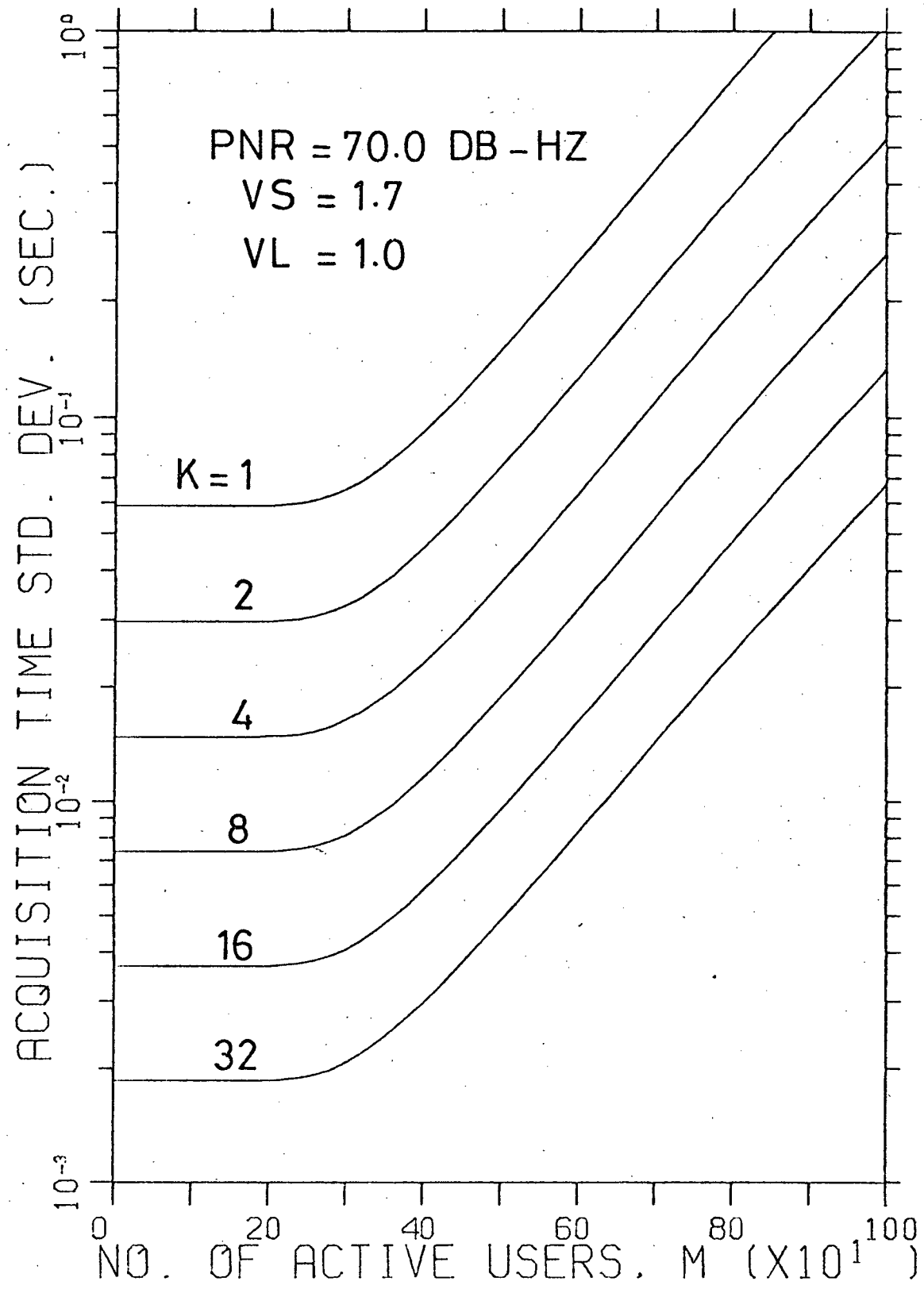

Fig. 3.7.10 Acquisition time standard deviation vs. number of active users M for various K values with PNR = 70.0 dB-Hz.

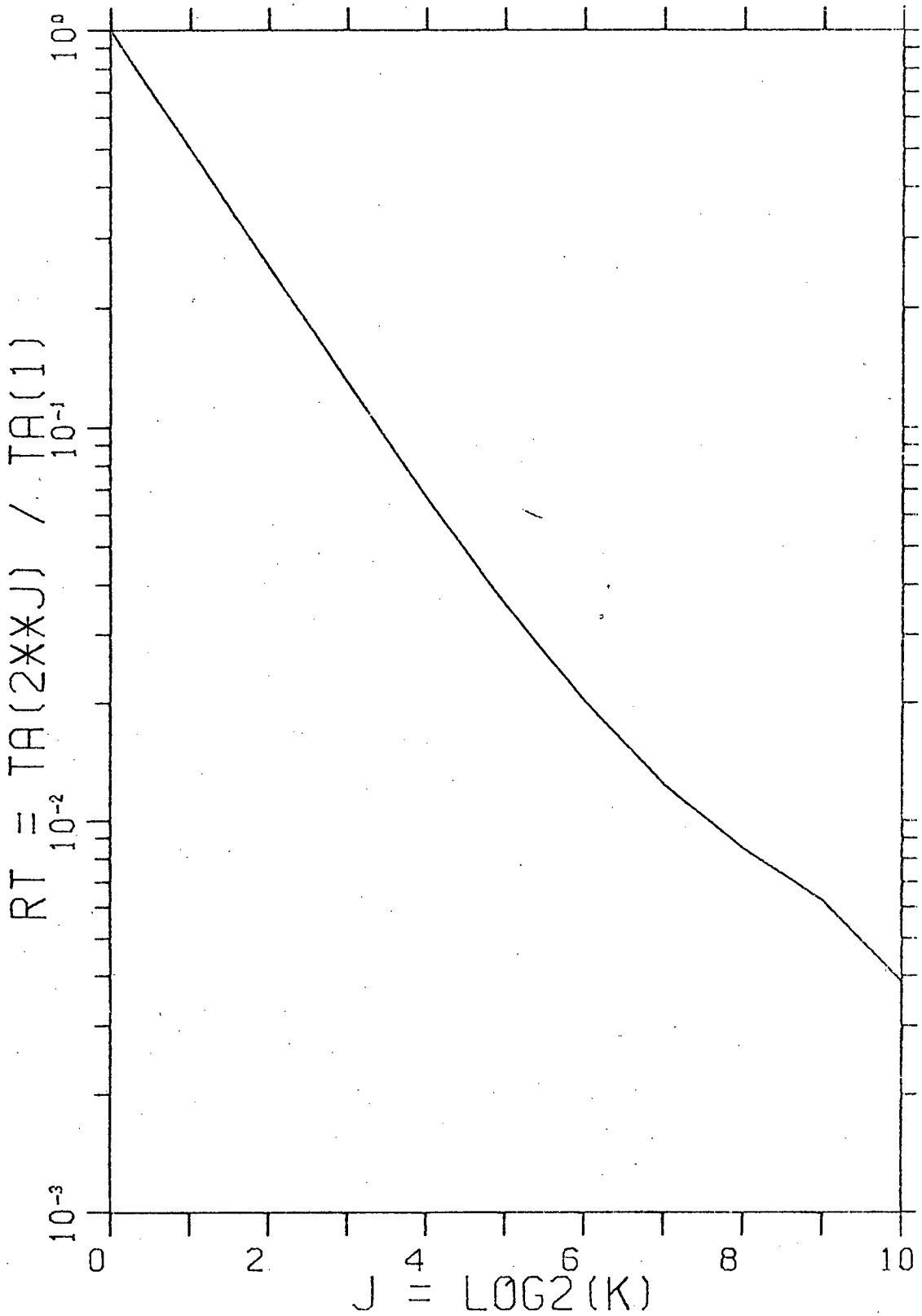

Fig. 3.7.11 Reduction of minimum mean acquisition time for various K values as fraction of minimum mean acquisition time for K = 1.

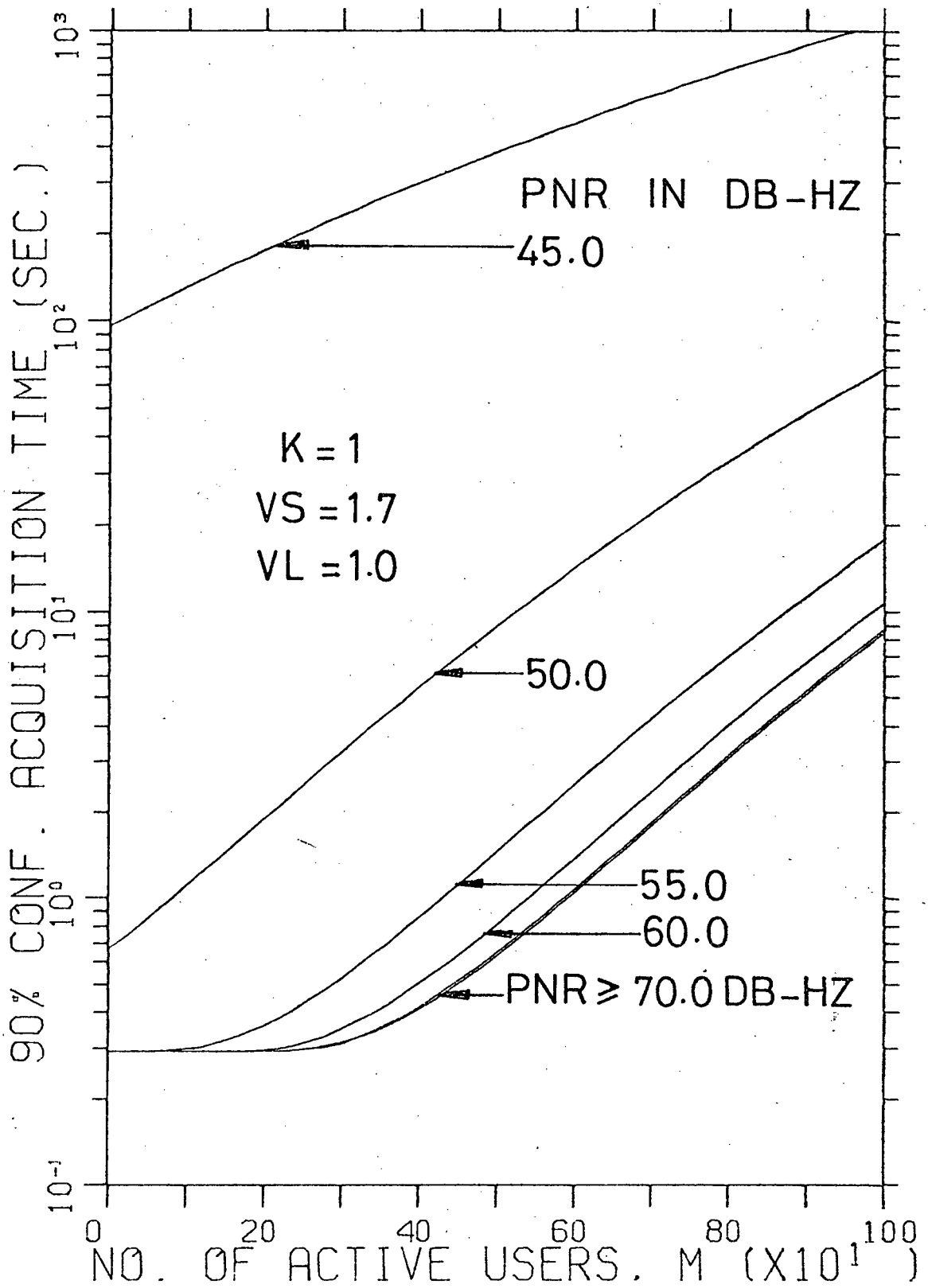

Fig. 3.7.12 Upper bound for 90% confident acquisition time vs. number of active users M.

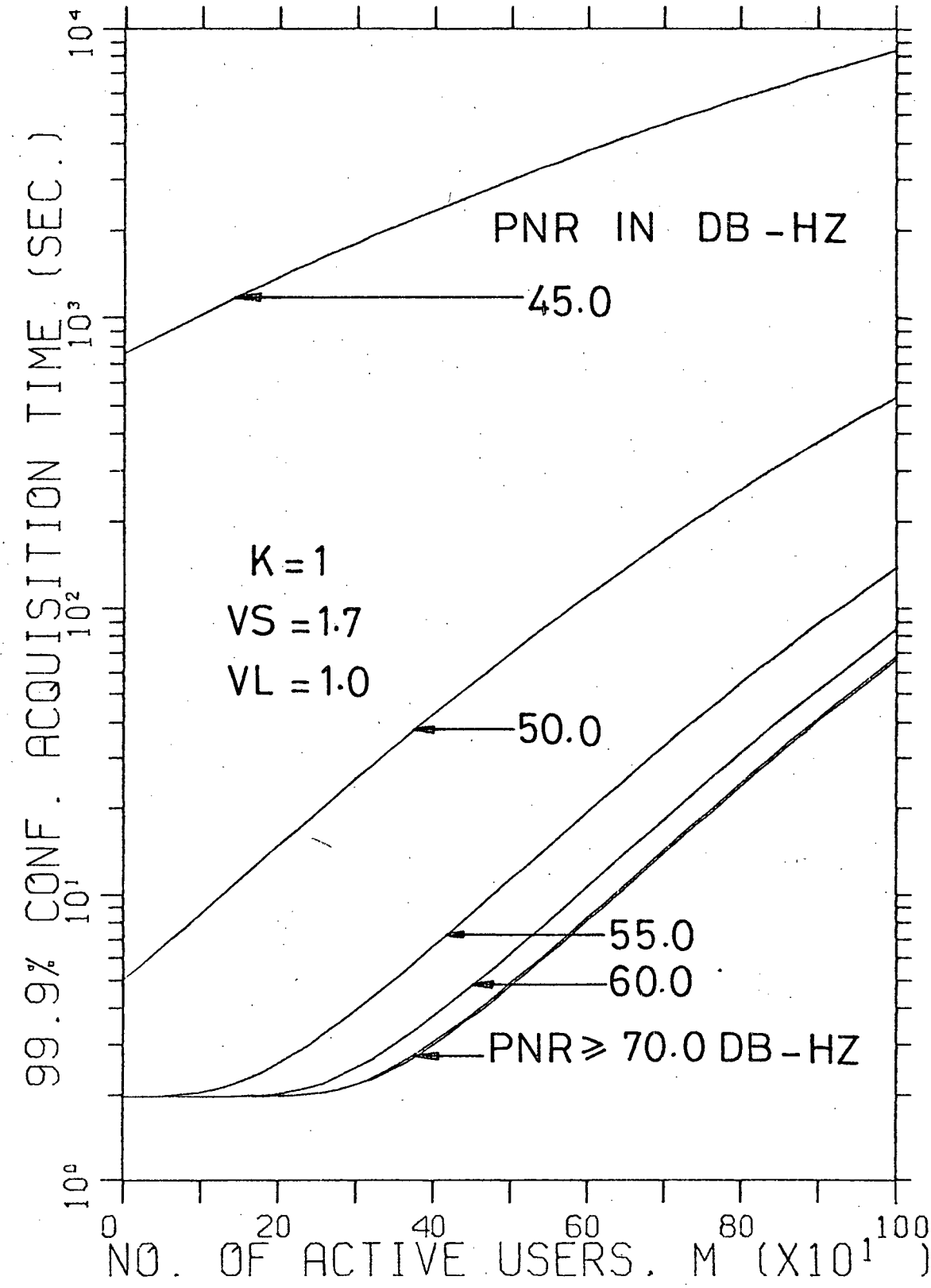

Fig. 3.7.13 Upper bound for 99.9% confident acquisition time vs. number of active users M.

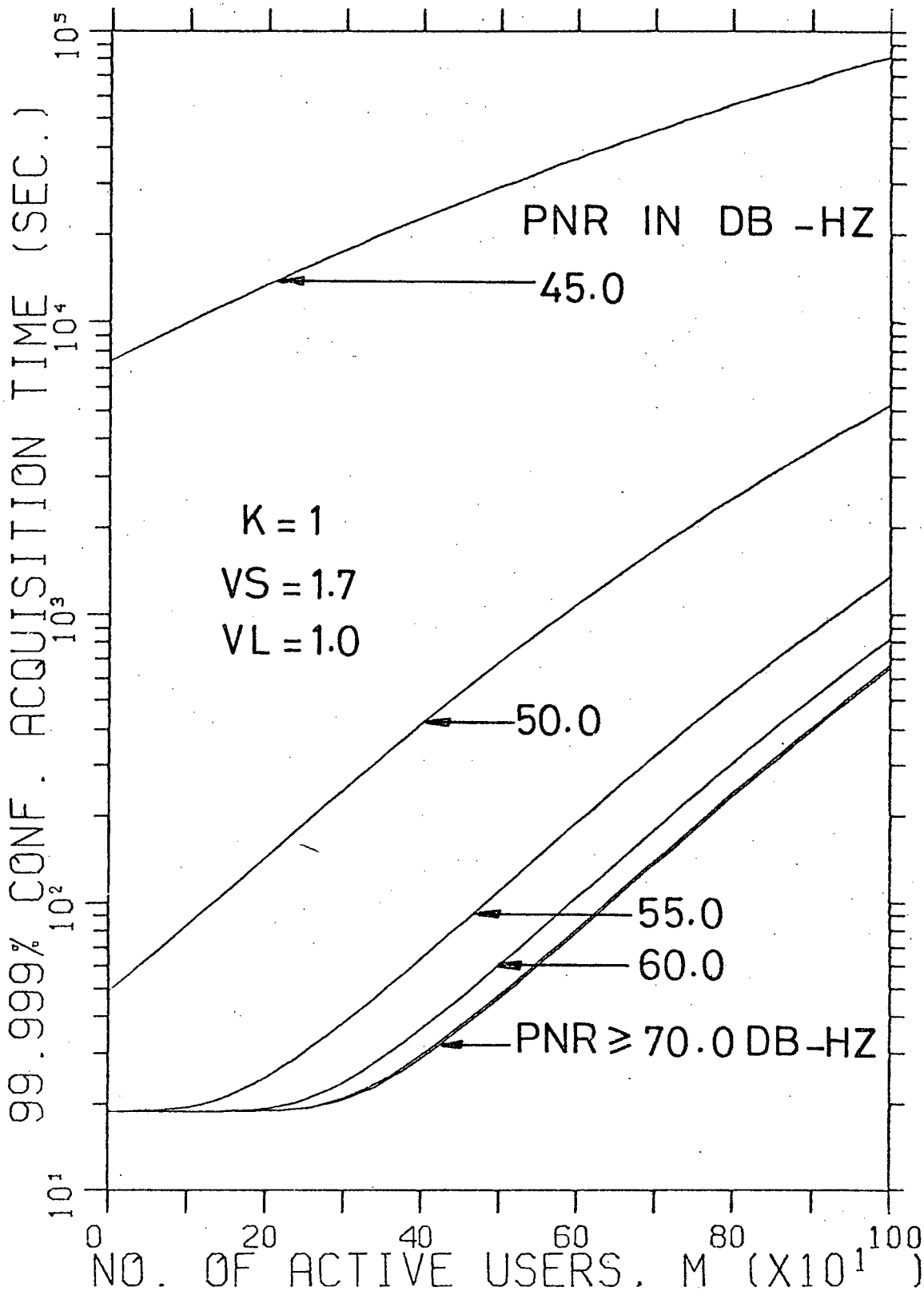

Fig. 3.7.14 Upper bound for 99.999% confident acquisition time vs. number of active users M.

The hold-in time is independent of search mode parameters. Figure 3.7.15 shows that mean hold-in time increases with decreasing V_L. Since V_L is constrained not to be less than 1.0 in order that false alarms are not favoured in the lock mode, it seems that $V_L = 1.0$ is an appropriate choice.

The mean and standard deviation of hold-in time are plotted against M for different values of PNR with K = 4 in Figs. 3.7.16 and 3.7.17, and with K = 32 in Figs. 3.7.18 and 3.7.19. Except at very low PNR's, these graphs show that the mean and standard deviation of hold-in time are approximately equal for given values of PNR and K. Comparison between the graphs for K = 4 and K = 32 reveals that increase in K results in decreases in the mean and standard deviation. This fact is further exemplified by Figs. 3.7.20 and 3.7.21 which also show that reductions in the mean and standard deviation of hold-in time occur at a decreasing rate as K increases. Therefore, when K is increased in order to reduce acquisition time, it is important to check that the mean hold-in time is not also reduced by such an extent that the synchronization loss probability is significantly increased. The hold-in time lower bounds for synchronization loss probabilities of 0.9, 0.999 and 0.99999, as given by the exponential approximation of eqn. (3.6.13), can be obtained by multiplying the scales of the mean hold-in time axis in the suitable graphs by factors of 0.1, 0.001 and 0.00001, respectively.

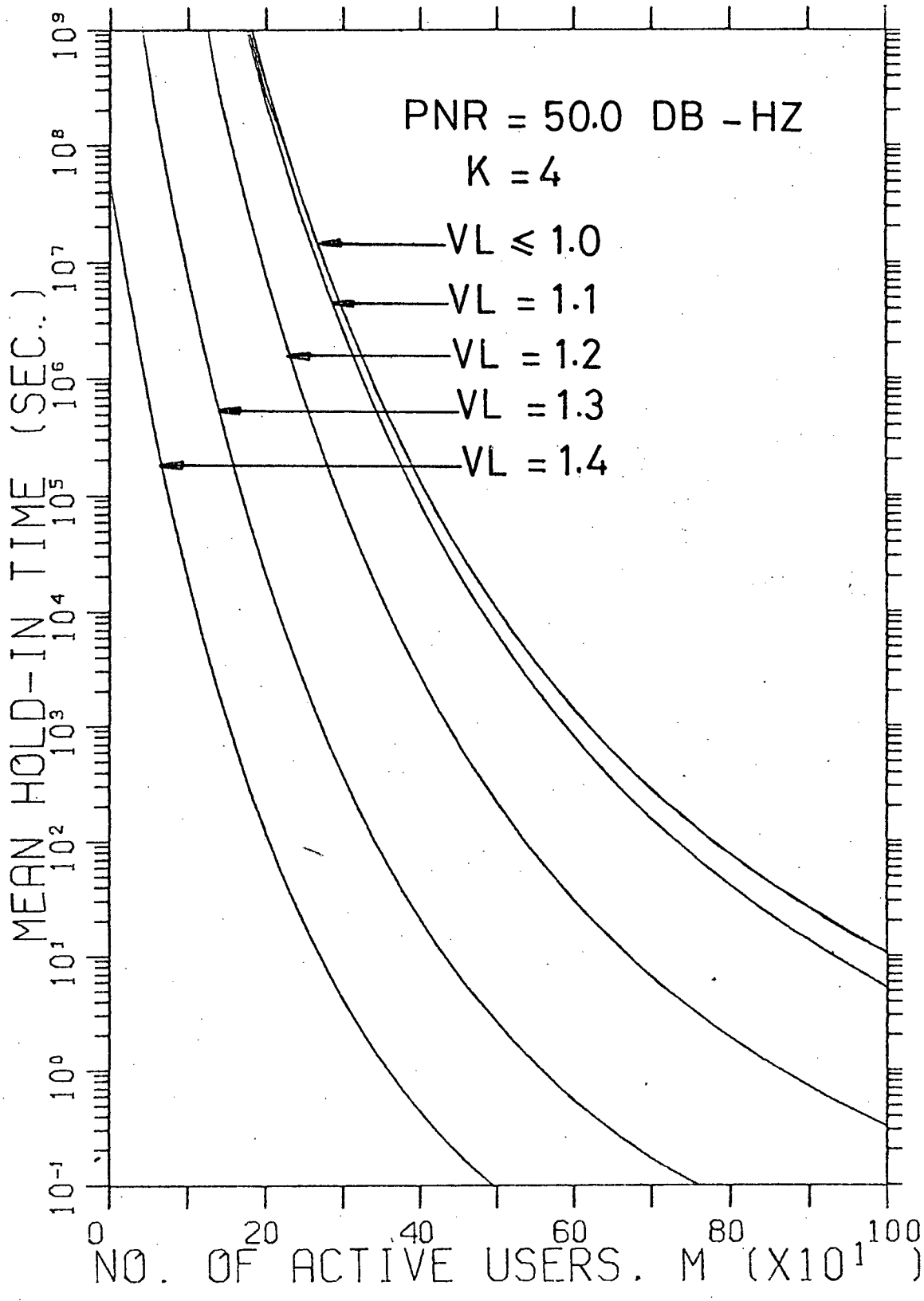

Fig. 3.7.15 Mean hold-in time vs. number of active users M for various V_L values.

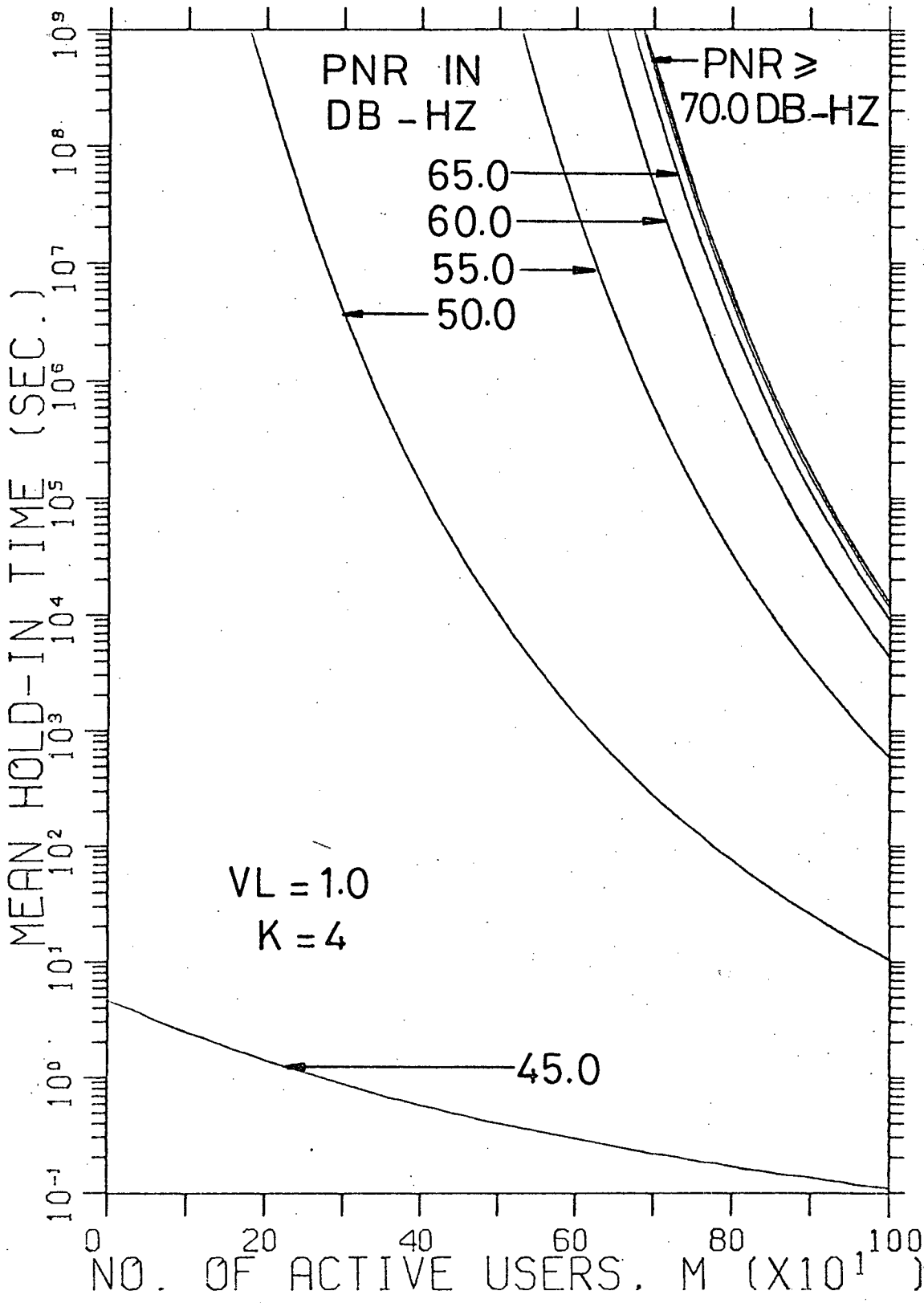

Fig. 3.7.16 Mean hold-in time vs. number of active users M for various PNR values with K = 4.

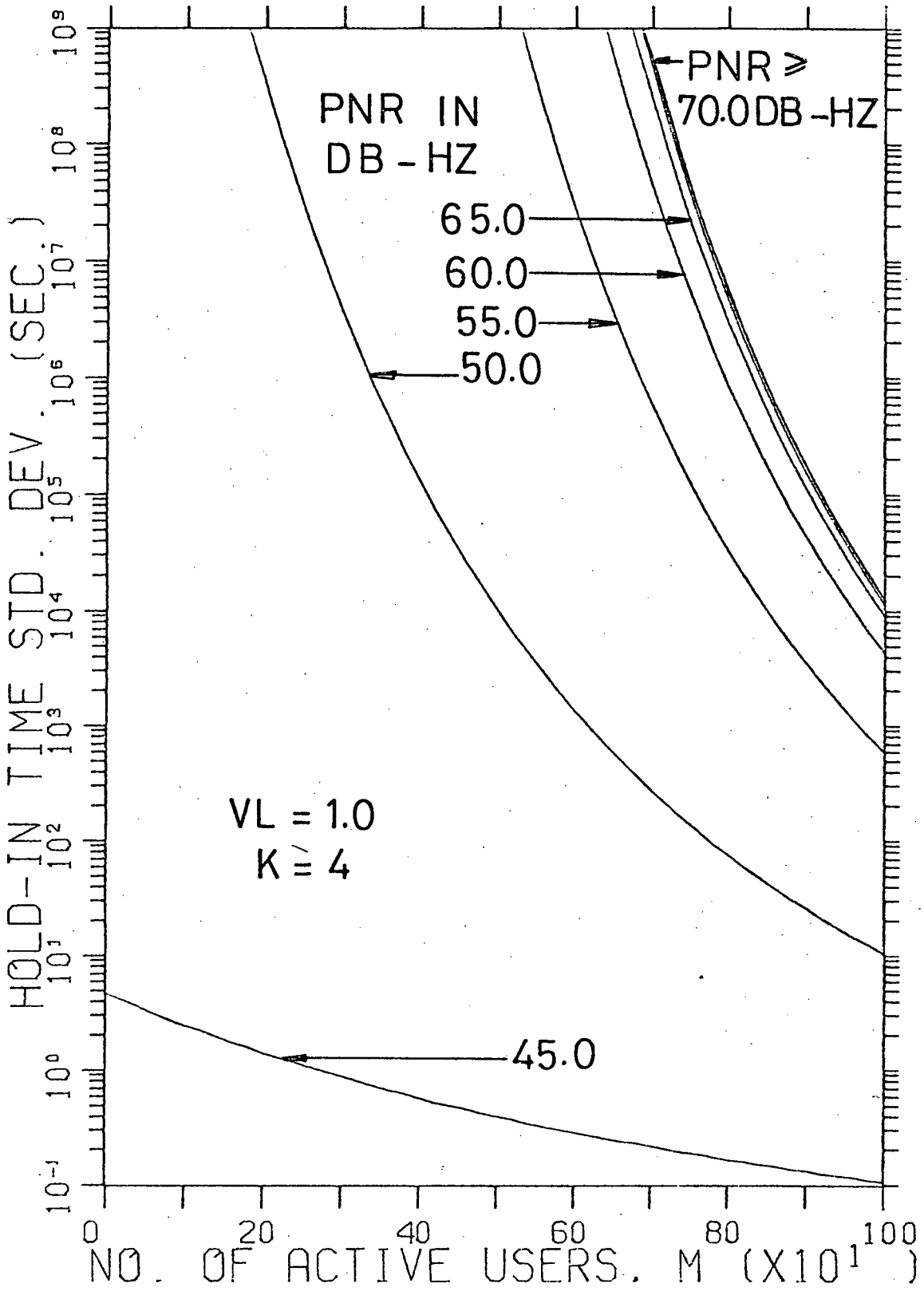

Fig. 3.7.17 Hold-in time standard deviation vs. number of active users M for various PNR values with K = 4.

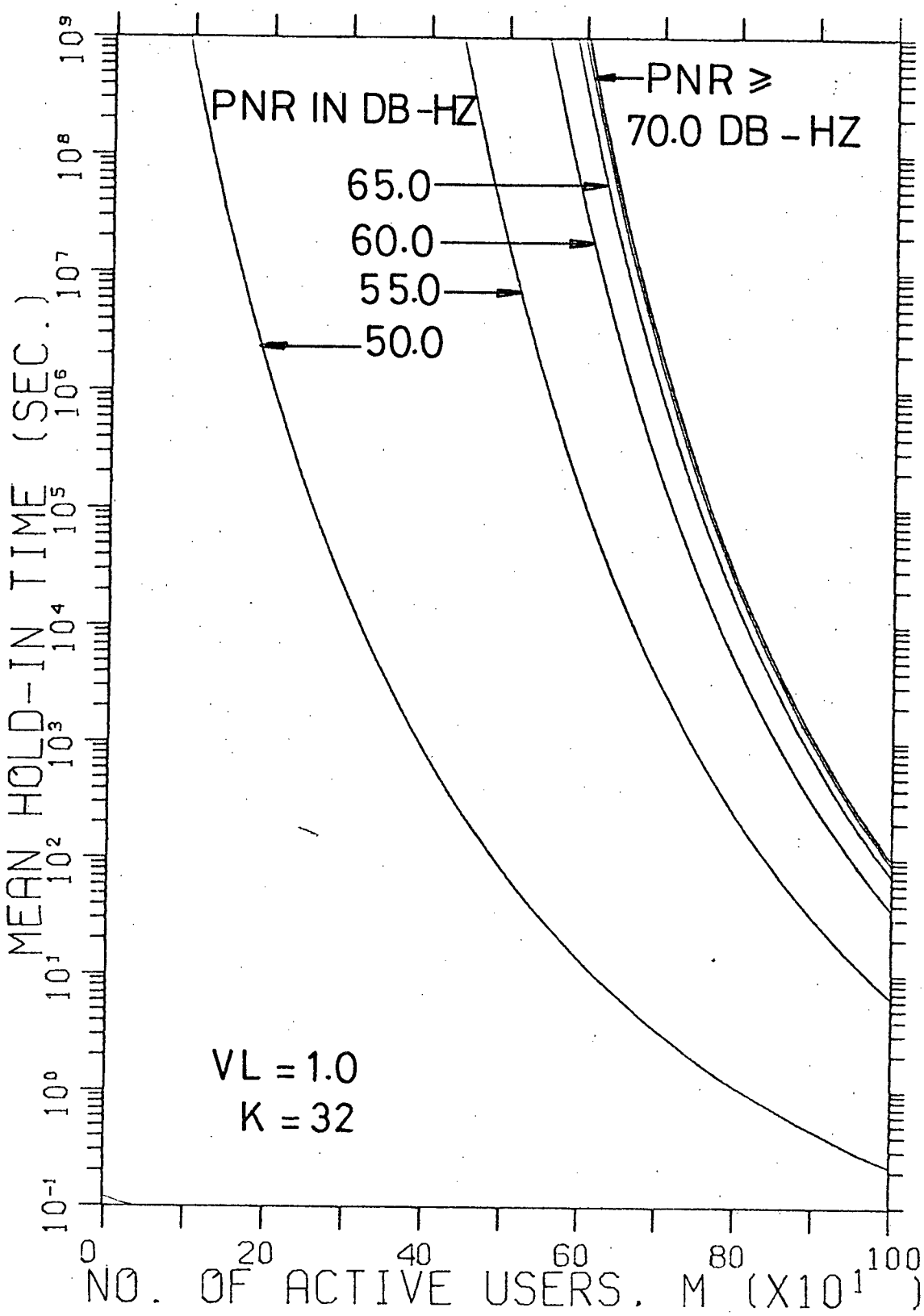

Fig. 3.7.18 Mean hold-in time vs. number of active users M for various PNR values with K = 32.

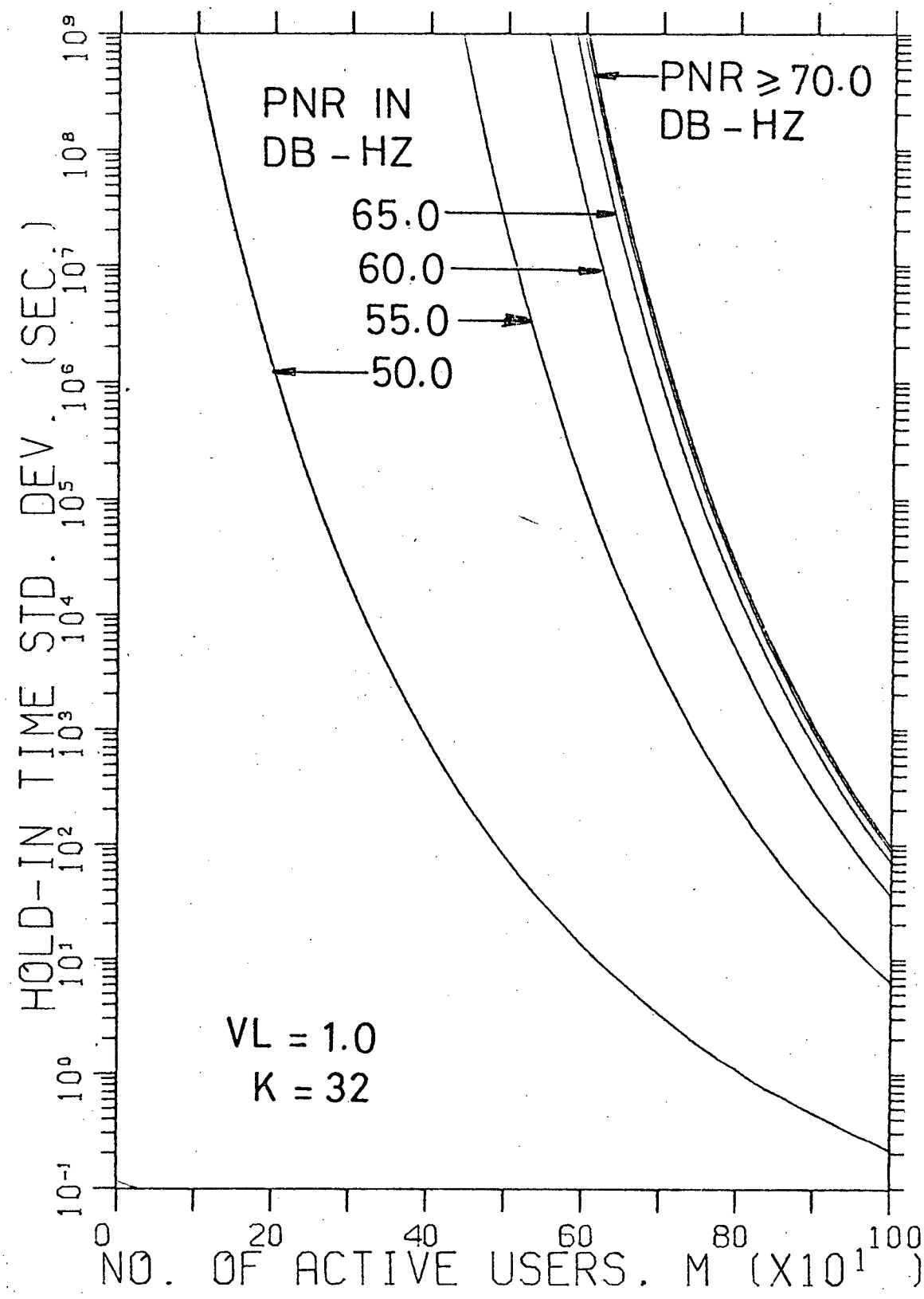

Fig. 3.7.19 Hold-in time standard deviation vs. number of active users M for various PNR values with K = 32.

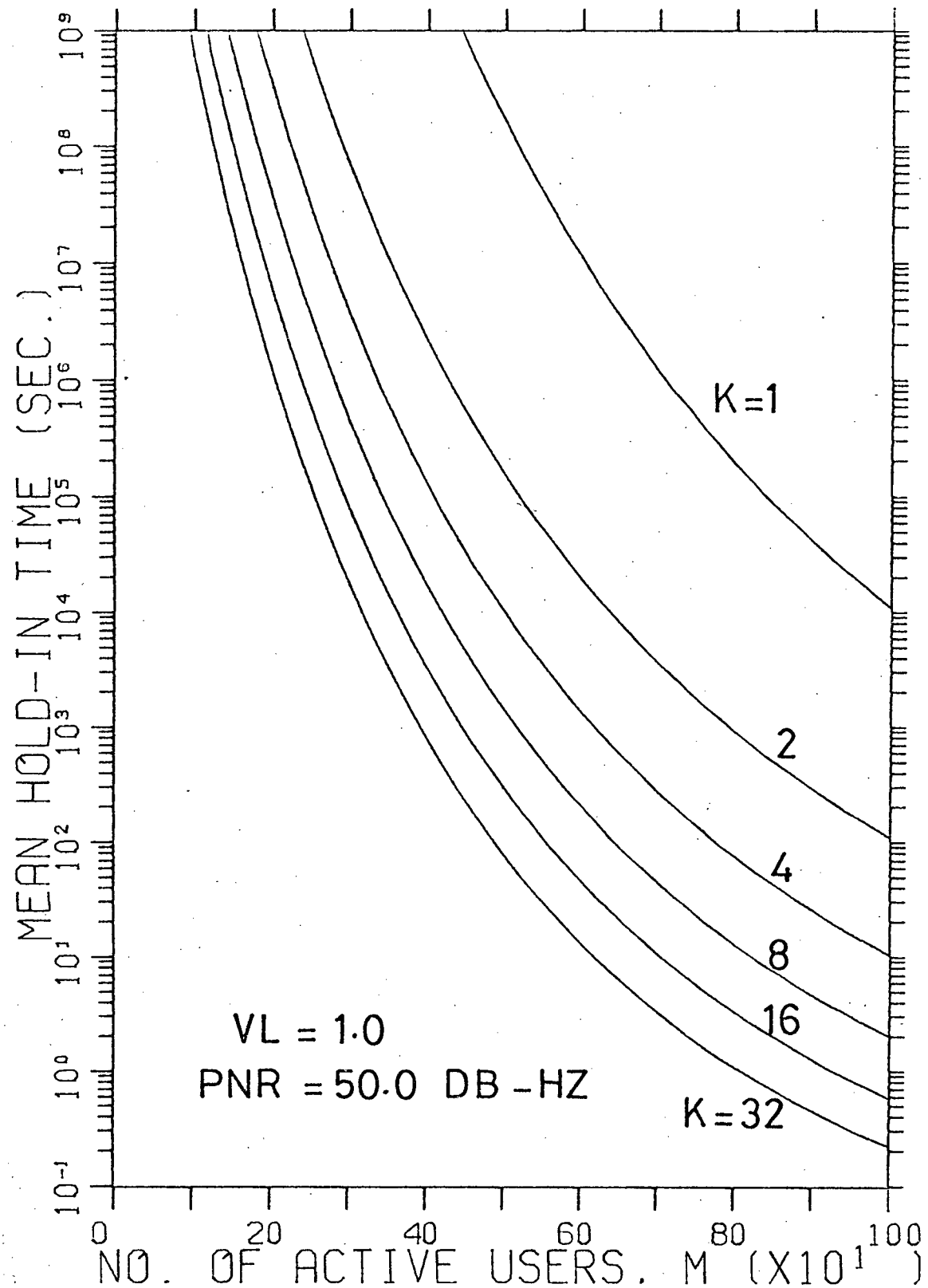

Fig. 3.7.20 Mean hold-in time vs. number of active users M for various K values.

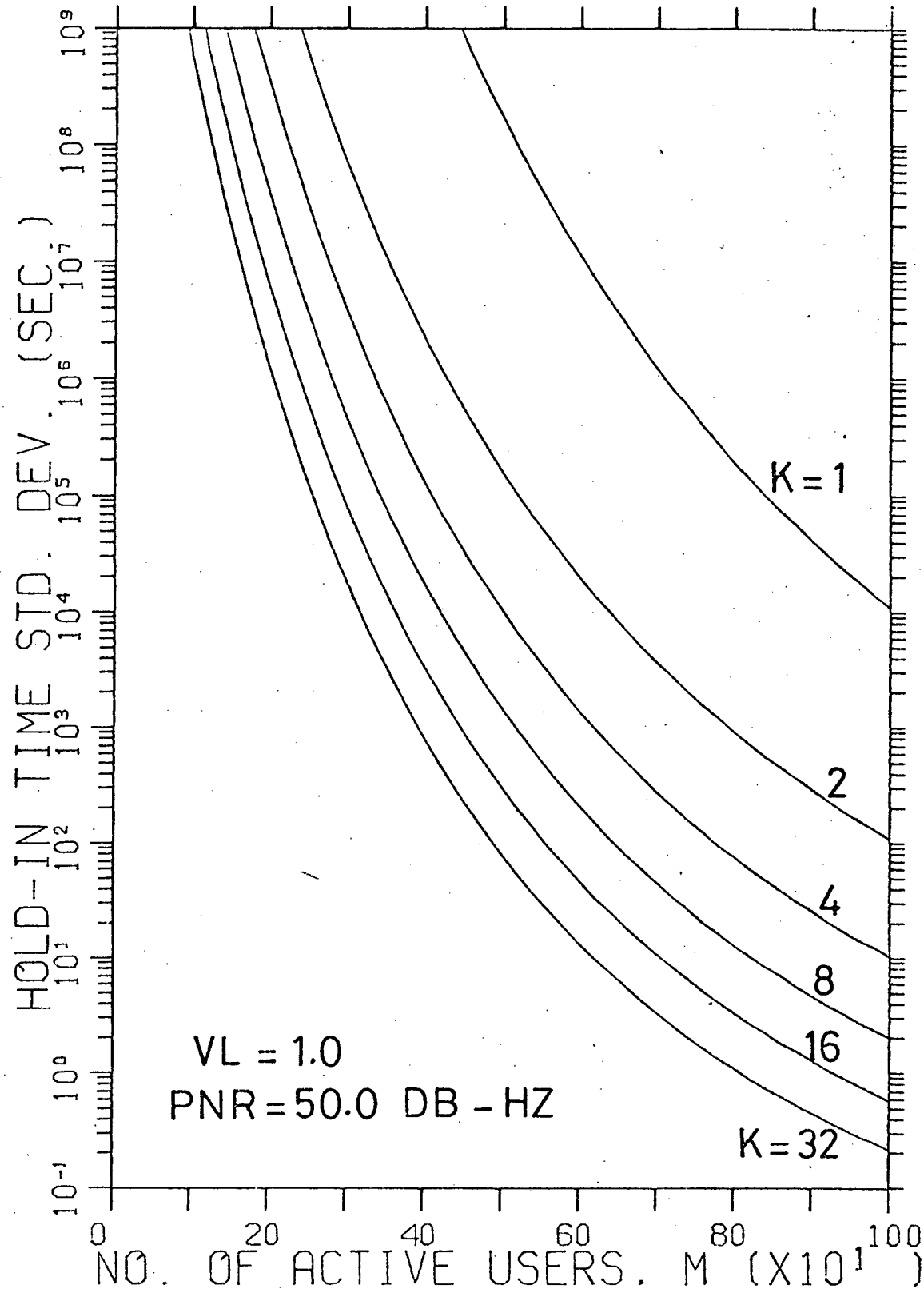

Fig. 3.7.21 Hold-in time standard deviation vs. number of active users M for various K values.

4. SSMA SYSTEM PERFORMANCE

4.1 Traffic Model

In an interactive data communication system, a user normally sends a message and waits for a response before sending another message. In a SSMA system, a user with a message to send may immediately become active in the channel until the message is correctly received. The user then remains idle until another message is ready. It is reasonable to assume that users access the channel independently, in which case the arrival of users and hence messages in the SSMA channel constitutes a Poisson random process [D6]. Let λ be the message arrival rate for the entire user population. The probability that m users (or messages) arrive during a time interval τ is

$$\Pr(m,\tau) = \frac{(\lambda\tau)^m}{m!} e^{-\lambda\tau} \quad , \quad \tau>0 \quad , \quad m = 0,1,2,\cdots \tag{4.1.1}$$

and the inter-arrival time is exponentially distributed with mean $1/\lambda$. The Poisson assumption is supported by traffic statistics [F1,D7] obtained from operational multiple access systems.

Restrictions on the length of messages generated by the users of a SSMA system is not really necessary. However, to facilitate comparison with ALOHA systems which restrict users' messages to a fixed length, messages in the SSMA system are also assumed to have a fixed length of ℓ bits/message. All messages are assumed to incorporate sufficient error detection channel coding so that bit-errors caused by channel noise or by loss of synchronization may be detected by the receiver with a negligible probability of undetected errors.

4.2 Protocols for SSMA Signal Transmission

A SSMA channel with M active users simultaneously sending messages to a central node is modelled in Section 2.2. For interactive data communications, the SSMA channel constitutes a forward channel, and transmissions from the node to the users, including acknowledgement messages, are handled by a separate return channel in an adjacent band. For maximum efficiency, messages addressed to different users are usually queued in the return channel, with a higher priority often assigned to acknowledgement messages.

Signal transmission protocols are procedures whereby users and nodes exchange information using the forward and return channels to facilitate code synchronization and correct message reception. The following discussions are restricted to protocols governing the transmission of messages from users to a central node.

Two important design criteria for SSMA protocols are minimization of average message delay D and maximization of the channel capacity (maximum attainable average throughput) C, given the message length ℓ, the received power to noise density ratio PNR, the average message service delay $\bar{T}_S$ (sum of average round trip propagation delay $2\bar{T}_P$ and average acknowledgement delay $\bar{T}_K$), the user population UP, and system parameters listed in Tables 2.3.1 and 3.7.1. In some cases the above criteria are not compatible and trade-offs are necessary. $\bar{T}_K$ is the time it takes for the central node to acknowledge establishment of synchronization or error-free reception of a message, and includes processing time at the node, queueing delay and transmission time for the acknowledgement message.

For small user populations (e.g. UP $\leq$ 200 at PNR $\geq$ 70 dB-Hz), receiver performance does not degrade appreciably when all users are active, compared to when a single user is active (see Fig. 2.3.1). Message delays and channel capacity are optimized in such cases if code synchronization between node and users is maintained at all times. Acquisition is necessary only in the infrequent event that the code synchronizer loses lock. Message delay consists of the propagation delay, a number of message transmissions to achieve error-free reception, and a number of service delays if each message transmission is acknowledged. The maximum channel capacity $C = UP \cdot R_m$ bits/sec, where R_m is the information bit rate, occurs when message interarrival time for each user is zero and message errors are negligible.

Further analysis will be restricted to systems with large user populations and large message interarrival times. In this case code acquisition is necessary before a new message is transmitted, and acquisition delay has major effects on message delay and channel capacity.

Figure 4.2.1 illustrates three possible protocols for SSMA signal transmission between an active member of a large user population and a central node.

Protocol A: An active user simply transmits the message repeatedly until being acknowledged by the node that the message has been correctly received (positive acknowledgement).

Protocol B: An active user first sends a synchronization preamble until being acknowledged that synchronization is established at the node. The user then sends the message as in Protocol A.

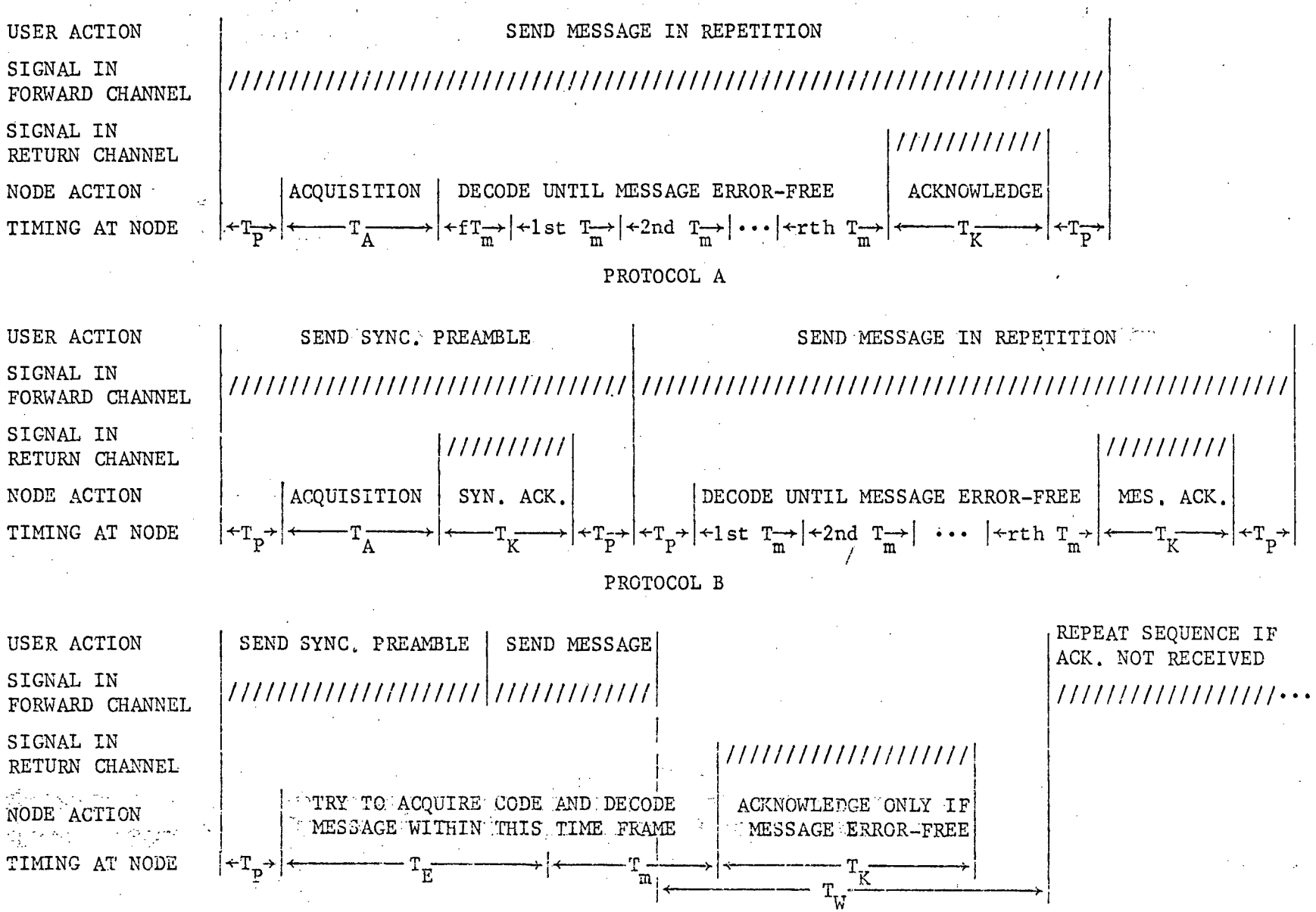

Fig. 4.2.1 Three protocols for SSMA signal transmission

In both Protocols A and B, if a positive acknowledgement is not received within a reasonable time T_R, channel or equipment failure may have occurred and other actions could be initiated by the user. The acquisition time confidence estimate derived in Section 3.5.3 is an important consideration in the determination of T_R.

Protocol C: An active user sends a synchronization preamble for a fixed duration T_E, followed by the message, sent once, with no repetitions. Successful acquisition followed by error-free reception of the message is acknowledged. If this acknowledgement is not received within a waiting time T_W, the preamble and message are sent again. This process repeats until the positive acknowledgement is received.

In Protocol C T_E and T_W are chosen to achieve given probabilities p_A and p_S that $T_A \leq T_E$ and $T_S < T_W$, where T_A and T_S are the acquisition time and service time random variables, respectively. Given p_A, T_E can be determined from the acquisition time confidence estimate derived in Section 3.5.3. This estimate is rather loose and gives a long delay, which can be reduced using a tighter estimate. However, knowledge of the acquisition time probability distribution is then necessary. If the probability distribution for T_S is also known, minimization of average delay with respect to p_A and p_S is possible.

Once synchronization has been achieved, transmitted data bits are decoded with bit-error probability p_B derived in Section 2.3. In an independent-error channel, the probability P_c of error-free reception of an ℓ-bit message is

$$P_c = (1-p_B)^{\ell}$$

$$\approx 1-\ell p_B \quad , \quad \ell p_B \ll 1 \tag{4.2.1}$$

For Protocols A and B, the average number of message repetitions before correct reception is therefore

$$\bar{r} = \sum_{r=1}^{\infty} r\, P_c(1-P_c)^{r-1} = 1/P_c \tag{4.2.2}$$

Similarly, for Protocol C the number of preamble/message transmissions before error-free reception is

$$\bar{r}_1 = \frac{1}{p_A p_S P_c} \tag{4.2.3}$$

Assuming that the number of active users is known and constant, let $\bar{T}_A$ be the mean acquisition time. The average message delays D for Protocols A, B and C are as follows:

$$D = \begin{cases} \bar{T}_P + \bar{T}_A + (\frac{1}{2} + \frac{1}{P_c})T_m \quad , & \text{Protocol A} \\ \bar{T}_P + \bar{T}_A + \bar{T}_S + T_m/P_c \quad , & \text{Protocol B} \\ [\bar{T}_p + T_E + T_m + (1-p_A p_S P_c)T_W]/(p_A p_S P_c) \quad , & \text{Protocol C} \end{cases} \tag{4.2.4}$$

where $T_m = \ell T_b$ is the message duration. Furthermore, the channel capacity C is a decreasing function of the average channel-occupation time $\bar{T}_{CO}$ (the average time during which an active user occupies the forward channel) which is given below for each of Protocols A, B and C.

$$\bar{T}_{CO} = \begin{cases} \bar{T}_S + \bar{T}_A + (\frac{1}{2} + \frac{1}{P_c})T_m \ , & \text{Protocol A} \\ 2\bar{T}_S + \bar{T}_A + T_m/P_c \ , & \text{Protocol B} \\ (T_E + T_m)/(p_A p_S P_c) \ , & \text{Protocol C} \end{cases} \qquad (4.2.5)$$

From eqns. (4.2.4) and (4.2.5), comparisons of average delay and channel capacity between Protocols A, B and C can be made as follows:

(i) Average delay for Protocol A is less than that for Protocol B and channel capacity for Protocol A is greater than that for Protocol B if $T_m/2 < \bar{T}_S$, and conversely.

(ii) Since $T_E > \bar{T}_A$ and $p_A p_S < 1$, average delay for Protocol B is less than that for Protocol C if $\bar{T}_S < T_E - \bar{T}_A$.

(iii) Similarly, average delay for Protocol A is less than that for Protocol C unless T_m is very large.

(iv) Note that $\bar{T}_{CO} < D$ for Protocol C but the converse is true for Protocols A and B. Therefore if $2\bar{T}_S$ is large compared with $T_E - \bar{T}_A$ (e.g. in cases where a large number of parallel correlators are used in the synchronizer, or in cases where round trip delays to a geosynchronous satellite are involved), Protocol C may yield a greater channel capacity than Protocols A or B. In this case a trade-off between average delay and channel capacity exists if $\bar{T}_S < T_E - \bar{T}_A < 2\bar{T}_S$.

The above discussions serve only as a rough guideline for protocol selection. More accurate delay analysis, as given in the following sections, must consider the number of active users as a random variable. Further analysis

necessitates the specifications of system parameters from which numerical results are obtained. It is assumed that $\bar{T}_P = 0$ and $\bar{T}_S = \bar{T}_K = 0.01$ sec., values typical for a terrestrial network, and that $\ell > 1000$ bits. Under such assumptions the application of Protocol B is appropriate.

4.3 Delay-Throughput Analysis for Protocol B

4.3.1 Effects of PNR and Delay Components on Total Delay

In Section 4.2, average message delay D and average channel-occupation time $\bar{T}_{CO}$ are derived for different protocols assuming that channel occupancy M is fixed. In reality, M varies in time as users access the channel at random and occupy the channel for a random duration. Thus variations in M must be taken into account when averaging message delay and channel-occupation time. It is desirable to express D and $\bar{T}_{CO}$ as functions of average channel occupancy $\bar{M}$ so that the average throughput corresponding to a given average delay may be obtained via Little's formula [K7],

$$\bar{M} = \lambda \bar{T}_{CO} \tag{4.3.1}$$

Unfortunately, no simple relationship exists between D (or $\bar{T}_{CO}$) and $\bar{M}$ because $\bar{T}_{CO}$ (and thus D) and $\bar{M}$ are inter-dependent. It is possible to gain some insight into the relationship between $\bar{T}_{CO}$ and $\bar{M}$ by examining the effects of individual delays and the PNR level on $\bar{T}_{CO}$ as function of M, again assumed to be fixed in time. Such examinations and subsequent analysis can only be pursued using numerical examples. Results will be obtained using system para-

meters shown in Tables 2.3.1 and 3.7.1, with $V_S = 1.7$, $V_L = 1.0$ and $\bar{T}_S = 0.01$ sec., and assuming co-channel users to be sources of Gaussian noise.

Figure 4.3.1 shows a family of $\bar{T}_{CO}$-vs.-M curves at different levels of PNR with K=1. These curves show that $\bar{T}_{CO}$ increases rapidly at a given M when PNR decreases below 60 dB-Hz. On the other hand, increase in PNR above 80 dB-Hz does not bring about any improvement (decrease) in $\bar{T}_{CO}$. For PNR $\geq$ 60 dB-Hz, a channel occupancy M_o exists such that $\bar{T}_{CO}$ is minimum and insensitive to changes in M whenever $M<M_o$. When $M>M_o$, $\bar{T}_{CO}$ increases rapidly with M. The parts of the curve where $M<M_o$, $M\approx M_o$ and $M>>M_o$ are called the "flat", "knee" and "ascent", respectively.

The flat of a $\bar{T}_{CO}$-vs.-M curve is very important for the operation of a SSMA channel because in this region small fluctuations in M do not affect the averages, $\bar{T}_{CO}$ and D, and operation of the channel is therefore stable. On the other hand, at the ascent of a $\bar{T}_{CO}$-vs.-M curve, increases in M cause $\bar{T}_{CO}$ to increase, which causes further increases in M and $\bar{T}_{CO}$, and so on. Operation of the channel is therefore unstable. Thus, stable operation of the SSMA channel with the given parameters is possible only if PNR $\gtrsim$ 60 dB-Hz with PNR = 70 dB-Hz being a good operating point. Given the shape of the $\bar{T}_{CO}$-vs.-M curves, it is reasonable to suggest that for PNR $\geq$ 60 dB-Hz; (i) $\bar{T}_{CO}$-vs.-$\bar{M}$ curves have the same shape as the $\bar{T}_{CO}$-vs.-M curves; (ii) the flats of corresponding $\bar{T}_{CO}$-vs.-$\bar{M}$ and $\bar{T}_{CO}$-vs.-M curves have the same level, but the knee of the $\bar{T}_{CO}$-vs.-$\bar{M}$ curve

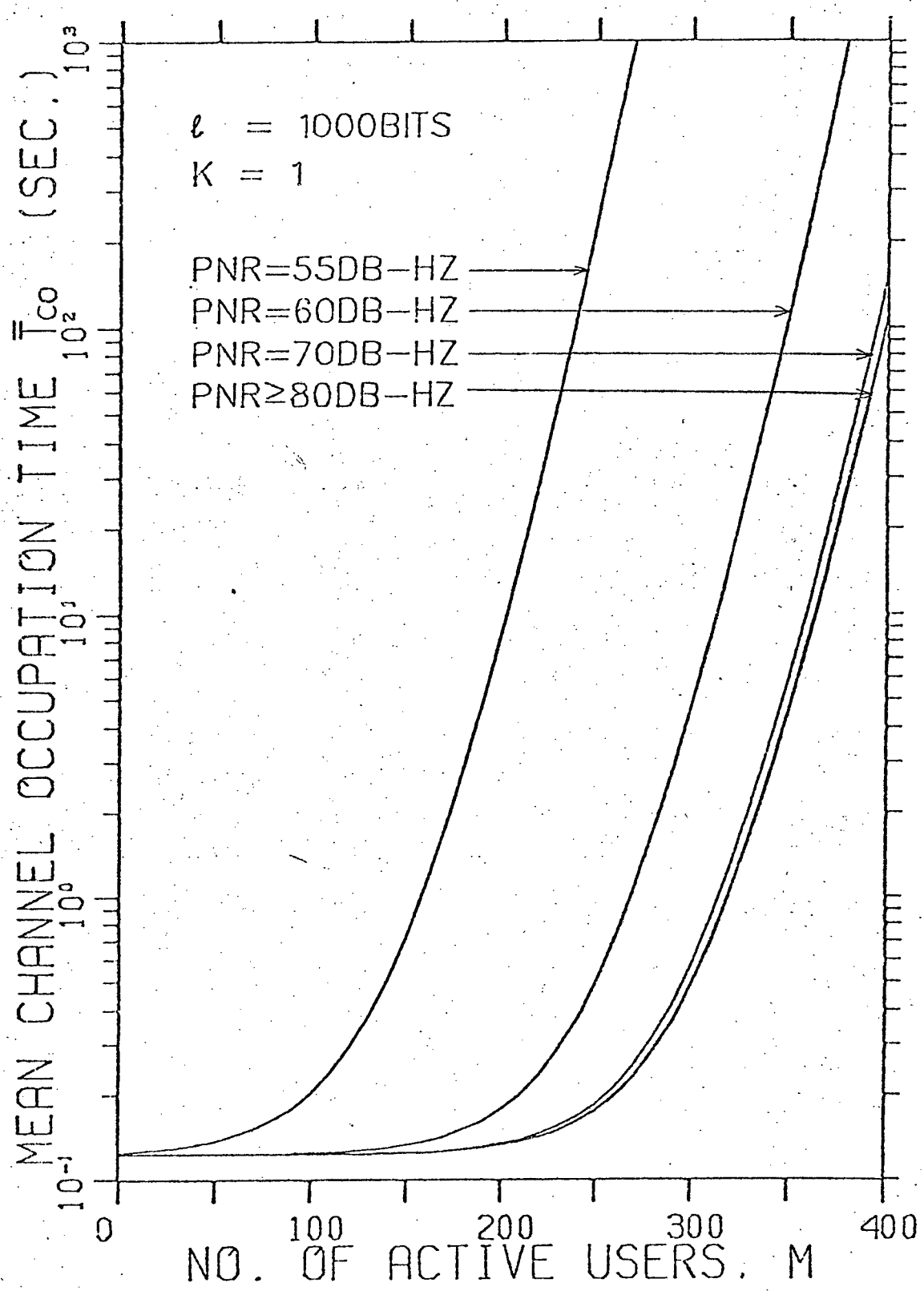

Fig. 4.3.1 Mean channel occupation time $\bar{T}_{CO}$ vs. number of active users M for various PNR values.

is closer to the origin, i.e., it occurs at $\bar{M}_o < M_o$; (iii) the ascent of the $\bar{T}_{CO}$ -vs.-$\bar{M}$ curve does not occur in reality because it corresponds to an unstable channel where M could increase indefinitely and $\bar{M}$ is thus undefined. However, this part of the curve will be included to facilitate discussions on channel stability in a later section.

Assuming that $\bar{T}_p$, $\bar{T}_K$ and thus $\bar{T}_S$ are independent of M, then $\bar{T}_{CO}$ and D, as given in eqns. (4.2.4) and (4.2.5), are related to M through the delay components $\bar{T}_A$ and T_m/P_c. Figure 4.3.2 gives a comparison between $\bar{T}_A$, T_m/P_c and $\bar{T}_{CO}$ as functions of M with PNR = 70 dB-Hz and K=1. It shows that both $\bar{T}_A$ and T_m/P_c are constant with respect to M for small values of M, and increase with M for large values of M, with T_m/P_c increasing at a much faster rate than $\bar{T}_A$. Therefore, the knee and ascent of the $\bar{T}_{CO}$-vs.-M curve are influenced mainly by T_m/P_c. Figure 3.4.2 also shows that with K=1, the level of the flat is caused mainly by $\bar{T}_A$ which is about five times T_m. However, $\bar{T}_A$ can be reduced to less than T_m if K>5.

4.3.2 Delays as Functions of Average Channel Occupancy

Assuming that $\bar{T}_p$ and $\bar{T}_K$ are independent of M, it is shown in Section 4.3.1 that T_m/P_c is the main cause for changes of $\bar{T}_{CO}$ and D relative to M. Therefore, fluctuations of M in time do not significantly change the contribution of $\bar{T}_A$ to $\bar{T}_{CO}$ calculated using a fixed M, provided that the envelope correlators of each synchronizer incorporates some form of automatic gain control which

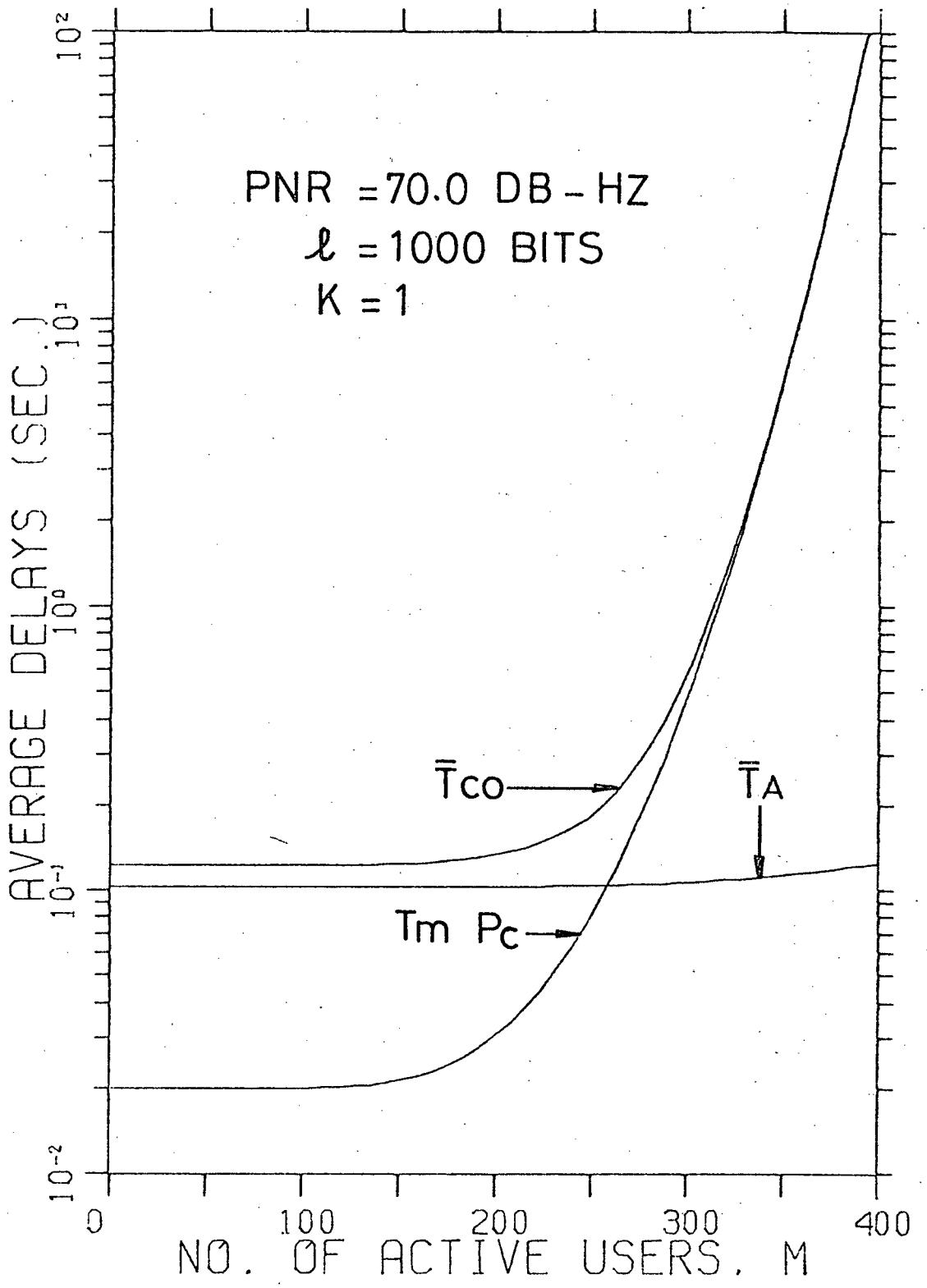

Fig. 4.3.2 Comparison of contributions of $\overline{T}_A$ and T_m/P_c to $\overline{T}_{CO}$ at different levels of channel occupancy.

responses to changes in M. On the other hand, re-evaluation of T_m/P_c to account for changes of M about a given average value $\bar{M}$ is necessary.

When M changes in time, P_c as given by eqn. (4.2.1) is no longer valid. Assuming that M does not change within each bit transmission period T_b (i.e. $\lambda T_b << 1$), and letting $p_B(M_k)$ be the bit-error probability for the k-th bit of a message, expressed as function of the channel occupancy M_k during the k-th bit period, then

$$P_c = \prod_{k=1}^{\ell} [1-p_B(M_k)]$$

$$\geq 1 - \sum_{k=1}^{\ell} p_B(M_k) \qquad (4.3.2)$$

Let $P_M(m)$ be the probability that M=m for a given value of $\bar{M}$. Further assume that values of M for adjacent bit periods are independent. Then the average probability of correctly receiving a message is bounded by

$$\bar{P}_c \geq 1 - \ell \bar{p}_B \qquad (4.3.3)$$

where

$$\bar{p}_B = \sum_{m=1}^{\infty} P_M(m)\, p_B(m) \qquad (4.3.4)$$

Thus replacing T_m/P_c by $T_m/\bar{P}_c$ in eqns. (4.2.4) and (4.2.5) would account for the fluctuations in M and result in expressions for D and $\bar{T}_{CO}$ as functions of $\bar{M}$. Assuming equality in (4.3.3), values of D and $\bar{T}_{CO}$ thus obtained are somewhat pessimistic and result in a steeper ascent.

The above analysis presumes the availability of the probability distribution for M. Unfortunately, analytical derivation of $P_M(m)$ is very difficult because it involves the interaction of different random processes in a complex manner. If T_{CO} is constant, then M has a Poisson distribution because the arrival process is Poisson. This leads to the hypothesis H_o that even if T_{CO} is random, the probability distribution of M is still Poisson. This hypothesis is tested by performing χ^2-tests to examine the goodness of fit between sets of data on frequency of each M value and corresponding sets of frequencies predicted by the Poisson distribution. Data are obtained from computer simulations of a discrete model of the system written in the GPSS simulation language[1] [G4]. Because the simulation runs are time consuming and expensive, only a representative set of parameters (ℓ=1000 bits, PNR=70 dB-Hz, K=1, V_s=1.7, V_L=1.0, other parameters as given in Tables 2.3.1 and 3.7.1) is used, with arrival rate λ ranging from 10 messages/sec. to 1000 messages/sec. In all cases considered, results[2] indicate acceptance of H_o with a 0.05 level of significance. Therefore, given average channel occupancy $\bar{M}$, the probability distribution for M is approximately

$$P_M(m) = \frac{\bar{M}^m}{m!} e^{-\bar{M}} \quad , \quad m=0,1,2,\cdots \tag{4.3.5}$$

---

[1]A program listing is given in Appendix 3.

[2]Results of goodness of fit tests are presented in Appendix 4.

The above results are not applicable to the knee and ascent of the $\bar{T}_{CO}$-vs.-$\bar{M}$ curve because here the channel is actually unstable. Nevertheless, $P_M(m)$ as given by eqn. (4.3.5) will be used for computation of the entire $\bar{T}_{CO}$-vs.-$\bar{M}$ curve so as to determine the position of the knee. Although this position is now subjected to some ambiguity, it is expected that this ambiguity is small.

Two families of $\bar{T}_{CO}$-vs.-$\bar{M}$ curves for different message lengths with K=1 and PNR = 60 dB-Hz and 70 dB-Hz are shown in Fig. 4.3.3. These curves all have the same shape. Increasing ℓ has the effect of translating a curve towards the upper-left corner, i.e. an increase in the level of the flat and a decrease in its length, as a result of increase in T_m and increasing rate of reduction of P_c relative to $\bar{M}$. $\bar{T}_{CO}$-vs.-$\bar{M}$ curves for different values of K with ℓ = 1024 bits and PNR = 70 dB-Hz are shown in Fig. 4.3.4. Evidently, when K increases to a value at which $\bar{T}_A < T_m$, further increases in K results in insignificant reduction in $\bar{T}_{CO}$ and are therefore not worthwhile. Note that similar D-vs.-$\bar{M}$ curves may be obtained by subtracting $\bar{T}_K$=0.01 sec. from the $\bar{T}_{CO}$ values.

4.3.3 Channel Stability

In the immediately preceding two sections it is stated that some parts of the $\bar{T}_{CO}$-vs.-$\bar{M}$ curves do not represent the actual channel behaviour because the channel is unstable with the result that the $\bar{M}$ values do not exist. An explanation of this phenomenon is offered in this section by exploring the relationships between $\bar{T}_{CO}$-vs.-$\bar{M}$ curves and the message arrival rate λ.

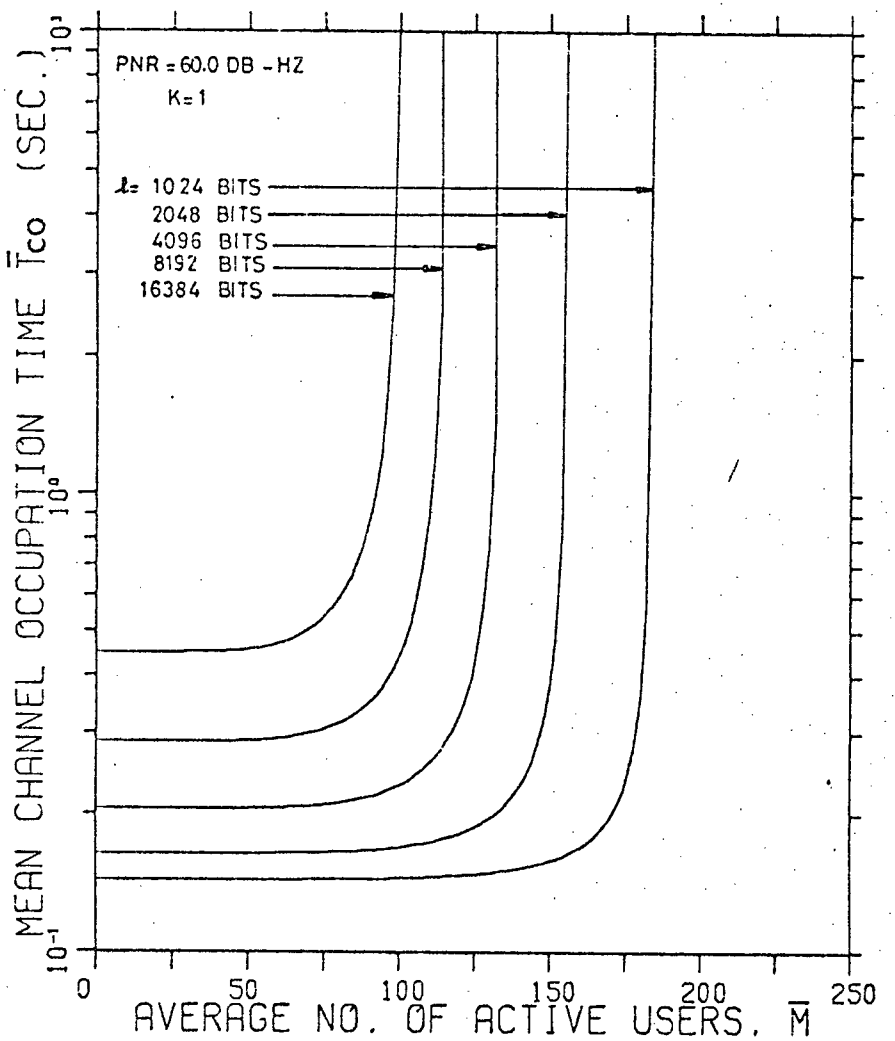

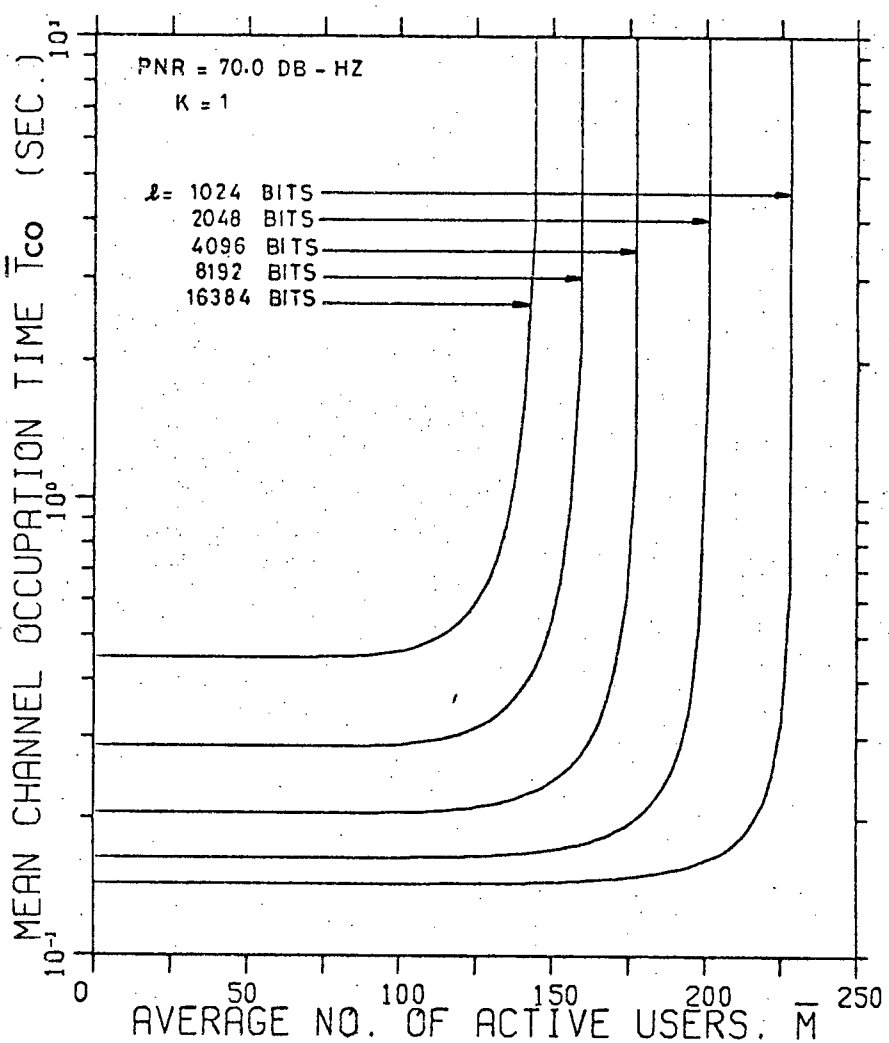

Fig. 4.3.3 Mean channel occupation time $\overline{T}_{CO}$ vs. average number of active users $\overline{M}$ for various message lengths ℓ.

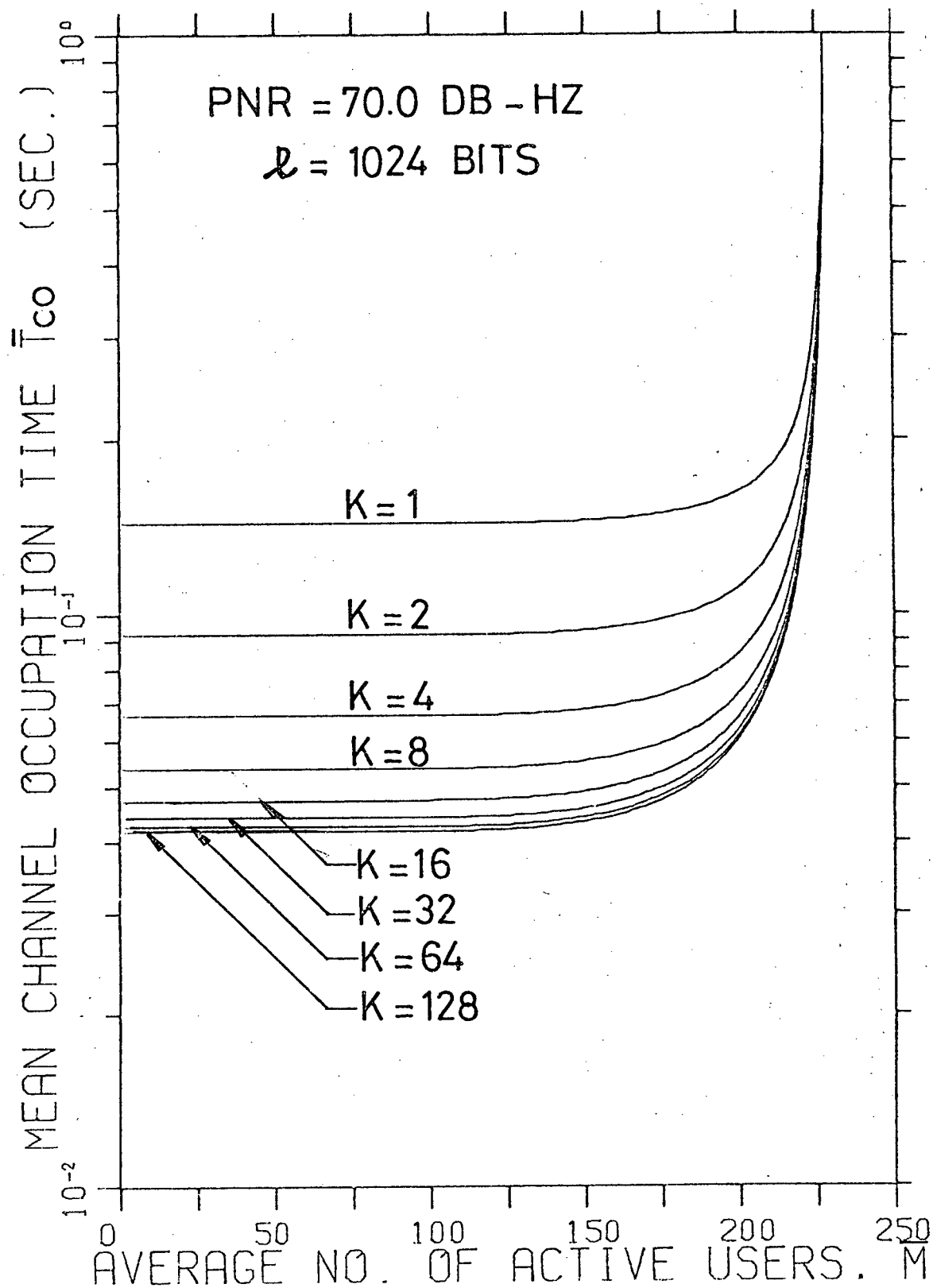

Fig. 4.3.4 Effect of increasing K on mean channel occupation time $\overline{T}_{CO}$.

$\bar{T}_{CO}$, $\bar{M}$ and λ are related by Little's formula given by eqn. (4.3.1). Given λ and an appropriate $\bar{T}_{CO}$-vs.-$\bar{M}$ curve, the values of $\bar{T}_{CO}$ and $\bar{M}$ satisfying Little's formula are given by the intersection of the $\bar{T}_{CO}$-vs.-$\bar{M}$ curve with a straight line through the origin with slope $1/\lambda$ (assuming scales for both axis are linear). Such intersections can be interpreted as the steady state operating point of the channel. The existence and number of steady state operating points may be classified under three possible cases illustrated in Fig. 4.3.5. For any given $\bar{T}_{CO}$-vs.-$\bar{M}$ curve, a critical arrival rate λ_{cr} exists such that

case 1: $\lambda > \lambda_{cr}$ and there are no operating points;

case 2: $\lambda = \lambda_{cr}$ and there is a unique operating point $(\bar{M}_1, \bar{T}_{CO1})$;

case 3: $\lambda < \lambda_{cr}$ and there are two operating points, $(\bar{M}_2, \bar{T}_{CO2})$ and $(\bar{M}_3, \bar{T}_{CO3})$.

The value $1/\lambda_{cr}$ is given by the slope of the line which goes through the origin and is tangent to the given $\bar{T}_{CO}$-vs.-$\bar{M}$ curve.

To analyze the channel stability for the three different cases, consider changes of channel occupancy in time. It is affected by the rates of arrival and departure of channel users. If there are M channel users and each spends T_{CO} sec. in the channel, the rate of departure is M/T_{CO}. Taking averages, therefore, yields

$$\frac{d\bar{M}}{dt} = \lambda - \frac{\bar{M}}{\bar{T}_{CO}} \qquad (4.3.6)$$

Consider $\bar{M}$ and $\bar{T}_{CO}$ in eqn. (4.3.6) as short term averages and apply the equation to the three cases.

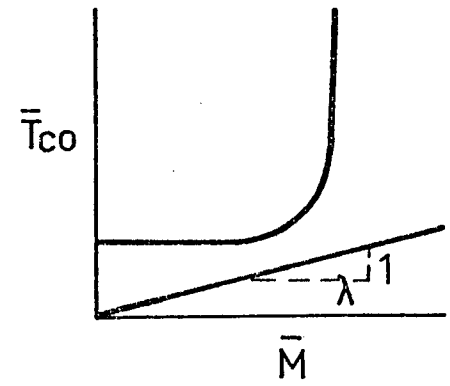

CASE 1: $\lambda > \lambda_{cr}$

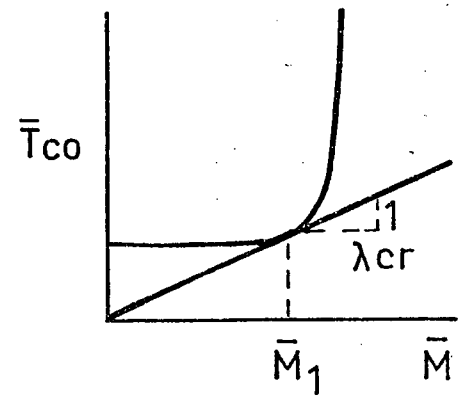

CASE 2: $\lambda = \lambda_{cr}$

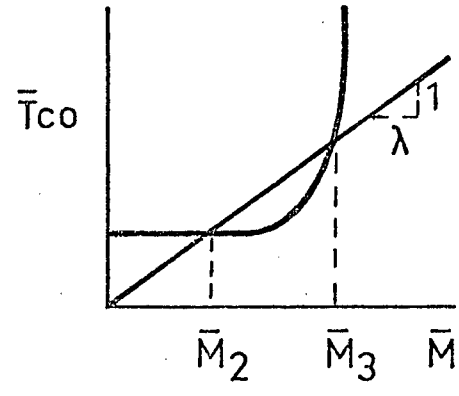

CASE 3: $\lambda < \lambda_{cr}$

Fig. 4.3.5 Graphical solutions of Little's formula as applied to the SSMA channel for three different cases of λ values.

case 1: $\lambda > \bar{M}/\bar{T}_{CO}$ for all $\bar{M}$, therefore $d\bar{M}/dt > 0$ and the channel occupancy increases without bound. The channel is unstable.

case 2: If $\bar{M} \neq \bar{M}_1$, then $\lambda > \bar{M}/\bar{T}_{CO}$ and $d\bar{M}/dt > 0$. Therefore if $\bar{M} < \bar{M}_1$, then $\bar{M}$ drifts toward $\bar{M}_1$ at which point $d\bar{M}/dt = 0$. However, if $\bar{M} > \bar{M}_1$, then $\bar{M}$ increases without bound. The channel is unstable because any small disturbance that causes positive deviation of the short term $\bar{M}$ from the operating point may lead to instability.

case 3: By the same arguments, the channel is unstable at operating point $(\bar{M}_3, \bar{T}_{CO3})$ but stable at operating point $(\bar{M}_2, \bar{T}_{CO2})$. At $\bar{M}_3$, a small increase in $\bar{M}$ causes it to drift towards infinity, whereas at $\bar{M}_2$, $\bar{M}$ always converges back to $\bar{M}_2$ after a disturbance causes $\bar{M}$ to deviate from $\bar{M}_2$, provided the distrubance is not large enough to cause $\bar{M}$ to reach or exceed $\bar{M}_3$.

The following conclusions may be drawn from the above discussions:

(i) The channel is always unstable if $\lambda \geq \lambda_{cr}$.

(ii) Stable operation of the channel is possible (at least in the short term) if $\lambda < \lambda_{cr}$. However, there is a non-zero probability that deterioration of receiver signal to noise ratio over a few message durations, caused by a large number of arrivals, an increase in noise, or fading, results in channel instability.

An unstable channel is said to have failed when average delays approach infinity. Although mean time to channel failure has been derived for slotted ALOHA channels [K3], similar analysis is not feasible for the SSMA channel. One expects that the mean time to channel failure is a decreasing function of

the "stability margin", defined as the distance between $\bar{M}_2$ and $\bar{M}_3$. Thus the SSMA channel may be expected to sustain stable operation for a long period of time if $\lambda \ll \lambda_{cr}$. λ_{cr} is plotted against message length ℓ with K=1,4,16 and with the limiting case where $T_A=0$, in Fig. 4.3.6 for PNR = 60 dB-Hz and Fig. 4.3.7 for PNR = 70 dB-Hz. Increasing K has the effect of increasing λ_{cr} at small values of ℓ, but such effect is not appreciable at large values of ℓ. The limiting case gives the maximum λ_{cr} for any given $\bar{T}_S$ and ℓ.

When channel failure occurs, both Protocols A and B described in Section 4.2 have provisions for recovery which require users to take appropriate action if no acknowledgement is received within T_R sec. of accessing the channel.

4.3.4 Delay-Throughput Characteristics and Channel Capacity

A necessary condition for the stable operation of a SSMA channel is that the average rate of message arrival at the channel equals the average rate of message departure. Therefore the average throughput S of a stable SSMA channel is simply

$$S = \lambda \text{ messages/sec.} \tag{4.3.7}$$

or

$$S = \lambda\ell \text{ bits/sec.} \tag{4.3.8}$$

The upper bound on S is called the channel capacity C. Since any $\lambda \geq \lambda_{cr}$ results in instability, whereas stable operation is possible for $\lambda < \lambda_{cr}$, the channel capacity is therefore

$$C = \lambda_{cr}\ell \text{ bits/sec.} \tag{4.3.9}$$

Delay-vs.-throughput curves (D-S curves) are obtained by plotting the

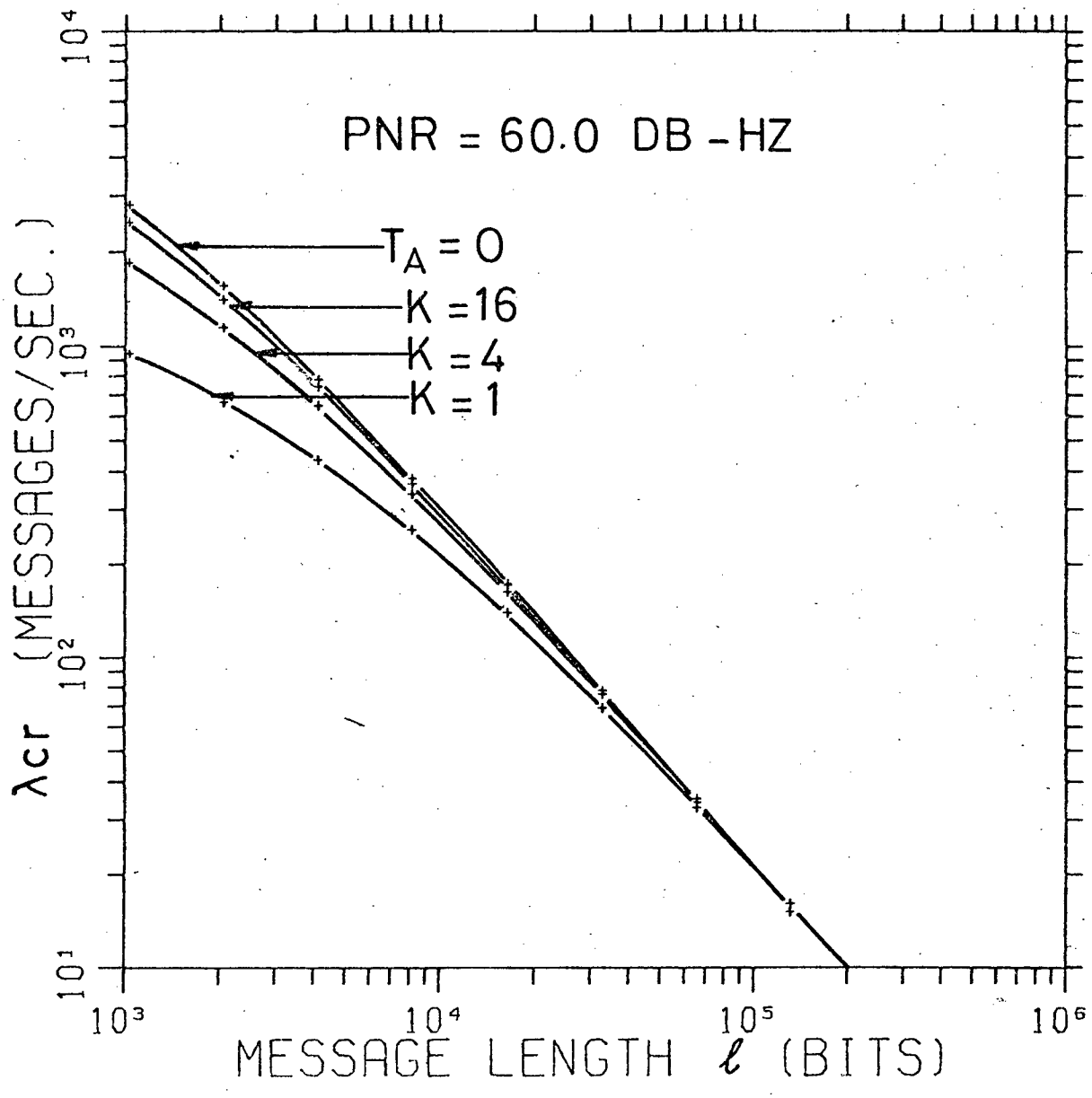

Fig. 4.3.6 Critical values of arrival rate λ_{cr} vs. message length ℓ, with PNR = 60.0 dB-Hz.

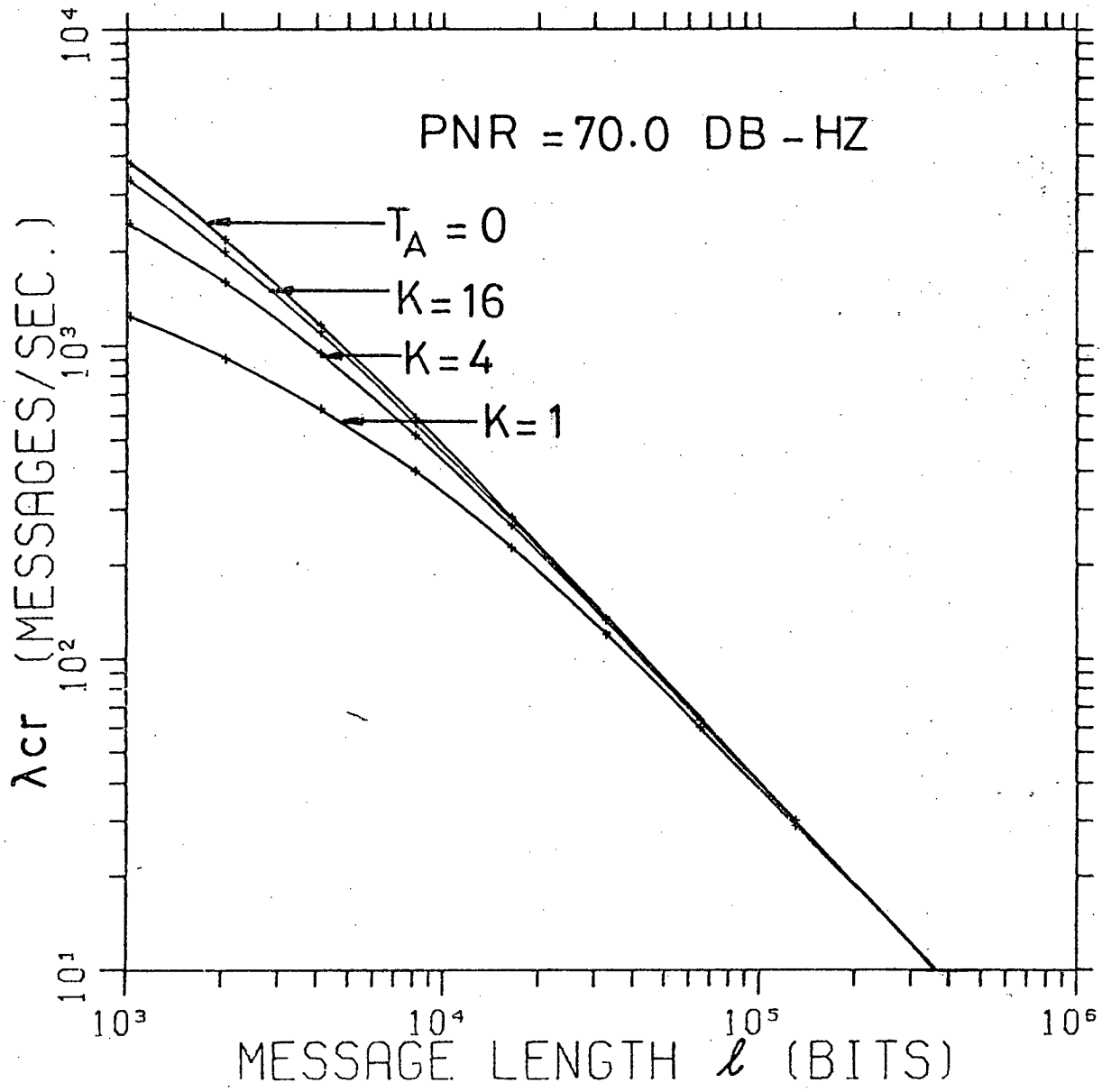

Fig. 4.3.7 Critical values of arrival rate λ_{cr} vs. message length ℓ, with PNR = 70.0 dB-Hz.

average delay D corresponding to a given average channel occupancy $\bar{M}$ against average throughput S calculated from eqn. (4.3.8) with

$$\lambda = \bar{M}/\bar{T}_{CO} \tag{4.3.10}$$

Families of D-S curves for different message lengths are shown in Fig. 4.3.8 with K=1,4 and PNR = 60 dB-Hz, and in Fig. 4.3.9 with K=1,4 and PNR = 70 dB-Hz. Each of these curves possesses the following general properties:

(i) A maximum throughput, corresponding to the channel capacity, exists.

(ii) The maximum throughput partitions the curve into two parts, a first part where average delay is relatively constant, and a second part where average delay increases without bound as throughput drops to zero.

(iii) The first part of the curve corresponds to the delay-throughput characteristic of the SSMA channel when it is stable in the steady state.

(iv) The second part of the curve indicates channel instability. When arrival rate is too high, the channel follows this curve upward and to the left in time so that eventually the channel fails.

Comparing the different curves, the following observations can be made:

(1) Average delay D increases with message length ℓ. D increases at a slower rate than ℓ when ℓ is small and the acquisition time and service time overhead is significant. When ℓ is large, D increases at the same rate as ℓ.

(2) When the channel is stable, the average delay is insensitive to changes in the PNR level, provided these changes do not cause the channel to become unstable.

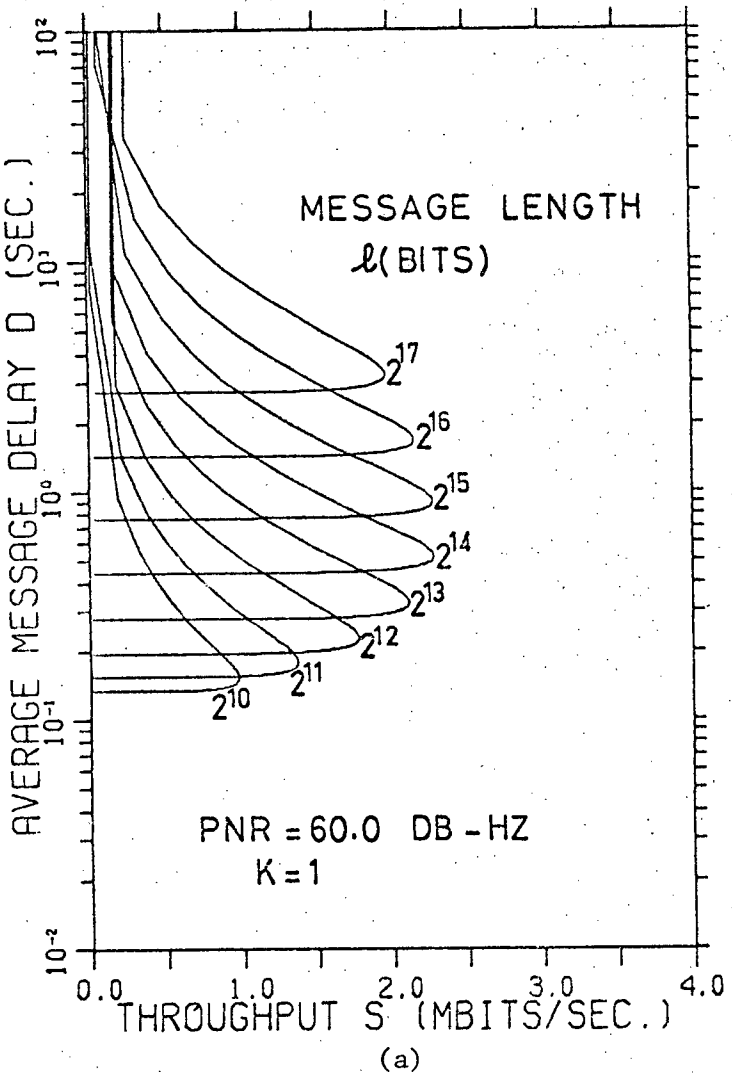

(a)

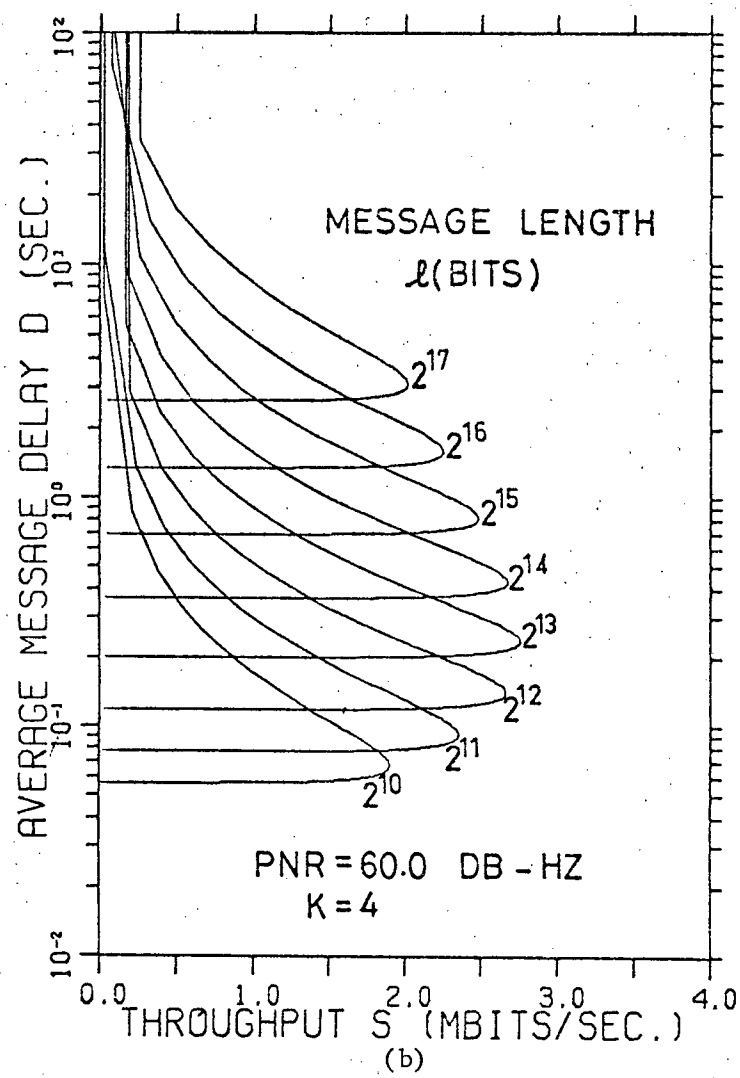

(b)

Fig. 4.3.8 SSMA delay-vs.-throughput curves for various message lengths with PNR = 60.0 dB-Hz and (a) K = 1, (b) K = 4.

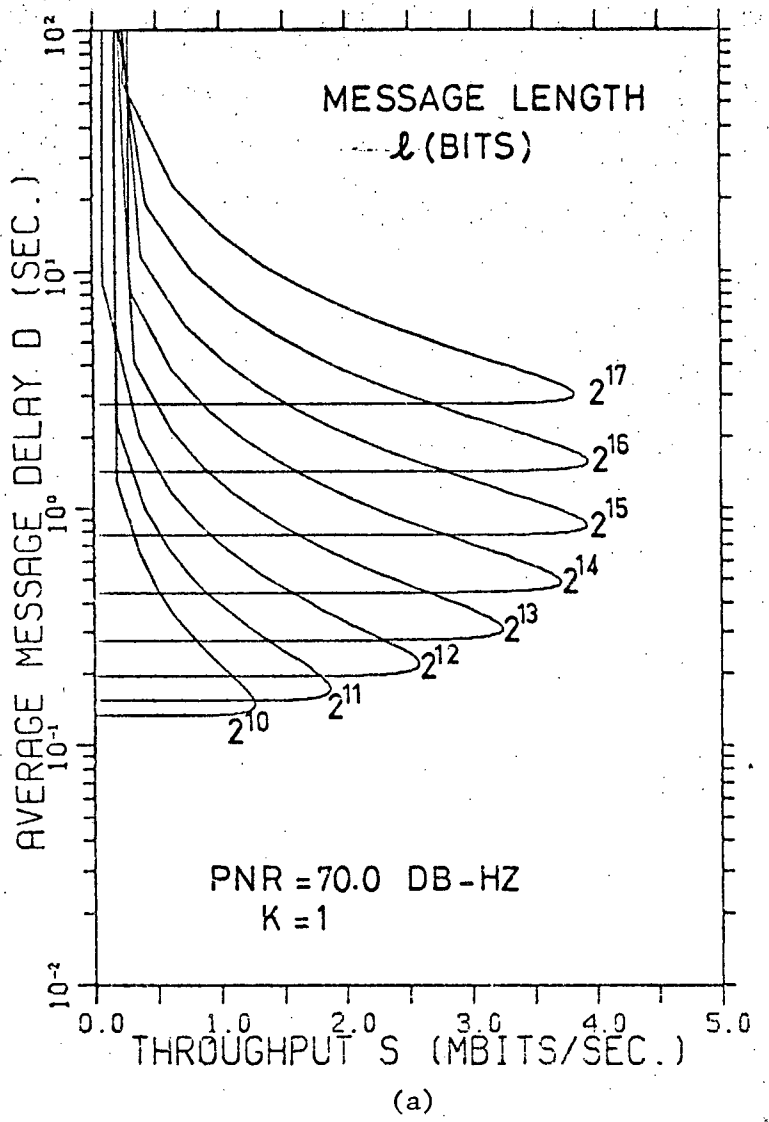

(a)

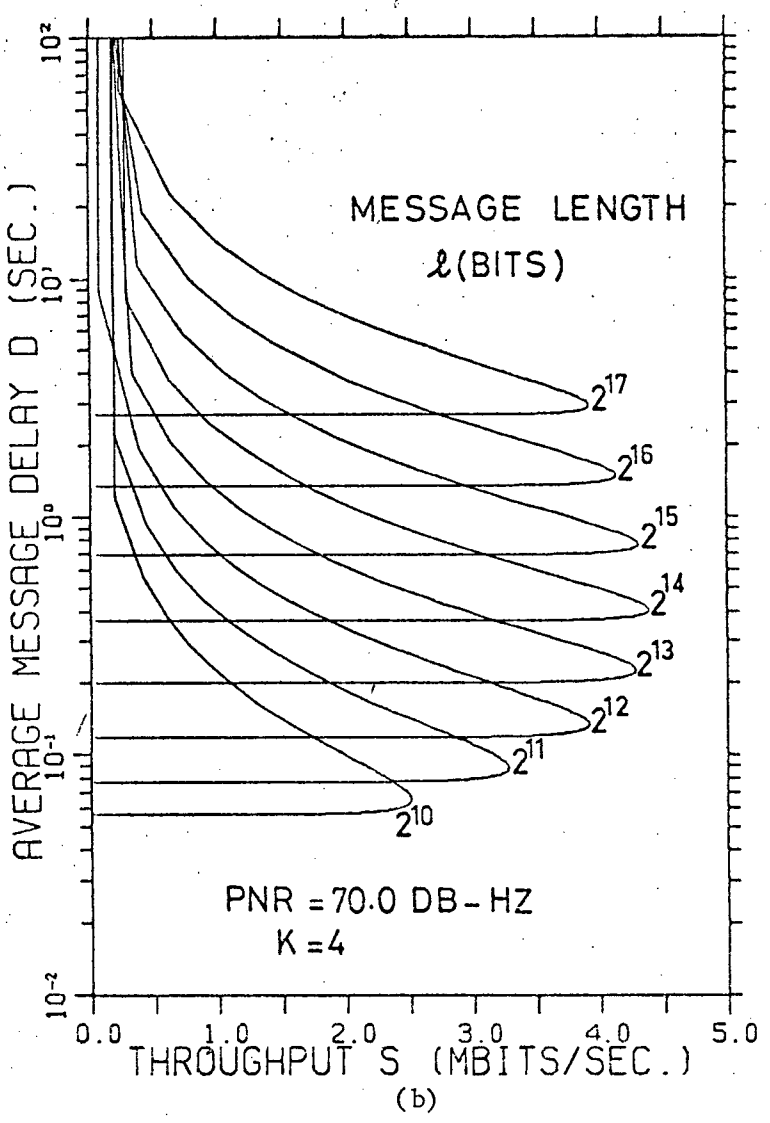

(b)

Fig. 4.3.9 SSMA delay-vs.-throughput curves for various message lengths with PNR = 70.0 dB-Hz and (a) K = 1, (b) K = 4

(3) When K is increased, D decreases, but at a decreasing rate. Decreases in D caused by increases in K become insignificant when ℓ or K are large.

(4) Channel capacity C increases when PNR is increased to 70 dB-Hz from 60 dB-Hz. In fact, C increases at a decreasing rate for increases of PNR to levels below 80 dB-Hz, and reaches a constant plateau for PNR $\geq$ 80 dB-Hz.

(5) C increases with K when ℓ is fixed. Such an increase becomes less significant at large values of ℓ.

(6) For any given values of PNR and K, C can be maximized with respect to ℓ.

Observations (5) and (6) above are further substantiated by Figs. 4.3.10 and 4.3.11, which show values of channel capacity versus message lengths for K=1,4,16 and for the limiting case, T_A=0, with PNR = 60 dB-Hz and PNR = 70 dB-Hz, respectively. The limiting case gives an upper bound to the achievable channel capacity for given values of PNR, ℓ and $\bar{T}_S$. These figures show that as K is increased, the optimum ℓ which maximizes C decreases and the maximum C is increased until it reaches the upper bound given by T_A=0, at which point the corresponding optimum ℓ is the lowest possible. Further decrease in the optimum value of ℓ and increase in the upper bound for C can only be achieved by decreasing the average service time $\bar{T}_S$. The two figures also show that increasing PNR from 60 dB-Hz to 70 dB-Hz results in increases in both the maximum C and the corresponding optimum ℓ, for any given K.

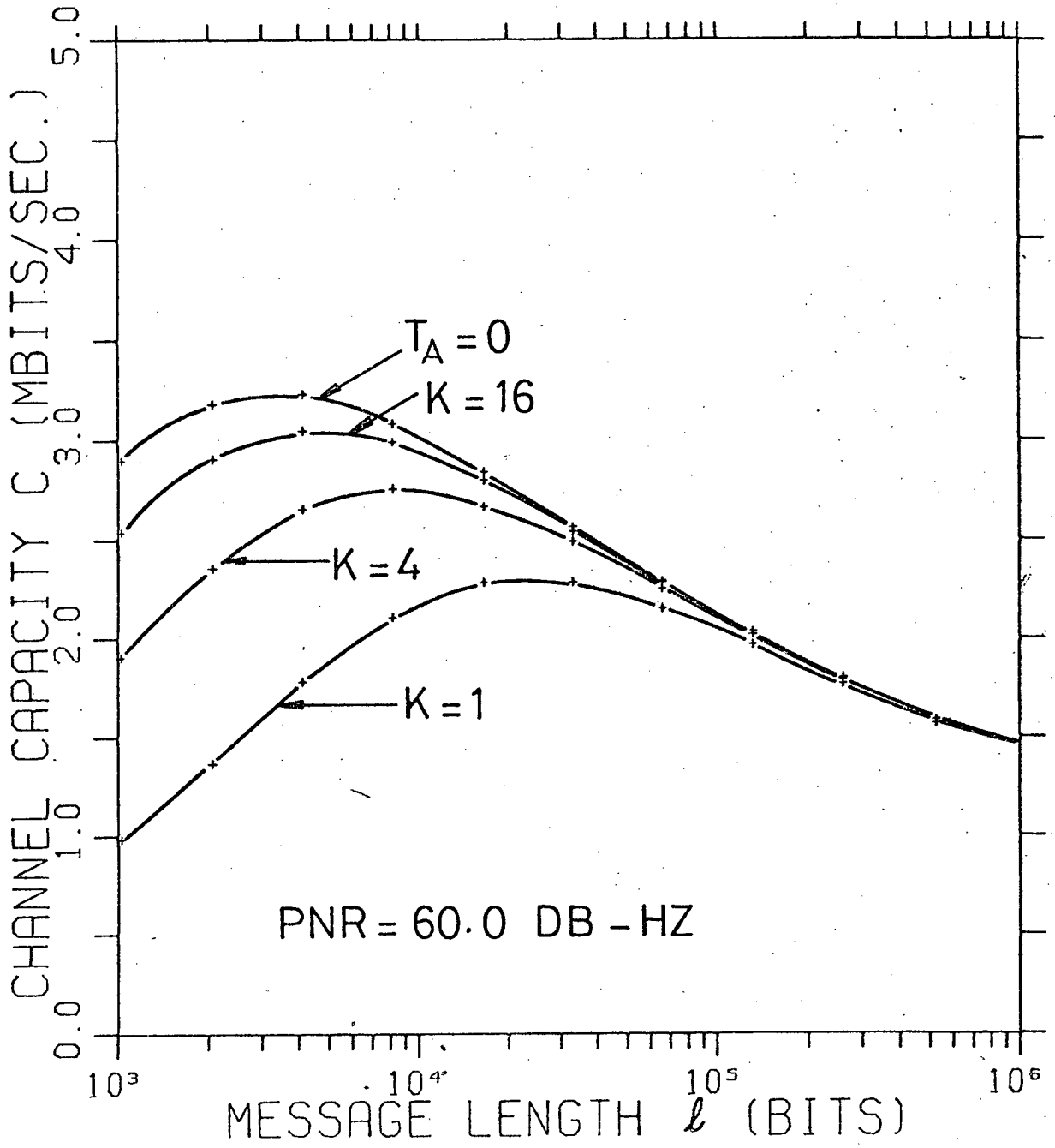

Fig. 4.3.10 SSMA channel capacity C vs. message length ℓ, with PNR = 60.0 dB-Hz.

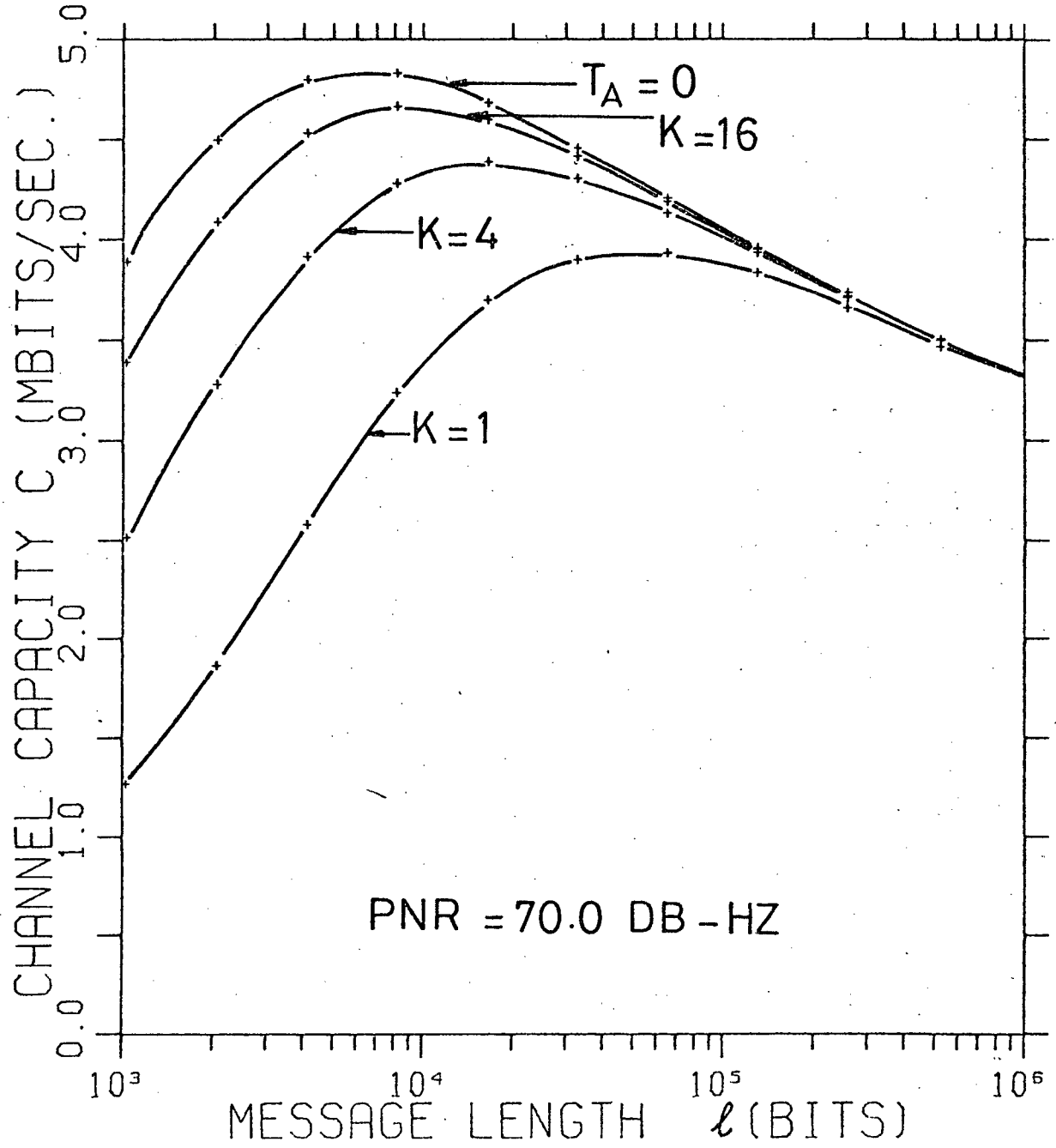

Fig. 4.3.11 SSMA channel capacity C vs. message length ℓ, with PNR = 70.0 dB-Hz.

The above results were obtained assuming users' codes are uncorrelated. If Gold's codes of length L=511 are used, results from Ch. 2 indicate that the above results remain valid if mean channel occupancy, average throughput and channel capacity are reduced by a factor of five.

5. COMPARISON WITH OTHER MULTIPLE ACCESS TECHNIQUES

5.1 Introduction

Contention multiple access schemes enable a number of users to access a broadcast channel independently without the complexity of centralized scheduling of dedicated frequency or time slots. Messages are usually assembled into fixed length packets for transmission.

The simplest contention scheme allows a user to transmit a packet whenever one is ready. When one user starts transmitting before another user has finished, a collision occurs which obliterate both users' packets and retransmissions are necessary. To minimize the chance of a collision between the same packets when retransmitting, retransmissions are randomly delayed according to a given delay distribution. Such a multiple access scheme is know as "pure ALOHA" and its system throughput was analysed by Abramson [A4].

In pure ALOHA systems, packet collisions reduce system throughput, and the maximum throughput or channel capacity is R/2e where R is the transmission data rate. The probability of packet collisions is reduced by half if all transmissions start at the beginning of fixed time slots whose lengths equal the packet duration. Such a multiple access scheme is known as "slotted ALOHA" and it doubles the channel capacity of a comparable pure ALOHA system. However, global block synchronization becomes necessary and increases system complexity. Delay-throughput characteristics and system stability for slotted ALOHA multiple access have been extensively studied [K1,K3,L1,C1].

In all the analysis cited above, it is assumed that received packets are error-free if they have not encountered any collisions. This assumption is

valid when bandwidth and hence data rate is limited but power is unlimited, so that a negligible receiver bit-error rate can be achieved. If packets are transmitted in a wideband channel with limited power the above assumption is usually unreasonable. Unfortunately, delay-throughput analysis for slotted and pure ALOHA under wideband, limited power situations is unavailable. In this case increasing the data rate increases both the channel capacity and the bit-error rate. In addition to packets destroyed by collisions, packets distorted by channel noise are also retransmitted. When the data rate increases to a level where distorted packets cause a significant fraction of all retransmission traffic, channel capacity ceases to increase. Thus a maximum channel capacity exists at an optimum data rate. Detailed analysis is given in Sections 5.2 and 5.3 for slotted ALOHA and pure ALOHA, respectively, assuming additive white Gaussian channel noise. This assumption applies to most time-invariant channels. Analysis for other channels can be obtained by substituting for the appropriate message-error rate.

Improved channel capacities are achieved by contention multiple access schemes which employ more sophisticated transmission protocols, for example, carrier sense multiple access [K4] and busy-tone multiple access [T1]. Further improvements in channel capacities are obtained by combining contention and scheduling, as in split-channel reservation multiple access [T2]. With increasing system complexity, channel capacity ultimately approaches that of a perfect scheduling M/D/1 queueing channel. In this case channel capacity is equal to the data rate if transmissions are error-free, and somewhat less if channel errors necessitate retransmissions. Section 5.4 shows that in wideband

power-limited situations, an optimum data rate again maximizes the channel capacity.

Since SSMA operates with very simple transmission protocols, it is reasonable to compare its delay-throughput performance against that of ALOHA, the simplest multiple access scheme, and queueing, the ultimate. In Section 5.5, such comparisons are conducted on an equal-bandwidth, equal-single-user-power basis, using the channel model described in Section 2.2. Because the available bandwidth is not fully utilized by the ALOHA and queueing channels at data rates optimum with respect to the system parameters considered for SSMA, delay-throughput performance of m pure ALOHA, slotted ALOHA or queueing channels operating in parallel is also included in the comparison, where m is the number of channels that can be fitted into the available bandwidth at optimum data rate.

5.2 Delay-Throughput Characteristics of a Slotted ALOHA Channel with Additive Gaussian Noise

Assume that packets of fixed length ℓ bits are transmitted under slotted ALOHA using binary PSK at a bit rate of R bits/second. The channel is thus partitioned into time slots of ℓ/R sec. duration. If exactly one packet is transmitted in a given time slot, then the probability P_c of correct reception is as follows, where PNR and p_B denote, respectively, the receiver signal power to noise density ratio and the bit-error probability:

$$P_c = (1 - p_B)^{\ell} \tag{5.2.1}$$

$$p_B = \frac{1}{2} \operatorname{erfc}\left(\sqrt{\frac{PNR}{R}}\right) \tag{5.2.2}$$

where

$$\operatorname{erfc}(x) = \frac{2}{\sqrt{\pi}} \int_x^{\infty} e^{-t^2}\, dt \tag{5.2.3}$$

Now consider the general situation where one or more packets may be transmitted in a given slot. Let S denote the channel throughput, G the channel traffic, and D the average packet delay in seconds. Both S and G are steady state average values in packets/slot. To facilitate analysis, assume that the system satisfies the following conditions:

(i) Arrival of new packets constitutes a Poisson random process characterized by channel throughput S.

(ii) Automatic retransmission request (ARQ) error control is incorporated in packet transmissions. A packet is said to be blocked if the receiver detects errors in one or more packet bits, with errors caused either by a packet collision or by random channel noise. A packet collision always causes all packets involved to be blocked. A blocked packet is retransmitted after a random delay uniformly distributed over K slots.

Packets transmitted in a given slot are distinguished either as newly generated, or as blocked in one of K immediately preceding slots. Following the notations in the throughput derivation for slotted ALOHA in [K1], let q_n be the probability that a newly generated packet is received without error, and q_t be the probability that a previously blocked packet is received without

error. The average number of retransmission until a packet is received without error is

$$\frac{G}{S} - 1 = \frac{1 - q_n}{q_t} \tag{5.2.4}$$

so that

$$S = \frac{q_t}{1 + q_t - q_n} G \tag{5.2.5}$$

Consider the event E_o that one of the K immediately preceding slots does not cause a retransmission in the given slot and let its probability be q_o. This event occurs if, in that previous slot, no packets were transmitted, one packet was transmitted and received without error, or one or more packets were blocked but retransmissions do not occur in the given slot. Assume that packets in previous slots are generated by a Poisson random process characterized by channel traffic G. Thus

$$\begin{aligned} q_o &= e^{-G} + P_c G e^{-G} + (1 - P_c)(1 - \tfrac{1}{K}) G e^{-G} + \sum_{m=2}^{\infty} \frac{G^m}{m!} e^{-G}(1 - \tfrac{1}{K})^m \\ &= e^{-\frac{G}{K}} + P_c \frac{G}{K} e^{-G} \end{aligned} \tag{5.2.6}$$

A packet newly generated in the given slot is received without error if the event E_o occurs for each of the K immediately previous slots, the packet is the only one generated, and this packet is not distorted by channel noise. Therefore

$$q_n = q_o^K e^{-S} P_c \tag{5.2.7}$$

Now consider a previously blocked packet transmitted in the given slot.

This packet was blocked in one of K immediately previous slots, namely the j-th slot. Let E_1 be the event that the packet transmitted in the given slot is received without error, E_2 be the event that the packet was blocked in the j-th slot because of random bit errors, and E_3 be the event that the packet was blocked in the j-th slot because of a packet collision. Since the events E_2 and E_3 are mutually exclusive, the probability of a previously blocked packet being received without error is

$$q_t = \Pr(E_1 | E_2 \cup E_3)$$
$$= \frac{\Pr(E_1 \cap E_2) + \Pr(E_1 \cap E_3)}{\Pr(E_2) + \Pr(E_3)} \tag{5.2.8}$$

The individual probabilities are evaluated as follows:

$$\Pr(E_2) = e^{-G}(1 - P_c) \tag{5.2.9}$$

$$\Pr(E_3) = 1 - e^{-G} \tag{5.2.10}$$

$$\Pr(E_1 \cap E_2) = e^{-G}(1 - P_c) q_o^{K-1} e^{-S} P_c \tag{5.2.11}$$

$$\Pr(E_1 \cap E_3) = q_o^{K-1} e^{-S} P_c \sum_{\ell=1}^{\infty} e^{-G} \frac{G^{\ell}}{\ell!} \left(1 - \frac{1}{K}\right)^{\ell}$$
$$= \left(e^{-\frac{G}{K}} - e^{-G}\right) q_o^{K-1} e^{-S} P_c \tag{5.2.12}$$

Substituting eqns. (5.2.9) to (5.2.12), inclusive into eqn. (5.2.8) yields

$$q_t = \frac{[e^{-\frac{G}{K}} - e^{-G} + e^{-G}(1 - P_c)]\, q_o^{K-1} e^{-S} P_c}{e^{-G}(1 - P_c) + 1 - e^{-G}}$$

$$= q_c\, q_o^{K-1}\, e^{-S}\, P_c \qquad (5.2.13)$$

where q_c is defined as

$$q_c = \frac{e^{-\frac{G}{K}} - e^{-G} P_c}{1 - e^{-G} P_c} \qquad (5.2.14)$$

Eqns. (5.2.5), (5.2.7) and (5.2.13) constitue a system of non-linear equations from which throughput S may be solved for any given values of K, P_c and G. Furthermore, the packet delay D may be calculated from

$$D = \frac{3}{2} T_m + T_s + \frac{1 - q_n}{q_t} [(1 + \frac{K}{2}) T_m + T_s] \qquad (5.2.15)$$

where $T_m = \ell/R$ is the packet transmission time and T_s is the service time including propagation delay and time for acknowledgement. From these calculations, a delay-vs.-throughput (D-S) curve may be plotted for specific values of ℓ, R, PNR and K. A typical set of D-S curves[1] is shown in Fig. 5.2.1, where ℓ, R and PNR are fixed and K varies for each curve. The envelope of such a set of curves describes the optimum throughput-delay characteristics of a slotted ALOHA system where K varies adaptively according to the level of channel traf-

---

[1]In all calculations for D, it is assumed that $T_s = 0.01$ sec.

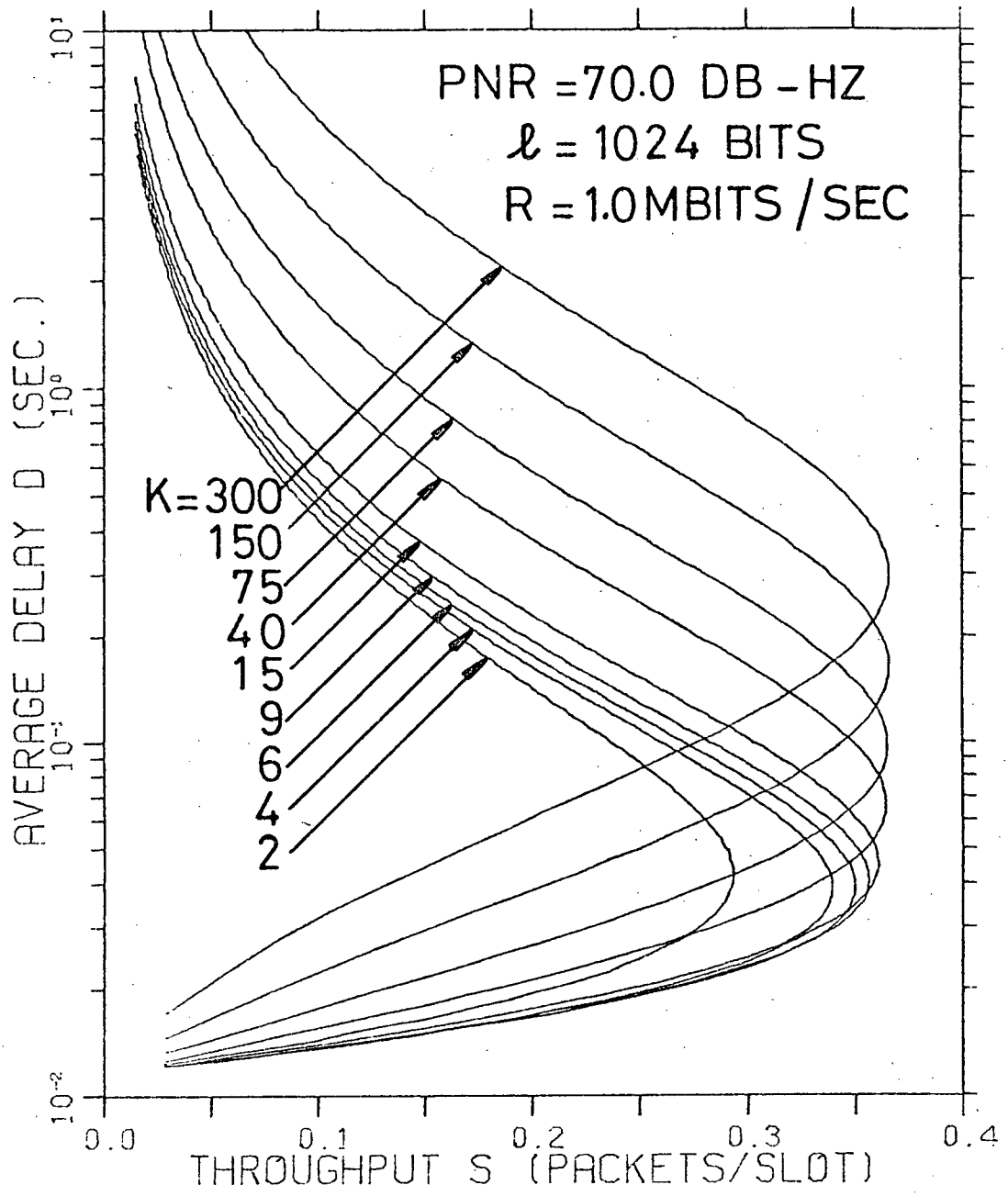

Fig. 5.2.1 A typical set of slotted ALOHA delay-vs.-throughput curves showing effects of different maximum retransmission delays in K slots.

fic. The maximum throughput for the optimized D-S curve is called the channel capacity C. For fixed values of ℓ and PNR an optimum bit rate R should exist to maximize the channel capacity C, assuming no bandwidth restrictions. This conclusion is based on the fact that an increase in R acts directly to increase the throughput; however, it also causes P_c to decrease which acts indirectly to decrease the throughput. Sets of optimized D-S curves[2] depicting the variation of delay-throughput characteristics and channel capacity with R, for fixed values of ℓ and PNR, are shown in Figs. 5.2.2 and 5.2.3. From these graphs optimum values of R (accurate to two significant digits) and the corresponding maximum channel capacities are obtained and tabulated in Table 5.2.1. Fig. 5.2.4 shows the relationships between packet length ℓ and D-S curves with channel capacities optimized over K and R, at fixed levels of PNR.

Table 5.2.1 and figures 5.2.2 to 5.2.4 inclusive, yield the following observations:

(i) At fixed PNR and ℓ values, there exists an optimum R at which channel capacity is maximized.

---

[2]To facilitate comparisons, throughput is converted to bits/sec. via the relation S bits/sec. = (S packets/slot)(ℓ bits/packet)/(ℓ/R sec./slot).

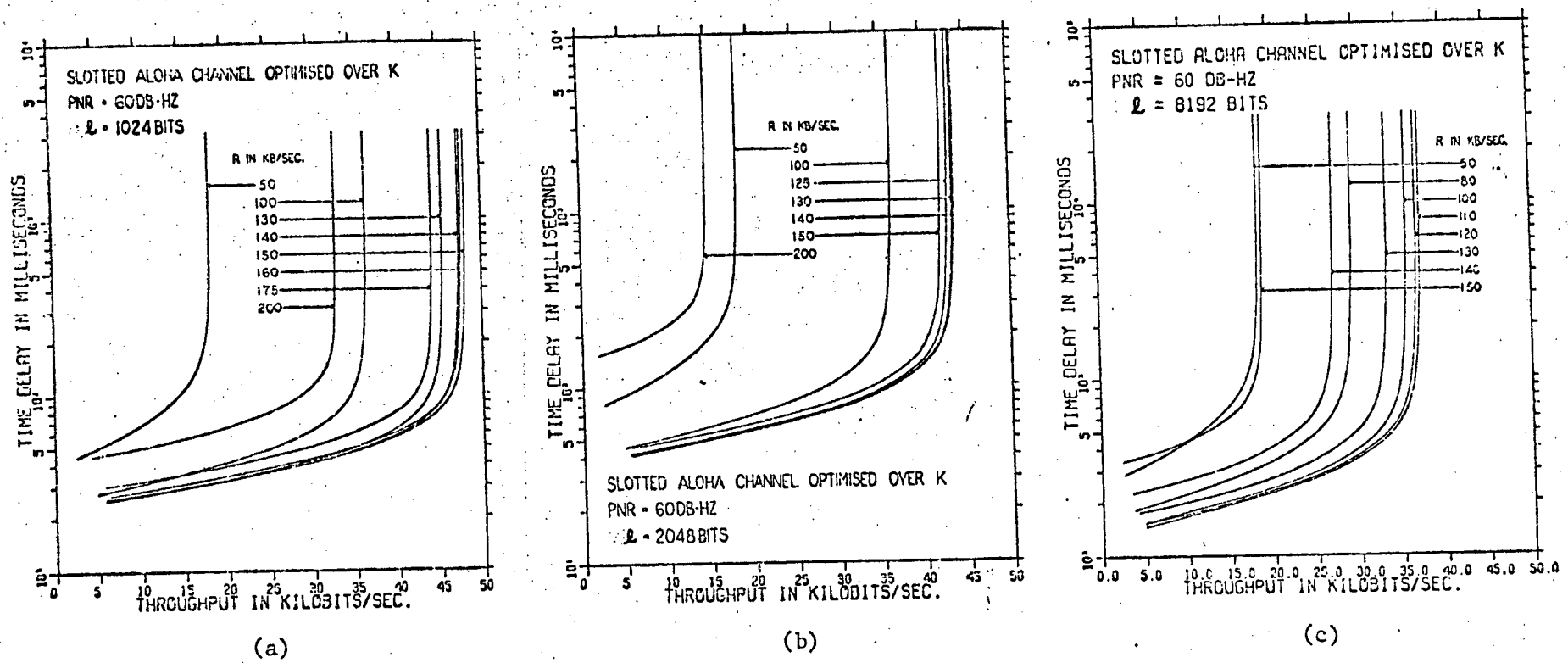

(a) (b) (c)

Fig. 5.2.2 Effects of different bit rates R on slotted ALOHA delay-vs.-throughput curves optimized over K with PNR = 60.0 dB-Hz and (a) ℓ = 1024 bits, (b) ℓ = 2048 bits, (c) ℓ = 8192 bits.

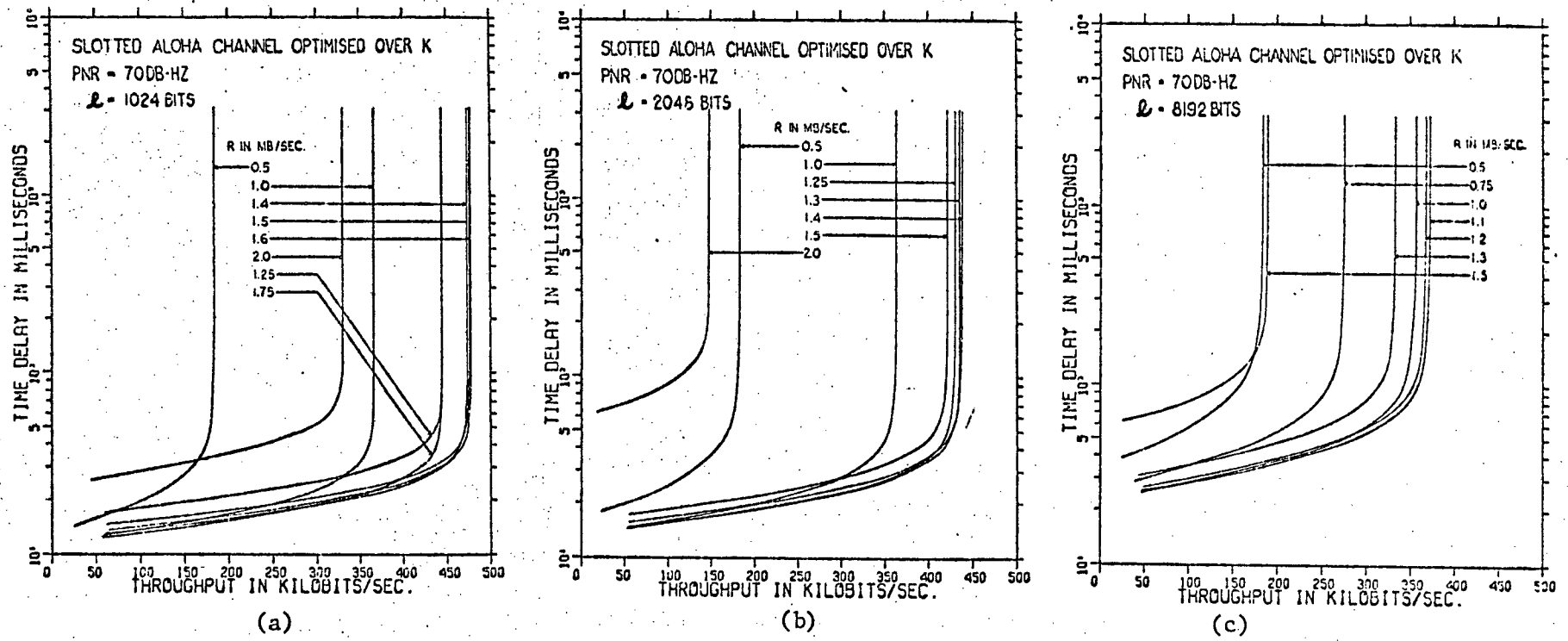

Fig. 5.2.3 Effects of different bit rates R on slotted ALOHA delay-vs.-throughput curves optimized over K with PNR = 70.0 dB-Hz and (a) ℓ = 1024 bits, (b) ℓ = 2048 bits, (c) ℓ = 8129 bits.

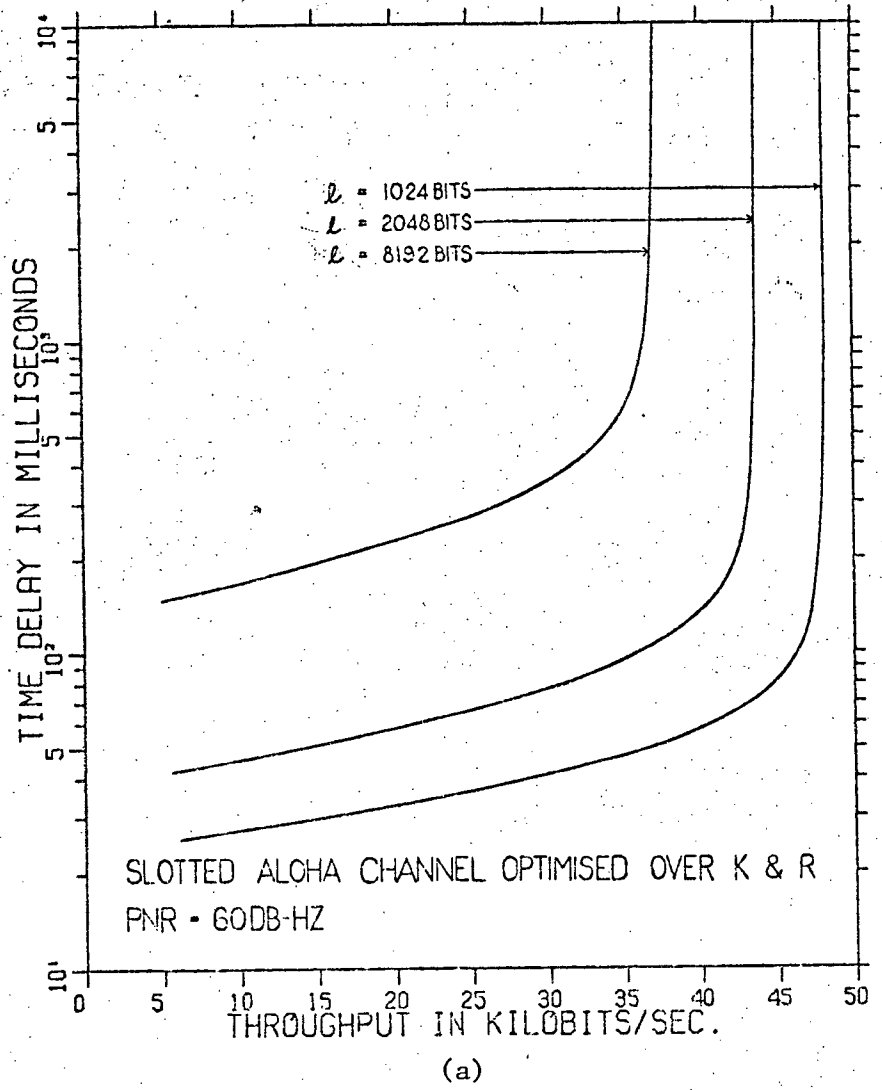

(a)

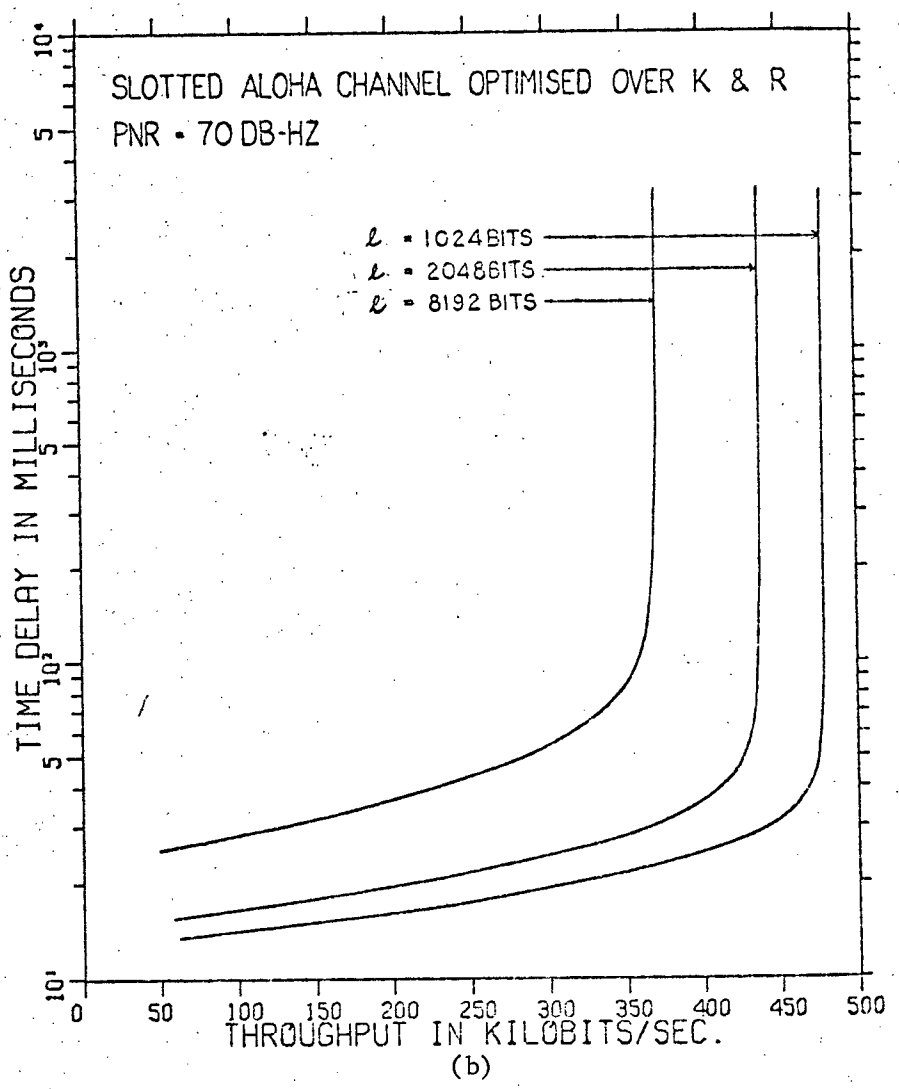

(b)

Fig. 5.2.4 Slotted ALOHA delay-vs.-throughput curves for different message lengths ℓ, optimized over K and R, with (a) PNR = 60.0 dB-Hz, (b) PNR = 70.0 dB-Hz.

Table 5.2.1 Optimum Values of Bit Rate R and Corresponding Maximum Channel Capacity C for Slotted ALOHA Channel with Additive Gaussian Noise

PNR (dB-Hz)	ℓ (bits)	R (bits/sec.)	C (bits/sec.)
60.0	1024	1.5×10^5	4.82×10^4
60.0	2048	1.4×10^5	4.37×10^4
60.0	8192	1.1×10^5	3.72×10^4
70.0	1024	1.5×10^6	4.77×10^5
70.0	2048	1.4×10^6	4.38×10^5
70.0	8192	1.1×10^6	3.72×10^5

(ii) At fixed PNR and ℓ, for any given level of throughput less than the channel capacity, there exists an optimum R, not necessarily the same as in (i), at which delay D is minimized.

(iii) Time delay D increases without bound as throughput approaches channel capacity, at which point the channel becomes unstable.

(iv) At a fixed level of PNR and throughput S, delay increases with packet length.

(v) Channel throughput decreases as packet length increases, if PNR and D are held constant.

5.3 Delay-Throughput Characteristics of a Pure ALOHA Channel with Additive Gaussian Noise

Let $T_m = \ell/R$ be the packet transmission time under pure ALOHA, where ℓ is the packet length and R is the transmission bit rate. A given packet is blocked either by collision with another packet transmitted within $\pm T_m$ sec. (the vulnerable period) of the start of transmission of the given packet, or as a result of Gaussian channel errors in the received packet. Assume that a blocked packet is retransmitted after a delay of $T_s + \tau$ sec. from the time of transmission of its last bit, where T_s is again the packet service time including propagation delay and acknowledgement time, and τ is a uniformly distributed random variable between 0 and T_r sec[1].

Given the received power to noise density ratio PNR, bit rate R and packet length ℓ, p_B and P_c are again given by eqns. (5.2.1) and (5.2.2).

Assume that new packets are generated by a Poisson random process with parameter λ_1. Therefore, average steady state channel throughput

$$S = \lambda_1 T_m \tag{5.3.1}$$

Consider a user who starts transmitting a packet at time t_o. Distin-

---

[1]Assume $T_r \geq 4 T_m$.

guishing this packet as either newly generated or previously blocked, let q_n be the probability that a newly generated packet is received without error, and q_t be the probability that a previously blocked packet is received without error. No attempt is made to further distinguish previously blocked packets as new packets or retransmissions. They are assumed to be generated by a Poisson process with parameter λ_2 such that average channel traffic

$$G = \lambda_2 T_m \tag{5.3.2}$$

The average number of retransmission until a packet is received without error is again

$$\frac{G}{S} - 1 = \frac{1 - q_n}{q_t} \tag{5.3.3}$$

so that

$$S = \frac{q_t G}{1 + q_t - q_n} \tag{5.3.4}$$

The probability q_n is derived as follows. The "vulnerable period" is the time interval $(t_o - T_m, t_o + T_m)$ in which initiation of any other packet transmissions causes a collision with the packet which begin transmission at t_o. A newly generated packet is successfully received if and only if the following events jointly occur:

E_a: no other new packets are generated in the vulnerable period;

E_b: no retransmissions of previously blocked packets begin in the vulnerable period; and

E_c: channel noise does not cause any bit errors. The probabilities for E_a and E_c are as follows:

$$\Pr(E_a) = e^{-2\lambda_1 T_m} = e^{-2S} \tag{5.3.5}$$

$$\Pr(E_c) = P_c \tag{5.3.6}$$

The derivation of $\Pr(E_b)$ is more involved. Assume that transmission of a packet started at time t and was blocked. Retransmission of this packet may start within the vulnerable period if the interval $(t+T_m+T_s,\ t+T_m+T_s+T_r)$ overlaps with the vulnerable period, as shown in Fig. 5.3.1. Thus the sole cause of retransmissions started in the vulnerable period is blocked transmissions generated in the interval $(t_o-T_s-T_r-2T_m,\ t_o-T_s)$. Partition this time interval into subintervals of equal length Δt and let Δt approach zero. Theories of Poisson processes stipulate probabilities in each subinterval as follows:

(i) $\lambda_2 \Delta t$ that one new or previously blocked packet was generated;

(ii) $1-\lambda_2 \Delta t$ that no packet was generated; and

(iii) a negligible probability that two or more packets were generated.

Let p(t) be the probability that a subinterval at $(t,\ t+\Delta t)$ does not cause a retransmission in the vulnerable period. Then

$$\Pr(E_b) = \prod_k p(t_k) \quad , \quad t_o-T_s-T_r-2T_m < t_k < t_o-T_s$$

$$= \exp\{\sum_k \ln\,[p(t_k)]\} \tag{5.3.7}$$

where ln(x) denotes the natural logarithm of x. Considering the amount of overlap in Fig. 5.3.1,

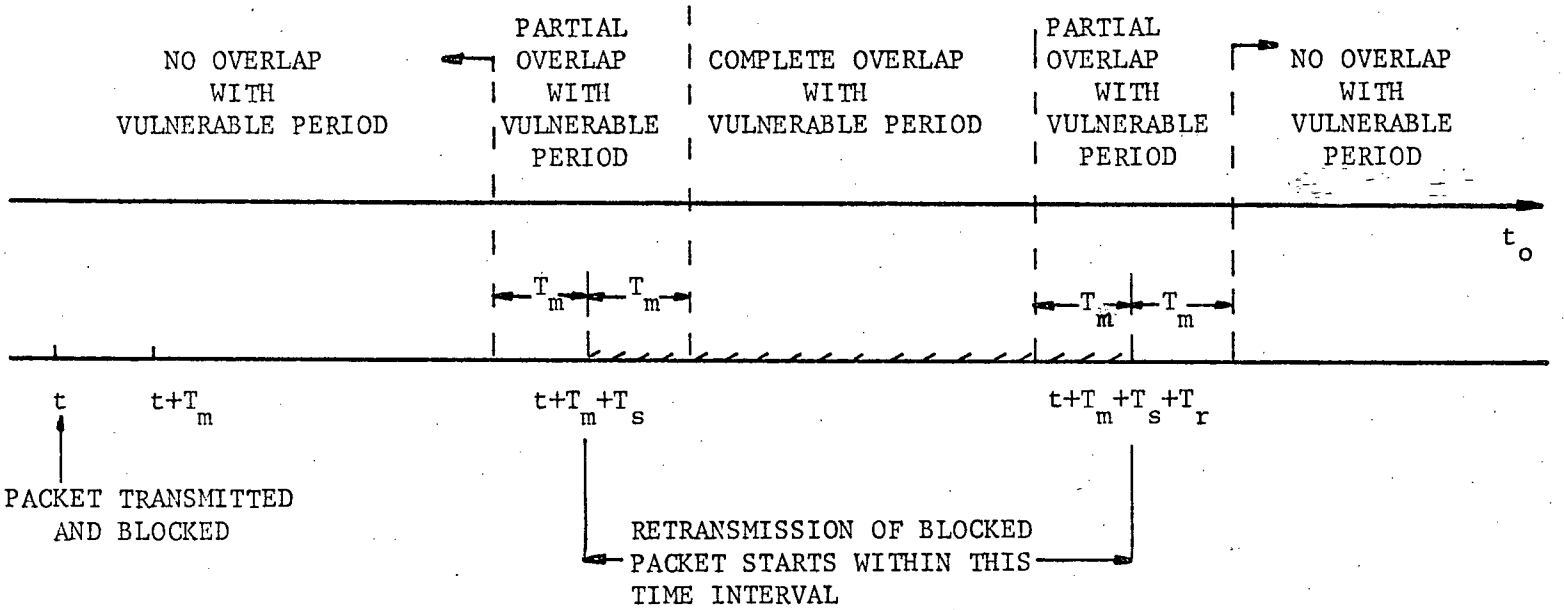

Fig. 5.3.1 Comparison between the time period in which retransmission of a packet, previously blocked at time t, may begin and the vulnerable period of a new transmission at time t_0. The extent of overlapping of the two time periods is proportional to the probability that the two packets collide.

$$p(t) = \begin{cases} 1-\lambda_2 \Delta t(1-e^{-2G_{P_c}})(t_o-t-T_s)/T_r\ , & t_o-2T_m-T_s<t<t_o-T_s \\ 1-\lambda_2 \Delta t(1-e^{-2G_{P_c}})2T_m/T_r\ , & t_o-T_s-T_r<t<t_o-2T_m-T_s \\ 1-\lambda_2 \Delta t(1-e^{-2G_{P_c}})(t+2T_m+T_s+T_r-t_o)/T_r\ , & t_o-2T_m-T_s-T_r<t<t_o-T_s-T_r \end{cases} \tag{5.3.8}$$

Since $\ln(1+x) \cong x$ for $x \ll 1$ and Δt approaches zero,

$$\ln[p(t)] \cong \begin{cases} -\lambda_2 \Delta t(1-e^{-2G_{P_c}})(t_o-t-T_s)/T_r\ , & t_o-2T_m-T_s<t<t_o-T_s \\ -\lambda_2 \Delta t(1-e^{-2G_{P_c}})2T_m/T_r\ , & t_o-T_s-T_r<t<t_o-2T_m-T_s \\ -\lambda_2 \Delta t(1-e^{-2G_{P_c}})(t+2T_m+T_s+T_r-t_o)/T_r\ , & t_o-2T_m-T_s-T_r<t<t_o-T_s-T_r \end{cases} \tag{5.3.9}$$

The function $-\ln[p(t)]/\Delta t$ is shown graphically in Fig. 5.3.2. The area under $-\ln[p(t)]/\Delta t$ in the j-th subinterval is simply $-\ln[p(t_j)]$. Hence $-\sum_k \ln[p(t_k)]$ equals the area under the trapezoid in Fig. 5.3.2, and

$$\begin{aligned} \sum_k \ln[p(t_k)] &= -\lambda_2(1-e^{-2G_{P_c}})2T_m \\ &= -2G(1-e^{-2G_{P_c}}) \end{aligned} \tag{5.3.10}$$

Therefore,

$$Pr(E_b) = e^{-2G(1-e^{-2G_{P_c}})} \tag{5.3.11}$$

and the probability of a newly generated packet being received without error is

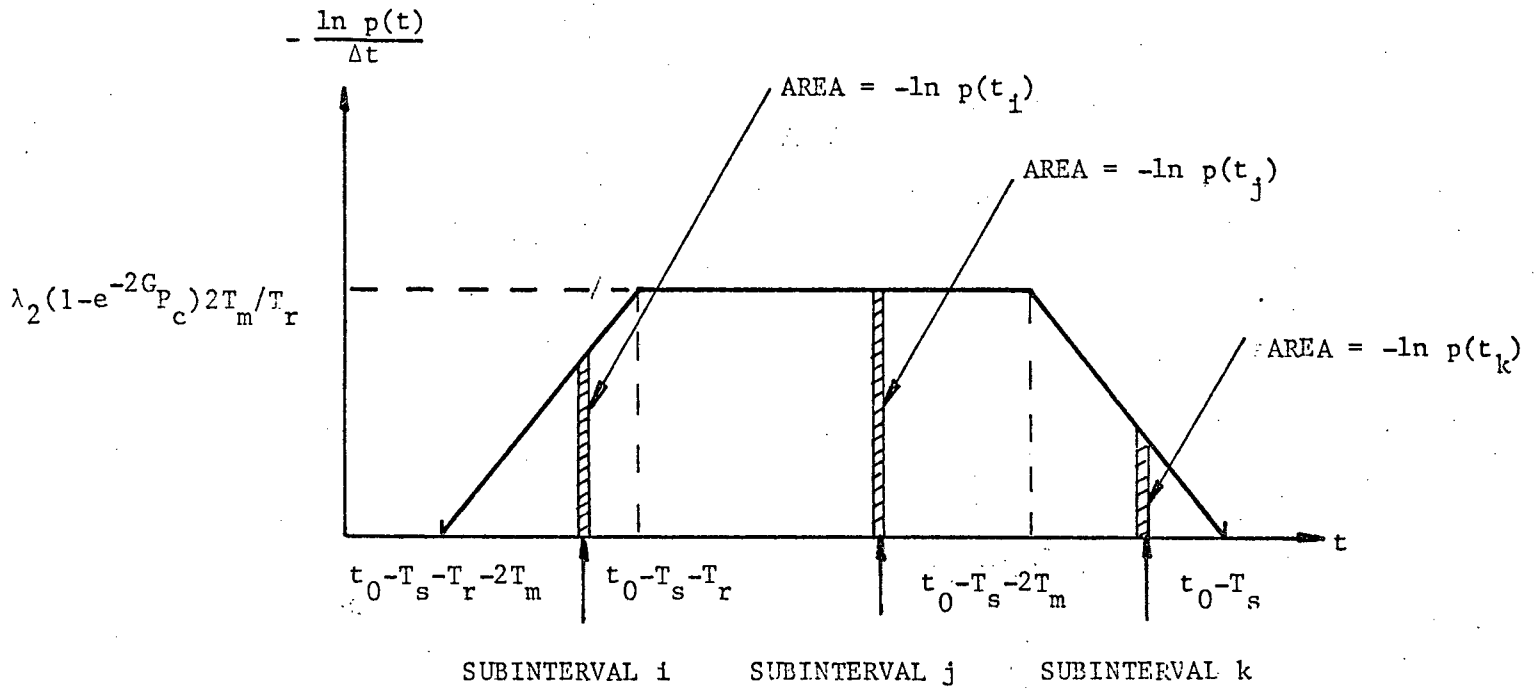

Fig. 5.3.2 $\{-\ln p(t)\}/\Delta t$ vs. t; p(t) is the probability that events occuring in the time interval (t, t+Δt) do not cause a retransmission within the vulnerable period of a packet transmitted at time t_0.

$$q_n = Pr(E_a)Pr(E_b)Pr(E_c)$$

$$= e^{-2S} e^{-2G(1-e^{-2G}P_c)} P_c \qquad (5.3.12)$$

To derive the probability q_n, assume that a packet was transmitted at time t_1 and was blocked, and that retransmission occurs at time t_0. The blockage at t_1 resulted from one of two mutually exclusive events.

E_1: a collision occurred, i.e. one or more additional packets were transmitted within the time interval $(t_1-T_m\ ,\ t_1+T_m)$;

E_2: no additional packets were transmitted in the time interval $(t_1-T_m,\ t_1+T_m)$ but one or more bit-errors were detected in the received packet.

From the retransmission delay distribution, t_1 is constrained within the time interval $(t_o-T_s-T_r-T_m\ ,\ t_o-T_s-T_m)$.

Define the event

E_3: no previously blocked packets (except the one transmitted at t_1) begin retransmission in the vulnerable period.

Let I_1 denote the time interval $(t_o-T_s-T_r-2T_m\ ,\ t_o-T_s)$ and I_2 denote the time interval $(t_1-T_m\ ,\ t_1+T_m)$. Note that I_1 includes I_2. Again partition I_1 into subintervals of equal duration Δt. If a subinterval $(t,t+\Delta t)$ does not fall within I_2, the probability $p(t)$ that this subinterval does not cause a retransmission in the vulnerable period is given by eqn. (5.3.8). For $t \in I_2$, this probability is modified as follows:

$$(p(t)|E_1,t\varepsilon I_2)=\begin{cases}1-[\lambda_2/(1-e^{-2G})]\Delta t(t_o-t-T_s)/T_r, & t_o-T_s-2T_m<t<t_o-T_s\\ 1-[\lambda_2/(1-e^{-2G})]\Delta t\ 2T_m/T_r, & t_o-T_s-T_r<t<t_o-T_s-2T_m\\ 1-[\lambda_2/(1-e^{-2G})]\Delta t(t+2T_m+T_s+T_r-t_o)/T_r, & t_o-T_s-T_r-2T_m<t<t_o-T_s-T_r\end{cases} \tag{5.3.13}$$

$$(p(t)|E_2,t\varepsilon I_2) = 1 \tag{5.3.14}$$

Taking natural logarithm and letting Δt approach zero yields

$$\ln(p(t)|E_1,t\varepsilon I_2)\cong\begin{cases}-[\lambda_2/(1-e^{-2G})]\Delta t(t_o-t-T_s)/T_r, & t_o-T_s-2T_m<t<t_o-T_s\\ -[\lambda_2/(1-e^{-2G})]\Delta t\ 2T_m/T_r, & t_o-T_s-T_r<t<t_o-T_s-2T_m\\ -[\lambda_2/(1-e^{-2G})]\Delta t(t+2T_m+T_s+T_r-t_o)/T_r, & t_o-T_s-T_r-2T_m<t<t_o-T_s-T_r\end{cases} \tag{5.3.15}$$

$$\ln(p(t)|E_2,t\varepsilon I_2) = 0 \tag{5.3.16}$$

Conditioned on t_1, the probability

$$(q_t|t_1) = e^{-2S}\ P_c\ .\ \Pr(E_3|E_1\cup E_2) \tag{5.3.17}$$

where

$$\Pr(E_3|E_1\cup E_2) = \frac{\Pr(E_1\cap E_3) + \Pr(E_2\cap E_3)}{\Pr(E_1) + \Pr(E_2)} \tag{5.3.18}$$

Evaluating each term in eqn. (5.3.18) yields

$$\Pr(E_1) = 1-e^{-2G} \tag{5.3.19}$$

$$Pr(E_2) = e^{-2G}(1-P_c) \tag{5.3.20}$$

$$Pr(E_1 \cap E_3) = P_r(E_3|E_1)Pr(E_1) \tag{5.3.21}$$

$$Pr(E_2 \cap E_3) = P_r(E_3|E_2)Pr(E_2) \tag{5.3.22}$$

Furthermore

$$Pr(E_3|E_1) = \prod_{\substack{\text{subintervals} \\ \varepsilon\, I_1-I_2}} p(t) \prod_{\substack{\text{subintervals} \\ \varepsilon\, I_2}} (p(t)|E_1)$$

$$= \exp\left\{ \sum_{\substack{\text{subintervals} \\ \varepsilon\, I_1-I_2}} \ln p(t) + \sum_{\substack{\text{subintervals} \\ \varepsilon\, I_2}} \ln (p(t)|E_1) \right\} \tag{5.3.23}$$

$$Pr(E_3|E_2) = \exp\left\{ \sum_{\substack{\text{subintervals} \\ \varepsilon\, I_1-I_2}} \ln p(t) + \sum_{\substack{\text{subintervals} \\ \varepsilon\, I_2}} \ln (p(t)|E_2) \right\} \tag{5.3.24}$$

Fig. 5.3.3 and Fig. 5.3.4 show how the summations in eqn. (5.3.23) and eqn. (5.3.24) are evaluated for different values of t_1. For the three range of t_1, the following results are obtained:

Case 1: $t_o-T_s-T_r-T_m<t_1<t_o-T_s-T_r+T_m$

$$-\ln Pr(E_3|E_1) = 2G(1-e^{-2G}P_c) + \frac{Ge^{-2G}[1+P_c(1-e^{-2G})]}{T_m T_r(1-e^{-2G})} \left\{ -\frac{(t_o-t_1)^2}{2} \right.$$

$$\left. +(T_s+T_r-T_m)(t_o-t_1) + 4T_m^2 - \frac{1}{2}(T_s+T_r-T_m)^2 \right\} \tag{5.3.25}$$

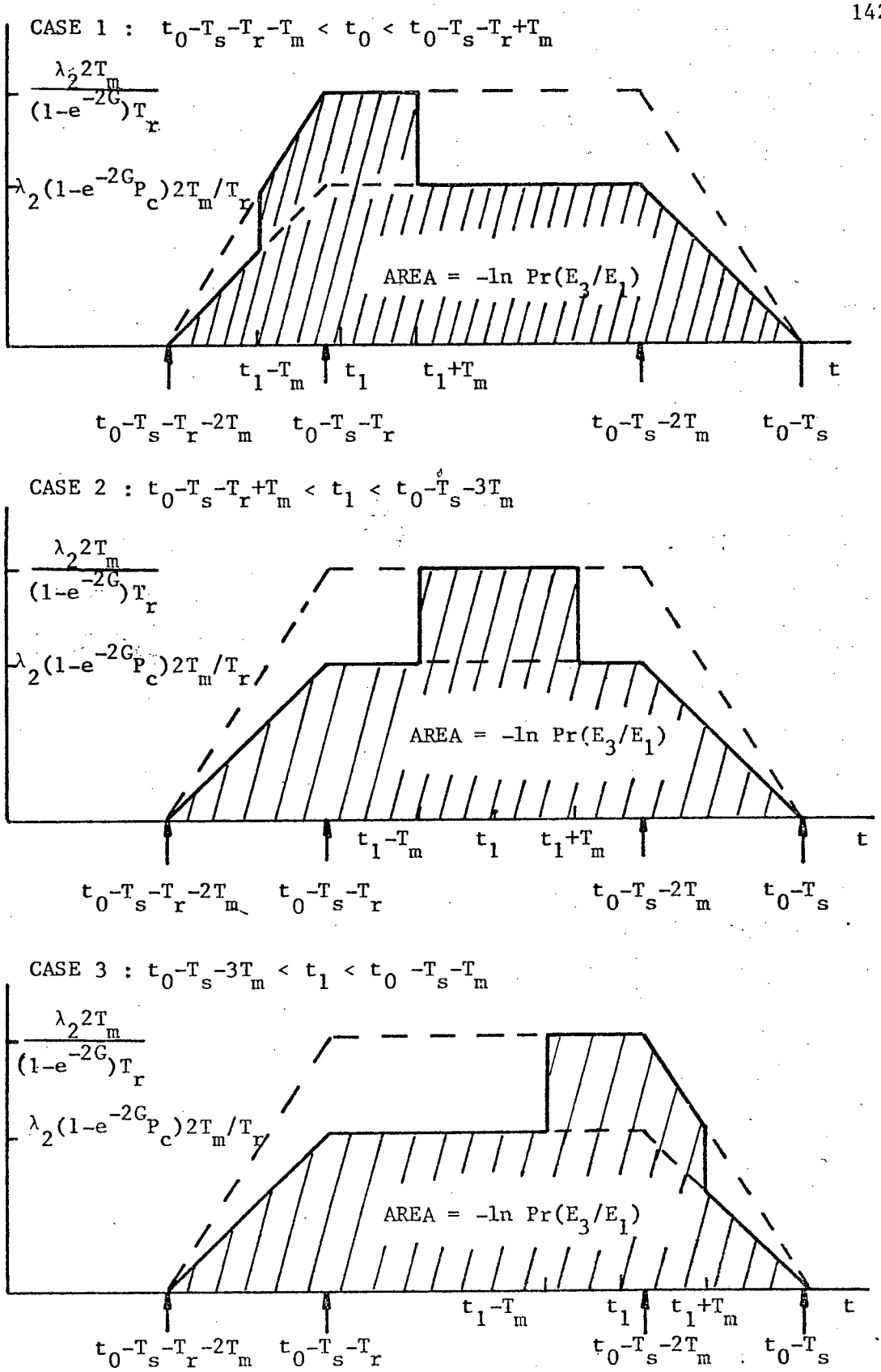

Fig. 5.3.3 Graphical evaluation of $-\ln\{Pr(E_3/E_1)\}$

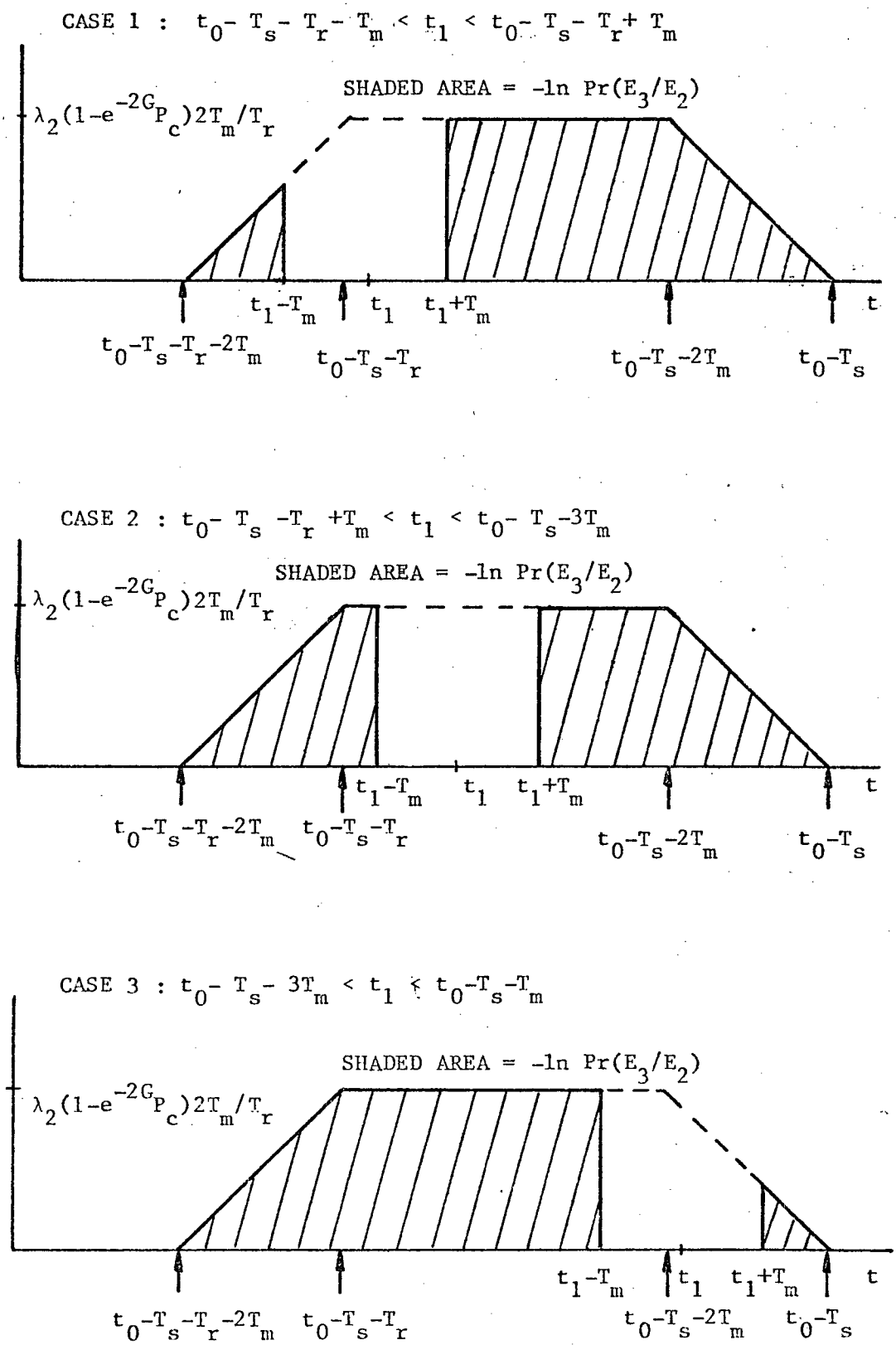

Fig. 5.3.4 Graphical evaluation of $-\ln\{\Pr(E_3/E_2)\}$

$$-\ln Pr(E_3|E_2) = 2G(1-e^{-2GP_c}) - \frac{G(1-e^{-2GP_c})}{T_m T_r}\left\{-\frac{(t_o-t_1)^2}{2}\right.$$

$$\left. + (T_s+T_r-T_m)(t_o-t_1) + 4T_m^2 - \frac{1}{2}(T_s+T_r-T_m)^2\right\} \qquad (5.3.26)$$

Case 2: $t_o-T_s-T_r+T_m<t_1<t_o-T_s-3T_m$

$$-\ln Pr(E_3|E_1) = 2G(1-e^{-2GP_c}) + \frac{4Ge^{-2G}[1+P_c(1-e^{-2G})]T_m}{T_r[1-e^{-2G}]} \qquad (5.3.27)$$

$$-\ln Pr(E_3|E_2) = 2G(1-e^{-2GP_c}) - 4G(1-e^{-2GP_c})T_m/T_r \qquad (5.3.28)$$

Case 3: $t_o-T_s-3T_m<t_1<t_o-T_s-T_m$

$$-\ln Pr(E_3|E_1) = 2G(1-e^{-2GP_c}) + (G/T_m T_r)[e^{-2G}/(1-e^{-2G})][1+P_c(1-e^{-2G})]$$

$$\{-(t_o-t_1)^2/2 + (T_s+3T_m)(t_o-t_1) + 4T_m^2-(T_s+3T_m)^2/2\} \qquad (5.3.29)$$

$$-\ln Pr(E_3|E_2) = 2G(1-e^{-2GP_c}) - (G/T_m T_r)(1-e^{-2GP_c})\{-(t_o-t_1)^2/2$$

$$+ (T_s+3T_m)(t_o-t_1) + 4T_m^2 - (T_s+3T_m)^2/2\} \qquad (5.3.30)$$

Let

$$f_1(G) = e^{-2G(1-e^{-2GP_c})} \qquad (5.3.31)$$

$$f_2(G) = \frac{Ge^{-2G}[1+P_c(1-e^{-2G})]}{T_m T_r(1-e^{-2G})} \tag{5.3.32}$$

$$f_3(G) = \frac{G(1-e^{-2GP_c})}{T_m T_r} \tag{5.3.33}$$

$$K_1 = T_s+T_r-T_m \tag{5.3.34}$$

$$K_2 = T_s+3T_m \tag{5.3.35}$$

Then

$$\Pr(E_3|E_1)=\begin{cases} f_1(G)\exp\{-f_2(G)[-\frac{1}{2}(t_o-t_1-K_1)^2+4T_m^2]\}, & t_o-K_1-2T_m<t_1<t_o-K_1 \\ f_1(G)\exp\{-4T_m^2 f_2(G)\}, & t_o-K_1<t_1<t_o-K_2 \\ f_1(G)\exp\{-f_2(G)[-\frac{1}{2}(t_o-t_1-K_2)^2+4T_m^2]\}, & t_o-K_2<t_1<t_o-K_2+2T_m \end{cases} \tag{5.3.36}$$

$$\Pr(E_3|E_2)=\begin{cases} f_1(G)\exp\{f_3(G)[-\frac{1}{2}(t_o-t_1-K_1)^2+4T_m^2]\}, & t_o-K_1-2T_m<t_1<t_o-K_1 \\ f_1(G)\exp\{4T_m^2 f_3(G)\}, & t_o-K_1<t_1<t_o-K_2 \\ f_1(G)\exp\{f_3(G)[-\frac{1}{2}(t_o-t_1-K_2)^2+4T_m^2]\}, & t_o-K_2<t_1<t_o-K_2+2T_m \end{cases} \tag{5.3.37}$$

and

$$(q_t|t_1) = \frac{e^{-2S}P_c[(1-e^{-2G})Pr(E_3|E_1) + e^{-2G}(1-P_c)Pr(E_3|E_2)]}{1-e^{-2G}P_c} \qquad (5.3.38)$$

The probability that a previously blocked packet is received without error is

$$q_t = \int_{-\infty}^{\infty} (q_t|t_1)\, f_{T_1}(t_1)dt_1 \qquad (5.3.39)$$

where $f_{T_1}(t_1)$ is the pdf for t_1 given by

$$f_{T_1}(t_1) = \begin{cases} 1/T_r\ , & t_o-T_s-T_r-T_m<t_1<t_o-T_s-T_m \\ \\ 0\ , & \text{elsewhere} \end{cases} \qquad (5.3.40)$$

The final result is therefore

$$q_t = e^{-2S}F(G,P_c,T_m,T_s,T_r) \qquad (5.3.41)$$

where, with $(t_o-t_1) = \tau$,

$$F(G,P_c,T_m,T_s,T_r) = \{P_c f_1(G)/[T_r(1-e^{-2G}P_c)]\}$$

$$\{(1-e^{-2G})\exp[-4T_m{}^2 f_2(G)][T_r-4T_m$$

$$+ \int_{K_1}^{K_1+2T_m} \exp(f_2(G)(\tau-K_1)^2/2)d\tau$$

$$+ \int_{K_2-2T_m}^{K_2} \exp(f_2(G)(\tau-K_2)^2/2)d\tau]$$

$$+ e^{-2G}(1-P_c)\exp[4T_m^2 f_3(G)][T_r-4T_m$$

$$+ \int_{K_1}^{K_1+2T_m} \exp(-f_3(G)(\tau-K_1)^2/2)d\tau$$

$$+ \int_{K_2-2T_m}^{K_2} \exp(-f_3(G)(\tau-K_2)^2/2)d\tau]\} \qquad (5.3.42)$$

Letting $\tau_1 = \tau-K_1$, $\tau_2 = \tau-K_2$, and $\tau_o = \tau_1 = \tau_2$ in eqn. (3.5.42) yields

$$F(G,P_c,T_m,T_s,T_r) = \{P_c f_1(G)/[T_r(1-e^{-2G}P_c)]\}$$

$$\{(1-e^{-2G})\exp[-4T_m^2 f_2(G)][T_r-4T_m$$

$$+ \int_{-2T_m}^{2T_m} \exp(f_2(G)\tau_o^2/2)d\tau_o]$$

$$+ e^{-2G}(1-P_c)\exp(4T_m^2 f_3(G)][T_r-4T_m$$

$$+ \int_{-2T_m}^{2T_m} \exp(-f_3(G)\tau_o^2/2)d\tau_o]\} \qquad (5.3.43)$$

Expressing T_r as $T_r=KT_m$, $K\geq 4$ and letting $x = \tau_o/T_m$, yields simplifications as follows to eqn. (5.3.43):

$$\tilde{F}(G,P_c,T_m,T_s,K) = \frac{P_c e^{-2G(1-P_c e^{-2G})}}{K(1-P_c e^{-2G})} \{(1-e^{-2G})e^{\frac{-4Ge^{-2G}[1+P_c(1-e^{-2G})]}{K(1-e^{-2G})}}$$

$$[K-4+\int_{-2}^{2} e^{\frac{Ge^{-2G}[1+P_c(1-e^{-2G})]}{K(1-e^{-2G})}\frac{x^2}{2}} dx] +$$

$$e^{-2G}(1-P_c)e^{\frac{4G(1-P_c e^{-2G})}{K}} [K-4+\int_{-2}^{2} e^{\frac{-G(1-P_c e^{-2G})}{K}\frac{x^2}{2}} dx]$$

(5.3.44)

where function F in eqn. (5.3.41) is replaced by $\tilde{F}$. Since solution to the integral $\int_o^x e^{t^2}dt$ is not available in closed form, the integrals in eqn. (5.3.44) must be evaluated using numerical methods.

It is interesting to note that for $K\to\infty$, the above results converge to those obtained using the Poisson assumption for channel traffic, i.e.

$$S = Ge^{-2G}P_c \qquad (5.3.45)$$

From eqns. (5.3.40) and (5.3.43) it follows that

$$\lim_{K\to\infty} q_t = e^{-2S} P_c e^{-2G(1-e^{-2G}P_c)} = q_n \tag{5.3.46}$$

and

$$\lim_{K\to\infty} \frac{S}{G} = \lim_{K\to\infty} q_t = q_n = e^{-2S} P_c e^{-2G(1-e^{-2G}P_c)} \tag{5.3.47}$$

By direct substitution, it can be confirmed that eqn. (5.3.45) is a solution of eqn. (5.3.47).

Given a set of values for G, P_c, T_m, T_s and T_r (or K), the variables S, q_n and q_t may be solved from a system of non-linear equations given by eqns. (5.3.4), (5.3.12) and (5.3.41). The corresponding average packet delay D is given by

$$D = T_m + T_s + \frac{(1-q_n)}{q_t}(T_m + T_s + T_r/2) \tag{5.3.48}$$

Using the results derived above, a delay-vs.-throughput (D-S) curve maybe plotted for given values of PNR, R, ℓ, T_s and K. Assuming T_s=0.01 sec., a typical family of D-S curves for various K with fixed PNR, R and ℓ is shown in Fig. 5.3.5. The envelope described by these curves represents the optimum throughput-delay characteristics of a pure ALOHA channel where K varies adaptively according to the level of channel traffic.

If the usable bit rate is not limited by channel bandwidth, the throughput-delay characteristics can be further optimized over the bit rate R by maximizing the channel capacity C (the maximum achievable throughput corresponding to the vertical portion of the envelope) or alternatively by minimizing the

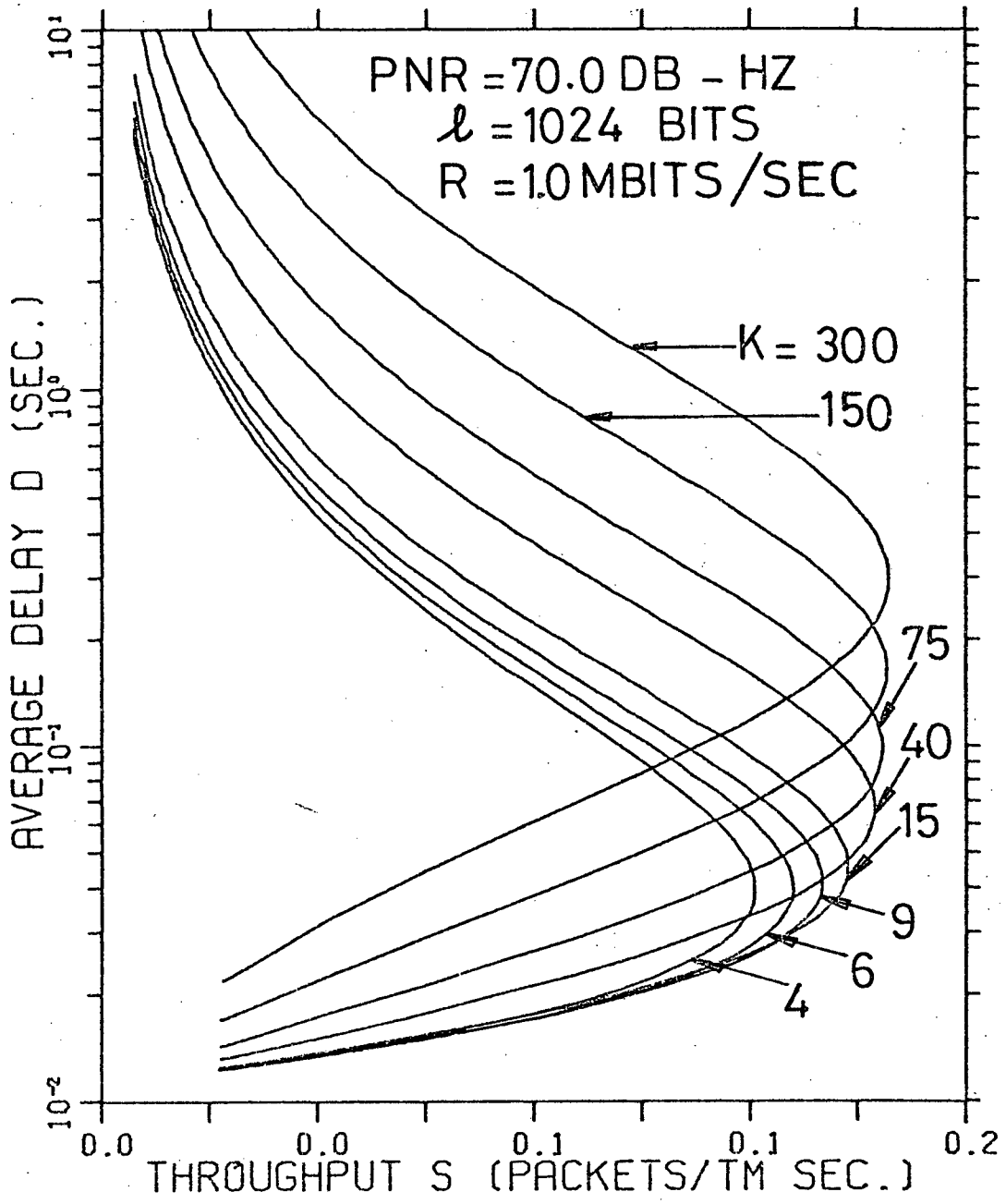

Fig. 5.3.5 A typical set of pure ALOHA delay-vs.-throughput curves showing effects of different maximum retransmission delays in KT_m sec.

time delay at a given level of channel throughput. Thus from each graph in Figs. 5.3.6 and 5.3.7 the channel capacity is visually optimized with respect to R and the results (accurate to two significant digits) are tabulated in Table 5.3.1. The effect of different message lengths on the throughput-delay characteristics (the D-S curves with C maximized are used) is illustrated in Fig. 5.3.8. These graphs show that throughput-delay characteristics of pure ALOHA are similar to that of slotted ALOHA. Specifically, the observations in Section 5.2 regarding Figs. 5.2.2 to 5.2.4 are also applicable to Figs. 5.3.6 to 5.3.8. Comparing Table 5.3.1 with Table 5.2.1, channel capacities for both pure ALOHA and slotted ALOHA are maximized at the same bit rate at given values of PNR and ℓ, and the maximum channel capacity for pure ALOHA is approximately half that of slotted ALOHA.

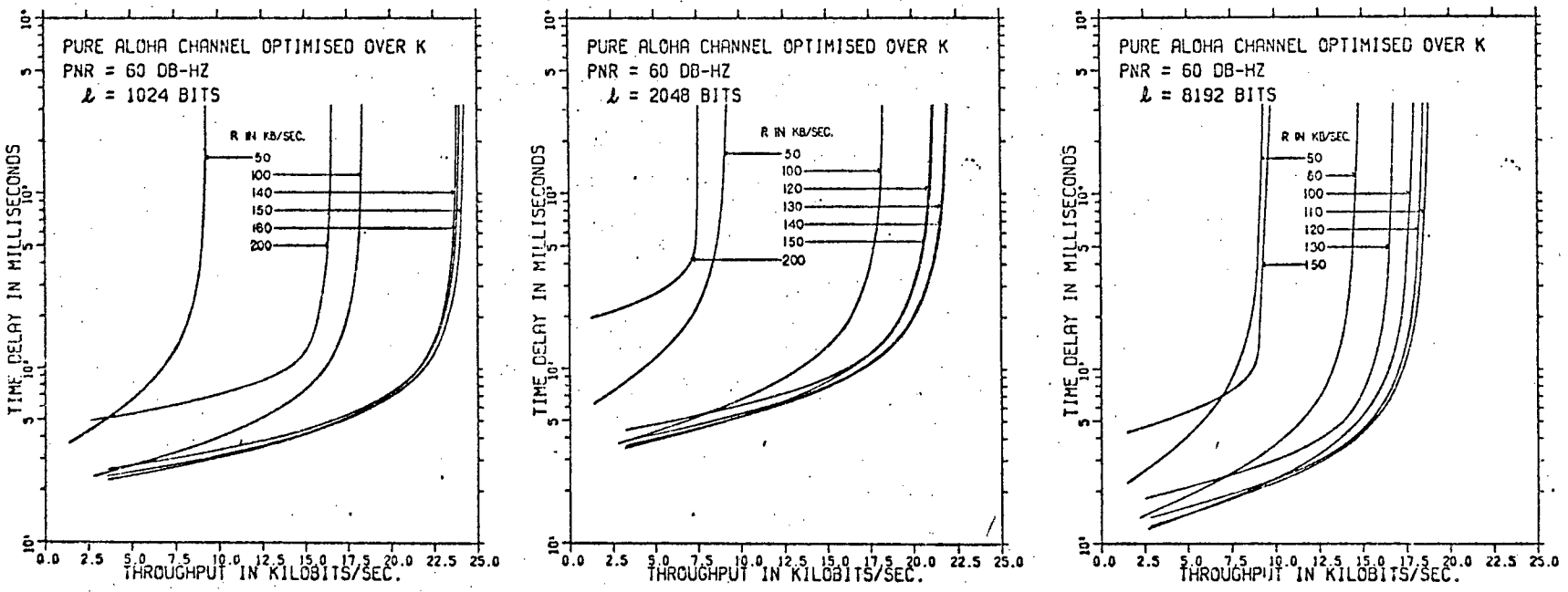

Fig. 5.3.6 Effects of different bit rates R on pure ALOHA delay-vs.-throughput curves optimized over K with PNR = 60.0 dB-Hz and (a) ℓ = 1024 bits, (b) ℓ = 2048 bits, (c) ℓ = 8192 bits.

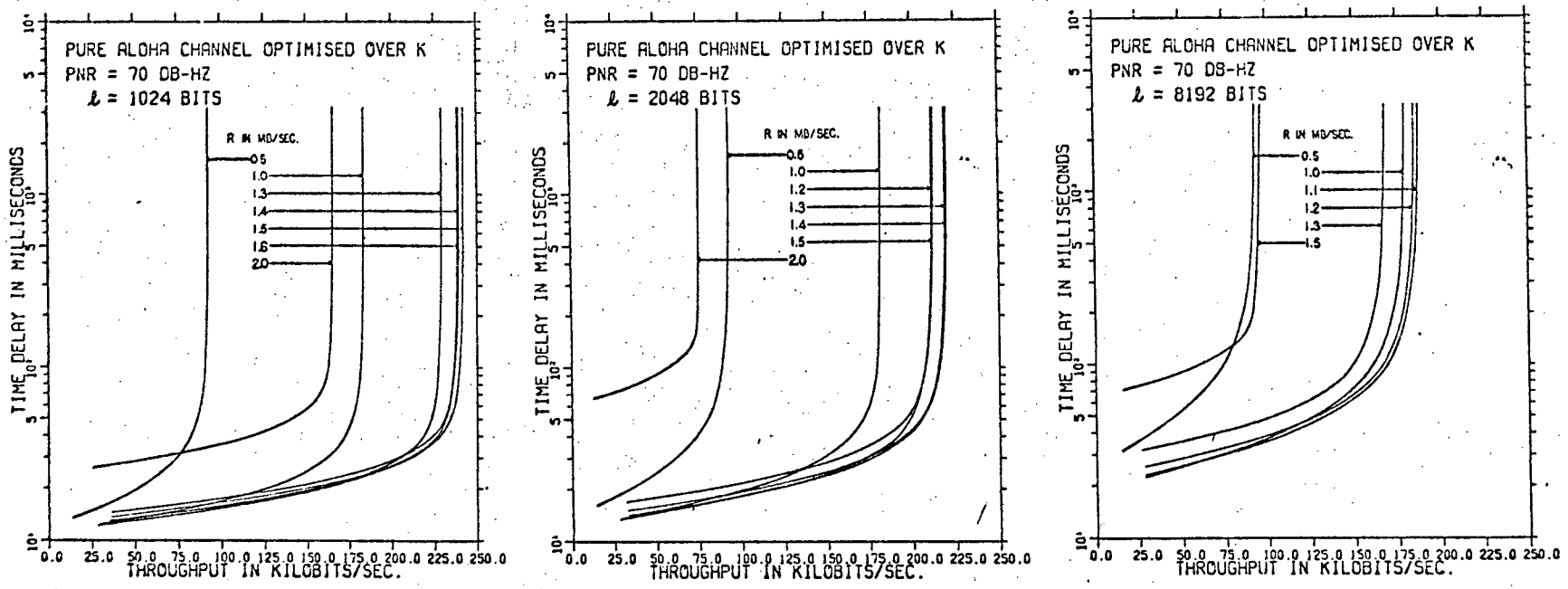

(a) (b) (c)

Fig. 5.3.7 Effects of different bit rates R on pure ALOHA delay-vs.-throughput curves optimized over K with PNR = 70.0 dB-Hz and (a) ℓ = 1024 bits, (b) ℓ = 2048 bits, (c) ℓ = 8192 bits.

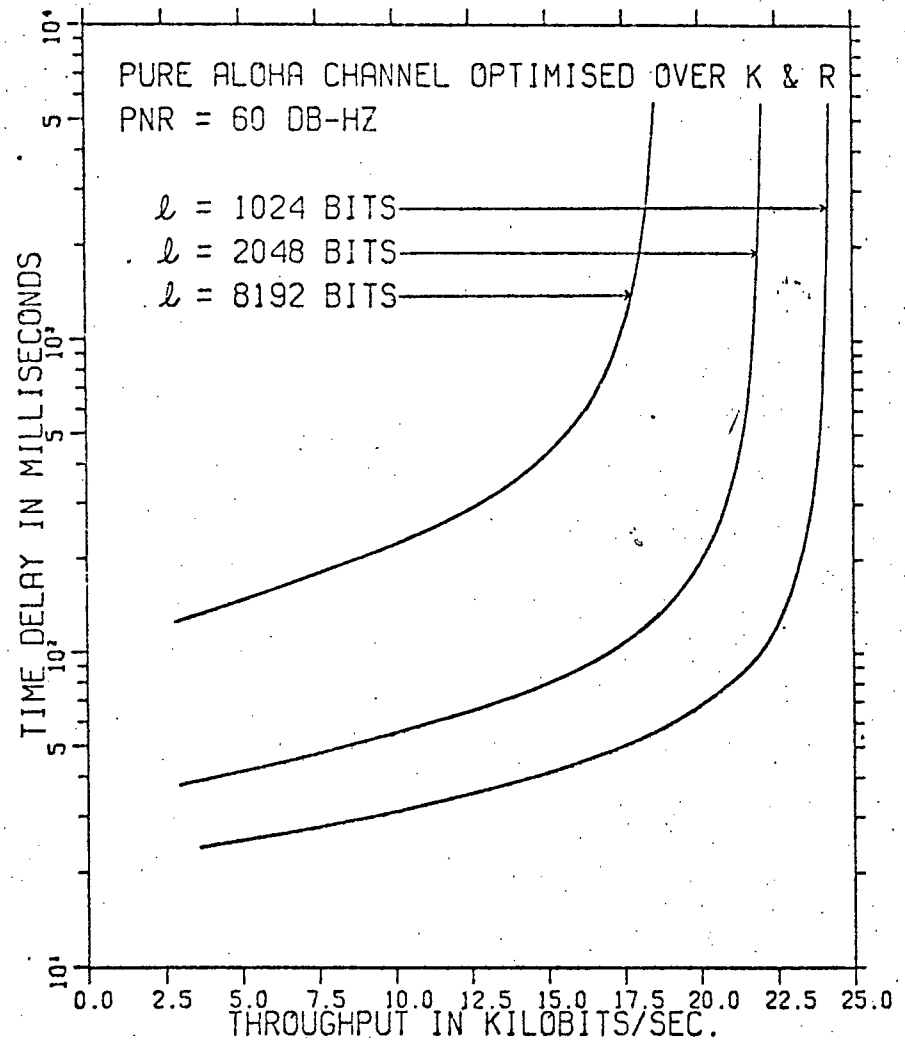

(a)

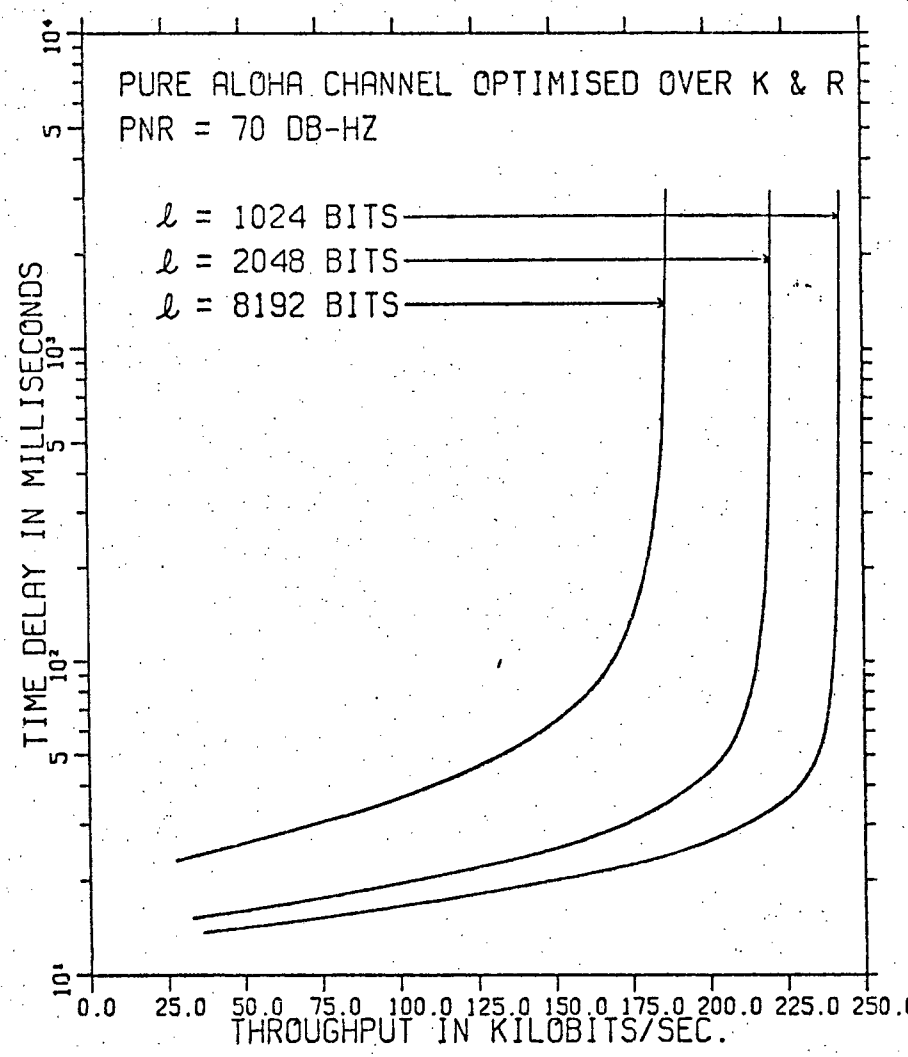

(b)

Fig. 5.3.8 Pure ALOHA delay-vs.-throughput curves for different message lengths ℓ, optimized over K and R, with (a) PNR = 60.0 dB-Hz, (b) PNR = 70.0 dB-Hz.

Table 5.3.1 Optimum Values of Bit Rate R and Corresponding Maximum Channel Capacity C for Pure ALOHA Channel with Additive Gaussian Noise

PNR(dB-Hz)	ℓ(bits)	R(bits/sec.)	C(bits/sec.)
60.0	1024	1.5×10^5	2.42×10^4
60.0	2048	1.4×10^5	2.19×10^4
60.0	8192	1.1×10^5	1.86×10^4
70.0	1024	1.5×10^6	2.42×10^5
70.0	2048	1.4×10^6	2.20×10^5
70.0	8192	1.1×10^6	1.87×10^5

5.4 Delay-Throughput Characteristics of a Queueing Channel with Additive Gaussian Noise

Consider a Gaussian noise channel serving a user population on a first-come-first-served basis and with perfect scheduling of transmission time so that no collision may occur on the channel. Assume messages have fixed length of ℓ bits/message and arrival of new messages constitutes a Poisson process with aggregate arrival rate λ messages/sec. Given the received signal-to-noise

density ratio PNR and the transmission bit rate R, message bits are received with bit-error probability p_B given by eqn. (5.2.2) and the probability P_c of error-free reception of a message is given by eqn. (5.2.1). A transmitted message is retained in a buffer at the transmitter until a positive acknowledgement of error-free reception is received. If a negative acknowledgement is received, the message rejoins the queue with a priority higher than that for new messages. The channel therefore constitutes a two priority class, head-of-the-line M/D/1 queue and the analysis in Section 3.6 of [K1] is applicable.

Let λ_n and λ_r be the arrival rate of new and retransmitted messages, respectively, and assume arrivals of new and retransmitted messages are Poisson and independent. Therefore

$$\lambda_n = \lambda \tag{5.4.1}$$

and

$$\lambda_r = \sum_{n=1}^{\infty} \lambda(1-P_c)^n = \lambda(1-P_c)/P_c \tag{5.4.2}$$

Define the channel utilization factor ρ as

$$\rho \triangleq \lambda T_m \tag{5.4.3}$$

where $T_m = \ell/R$ is the message duration. Therefore, the channel utilization factors ρ_n and ρ_r for new and retransmitted messages are, respectively,

$$\rho_n = \lambda T_m \tag{5.4.4}$$

$$\rho_r = \lambda T_m(1-P_c)/P_c \tag{5.4.5}$$

Define

$$\sigma_n \triangleq \rho_n + \rho_r = \lambda T_m / P_c \tag{5.4.6}$$

$$\sigma_r \triangleq \rho_r = \lambda T_m (1-P_c)/P_c = (1-P_c)\sigma_n \tag{5.4.7}$$

Then Cobham's result in Section 3.6 of [K1] gives the following solution to the average waiting time $\bar{W}_n$ and $\bar{W}_r$ for new and retransmitted messages, respectively.

$$\bar{W}_n = \frac{\bar{W}_o}{(1-\sigma_n)(1-\sigma_r)} \tag{5.4.8}$$

$$\bar{W}_r = \frac{\bar{W}_o}{(1-\sigma_r)} \tag{5.4.9}$$

$\bar{W}_o$ is the average residual transmission time for a message transmission in progress when another message joins the queue, and is given by

$$\bar{W}_o = \frac{T_m^2}{2}(\lambda_n+\lambda_r) = \frac{\lambda T_m^2}{2P_c} \tag{5.4.10}$$

The average delay D for error-free reception of a message is therefore

$$D = \bar{W}_n + (\bar{T}_s + \bar{W}_r + T_m)/P_c - (\bar{T}_s + \bar{W}_r) \tag{5.4.11}$$

where $\bar{T}_s$ is the average service delay, including round-trip propagation time and acknowledgement delay. Waiting time $\bar{W}_n$ and hence D become unbounded as λ approaches P_c/T_m and σ_n approaches one. When D is finite, the corresponding average throughput S in bits/sec. for a given λ is

$$S = \rho_n R = \lambda T_m R \quad , \quad \lambda < P_c/T_m \tag{5.4.12}$$

When D is infinite, S reaches its maximum value known as the channel capacity C which is given by

$$C = P_c R \tag{5.4.13}$$

Curves of D-vs.-S are plotted for the queueing channel discussed above for various R values, with ℓ=1024, 2048 and 8192 bits/message in Figs. 5.4.1 and 5.4.2, where PNR = 60 dB-Hz and 70 dB-Hz, respectively. These graphs show that if R is not constrained (e.g. by the available bandwidth), then as in ALOHA channels, channel capacity C is maximized at an optimum value of R for any given PNR and ℓ. Optimum values of R (accurate to two significant digits) and corresponding maximum value of C are tabulated in Table 5.4.1 for PNR = 60 and 70 dB-Hz and ℓ = 1024, 2048 and 8192 bits/message. The relationships between D-vs.-S curves with maximized channel capacity and different message lengths are shown by two graphs in Fig. 5.4.3 for PNR = 60 and 70 dB-Hz, respectively.

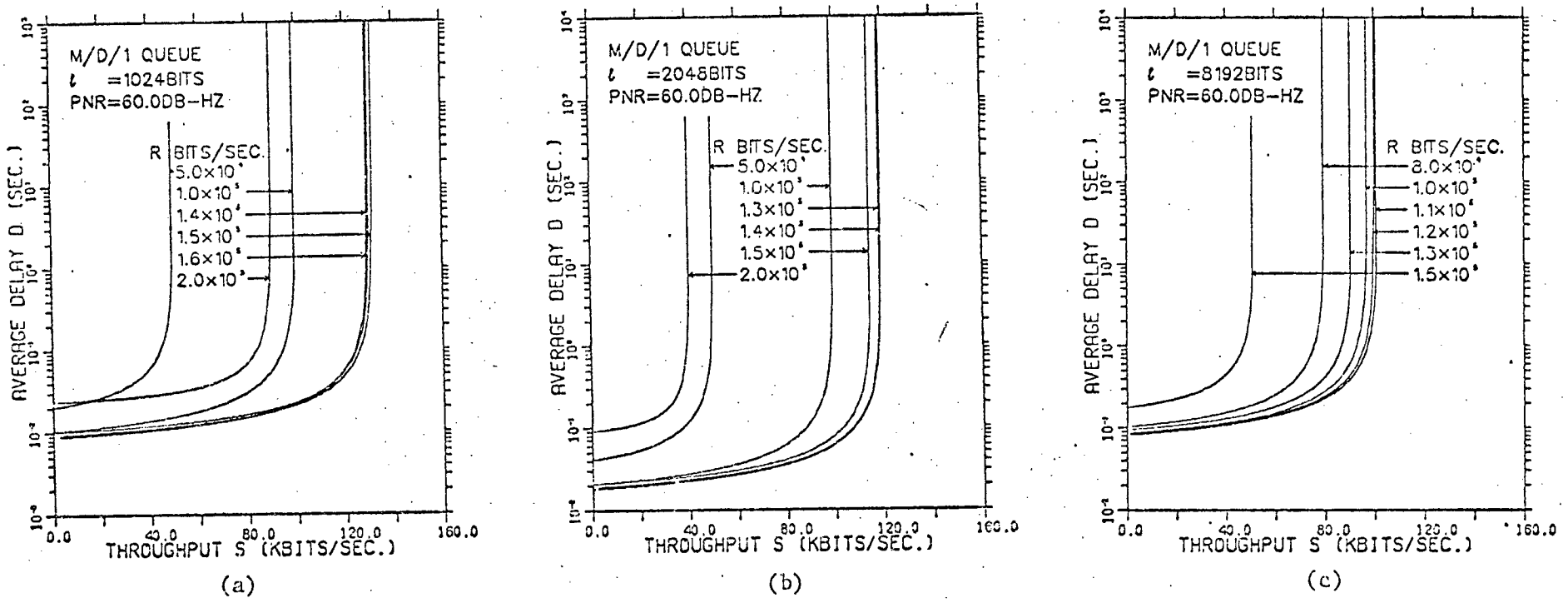

Fig. 5.4.1 Effects of different bit rates R on M/D/1 queueing delay-vs.-throughput curves with PNR = 60.0 dB-Hz and (a) ℓ = 1024 bits, (b) ℓ = 2048 bits, (c) ℓ = 8192 bits.

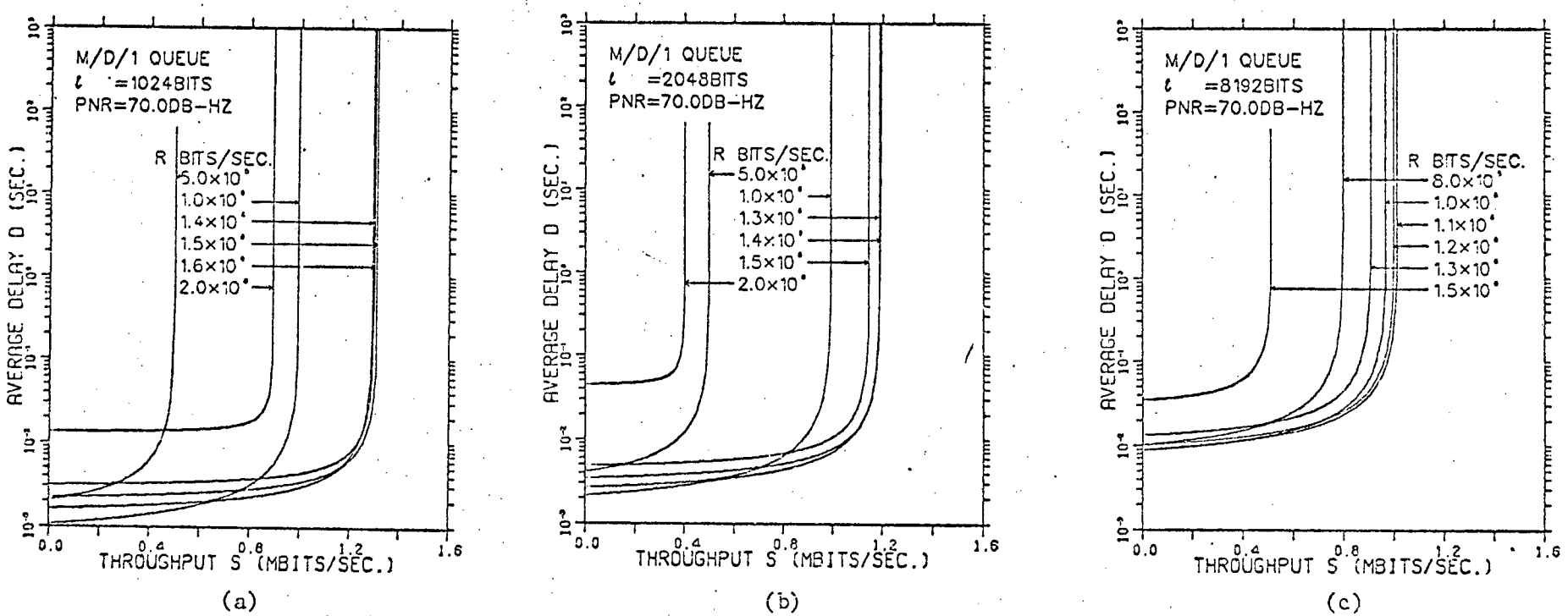

Fig. 5.4.2 Effects of different bit rates R on M/D/1 queueing delay-vs.-throughput curves with PNR = 70.0 dB-Hz and (a) ℓ = 1024 bits, (b) ℓ = 2048 bits, (c) ℓ = 8192 bits.

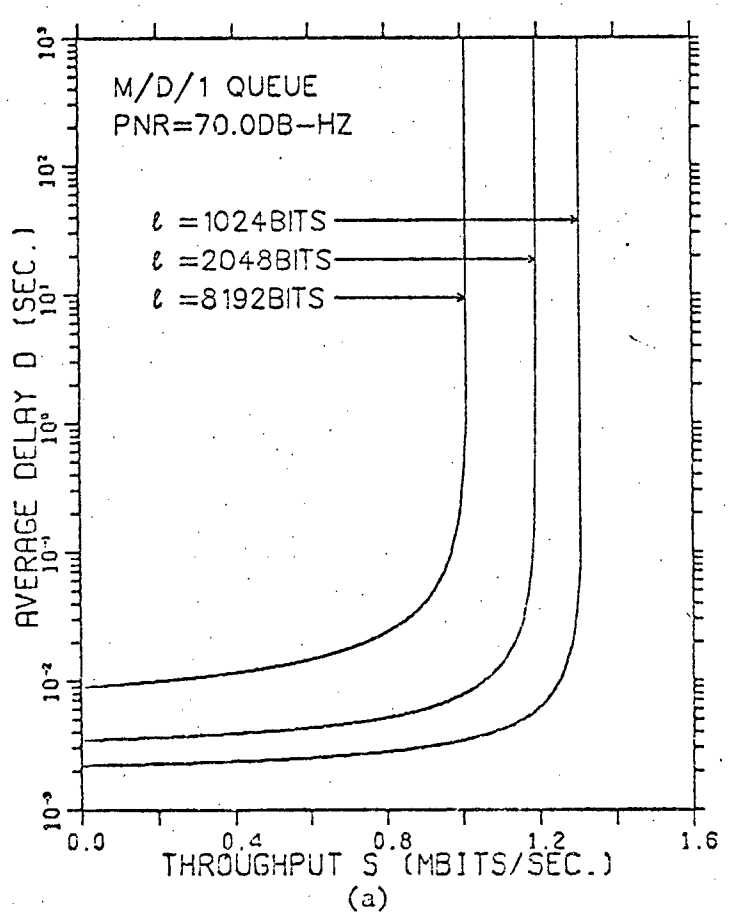

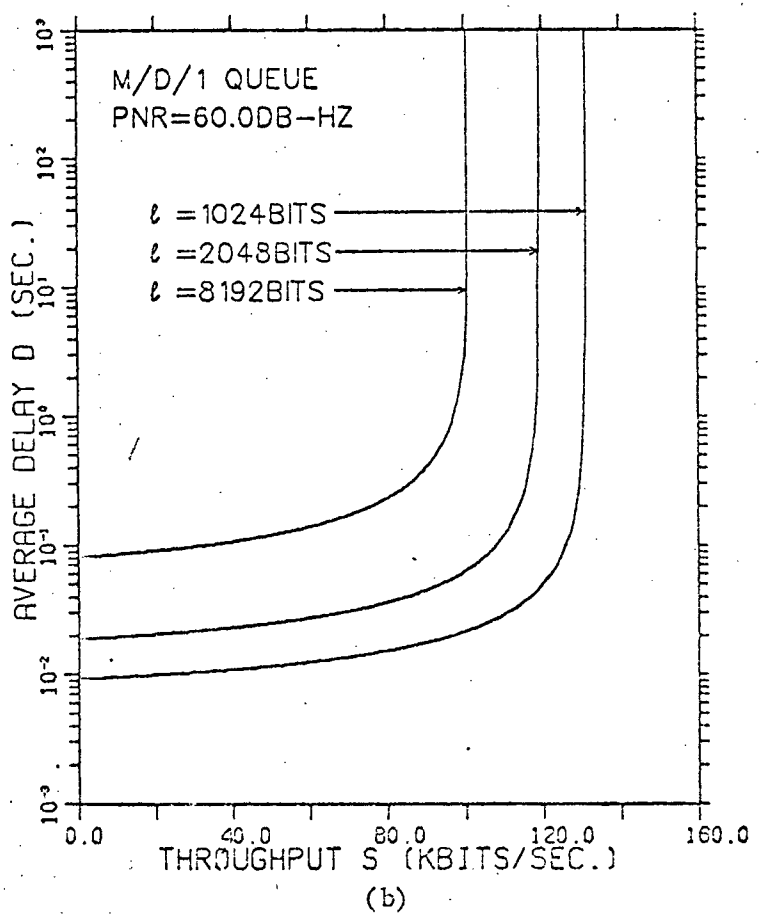

Fig. 5.4.3 M/D/1 queueing delay-vs.-throughput curves for different message lengths ℓ, with (a) PNR = 60.0 dB-Hz, (b) PNR = 70.0 dB-Hz.

Table 5.4.1 Optimum Values of Bit Rate R and Corresponding Maximum Channel Capacity C for M/D/1 Queueing Channel with Additive Gaussian Noise

PNR (dB-Hz)	ℓ (bits)	R (bits/sec)	C (bits/sec)
60.0	1024	1.5×10^5	1.31×10^5
60.0	2048	1.4×10^5	1.19×10^5
60.0	8192	1.1×10^5	1.01×10^5
70.0	1024	1.5×10^6	1.31×10^6
70.0	2048	1.4×10^6	1.19×10^6
70.0	8192	1.1×10^6	1.01×10^6

Comparison with the results in Sections 5.2 and 5.3, shows that the delay-throughput characteristics for M/D/1 queueing channel are similar to those of pure and slotted ALOHA channels optimized over retransmission delay distribution. Thus observations (i) to (v) stated in Section 5.2 are applicable to the queueing channel, with the exception that although delay becomes unbounded when throughput approaches channel capacity, the queueing channel does not become unstable as do ALOHA channels. It is also of interest to note that, given PNR and ℓ values, the bit rates which maximize channel capacities are the same for queueing, slotted ALOHA and pure ALOHA, and the corresponding maximum channel

capacities for these multiple access schemes have the ratio of 1:1/e:1/2e approximately, which is the same as the capacity ratio for these schemes operating in a noiseless channel. Channel noise affects the three multiple access schemes in a way which leaves their relative performance unchanged.

5.5 Comparison of Delay-Throughput Characteristics Between SSMA, Pure ALOHA, Slotted ALOHA and Queueing Channels

In this section, delay-throughput characteristics of SSMA, pure ALOHA, slotted ALOHA and queueing channels are compared under the conditions that messages of equal length ℓ are transmitted in all multiple access channels with equal single user power to noise-density ratio PNR and equal available transmission bandwidth B_t. These multiple access channels are assumed to conform to the channel model presented in Section 2.2, that is, each channel connects the user population to a central node in a star configuration. Delay-vs.-throughput curves for the above multiple access channels are shown in Figs. 5.5.1 to 5.5.6 inclusive for PNR = 60 and 70 dB-Hz, ℓ = 1024, 2048 and 8192 bits/message and B_t = 51.1 MHz.

Because the actual transmission bandwidths for pure ALOHA, slotted ALOHA and queueing at bit rate R which maximizes the channel capacity for the given values of PNR and ℓ are much less than B_t, these multiple access schemes are penalized by having excessive unused bandwidth. To perform more meaningful comparisons, the figures also include delay-vs.-throughput curves for m pure ALOHA, slotted ALOHA or queueing channels operating in parallel. These curves are obtained assuming that all users have the same arrival rate and each user is permanently assigned to one of m channels with identical delay-throughput

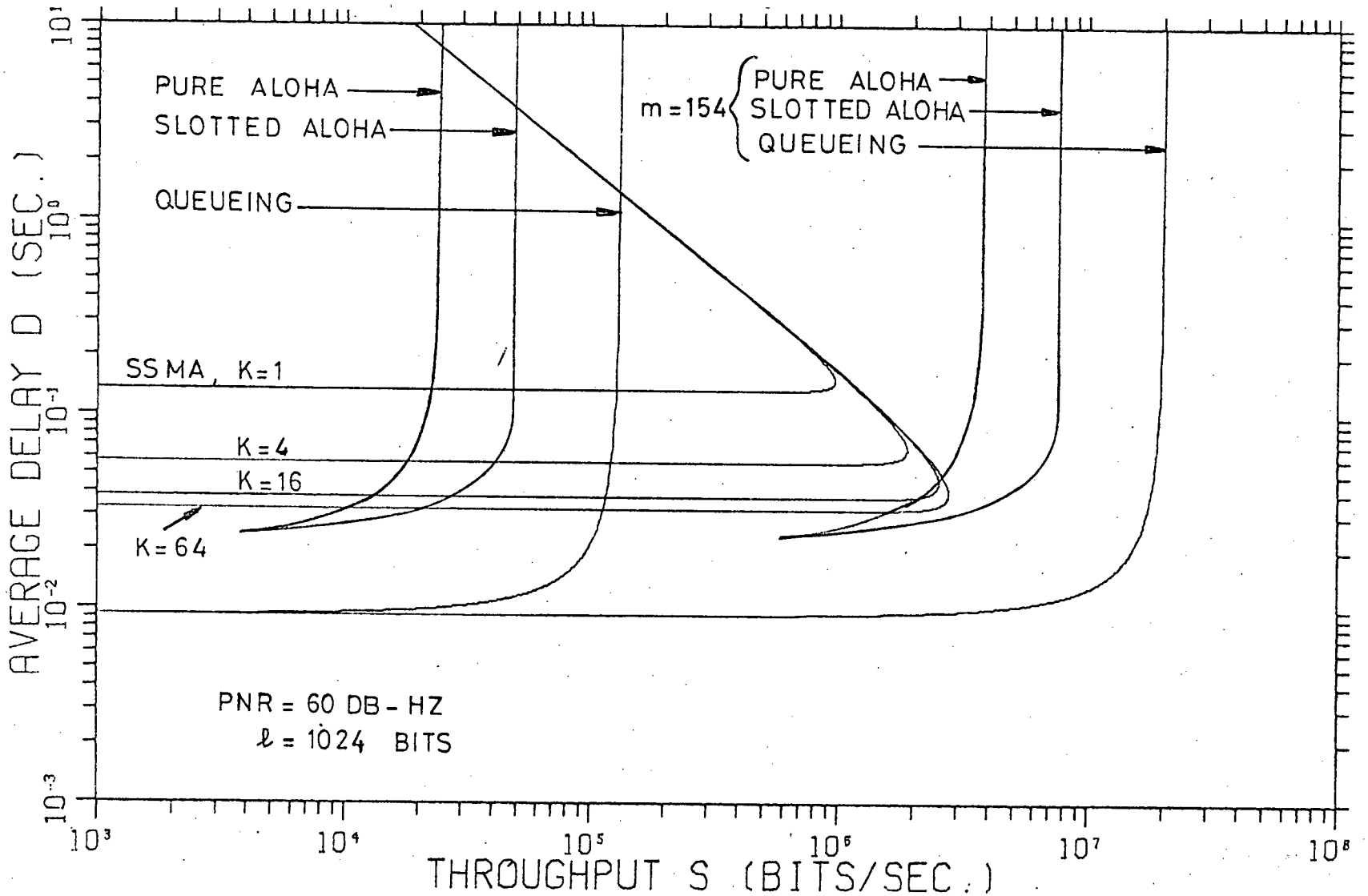

Fig. 5.5.1 Comparison of delay-throughput characteristics between SSMA, pure ALOHA, slotted ALOHA and queueing with PNR = 60.0 dB-Hz and ℓ = 1024 bits.

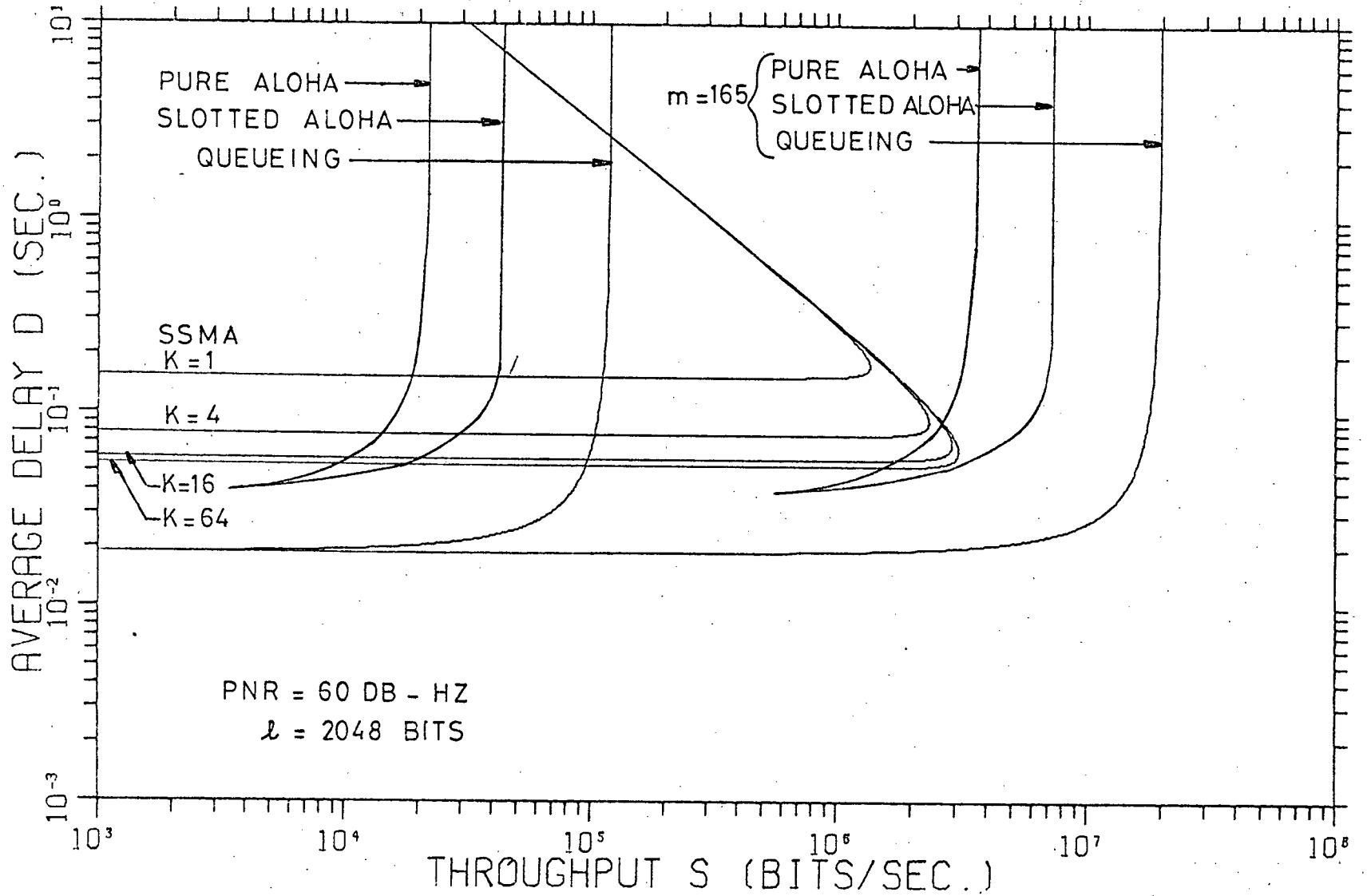

Fig. 5.5.2 Comparison of delay-throughput characteristics between SSMA, pure ALOHA, slotted ALOHA and queueing with PNR = 60.0 dB-Hz and ℓ = 2048 bits.

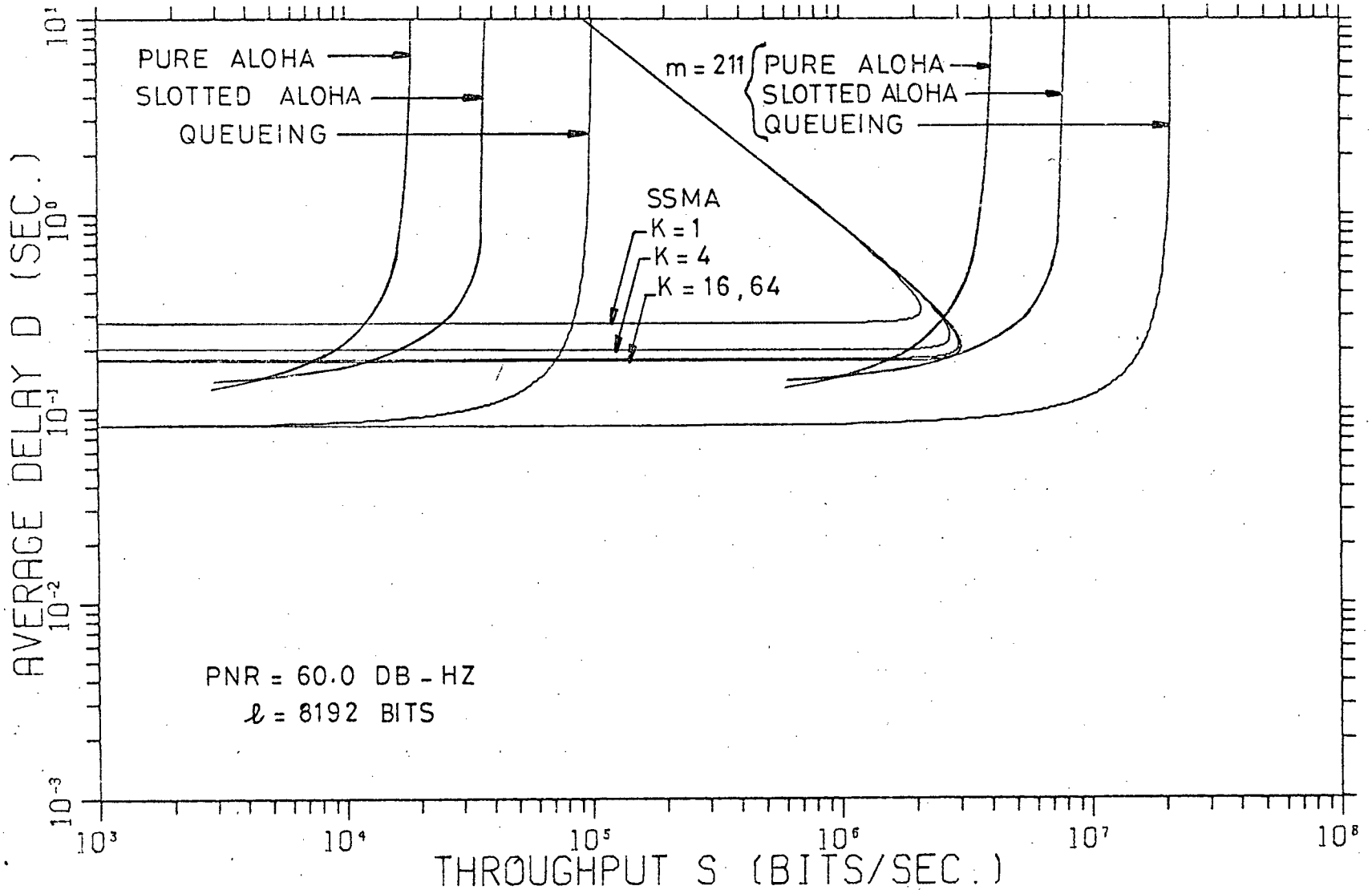

Fig. 5.5.3 Comparison of delay-throughput characteristics between SSMA, pure ALOHA, slotted ALOHA, and queueing with PNR = 60.0 dB-Hz and ℓ = 8192 bits.

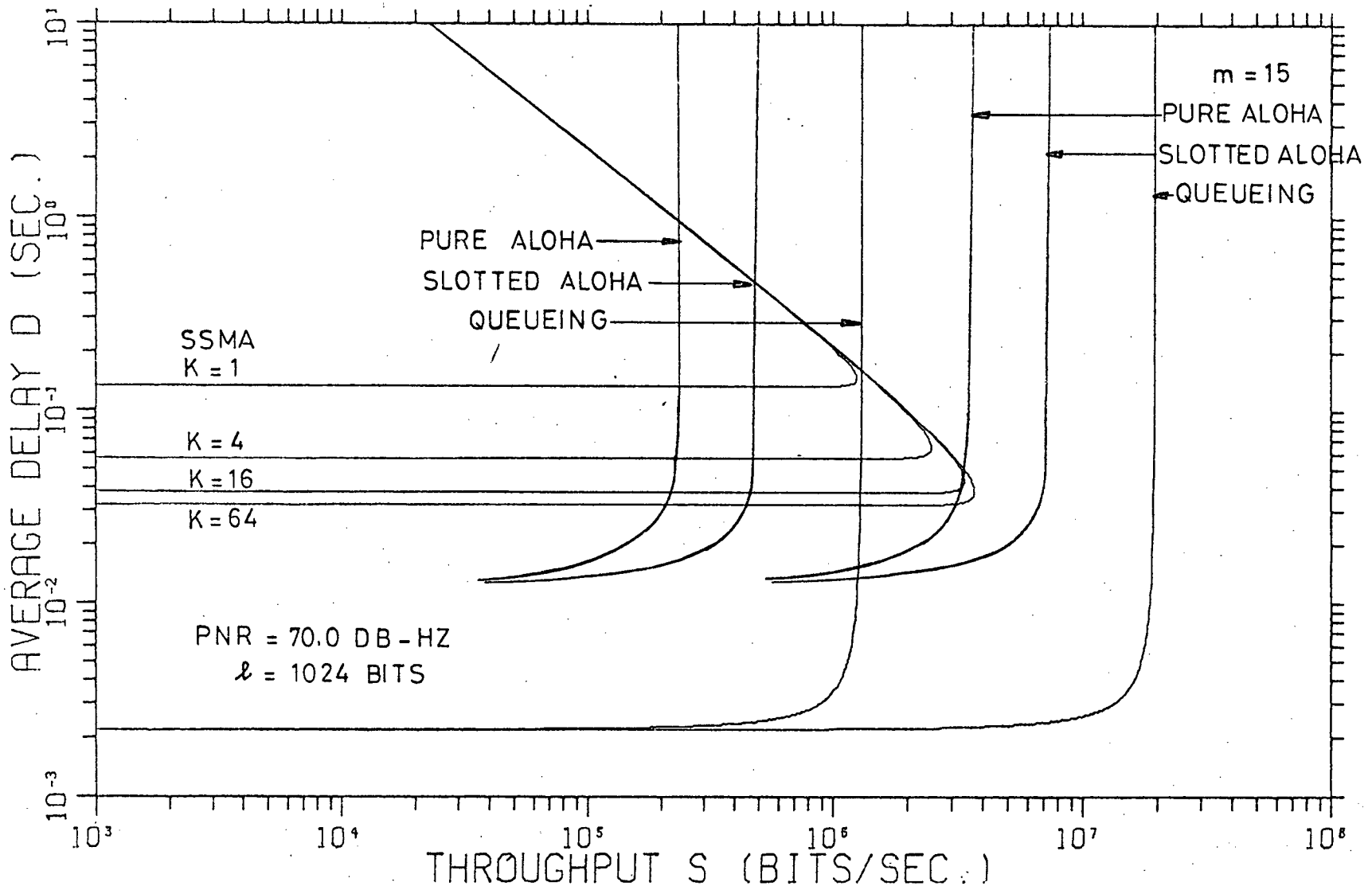

Fig. 5.5.4 Comparison of delay-throughput characteristics between SSMA, pure ALOHA, slotted ALOHA and queueing with PNR = 70.0 dB-Hz and ℓ = 1024 bits.

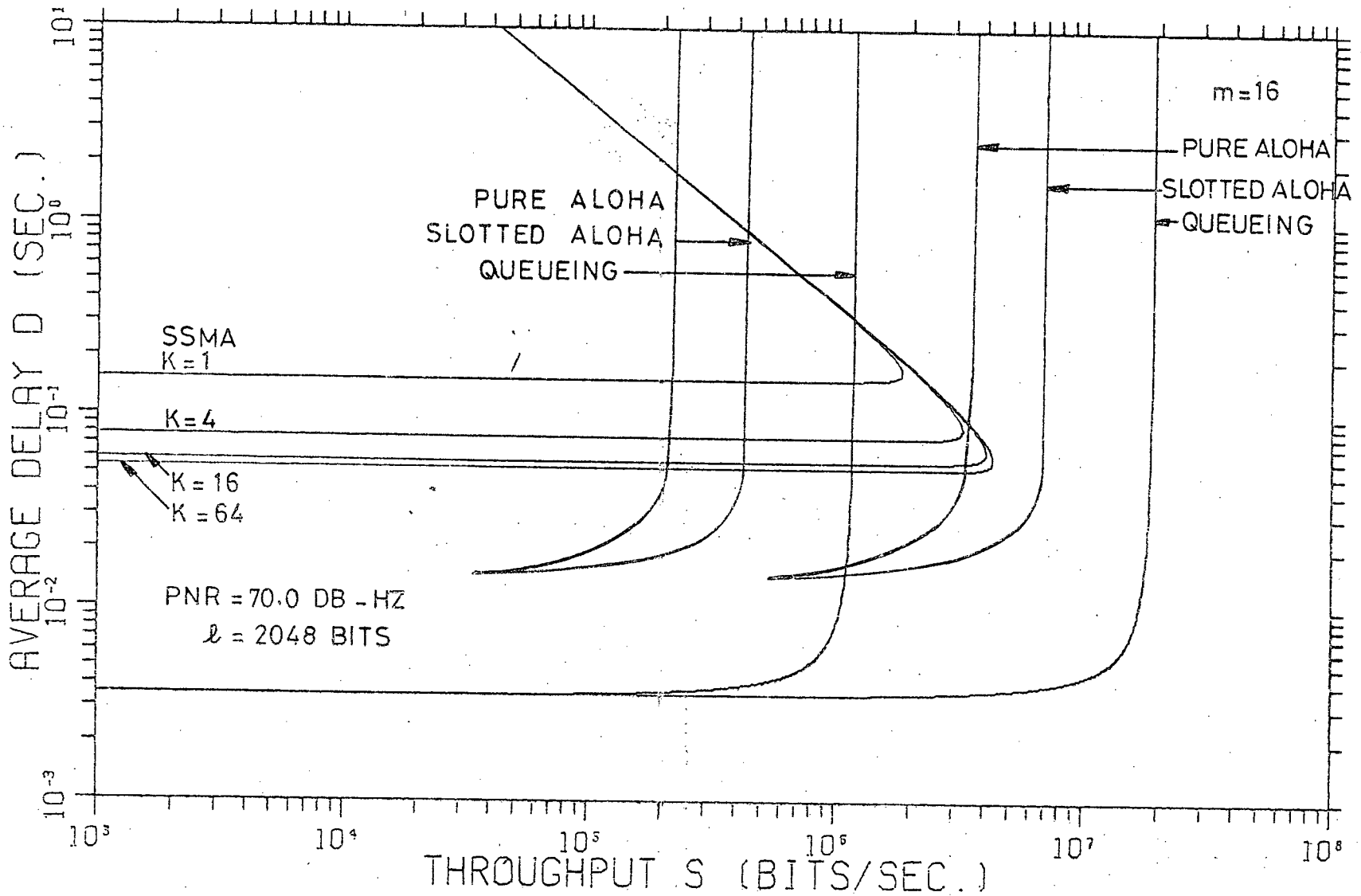

Fig. 5.5.5 Comparison of delay-throughput characteristics between SSMA, pure ALOHA, slotted ALOHA and queueing with PNR = 70.0 dB-Hz and ℓ = 2048 bits.

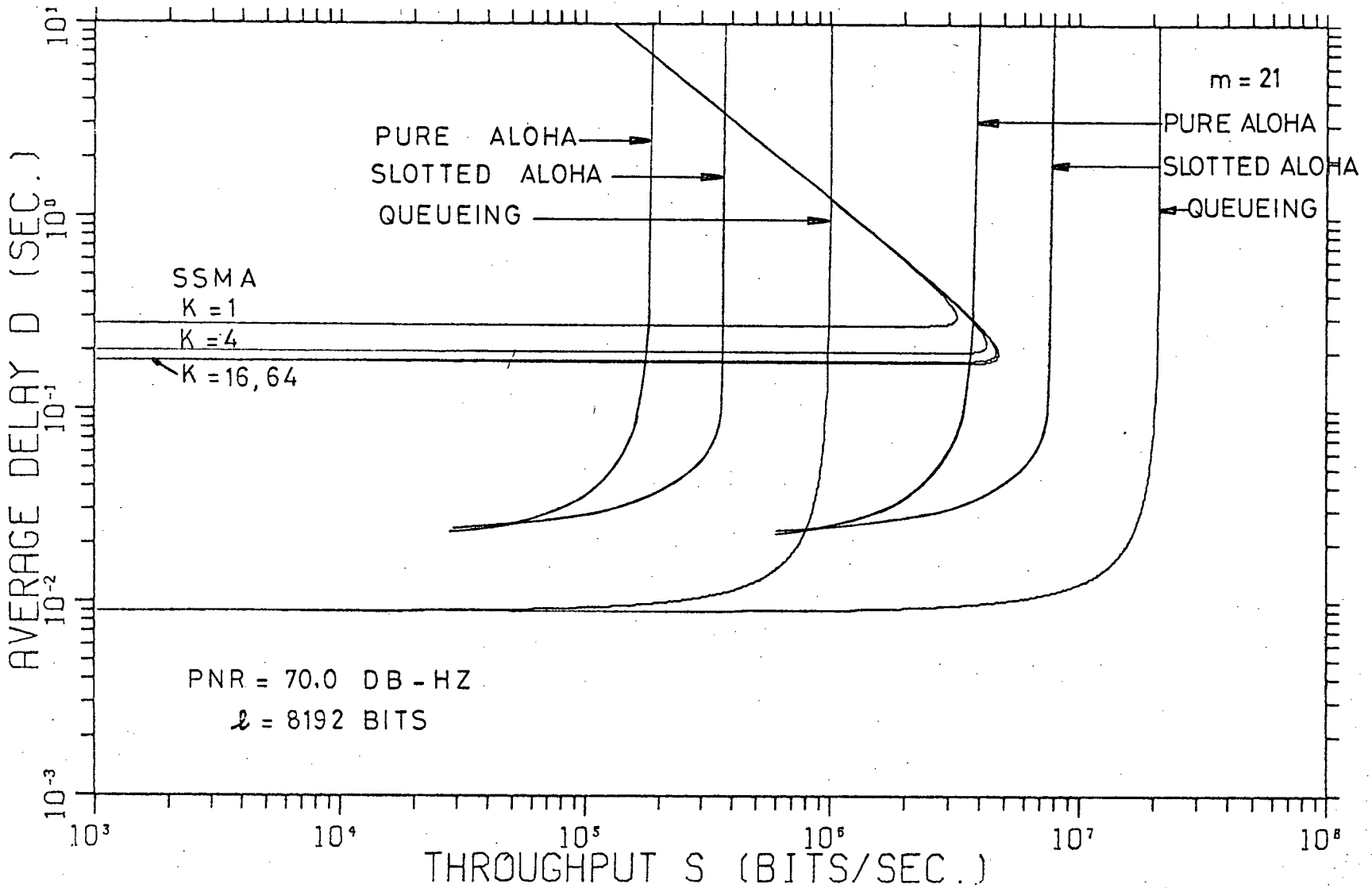

Fig. 5.5.6 Comparison of delay-throughput characteristics between SSMA, pure ALOHA, slotted ALOHA and queueing with PNR = 70.0 dB-Hz and ℓ = 8192 bits.

characteristics. It is further assumed that the central node has m receivers, one for each of the m channels. Thus the overall throughput is m times the throughput of a single channel, and average delay is unchanged. Assuming that guard bands occupy at least 10% of channel bandwidth, then

$$m = \text{trunc}\left(B_t/2.2R\right) \tag{5.5.1}$$

where trunc(x) is the integer part of real number x. This lower-bounds the delay-throughput characteristics for full load-sharing among the m channels, the analysis for which is quite unwieldy. The above results are also applicable to a fully meshed network in which each user receives in one of m channels and which traffic matrix is such that off diagonal elements are all equal.

The following observations can be made regarding Figs. 5.5.1 to 5.5.6:

(i) SSMA possesses a higher channel capacity than the other schemes operating over a single channel, except that queueing yields a higher capacity then SSMA with K=1 when PNR = 70 dB-Hz and ℓ = 1024 bits/-message.

(ii) SSMA possesses a lower channel capacity than other schemes operating over m channels, except that at PNR = 70 dB-Hz capacity for m pure ALOHA channels is lower than that of SSMA with $K \geq 64$ for ℓ = 1024 bits, $K \geq 16$ for ℓ = 2048 bits and $K \geq 4$ for ℓ = 8192 bits.

(iii) The difference in channel capacities in (i) changes in favour of SSMA as ℓ increases, PNR decreases, or K increases. The same is true for the channel capacity differences in (ii), except that changes in PNR have the apposite effect.

(iv) When throughput levels of all multiple access schemes are much less than the respective channel capacities, SSMA gives the longest and queueing gives the shortest average delay. The average delays for the ALOHA channels are between the two extremes. The difference between the two extremes decreases as ℓ increases, PNR decreases or K increases. The effect of increasing K to reduce this delay difference diminishes as ℓ increases.

(v) At throughput values greater than the channel capacity of a single pure ALOHA, slotted ALOHA or queueing channel and less than the channel capacity of SSMA (such values exist for some values of K in all cases considered), average delay for SSMA is less than that of the other schemes.

(vi) In all cases considered, for some values of K there exists a range of throughput values at which average delay for SSMA is less than that of m-parallel pure ALOHA channels.

(vii) The average delays for all multiple access schemes considered are quite acceptable when operating well below channel capacity.

In general, the following remarks are relevant to comparisons between delay-throughput characteristics of SSMA, pure ALOHA, slotted ALOHA and queueing channels:

(1) SSMA derives its multiple access capabilities from operating at a data rate lower than what it takes to accomplish a reasonable message error rate in other channels (50 Kbits/sec for SSMA vs. 1.5 Mbits/sec for other schemes at PNR = 70 dB-Hz with ℓ = 1024 bits). Therefore, at low throughput values SSMA is inferior because of its longer message

duration. Under such condition SSMA delays may be lowered by increasing information bit rate and thus decreasing processing gain, but this could lead to increase in cross-correlation which would tend to counteract any improvement.

(2) At moderately high throughput levels, SSMA is superior to single channel ALOHA or queueing because of its higher channel capacity. However, single channel ALOHA or queueing only uses a fraction of the transmission bandwidth of SSMA.

(3) If m ALOHA or queueing channels are fitted into the transmission bandwidth of SSMA, then both slotted ALOHA and queueing give channel capacities and delays superior to those of SSMA. However, performance of m channel pure ALOHA is quite comparable to that of SSMA. SSMA is especially favourable for long messages.

(4) Increasing PNR improves the performance of single channel ALOHA or queueing more than that of SSMA. In fact at approximately PNR = 85 dB-Hz optimum single channel ALOHA or queueing would occupy the entire B_t with the resulting delay-throughput characteristics much better than those of m channels operating at a lower PNR level. However, the delay-throughput characteristics of SSMA would show little improvement from that obtained at PNR = 70 dB-Hz.

(5) Channel capacity and average delay for SSMA are both affected by the average service time $\bar{T}_s$ and could both benefit from its reduction. However, reduction of service time only helps to decrease delay in

ALOHA and queueing channels, and has no effect on their channel capacity.

(6) The above comparison is based on the assumption that messages have fixed length. If message lengths are variable, average delays increase from a little for SSMA to probably very much for slotted ALOHA. Average delays only depend on mean message duration for SSMA, and depend on mean and variance of message duration for queueing. Analysis on effects of variable message lengths on ALOHA channels is unavailable and is probably very complicated.

(7) The above results for SSMA were obtained assuming that users' codes are uncorrelated. If Gold's codes of the given length were used, a five times reduction in throughput would result, and whatever advantages in channel capacity SSMA presents over other schemes would be severely reduced.

Delay-throughput characteristics are important factors in the choice of multiple access schemes for data communication networks. The above comparisons of delay-throughput characteristics between SSMA, pure ALOHA, slotted ALOHA and queueing show that the performance of SSMA is quite acceptable compared to that of slotted ALOHA and queueing, and is very favourable compared to that of pure ALOHA. SSMA is particularly suitable for applications where average message length is quite long, power is limited, a wide transmission bandwidth is available and its efficient utilization is not, therefore, a primary consideration.

6. CONCLUSIONS

6.1 Summary of Results

This thesis presents a comprehensive evaluation of the delay-throughput performance of an asynchronous direct sequence SSMA interactive data communication system based on a centralized network configuration. Results that constitute original contributions are summarized below:

(i) A code synchronizer with K parallel correlators was proposed, developed and analyzed. In particular, means, standard deviations and confidence estimates for acquisition time and hold-in time were derived. Effects of changes in some synchronizer parameters on the above performance meansures were investigated. It was shown that reduction in mean acquisition time is proportional to an increase in K. Application of the above results to the special case K = 1 (Hopkins' synchronizer) were presented. (These results together with their implications regarding protocol design are being published [L2].)

(ii) Three protocols suitable for SSMA communications under various operating conditions were developed and analyzed.

(iii) SSMA delay-throughput characteristics were obtained for Protocol B using a given set of system parameters and assuming uncorrelated users' codes. It was shown that average delays stay relatively constant for traffic levels less than the channel capacity, whereas average delays increase without bound and throughput levels diminish to zero for traffic levels exceeding channel capacity. Relationships

between channel capacity, channel stability, message arrival rate, message length, PNR level and the number K of parallel correlators in the synchronizer were considered. Results show that channel capacity can be maximized with respect to message length. Increasing K generally reduces total delay and increases the channel capacity. Using the analysis procedures developed, SSMA delay-throughput characteristics for other protocols using different system parameters could be pursued.

(iv) Delay-throughput analysis for slotted ALOHA channels was extended to include the effects of Gaussian channel noise. A novel approach was used to obtain the delay-throughput characteristics of pure ALOHA channels under the influence of Gaussian noise. A priority queueing model was established to facilitate delay-throughput analysis of Gaussian channels with perfectly scheduled transmission, with re-transmissions at a higher priority for messages degraded by bit-errors. At any given PNR level and given message length, capacities of these channels can be maximized with respect to transmission bit rate. Results also show that the relative performance of these channels subjected to the corruption of Gaussian noise are unchanged when compared to noise-free channel performance.

(v) Delay-throughput comparisons for SSMA, pure and slotted ALOHA, and queueing were presented. Also included in these comparisons are the delay-throughput characteristics of m parallel pure ALOHA, slotted ALOHA or queueing channels which fit the transmission bandwidth for SSMA. These comparisons show that delays in the SSMA channel are

longer than those in the other channels when operating at throughput levels which are much less than the capacities of all the channels. The capacity of the SSMA channel is generally higher than that of a single ALOHA or queueing channel but lower than that of multiple slotted ALOHA or queueing channels. The capacities of SSMA and multiple pure ALOHA channels are approximately equal.

In conclusion, our results show that under the specified conditions the delay-throughput performance of SSMA is comparable to other multiple accessing schemes considered. Because SSMA protocols are comparable in simplicity to the pure ALOHA protocol, and are less complicated than those of slotted ALOHA and perfect scheduling, SSMA presents a viable alternative to other multiple accessing schemes. SSMA is especially favorable for transmission of long messages in a wideband channel using a limited amount of power. For short message lengths, much improvement in SSMA delay-throughput characteristics may be realized by increasing the number of parallel correlators in the synchronizer.

6.2 Suggestions for Further Work

Delay-throughput performance of SSMA was analyzed in the preceding chapters assuming a particular system configuration and receiver structure. Comprehensive studies of spread-spectrum communications in general and SSMA in particular are scarce, and much opportunity exists for further study. Some would undoubtedly involve application or modification of our methods and results. Listed below are some areas of interest.

6.2.1 Enhancement of Receiver Performance through Interference Cancellation

In a centralized network all SSMA receivers are located at the central node. Thus interference cancellation can be achieved by subtracting the information extracted by one receiver from the received signal of all other receivers. Analysis by Kashihara [K8] shows that this technique virtually eleminates co-channel interference of other users at high PNR levels. It is of interest to examine the delay-throughput performance of a SSMA system incorporating this processing technique.

6.2.2 Different Power Levels for Acquisition and Message Transmission

It has been shown that for PNR $\gtrsim$ 60 dB-Hz, message retransmissions resulting from bit-errors result in rapid increases in SSMA delay when channel occupancy exceeds a certain level, whereas acquisition delay does not begin to increase rapidly until channel occupancy has reached a much higher level. If a lower power level were used for transmission of the acquisition preamble and a higher power level for transmission of the message, then the level of channel occupancy at which retransmission delay begins to increase rapidly would be increased, and the level at which acquisition delay begin to increase rapidly would be reduced. An overall increase in channel capacity would result. The extent to which optimal assignment of the two different power levels could increase channel capacity is of interest.

6.2.3 Effect of Various Modulation Schemes on Direct Sequence SSMA Performance

Applications of quadriphase and M-ary modulation schemes to direct sequence spread-spectrum communications have been investigated [P4, S6]. It is of interest to examine how applications of these modulation schemes affect overall system performance, and synchronizer performance in particular.

6.2.4 Extension of Results to Other Spread-Spectrum Techniques

Other spread-spectrum techniques such as time and frequency hopping, and hybrids of various techniques are also suitable for SSMA applications. Receiver structure and modulation formats for these techniques are quite different from those of direct sequence. With suitable modifications our results should be applicable to SSMA systems using these other techniques.

6.2.5 Extension of Results to Fully Connected Network

Two problems related to the application of SSMA to a fully connected network were cited in Section 2.2. The power control problem can be overcome by transponding which enables all users to impart the same PNR to any one receiving site, but this PNR level may differ from one receiving site to another. If the PNR levels at all receiving sites are at least 70 dB-Hz for the system which parameters are given in our numerical examples, then essentially uniform performance is attained at all receiving sites. The contention problem arises if there is only one receiver per site, and results in degradation in delay-throughput performance. Analysis of the effects of contention to SSMA performance is probably very involved. A similar but

possibly simpler problem is the effect of contention to the performance of a multi-channel ALOHA system in a fully connected network.

6.2.6 Exploration of New Coding Schemes

Coding schemes which produce code sets with large numbers of elements and low cross-correlation between elements are essential to the successful operation of a SSMA system, especially if a large user population is to be served. Continuing effort in the development of suitable coding schemes would be useful.

6.2.7 Extension of Results to Non-Gaussian Channels

Derivation of appropriate SNR expressions for SSMA in non-Gaussian channels such as fading channels and hard-limiting channels enables direct application of our results for SSMA performance evaluations. It is anticipated that the inherent frequency diversity will give SSMA additional advantages over other multiple access techniques for applications in non-Gaussian channels.

6.2.8 Application of Decision Feedback to Improve Channel Stability

In a centralized random access network, when the propagation delay is short, it is possible to improve channel stability by using estimates of channel statistics at the central node to generate decision feedback over the return channel, thus limiting further access when the channel is close to saturation. Delay-throughput analysis for a decision feedback protocol is of interest.

REFERENCES

A1 J.M. Aein, "Multiple access to a hard-limiting communication satellite repeater," IEEE Trans. Space Electronics and Telemetry, vol. SET-10, pp. 159-167, Dec. 1964.

A2 D.R. Anderson and P.A. Wintz, "Analysis of a spread-spectrum multiple-access system with a hard limiter," IEEE Trans. Comm. Tech., vol. COM-17, pp. 285-290, April 1969.

A3 D.R. Anderson, "A new class of cyclic codes," SIAM J. Appl. Math., vol. 16, pp. 181-197, Jan. 1968.

A4 N. Abramson, "The throughput of packet broadcasting channels," IEEE Trans. Comm., vol. COM-25, pp. 117-128, Jan. 1977.

B1 D.T. Bell, Jr., J.D. Holmes and R.V. Ridings, "Application of acoustic surface-wave technology to spread spectrum communications," IEEE Trans. Sonics and Ultrasonics, vol. SU-20, pp. 181-189, Apr. 1973.

B2 D.D. Buss, D.R. Collins, W.H. Bailey and C.R. Reeves, "Transversal filtering using charge-transfer devices," IEEE J. Solid-State Circuits, vol. SC-8, pp. 138-146, Apr. 1973.

B3 H.O. Burton and D.D. Sullivan, "Errors and error control," Proc. IEEE, vol. 60, pp. 1293-1301, No. 1972.

C1 A.B. Carleial and M.E. Hellman, "Bistable behaviour of ALOHA-type systems," IEEE Trans. Comm., vol. COM-23, pp. 401-409, Apr. 1975.

C2 G.R. Cooper, "Multi-service aspects of spread-spectrum mobile communication systems," Conference Record of MIDCON/78, Dallas, Texas, Dec. 12-14, 1978, Electrical and Electronics Exhibitions, Inc.

C3 G.R. Cooper and R.W. Nettleton, "A spread-spectrum technique for high-capacity mobile communications," IEEE Trans. Vehicular Tech., vol. BT-27, pp. 264-275, Nov. 1978.

D1 R.C. Dixon, Spread Spectrum Systems. New York: Wiley & sons, 1976.

D2 R.C. Dixon, Ed., Spread Spectrum Techniques. New York: IEEE Press, 1976.

D3 R.W. Donaldson, Design of Distributed Computer-Communication Networks, pp. 40-41. Report to the Department of Communications, Ottawa, Canada, July 1977.

D4 R.C. Dixon, "100 MHz. pseudonoise code generator," TRW Systems Group, Report IOC7325.2-19, July 1968.

D5 W.B. Davenport, Jr., Probability and Random Processes, Ch. 7. New York: McGraw Hill, 1970.

D6 W.B. Davenport, Jr., Probability and Random Processes, Ch. 13. New York: McGraw Hill, 1970.

D7 A.L. Dudick, E. Fuchs and P.E. Jackson, "Data traffic measurements for inquiry-response computer communications system," Proc. IFIP, pp. 634-641, Ljubljana, Yugoslavia, Aug. 1971.

E1 J. Eldon, "Correlation - a powerful technique for digital signal processing," TRW LSI Products LSI Publication TP17A, La Jolla, California, Dec. 1980.

F1 E. Fuchs and P.E. Jackson, "Estimates of distributions of random variables for certain computer communication traffic models," Comm. ACM, vol. 13, pp. 752-757, Dec. 1970.

G1 D.A. Gandolfo, G.D. O'Clock, and C.L. Grasse, "Acoustic surface wave sequence generators and matched filters with adjustable taps," IEEE Int. Microwave Symp. Dig., pp. 60-61, May 1971.

G2 R. Gold, "Optimal binary sequences for spread spectrum multiplexing, "IEEE Trans. Information Theory, vol. IT-13, pp. 619-621, Oct. 1967.

G3 D.P. Grybos and G.R. Cooper, "A receiver feasibility study for the spread-spectrum high capacity mobile radio system," Conf. Rec. Vehicular Tech. Society, Denver, CO., Mar. 22-24, 1978.

G4 G. Gordon, The Application of GPSS V to Discrete System Simulation, Englewood Cliffs, N.J.: Prentice Hall, 1975.

H1 H.P. Hartmann, "Analysis of a dithering loop for PN code tracking," IEEE Trans. Aerospace Electronic Systems, vol. AES-10, pp. 2-9, Jan. 1974.

H2 J.K. Holmes and C.C. Chen, "Acquisition time performance of PN spread-spectrum systems," IEEE Trans. Comm., vol. COM-25, pp. 778-784, Aug. 1977.

H3 P.M. Hopkins, "A unified analysis of pseudonoise synchronization by envelope correlation," IEEE Trans. Comm., vol. COM-25, pp. 770-778, Aug. 1977.

H4 P.S. Henry, "Spectrum efficiency of a frequency-hopped-DPSK spread-spectrum mobile radio system," IEEE Trans. Vehicular Tech., vol. VT-28, pp. 327-332, Nov. 1979.

K1 L. Kleinrock, Queueing Systems, Vol. 2: Computer Applications. New York: Wiley & Sons, 1976.

K2 L. Kleinrock, "On resource sharing in a distributed communication environment," IEEE Comm. Magazine, vol. 17, pp. 27-33, Jan. 1979.

K3 L. Kleinrock and S.S. Lam, "Packet swithcing in a multiaccess broadcast channel: performance evaluation," IEEE Trans. Comm., vol. COM-23, pp. 410-423, Apr. 1975.

K4 L. Kleinrock and F.A. Tobagi, "Packet switching in radio channels: part I - carrier sense multiple-access modes and their throughput-delay characteristics," IEEE Trans. Comm., vol. COM-23, pp. 1400-1416, Dec. 1975.

K5 C.C. Kilgus, "Pseudonoise code acqusition using majority logic decoding," IEEE Trans. Comm., vol. COM-21, pp. 772-774, June 1973.

K6 R.E. Kahn, S.A. Gronemeyer, J. Burchfiel and R.C. Kunzelman, "Advances in packet radio technology," Proc. IEEE, vol. 66, pp. 1468-1496, Nov. 1978.

K7 J.G. Kemeny and J.L. Snell, Finite Markov Chains. Princeton, N.J.: Van Nostrand Co., 1969.

K8 T.K. Kashihara, "Adaptive cancellation of mutual interference in spread spectrum multiple access," Proc. ICC'80, pp. 44.4.1-44.4.5, Seattle, Washington, June 1980.

L1 S.S. Lam and L. Kleinrock, "Packet switching in a multiaccess broadcast channel: dynamic control procedures," IEEE Trans. Comm. vol. COM-23, pp. 891-904, Sept. 1975.

L2 V.C.M. Leung and R.W. Donaldson, "Confidence estimates for acquisition times and hold-in times for PN-SSMA synchronizer employing envelope correlation," IEEE Trans. Comm., vol. COM-30, Jan. 1982.

M1 J. Martin, Design of Man-Computer Dialogues. Eaglewood Cliffs, N.J.: Prentice Hall, 1973.

M2 S.A. Musa and W. Wasylkiwskyj, "Co-channel interference of spread spectrum systems in a multiple user environment," IEEE Trans. Comm., vol. COM-26, pp. 1405-1413, Oct. 1978.

M3 M.B. Milstein and P.K. Das, "Spread spectrum receiver using surface acoustic wave technology," IEEE Trans. Comm., vol. COM-25, pp. 841-847, Aug. 1977.

M4 J.E. Mazo, "Some theoretical observations on spread-spectrum communications," The Bell System Technical Journal, vol. 58, pp. 2013-2023, No. 1979.

M5 J.I. Marcum, "A statistical theory of target detection by pulsed radar, mathematical appendix," IRE Trans., vol. IT-6, pp. 269-288, Apr. 1960.

N1 R.W. Nettleton and G.R. Cooper, "Error performance of a spread-spectrum mobile communications system in a rapidly-fading environment," Conf. Rec. NTC'77, Los Angeles, CA, Dec. 5-7, 1977.

N2 R.W. Nettleton and G.R. Cooper, "Mutual interference in cellular LMR systems: narrowband and broadband techniques compared," MIDCON 1977 Session Reprint, Session 9, Chicago, IL, Nov. 1977.

N3 R.W. Nettleton and G.R. Cooper, "Spectral efficiency in cellular land-mobile communications: a spread-spectrum approach," Technical Report TR-EE 78-44, Purdue University, Oct. 1978.

P1 M.B. Pursley, "Performance evaluation for phase-coded spread-spectrum multiple-access communication - part I: system analysis," IEEE Trans. Comm.. vol. COM-25, pp. 795-799, Aug. 1977.

P2 M.B. Pursley and D.V. Sarwate, "Performance evaluation for phase-coded spread-spectrum multiple-access communication - part II: code sequence analysis," IEEE Trans. Comm., vol. COM-25, pp. 800-803, Aug. 1977.

P3 A Papoulis, Probability, Random Variables, and Stochastic Processes. New York: McGraw-Hill, 1965.

P4 M.B. Pursley, F.D. Garber and J.S. Lehnert, "Analysis of generalized quadriphase spread-spectrum communications," Proc. ICC'80, pp. 15.3.1-15.3.6, Seattle, Washington, June 1980.

R1 W.B. Rouse, "Design of man-computer interface for on-line interactive systems," Proc. IEEE, vol. 63, pp. 847-857, June 1975.

R2 D. Raychaudhuri, "Performance analysis of random-access packet-switched code division multiple access systems," IEEE Trans. Comm., vol. COM-29, pp. 895-901, June 1981.

S1 J.W. Schwartz, J.M. Aein and J. Kaiser, "Modulation techniques for multiple access to a hard-limiting satellite repeater," Proc. IEEE, vol. 54, pp. 763-777, May 1966.

S2 G. Solomon, "Optimal frequency hopping sequences for multiple access", Proc. Symp. Spread Spectrum Comm., Naval Electronics Lab., Mar. 1973.

S3 J.J. Spilker, Jr. and D.T. Magill, "The delay-lock discriminator - an optimum tracking device," Proc. IRE, vol. 49, pp. 1403-1416, Sept. 1961.

S4 G.F. Sage, "Serial synchronization of pseudonoise systems," IEEE Trans. Comm. Tech., vol. COM-12, pp. 123-127, Dec. 1964.

S5 J.J. Spilker, Jr., "Delay-lock tracking of binary signals," IEEE Trans. Space Electronics and Telemetry, vol. SET-9, pp. 1-8, Mar. 1963.

S6 D.L. Schilling, L.B. Milstein, R.L. Pickholtz and R.W. Brown, "Optimization of the processing gain of an M-ary direct sequence spread spectrum communication system," IEEE Trans. Comm., vol. COM-28, pp. 1389-1398, Aug. 1980.

T1 R.A. Tobagi and L. Kleinrock, "Packet switching in radio channels: part II - the hidden terminal problem in carrier sense multiple-access and the busy-tone solution," IEEE Trans. Comm., vol. COM-23, pp. 1417-1433, Dec. 1975.

T2 F.A. Tobagi and L. Lkeinrock, "Packet swithcing in radio channels: part III - polling and (dynamic) split-channel reservation multiple access," IEEE Trans. Comm., vol. COM-24, pp. 832-844, Aug. 1976.

V1 R. Van Slyke and H. Frank, "Network reliability analysis: Part 1," Networks, vol. 1, No. 3, pp. 279-290, 1972.

V2 P.A. DeVito, P.H. Carr, W.J. Kearns and J.H. Silva, "Encoding and decoding with elastic surface wvaes at 10 Megabits per second," Proc. IEEE, vol. 59, pp. 1523-1525, Oct. 1971.

W1 R.B. Ward, "Acquisition of Pseudonoise signals by sequential estimation," IEEE Trans. Comm., vol. COM-13, pp. 475-483, Dec. 1965.

W2 R.B. Ward and K.P. Yiu, "Acquisition of pseudonoise signals by recursion-aided sequential estimation," IEEE Trans. Comm., vol. COM-25, pp. 784-794, Aug. 1977.

Y1 K. Yao, "Error probability of asynchronous spread spectrum multiple access communications systems," IEEE Trans. Comm., vol. COM-25, pp. 803-809, Aug. 1977.

Y2 R.D. Yates and G.R. Cooper, "Design of large signal sets with good aperiodic correlation properties," Technical Report TR-EE 66-13, Purdue University, Sept. 1966.

Y3 P.S. Yu and S. Lin, "An efficient selective-repeat ARQ scheme for satellite channels and its throughput analysis," IEEE Trans. Comm., vol. COM-29, pp. 353-363, Mar. 1981.

Z1 R.E. Ziemer and W.H. Tranter, Principles of Communications, Ch. 7, Boston, Mass.: Houghton Mifflin Co., 1976.

Appendix 1. Derivation of Equation (2.3.6)

Consider the receiver block diagram in Fig. 2.1.1(b), and let x(t) and y(t) be the input and output signals, respectively, of the low pass filter which has the transfer function

$$H(f) = \begin{cases} 1 & , |f| < B_m \\ 0 & , |f| > B_m \end{cases} \tag{A1.1}$$

Let u(t) be the locally generated signal which is synchronized to the i-th user's tranmission. Let the random phases and delays of all transmitted signals, $s_k(t)$, be measured with reference to $s_i(t)$. Therefore, $\theta_i=0$, $\tau_i=0$ and

$$u(t) = \sqrt{2}\ c_i(t) \cos(\omega_c t) \tag{A1.2}$$

Let $x^N(t)$ and $y^N(t)$ be the noise components of x(t) and y(t), respectively, contributed by n(t) and $s_k(t)$, $k \neq i$.

Modelling all PN signals as band-limited, uncorrelated Gaussian white noise, yields the power spectra for $s_k(t)$ and u(t) as follows:

$$S_{s_k}(f) = \begin{cases} P/2B_t & , |f \pm f_c| < B_t/2 \\ 0 & , \text{elsewhere} \end{cases} \tag{A1.3}$$

and

$$S_u(f) = S_{s_k}(f)/P \tag{A1.4}$$

where $f_c = \omega_c/2\pi$.

The power spectrum for n(t) is

$$S_n(f) = N_o/2 \tag{A1.5}$$

Convolution of $S_u(f)$ with the sum of $S_n(f)$ and $(M-1)S_{s_k}(f)$ results in the following spectrum for $x^N(t)$.

$$S_{x^N}(f) = \begin{cases} \frac{N_o}{2} + \frac{(M-1)P}{2B_t}\left(1 - \frac{2|f|}{B_t}\right) & , \quad |f| < \frac{B_t}{2} \\ \frac{N_o}{2} + \frac{(M-1)P}{4B_t}\left(1 - \frac{2|f \pm 2f_o|}{B_t}\right), & |f \pm 2f_o| < \frac{B_t}{2} \\ \frac{N_o}{2} & , \quad \text{elsewhere} \end{cases} \tag{A1.6}$$

Since $B_m \ll B_t$, low-pass filtering results in the following spectrum for $y^N(t)$.

$$\begin{aligned} S_{y^N}(f) &\cong S_{x^N}(0) = \frac{N_o}{2} + \frac{(M-1)P}{2B_t} = N_D \quad , |f| \leq B_m \\ S_{y^N}(f) &= 0 \qquad\qquad\qquad\qquad\quad , |f| > B_m \end{aligned} \tag{A1.7}$$

The corresponding autocorrelation function for $y^N(t)$ is

$$R_{y^N}(\tau) = 2B_m N_D \frac{\sin(2\pi B_m \tau)}{2\pi B_m \tau} \tag{A1.8}$$

It follows that

$$\begin{aligned} E[(a^N(T_b))^2] &= E\left[\int_o^{T_b}\int_o^{T_b} y^N(t)\, y^N(\tau) dt\, d\tau\right] \\ &= \int_o^{T_b}\int_o^{T_b} R_{y^N}(t-\tau) dt\, d\tau \\ &= \frac{N_D}{2\pi^2 B_m}\int_o^{2\pi}\int_o^{2\pi} \frac{\sin(x-y)}{x-y}\, dx\, dy \end{aligned} \tag{A1.9}$$

where the substitution $T_b = 1/B_m$ has been made. Evaluating the double integral in eqn. (A1.9) by numerical methods, yields the result given by eqn. (2.3.6),

$$\mathrm{Var}[a^N(T_b)] = 0.9\ N_D/B_m \qquad \text{(A1.10)}$$

Appendix 2. Derivation of Equation (2.3.11)

In addition to signals defined in Ch. 2 and Appendix 1, let $x_k(t)$, $y_k(t)$ and $a^k(t)$ be the components of x(t), y(t) and a(t), respectively, contributed by the k-th active user of the channel. Consider the i-th reciever. For $k \neq i$,

$$x_k(t) = s_k(t)\, u(t)$$

$$= \sqrt{P}\ \ c_i(t)c_k(t-\tau_k)\{\cos(\omega_c \tau_k - \Theta_k) + \cos[\omega_c(2t-\tau_k) + \Theta_k]\} \qquad \text{(A2.1)}$$

The low pass filter removes the double frequency term to give

$$y_k(t) = \sqrt{P}\ \ c_i(t)c_k(t-\tau_k)\cos(\omega_c \tau_k - \Theta_k) * 2B_m \frac{\sin(2\pi B_m t)}{2\pi B_m t} \qquad \text{(A2.2)}$$

where * denotes convolution.

Expanding the code sequences $c_i(t)$ and $c_k(t)$ into series of pulse train yields

$$c_i(t) = \sum_{m=-\infty}^{\infty} a_m p(t-mT_c) \qquad \text{(A2.3)}$$

$$c_k(t) = \sum_{n=-\infty}^{\infty} b_n p(t-nT_c) \qquad \text{(A2.4)}$$

where $\{a_m\}$ and $\{b_n\}$ are the sequences of code symbols with values of ± 1 and period L corresponding to $c_i(t)$ and $c_k(t)$, and p(t) is a pulse defined by

$$p(t) = \begin{cases} 1 \ , & 0 \leq t \leq T_c \\ 0 \ , & \text{elsewhere} \end{cases} \qquad \text{(A2.5)}$$

In eqns. (As.3) to (A2.5) inclusive, T_c is the pulse duration of the spread-spectrum codes. Therefore

$$c_i(t)c_k(t-\tau_k) = \sum_{m=-\infty}^{\infty} a_m p(t-mT_c) \sum_{n=-\infty}^{\infty} b_n p(t-nT_c-\tau_k) \tag{A2.6}$$

This product is zero for all values of t except where the pulses overlap.

Define r_k and d_k as follows:

$$r_k = \text{trunc}\ (\tau_k/T_c) \tag{A2.7}$$

$$d_k = \tau_k - r_k T_c \tag{A2.8}$$

where trunc(x) is the largest integer less than or equal to real number x. Then eqn. (A2.6) becomes

$$c_i(t)\ c_k(t-\tau_k) = \sum_{m=-\infty}^{\infty} [a_m b_{m-r_k-1} p_1(t-mT_c) + a_m b_{m-r_k} p_2(t-mT_c)] \tag{A2.9}$$

where $p_1(t)$ and $p_2(t)$ are pulses defined by

$$p_1(t) = \begin{cases} 1 & , \quad 0 \leq t \leq d_k \\ 0 & , \quad \text{elsewhere} \end{cases} \tag{A2.10}$$

$$p_2(t) = \begin{cases} 1 & , \quad d_k \leq t \leq T_c \\ 0 & , \quad \text{elsewhere} \end{cases} \tag{A2.11}$$

Because $1/B_m = T_b = LT_c$, $T_c \ll 1/B_m$ and $\sin(2\pi B_m t)/2\pi B_m t$ may be considered as a constant within any time interval of length T_c. Therefore

$$p_1(t-mT_c) * \frac{\sin(2\pi B_m t)}{2\pi B_m t} \cong \frac{d_k \sin[2\pi B_m (t-mT_c)]}{2\pi B_m (t-mT_c)} \tag{A2.12}$$

$$p_2(t-mT_c) * \frac{\sin(2\pi B_m t)}{2\pi B_m t} \cong \frac{(T_c-d_k)\sin[2\pi B_m (t-mT_c)]}{2\pi B_m (t-mT_c)} \tag{A2.13}$$

Define the function $f_{ik}(m, \tau_k)$ by

$$f_{ik}(m, \tau_k) = a_m b_{m-r_k-1} d_k + a_m b_{m-r_k} (T_c - d_k) \tag{A2.14}$$

Since a_m and b_m are periodic in m with period L, so is $f_{ik}(m, \tau_k)$; thus

$$f_{ik}(m+nL, \tau_k) = f_{ik}(m, \tau_k), \text{ any integer } n \tag{A2.15}$$

Substituting for $c_i(t)c_k(t-\tau_k)$, eqn. (A2.2) becomes

$$\begin{aligned} y_k(t) &= \sqrt{P}2B_m \cos(\omega_c T_k - \theta_k) \sum_{n=-\infty}^{\infty} \sum_{m=1}^{L} \{f_{ik}(m+nL, \tau_k) \\ &\qquad \frac{\sin[2\pi B_m (t-mT_c-nLT_c)]}{2\pi B_m (t-mT_c-nLT_c)}\} \\ &= \sqrt{P}2B_m \cos(\omega_c \tau_k - \theta_k) \sum_{m=1}^{L} f_{ik}(m, \tau_k) \\ &\qquad \sum_{n=-\infty}^{\infty} \frac{\sin[2\pi B_m (t-mT_c-nT_b)]}{2\pi B_m (t-mT_c-nT_b)} \\ &= \sqrt{P}2B_m \cos(\omega_c \tau_k - \theta_k) \sum_{m=1}^{L} f_{ik}(m, \tau_k) g(t-mT_c) \end{aligned} \tag{A2.16}$$

where the function g is defined as follows:

$$g(t) \triangleq \sum_{n=-\infty}^{\infty} \frac{\sin[2\pi B_m (t-nT_b)]}{2\pi B_m (t-nT_b)} \tag{A2.17}$$

Note that g(t) is periodic in t with period T_b and that value of g(t) may be computed to a satisfactory degree of accuracy using numerical methods.

Integration of $y_k(t)$ followed by sampling yields

$$a^k(T_b) = \int_o^{T_b} \sqrt{P}2B_m \cos(\omega_c T_k - \Theta_k) \sum_{m=1}^{L} f_{ik}(m,\tau_k) g(t-mT_c)dt$$

$$= \sqrt{P}2B_m \cos(\omega_c T_k - \Theta_k) \sum_{m=1}^{L} f_{ik}(m, \tau_k) \int_o^{T_b} g(t)dt \qquad \text{(A2.18)}$$

In eqn. (A2.18) integration is over one period of g(t). Therefore $g(t-mT_c)$ may be replaced by g(t). Numerical integration gives the following result:

$$\int_o^{T_b} g(t)dt \cong T_b/2 = 1/2B_m \qquad \text{(A2.19)}$$

Define the maximum cross-correlation between the code sequences as

$$\psi_{max} = \max_{i,j,\tau} \int_o^{T_b} c_i(t)c_j(t+\tau)dt$$

$$= \max_{i,k,\tau} \sum_{m=1}^{L} f_{ik}(m,\tau) \qquad \text{(A2.20)}$$

Making appropriate substitutions, an upper bound for the mean squared value of $a^k(T_b)$ is therefore given by

$$E[(a^k(T_b))^2] \leq E[P\psi_{max}^2 (1+\cos(2\omega_c \tau_k - \Theta_k))/2] \qquad \text{(A2.22)}$$

Since

$$E[\cos(2\omega_c \tau_k - \Theta_k)] = 0 \qquad \text{(A2.23)}$$

it follows that

$$E[(a^k(T))^2] \leq P\psi_{max}^2/2 \qquad \text{(A2.24)}$$

Applying the results in Appendix 1 to the Gaussian channel noise only,

the contribution of channel noise to $a^N(T_b)$ is

$$a^n(T_b) = 0.45\ N_o/B_m \tag{A2.25}$$

Summing all contributions, results in $\mathrm{Var}[a^N(T_b)]$ being bounded as follows:

$$\mathrm{Var}[a^N(T_b)] \leq (M-1)\psi_{max}^2\ P/2 + 0.45\ N_o/B_m \tag{A2.26}$$

which is the result given by eqn. (2.3.11).

APPENDIX 3. GPSS PROGRAM FOR SIMULATION OF SSMA CHANNEL

```
      REALLOCATE  XAC,3700
*************************** SSMA-RT ****************************
*                                                              *
*  TO SIMULATE A SSMA COMMUNICATION SYSTEM WITH RETRANSMISSION  *
*  ON MESSAGE ERRORS. ASSUME:                                  *
*  (1) EXPONENTIALLY DISTRIBUTED INTERARRIVAL TIME;            *
*  (2) FIXED MESSAGE LENGTH;                                   *
*  (3) UNIFORMLY DISTRIBUTED ACQUISITION TIME;                 *
*  (4) FIXED SERVICE TIME OF 0.01 SEC.;                        *
*  (5) FIXED BIT-ERROR RATE FOR TRANSMISSION OF EACH BIT;      *
*  (6) MESSAGE TRANSMISSION REPEATED UNTIL ERROR-FREE.         *
*  MESSAGE DELAYS ARE TABULATED. CHANNEL OCCUPANCY IS SAMPLED  *
*  AT FIXED INTERVALS AND TABULATED.                           *
*                                                              *
****************************************************************
      SIMULATE
*
* DEFINE FUNCTIONS
*
XPDIS FUNCTION  RN1,C24       INVERTED EXPONENTIAL DISTRIBUTION
0,0/.1,.104/.2,.222/.3,.355/.4,.509/.5,.69/.6,.915/.7,1.2
.75,1.38/.8,1.6/.84,1.83/.88,2.12/.9,2.3/.92,2.52/.94,2.81
.95,2.99/.96,3.2/.97,3.5/.98,3.9/.99,4.6/.995,5.3/.998,6.2
.999,7/.9998,8
PBIT  FUNCTION  S$CHANL,C13   ERRORS/1000BITS VS CHN.OCP. AT 70DB-HZ
0,0/125,0/205,1/254,2/285,3/308,4/347,6/380,8/408,10
460,14/550,22/672,34/828,50/
*
* SIMULATION  OF INDIVIDUAL USERS
*
      GENERATE  XH$IARRT,FN$XPDIS,,,,1PH  CREATE AN ARRIVAL
      ENTER     CHANL             INCREMENT CHANNEL OCCUPANCY
      ADVANCE   XH$TACQ,XH$TACQ   ACQUISITION DELAY
      ADVANCE   XH$TSERV          SERVICE DELAY
TRAN  ASSIGN    1,XH$MLEN,PH      SET UP BIT COUNTER
      LOGIC R   1                 RESET BIT-ERROR SWITCH
NXBIT TEST L    RN8,FN$PBIT,CORR  GO TO CORR IF NO BIT-ERROR
      LOGIC S   1               SET BIT ERROR SWITCH
CORR  ADVANCE   XH$TBIT         TRANSMISSION TIME FOR 1 BIT
      ASSIGN    1-,1,PH         DECREMENT BIT COUNTER
      TEST E    PH1,0,NXBIT     ALL BITS TRANSMITTED? IF NOT, GOTO NXBIT
      GATE LR   1,TRAN          RETRANSMIT IF BIT-ERRORS OCCURED
      TABULATE  DELAY           DELAY TABULATED AFTER MESSAGE ERROR-FREE
      ADVANCE   XH$TSERV        SERVICE DELAY FOR ACKNOWLEDGEMENT
      LEAVE     CHANL           DECREMENT CHANNEL OCCUPANCY
      TERMINATE                 SIMULATION OF 1 USER COMPLETED
```

```
*
* COLLECT STATISTICS FOR CHANNEL OCCUPANCY
*
      GENERATE    XH$SAMPT,,,,,0PH  SAMPLE AT REGUALR INTERVAL
      TABULATE    NUSER  TABULATE CHANNEL OCCUPANCY
      TERMINATE   1
*
* INITIALIZE SAVEVALUES
*
      INITIAL     XH$TBIT,2         BIT TRANSMISSION TIME 0.02 MSEC.
      INITIAL     XH$TSERV,1000     SERVICE TIME 0.01 SEC.
      INITIAL     XH$TACQ,10000     MEAN ACQUISITION TIME 0.1 SEC.
      INITIAL     XH$IARRT,125      IARRT 0.00125SEC., 800MES./SEC.
      INITIAL     XH$SAMPT,750      SAMPLING INTERVAL 0.0075SEC.
      INITIAL     XH$MLEN,1000      MESSAGE LENGTH 1000 BITS
*
* DEFINE TABLES
*
DELAY TABLE       M1,3000,1000,24
NUSER TABLE       S$CHANL,60,1,100
*
* CONTROL
*
      START       18,NP             INITIALIZE CHANNEL
      RESET
      START       500               COLLECT 500 SAMPLES
      CLEAR       XH2-XH5
NUSER TABLE       S$CHANL,90,1,100
      INITIAL     XH$IARRT,100      IARRT 0.001SEC., 1000MES./SEC.
      INITIAL     XH$SAMPT,700      SAMPLING INTERVAL 0.007SEC.
      START       19,NP             INITIALIZE CHANNEL
      RESET
      START       500               COLLECT 500 SAMPLES
      END
```

Appendix 4. Goodness-of-Fit Tests

The following is the summary of a number of goodness-of-fit tests performed between the distributions of channel occupancy obtained from simulations of a SSMA channel and exponential distributions whose expected values equal the corresponding channel occupancy averages. Data were obtained for PNR = 70 dB-Hz and ℓ = 1000 bits/message, with λ ranging from 10 to 1000 messages/sec. In the simulations it was assumed that acquisition delays were uniformly distributed between 0 and twice the mean value for a synchronizer with K = 1, V_S = 1.7, V_L = 1.0. This assumption is reasonable for the PNR level and range of channel occupancies considered because the mean and standard deviation of acquisition time are minimum and have the ratio of standard deviation/mean $\cong$ 0.6 $\cong 1/\sqrt{3}$, the corresponding ratio for a uniform distribution.

To test the hypothesis

$$H_o: \quad Pr(M=m) = \frac{\bar{M}^m}{m!} e^{-\bar{M}}$$

against 500 channel occupancy samples obtained from simulation, where $\bar{M}$ is the sample mean, data and results are tabulated below.

Case 1: $\lambda = 10$ messages/sec.

$\bar{M} = 1.441$

Channel Occupancy M	Observed Frequency O_i	Expected Frequency E_i	$\frac{(O_i-E_i)^2}{E_i}$
0	116.	118.35	0.046
1	177.	170.54	0.245
2	119.	122.87	0.122
3	58.	59.02	0.018
4	19.	21.26	0.241
5 to 6	11.	7.60	1.522

$$\sum \frac{(O_i-E_i)^2}{E_i} = 2.194$$

Number of degrees of freedom = 5

$$\chi^2_{0.05} = 11.070 > 2.194$$

Therefore, we fail to reject H_o at a 0.05 level of significance.

Case 2: $\lambda = 50$ messages/sec.

$\bar{M} = 6.775$

Channel Occupancy M	Observed Frequency O_i	Expected Frequency E_i	$\frac{(O_i-E_i)^2}{E_i}$
0 to 2	21.	17.54	0.681
3	26.	29.59	0.436
4	48.	50.12	0.090
5	62.	67.92	0.516
6	88.	76.69	1.667
7	74.	74.23	0.001
8	63.	62.86	0.000
9	47.	47.32	0.002
10	35.	32.06	0.270
11	9.	19.75	5.848
12	11.	11.15	0.002
13	8.	5.81	0.826
14 to 16	6.	4.62	0.413

$$\sum \frac{(O_i-E_i)^2}{E_i} = 10.752$$

Number of degrees of freedom = 12

$$\chi^2_{0.05} = 21.016 > 10.752$$

Therefore, we fail to reject H_o at a 0.05 level of significance.

Case 3: λ = 100 message/sec.

$\bar{M}$ = 13.717

Channel Occupancy M	Observed Frequency O_i	Expected Frequency E_i	$\frac{(O_i-E_i)^2}{E_i}$
0 to 6	7.	8.45	0.248
7	9.	10.00	0.101
8	19.	17.15	0.199
9	29.	26.14	0.313
10	41.	35.86	0.738
11	44.	44.71	0.011
12	41.	51.11	2.001
13	60.	53.93	0.683
14	44.	52.84	1.479
15	47.	48.32	0.036
16	55.	41.43	4.447
17	27.	33.43	1.235
18	22.	25.47	0.473
19	21.	18.39	0.370
20	12.	12.61	0.030
21	13.	8.24	2.752
22 to 26	9.	11.42	0.512

$$\sum \frac{(O_i-E_i)^2}{E_i} = 15.630$$

Number of degrees of freedom = 16.

$$\chi^2_{0.05} = 26.296 > 15.630$$

Therefore, we fail to reject Ho at a 0.05 level of significance.

Case 4: λ = 200 message/sec. $\bar{M}$ = 28.271

Channel Occupancy M	Observed Frequency O_i	Expected Frequency E_i	$\frac{(O_i-E_i)^2}{E_i}$
0 to 17	6.	7.96	0.482
18	6.	5.48	0.049
19 to 20	11.	19.68	3.830
21	14.	15.52	0.149
22	23.	19.94	0.469
23	23.	24.51	0.093
24	24.	28.87	0.823
25	27.	32.65	0.978
26	35.	35.50	0.007
27	51.	37.18	5.141
28	40.	37.54	0.162
29	38.	36.59	0.054
30	37.	34.48	0.184
31	36.	31.45	0.659
32	35.	27.78	1.875
33	27.	23.80	0.430
34	23.	19.79	0.520
35	18.	15.99	0.254
36	11.	12.55	0.192
37 to 38	8.	16.73	4.554
39 to 42	7.	13.05	2.803

$$\sum \frac{(O_i-E_i)^2}{E_i} = 23.708$$

Number of degrees of freedom = 20.

$$\chi^2_{0.05} = 31.410 > 23.708$$

Therefore, we fail to reject H_o at a 0.05 level of significance.

Case 5: λ = 400 message/sec. $\bar{M}$ = 56.605

Channel Occupancy M	Observed Frequency O_i	Expected Frequency E_i	$\frac{(O_i-E_i)^2}{E_i}$
0 to 39	6.	4.31	0.667
40 to 42	7.	8.83	0.378
43 to 44	10.	11.65	0.235
45	6.	8.25	0.613
46	9.	10.15	0.130
47	12.	12.22	0.004
48	15.	14.42	0.024
49	12.	16.65	1.300
50	25.	18.85	2.004
51	20.	20.93	0.041
52	26.	22.78	0.456
53	25.	24.33	0.019
54	32.	25.50	1.656
55	23.	26.25	0.401
56	23.	26.53	0.469
57	29.	26.35	0.268
58	29.	25.71	0.421
59	22.	24.67	0.289
60	22.	23.27	0.070
61	23.	21.60	0.091
62	25.	19.72	1.416
63	19.	17.71	0.093
64	10.	15.67	2.050
65	13.	13.64	0.030
66	10.	11.70	0.248
67	9.	9.89	0.079
68	10.	8.23	0.381
69 to 70	7.	12.21	2.224
71 to 72	7.	7.77	0.077
73 to 74	7.	4.68	1.146
75 to 77	7.	3.51	3.466

$$\sum \frac{(O_i-E_i)^2}{E_i} = 20.745$$

Number of degrees of freedom = 30.

$$\chi^2_{0.05} = 43.773 > 20.745$$

Therefore, we fail to reject Ho at a 0.05 level of significance.

Case 6: λ = 500 message/sec. $\bar{M}$ = 70.553

Channel Occupancy M	Observed Frequency O_i	Expected Frequency E_i	$\frac{(O_i-E_i)^2}{E_i}$
0 to 55	7.	16.38	5.374
56 to 57	11.	11.83	0.058
58	10.	7.96	0.523
59	9.	9.52	0.028
60	6.	11.19	2.409
61	10.	12.95	0.670
62	12.	14.73	0.506
63	11.	16.50	1.832
64	20.	18.19	0.181
65	20.	19.74	0.003
66	17.	21.10	0.709
67	26.	22.22	0.643
68	23.	23.06	0.000
69	28.	23.57	0.831
70	29.	23.76	1.155
71	25.	23.61	0.082
72	29.	23.14	1.486
73	30.	22.36	2.610
74	32.	21.32	5.351
75	30.	20.06	4.931
76	25.	18.62	2.188
77	15.	17.06	0.249
78	14.	15.43	0.133
79	16.	13.78	0.357
80	11.	12.15	0.109
81	9.	10.59	0.238
82	9.	9.11	0.001
83 to 84	9.	14.24	1.931
85 to 87	7.	13.42	3.069

$$\sum \frac{(O_i-E_i)^2}{E_i} = 37.744$$

Number of degrees of freedom = 28.

$$\chi^2_{0.05} = 41.337 > 37.744$$

Therefore, we fail to reject H_o at a 0.05 level of significance.

Case 7: λ = 800 message/sec. $\bar{M}$ = 112.359

Channel Occupancy M	Observed Frequency O_i	Expected Frequency E_i	$\frac{(O_i-E_i)^2}{E_i}$
0 to 91	5.	10.91	3.198
92 to 93	7.	6.42	0.053
94 to 95	10.	9.16	0.077
96 to 97	11.	12.54	0.188
98	5.	7.71	0.955
99	9.	8.75	0.007
100	9.	9.84	0.071
101	9.	10.94	0.345
102	12.	12.05	0.000
103	7.	13.15	2.876
104	12.	14.21	0.343
105	8.	15.20	3.412
106	20.	16.11	0.937
107	18.	16.92	0.069
108	21.	17.60	0.655
109	19.	18.15	0.040
110	14.	18.54	1.110
111	19.	18.76	0.003
112	22.	18.82	0.536
113	34.	18.72	12.482
114	26.	18.45	3.093
115	16.	18.02	0.227

. . .continued

Case 7: λ = 800 message/sec. $\bar{M}$ = 112.359

Channel Occupancy M	Observed Frequency O_i	Expected Frequency E_i	$\frac{(O_i-E_i)^2}{E_i}$
116	21.	17.46	0.719
117	20.	16.76	0.624
118	23.	15.96	3.102
119	8.	15.07	3.319
120	13.	14.11	0.088
121	16.	13.10	0.640
122	13.	12.07	0.072
123	15.	11.03	1.433
124	7.	9.99	0.895
125	7.	8.98	0.436
126	5.	8.01	1.130
127	5.	7.08	0.613
128	11.	6.22	3.676
129 to 130	7.	10.10	0.950
131 to 133	7.	10.32	1.068
134 to 143	6.	11.58	2.692

$$\sum \frac{(O_i-E_i)^2}{E_i} = 52.134$$

Number of degrees of freedom = 37.

$$\chi^2_{0.05} = 52.192 > 52.134$$

Therefore, we fail to reject H_o at a 0.05 level of significance.

Case 8: λ = 1000 message/sec. $\bar{M}$ = 141.500

Channel Occupancy M	Observed Frequency O_i	Expected Frequency E_i	$\frac{(O_i-E_i)^2}{E_i}$
0 to 116	5.	6.21	0.236
116 to 117	5.	3.53	0.613
118 to 119	5.	5.07	0.001
120 to 121	6.	7.05	0.156
122 to 123	10.	9.47	0.029
124	5.	5.78	0.106
125	6.	6.55	0.046
126	5.	7.35	0.753
127	11.	8.19	0.962
128	10.	9.06	0.098
129	8.	9.93	0.376
130	12.	10.81	0.130
131	9.	11.68	0.615
132	14.	12.52	0.175
133	7.	13.32	2.999
134	9.	14.07	1.824
135	16.	14.74	0.107
136	18.	15.34	0.462
137	15.	15.84	0.045
138	18.	16.24	0.190
139	21.	16.54	1.205
140	15.	16.71	0.176
141	18.	16.77	0.090
142	18.	16.71	0.099
143	21.	16.54	1.203
144	19.	16.25	0.465
145	12.	15.86	0.939
146	17.	15.37	0.173

. . .continued

Case 8: λ = 1000 message/sec. $\bar{M}$ = 141.500

Channel Occupancy M	Observed Frequency O_i	Expected Frequency E_i	$\frac{(O_i-E_i)^2}{E_i}$
147	11.	14.80	0.974
148	15.	14.15	0.052
149	13.	13.43	0.014
150	9.	12.67	1.064
151	9.	11.88	0.696
152	22.	11.05	10.837
153	7.	10.22	1.017
154	16.	9.39	4.646
155	7.	8.58	0.290
156	7.	7.78	0.078
157	12.	7.01	3.551
158 to 159	8.	11.87	1.260
160	5.	4.94	0.001
161	12.	4.34	13.500
162 to 165	6.	12.36	3.276
166 to 173	6.	9.73	1.428

$$\sum \frac{(O_i-E_i)^2}{E_i} = 56.952$$

Number of degrees of freedom = 43.

$$\chi^2_{0.05} = 59.300 > 56.952$$

Therefore, we fail to reject H_o at a 0.05 level of significance.